The Impact of Aerobic Exercise on Brain's White Matter Integrity in the Alzheimer's disease and the Aging Population

BY

Rodrigo Dennis Perea Camargo

Submitted to the Bioengineering Program in the School of Engineering and the Graduate Faculty of the University of Kansas in partial fulfillment of the requirements for the degree of Doctor of Philosophy

_____
Chairperson Robyn A. Honea, DPhil

_____
Eric D. Vidoni, PT. PhD

_____
Sara E. Wilson, PhD

_____
Xinmai Yang, PhD

_____
William M. Brooks, PhD

_____
Jeffrey M. Burns, MS. MD

Date Defended: _____

The Dissertation Committee for Rodrigo Dennis Perea Camargo certifies that this is the approved version of the following dissertation:

The Impact of Aerobic Exercise on Brain's White Matter Integrity in the Alzheimer's disease and the Aging Population

_____
Chairperson Robyn A. Honea, DPhil

Date approved: _____

Abstract

The brain is the most complex organ in the body. Currently, its complicated functionality has not been fully understood. However, in the last decades an exponential growth on research publications emerged thanks to the use of *in-vivo* brain imaging techniques. One of these techniques pioneered for medical use in the early 1970s was known as nuclear magnetic resonance imaging based (now called magnetic resonance imaging [MRI]). Nowadays, the advances of MRI technology not only allowed us to characterize volumetric changes in specific brain structures but now we could identify different patterns of activation (e.g. functional MRI) or changes in structural brain connectivity (e.g. diffusion MRI). One of the benefits of using these techniques is that we could investigate changes that occur in disease-specific cohorts such as in the case of Alzheimer's disease (AD), a neurodegenerative disease that affects mainly older populations. This disease has been known for over a century and even though great advances in technology and pharmacology have occurred, currently there is no cure for the disease. Hence, in this work I decided to investigate whether aerobic exercise, an emerging alternative method to pharmacological treatments, might provide neuroprotective effects to slow down the evident brain deterioration of AD using novel *in-vivo* diffusion imaging techniques. Previous reports in animal and human studies have supported these exercise-related neuro-protective mechanisms. Concurrently in AD participants, increased brain volumes have been positively associated with higher cardiorespiratory fitness levels, a direct marker of sustained physical activity and increased exercise. Thus, the goal of this work is to investigate further whether exercise influences the brain using structural connectivity analyses and novel diffusion imaging techniques that go beyond volumetric

characterization. The approach I chose to present this work combined two important aspects of the investigation. First, I introduced important concepts based on the neuro-scientific work in relation to Alzheimer's diseases, *in-vivo* imaging, and exercise physiology (Chapter 1). Secondly, I tried to describe in simple mathematics the physics of this novel diffusion imaging technique (Chapter 2) and supported a tract-specific diffusion imaging processing methodology (Chapter 3 and 4). Consequently, the later chapters combined both aspects of this investigation in a manuscript format (Chapter 5-8). Finally, I summarized my findings, include recommendations for similar studies, described future work, and stated a final conclusion of this work (Chapter 9).

Acknowledgements

This five-year journey in the neuro-imaging world has been interesting, exciting, ambitious, stressful, and most importantly, crucial for my professional development. Prior to focusing my attention to this field, I didn't realize how much would fit my curiosity to combine technical and scientific skills in the biology and understanding of the brain, an organ that I've always been fascinated and also intimated to study it. It's been a great and long journey for me here in Kansas. Hence, I need to thank my university, The School of Engineering, and The Bioengineering Program for allowing me to continue my education.

Additionally, I would like to thank the University of Kansas Alzheimer's disease Center, Dr. Jeff Burns, all the faculty and staff members, and participants who directly or indirectly provided me the necessary information to continue with my investigation. I also would like to thank my mentor Dr. Robyn Honea who I envisioned as a role model since I started working as a research assistant before starting my doctoral education. I will always be thankful for her patience when mentoring me, her infinite advice, and for allowing me to expand my knowledge in the neuro-imaging world with patience, outstanding motivation, and trust in my skills. To Dr. Eric Vidoni who also mentored me with excellent advice not only to finish my work but also to continue my professional career path. Thanks to both, I believe I have gained another perspective for addressing neuroscience-related problems as well as the importance for communicating very complex concepts in a simple easy-to-understand manner.

Finally I would like to thank my family. Muchísimas gracias por brindarme siempre el apoyo, confianza, paciencia y amor que necesito. Gracias a uds. por ayudarme a crecer y llegar a cumplir mis metas. Mis logros siempre serán dedicados a uds. Los amo!

Table of Contents

List of Figures

Chapter 1: Introduction.

Chapter 2: From diffusion weighted imaging to the tensor calculation.

Chapter 3: A comparative white matter study with Parkinson's disease, Parkinson's disease with dementia and Alzheimer's disease.

Chapter 4: Diffusion tensor imaging and Alzheimer's disease: a comparison between tract-based spatial statistics (TBSS) and tract-of-interest (TOI).

Chapter 5: Cardiorespiratory fitness and white matter integrity in early Alzheimer's disease.

Chapter 6: A longitudinal assessment of brain neuroplasticity and exercise intensity in healthy older adults: a 26-week intervention study

Chapter 7: The effects of aerobic exercise on brain's white matter integrity in the Alzheimer's disease population: a 26-week intervention

Chapter 8: Aerobic exercise and thalamo-cortical connectivity in the Alzheimer's disease population: a 26-week exercise intervention study

List of Tables

Chapter 3: A comparative white matter study with Parkinson's disease, Parkinson's disease with dementia and Alzheimer's disease.

Chapter 4: Diffusion tensor imaging and Alzheimer's disease: a comparison between tract-based spatial statistics (TBSS) and tract-of-interest (TOI).

Chapter 5: Cardiorespiratory fitness and white matter integrity in early Alzheimer's disease.

Chapter 6: A longitudinal assessment of brain neuroplasticity and exercise intensity in healthy older adults: a 26-week intervention study

Chapter 7: The effects of aerobic exercise on brain's white matter integrity in the Alzheimer's disease population: a 26-week intervention

Chapter 8: Aerobic exercise and thalamo-cortical connectivity in the Alzheimer's disease population: a 26-week exercise intervention study

Chapter 1

Introduction

1.1 THE BRAIN AS A CONTROL SYSTEM

From an engineering standpoint, every decision, thought, or action we take at a specific time can be described of as a very well organized and powerful closed-loop control system. Figure 1.1 depicts a simple representation of this idea. Let's take, for example, a simple conversation happening at a given time (t) between two people. If both communicate successfully (e.g. speaking the same language), one of them could ask a question (reference input) that will trigger a response in the other person (output). Even though the context will be similar, the response could be informal or formal, very detailed or vague, loud or quiet, depending on the environment and the relationship between both. The response and its characteristics will be controlled by our very complicated, convoluted, and high efficient controller (e.g. our brain acting as a controller unit, Figure 1.1). Now depending on the response and reaction of the person who asked the question, the conversation could continue leading to a more interesting talk or else it could terminate abruptly. For any of these stages to occur, our system needs some additional response (a feedback loop, r(t+1)) on how the conversation unfolds. This feedback input will lead our system to output the next task or, in this case, communicate another message at time (t+1). The simplistic block diagram in Figure 1.1 depicts how the brain works for every basic and complex scenario happening in our life. A growing field known as a neural network is devoted to understanding this concept but covering this field of work goes beyond my dissertation.

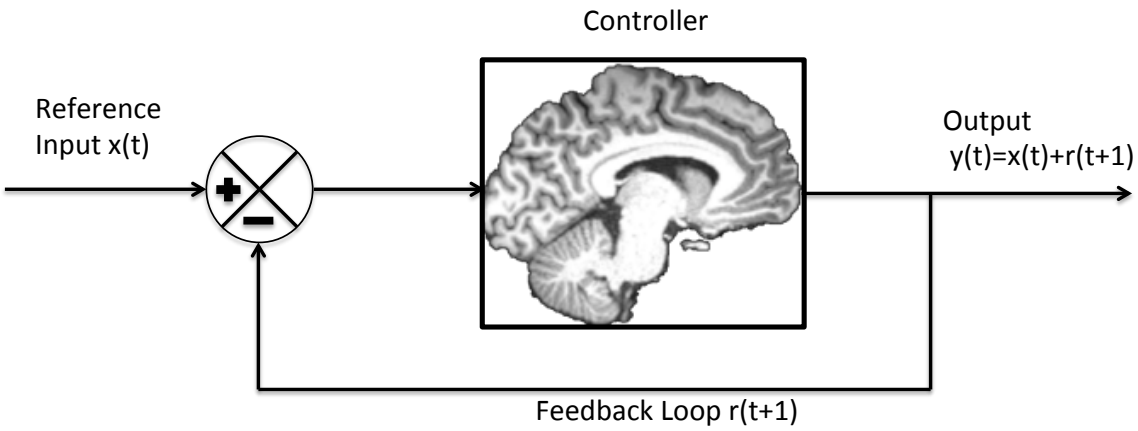

Figure 1.1. Simplistic closed-loop control system depicting the functionality of the brain.

In summary, this complex, chaotic, and highly interconnected control system produces a specific output (e.g. physical action) at time (t+1) when a reference input and controlled feedback (e.g. response action) are given at time (t). However, with our current technology, we have not yet understood how this abundantly wired system executes and determines every action. In addition, we do not know when or why it malfunctions or deteriorates when aging leads to neurodegenerative diseases. The following quote states an interesting explanation for our lack of understanding,

"If the brain was so simple we could understand it, we would be so simple that we couldn't." - Lyall Watson

The brain is composed of a chaotic network of hundred billions of neurons. Each connected on average to 7,000 other neurons leading to approximately 10^{15} (a quadrillion) synapses that fired at the same time in a 3-year-old child. This number decreases with time and varies in every adult ranging from 10^{14} to $5x10^{14}$ synapses (100 to 500 trillion!). Synapses occur when long axonal terminals of a neuron pass their information to dendrite

terminals located in the soma. If we were to line up every single axon from an adult's brain with each other in parallel, these axons would be able to circle the circumference of the earth 4 and half times. That being said, an adult human brain contains around 109,000 (176,000) kilometers of wiring known as myelinated and unmyelinated axons making it the most complex and chaotic organism, a product of millions of years of natural selection (Darwin, 1872).

Since birth the development of the brain is very plastic as investigated by the advancements of current *in-vivo* imaging technology in the few decades (Leipsic, 1901). It preserves stronger connections, and weakens or recycles information that is not as important. For example, we can remember peculiar memories that happened decades ago. However, we have a hard time recalling more recent events that happened even days ago (e.g. do you remember what clothes you wore a week ago?). Similarly as we age, the brain undergoes neurodegeneration; the brain connections start to malfunction leading to forgetfulness and incorrect outputs in our control system analogy (Bartzokis, 2004) When these changes impact normal life, this malfunction is clinically treated and diagnosed as a dementia pathology, being Alzheimer's disease the most common. The reason for the malfunction is still unknown. However with *in-vivo* imaging, we can characterize what happens with these connections in a macro-scale resolution (~1-3 mm^3) using magnetic resonance imaging (MRI). More specifically, using a novel imaging sequence known as diffusion tensor imaging (DTI). Thus in this dissertation, I will explore how we can slow down or ameliorate this age-related neurodegeneration. I will investigate the importance of environmental factors (e.g. feedback loop in our control system analogy) such as aerobic exercise and physical activity on slowing down the malfunctioning of our brain

connectivity, specifically in older adults with and without dementia.

1.2 ALZHEIMER'S DISEASE

Dr. Alois Alzheimer (Germany 1864 – 1915). Retrieved from (Lorenzo, 2012)

Alzheimer's disease (AD) is a progressive neurodegenerative disease characterized by a progressive memory loss and brain deterioration. Dr. Alois Alzheimer diagnosed the first case in 1901 in a 51-year-old woman known as Auguste Deter, who presented a profound memory loss, abnormal suspicion about her family and friends, and worsening of psychological changes. After five years the woman died, and brain autopsy revealed abnormal atrophy and anomalous deposits in and around the nerve cell. Over more than a century ago, advances in understanding the disease have emerged yet the cause of the disease is still unknown. Consequently, there is no cure for the disease. However, potential risk factors have been identified such as aging (the greatest risk factor), genetics, family history, vascular disease, gender (women are more likely to develop AD), and a careless lifestyle (lack of exercise, smoking, or poor diet). One in nine people over the age of 65 will have AD, and the incidence will increase to one in three over the age of 85 (Thies et al., 2013). However, AD is also present in young adults (~30 to 40 years of age) but with smaller percentages (~5% of the US population). This early manifestation is known as early-onset AD with genetics being the greatest risk factor. In this work, I will only focused on the late onset manifestation of AD.

Clinical early symptoms include mild forgetfulness or confusion and are often neglected due to concurrent mild cognitive worsening due to advanced aging. However

over the course of time, these changes worsen and become noticeable to family members, close friends, and co-workers. With the advances of *in-vivo* imaging (Section 1.3), increased abnormal deposits of amyloid plaque formation in the brain can now be identified even at a non-symptomatic stage. This non-symptomatic stage is currently known as the preclinical AD stage and can last years or even decades (Johnson et al., 2012a). The first clinical stage in AD is known as mild cognitive impairment (MCI). During this stage, mild changes in memory and thinking abilities start to appear but are subtle enough that do not affect work, relationships, or daily functions. Not all the patients diagnosed with MCI will develop AD. Other possible causes for developing MCI include depression or temporary forgetfulness due to other medical complications. However, if the disease progresses, worsening of memory and thinking abilities become clearer, and the person progresses to the next stage known as mild dementia due to AD. At this stage, people have difficulty remembering recently learned information and eventually start asking the same question many times. Problem-solving skills and sound judgments are also affected by difficulties in planning family events or balancing financial situations. Disorientation (e.g. getting lost even in familiar places, losing or misplacing belongings), difficulty organizing and expressing thoughts, and changes in personalities (e.g. withdrawn, irritability or anger) are also present at this stage. Worsening of these domains over the course of time lead to the next clinical stage known as moderate dementia due to AD. Moderate AD patients cannot keep track of time, recognize belongings, cannot remember personal history details (e.g. phone number, address), need help with daily activities (e.g. proper clothing, bathing), and in some cases have significant personality changes (e.g. restless or agitated) with possible aggressive or physical outbursts. The final stage of AD is known as severe dementia due to

AD. Patients with severe dementia cannot communicate coherently, need help with daily personal care (e.g. eating, dressing, using the bathroom), and have progressive worsening in physical abilities (e.g. cannot walk alone, rigid muscles, cannot swallow or control bladder and bowel muscles). Eventually people who have severe AD will die. Pneumonia is a common death cause for severe AD patients due to impaired swallowing of food and drinks leading to infection. Other causes of death include falls, cardiovascular complications and urinary tract infection (Todd et al., 2013).

Pathologically, the brain starts to atrophy as the disease progresses and aggregates such as extracellular amyloid beta plaques and intracellular tau fibrillary tangles start to accumulate. These plaques and tangles are the histopathological gold standards for diagnosing AD *post-mortem*. Even though neurobiological mechanisms could explain the formation of these plaques and tangles, it is not known whether these deposits precede and trigger the disease or are consequences of yet unknown neuro-related mechanisms. The mechanism of amyloid beta plaques formation starts when proteolytic enzymes (enzymes that break down proteins) incorrectly cleave a type of cellular inter-membrane protein known as amyloid precursor protein (APP). In the "normal" non-amyloidogenic pathway, two proteolytic enzymes known as alpha-secretase and gamma secretase cleave APP leaving extracellular soluble fragments of APP (sAPP, Figure 1.2a). These sAPP fragments are thought to benefit neurons by regulating the metabolism of APP and by influencing alpha and beta-secretases (Perneczky et al., 2014). On the other hand, when APP is cleaved by beta and gamma secretases, insoluble and toxic short fragments known as beta amyloids start to aggregate and eventually form amyloid beta plaques (Figure 1.2b). These toxic amyloid plaques accumulate in the extracellular spaces of the neuronal tissue and interfere

with neuronal function leading eventually to neuronal death.

Another neuro-pathological mechanisms manifests inside the neuronal cells, where tau neurofibrillary tangles start to form from disrupted tau proteins. Healthy tau proteins are essential for stabilizing microtubules and maintaining the structure of the cell and nutrient transportation (Figure 1.3b). However in AD, these tau proteins become defective and can no longer stabilize neuronal microtubules. Then, unstable tau proteins aggregate within the neurons and eventually cause disruption and neuronal cell death (Figure 1.3e).

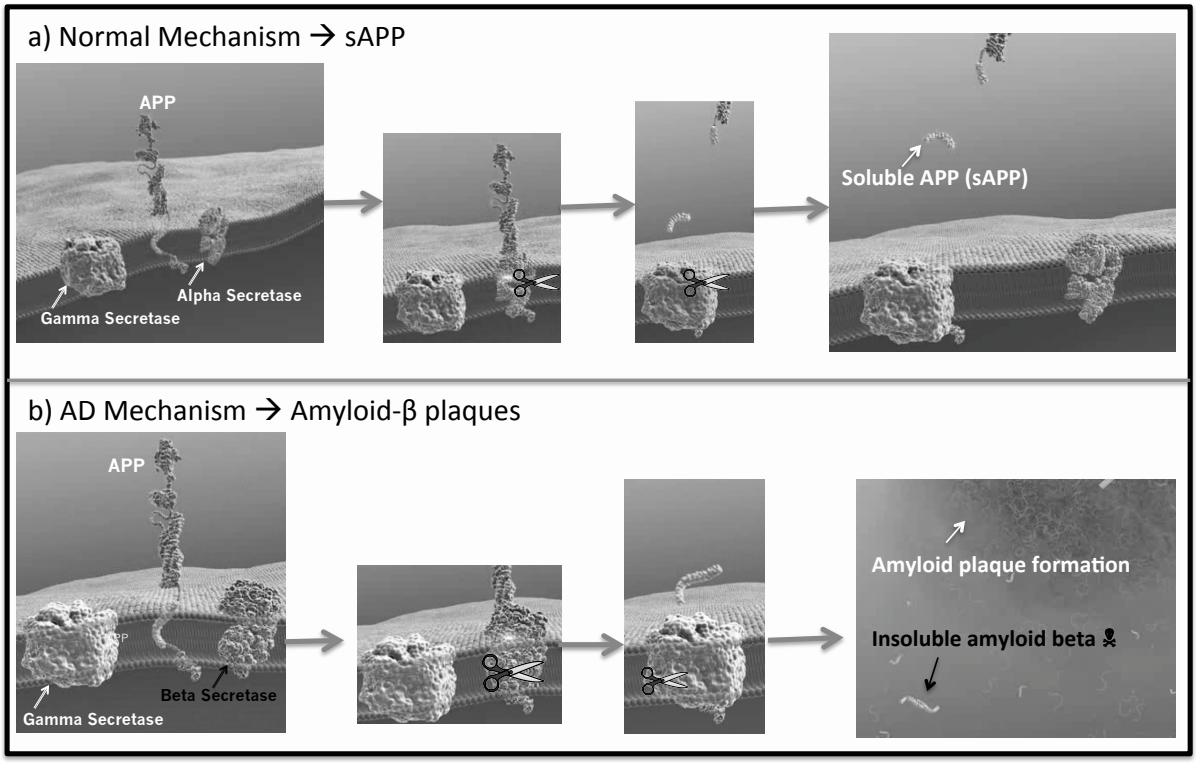

Figure 1.2 Neurobiological formation of soluble APP (a) and amyloid plaque formation (b) in the neuronal cell membrane. Retrieved from (NIA, 2014) in the public domain.

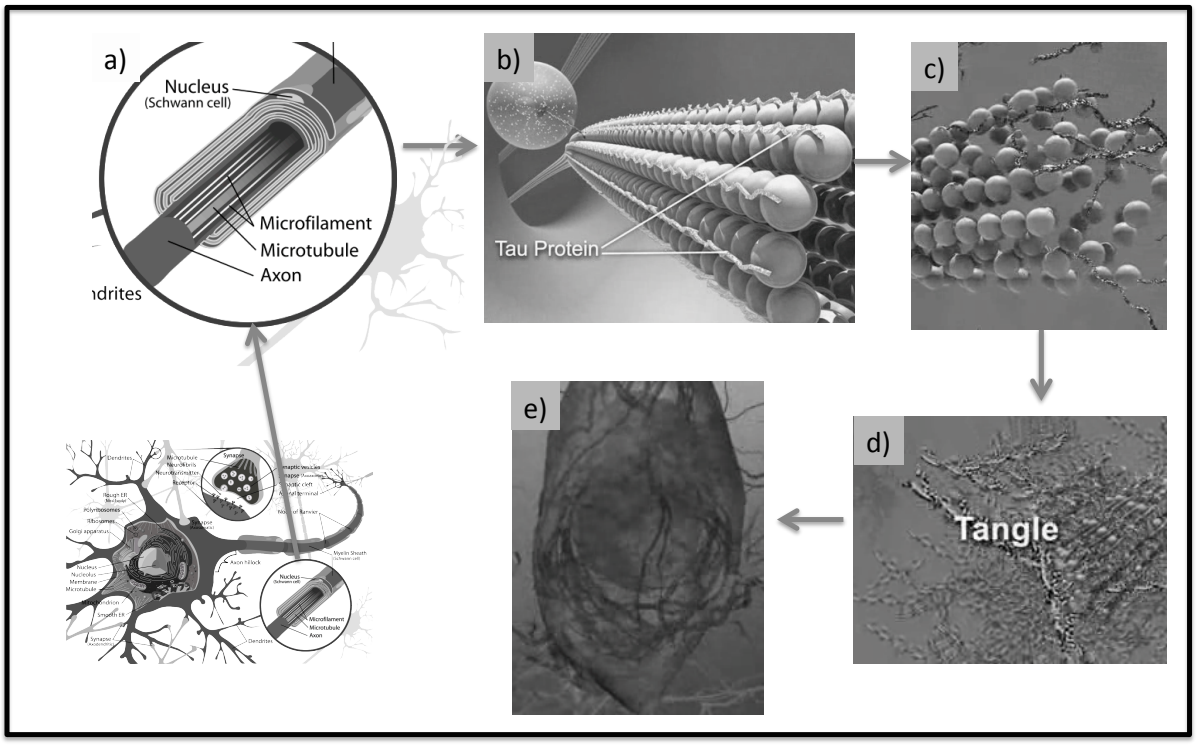

Figure 1.3 Neurobiological formation of neurofibrillary tau-tangles (a-d) and cell death (e). Retrieved from (NIA, 2014)from the public domain.

At early stages, the formation of amyloid-beta plaques and neurofibrillary tau tangles are specific to brain regions, and as the disease progresses, these aggregates disperse throughout the brain leading to global brain deterioration. Brain regions affected early in AD are the medial temporal lobe and hippocampus, which are areas involved in learning, memory, visual item recognition, auditory processing and emotion (Banich and Compton, 2010)(Figure 1.4a). When these domains are affected, clinical symptoms start to appear leading to the first diagnosis of the disease. However, as the disease progresses, brain atrophy spread throughout the entire brain involving more posterior and anterior brain regions. Moderate AD patients have more progressive deterioration involving more posterior-parietal regions while decreased cognitive changes reveal higher difficulties of

communication, loss of memory, and orientation (Figure 1.4b). In severe AD, the whole brain undergoes atrophy. Consequently, an extensive increase in plaques and tau tangles formation throughout the brain (Braak and Braak, 1991b) (Figure 1.3c). At this stage, patients cannot perform daily activities, have trouble communicating and have a lack of self-care due to a complete brain deterioration.

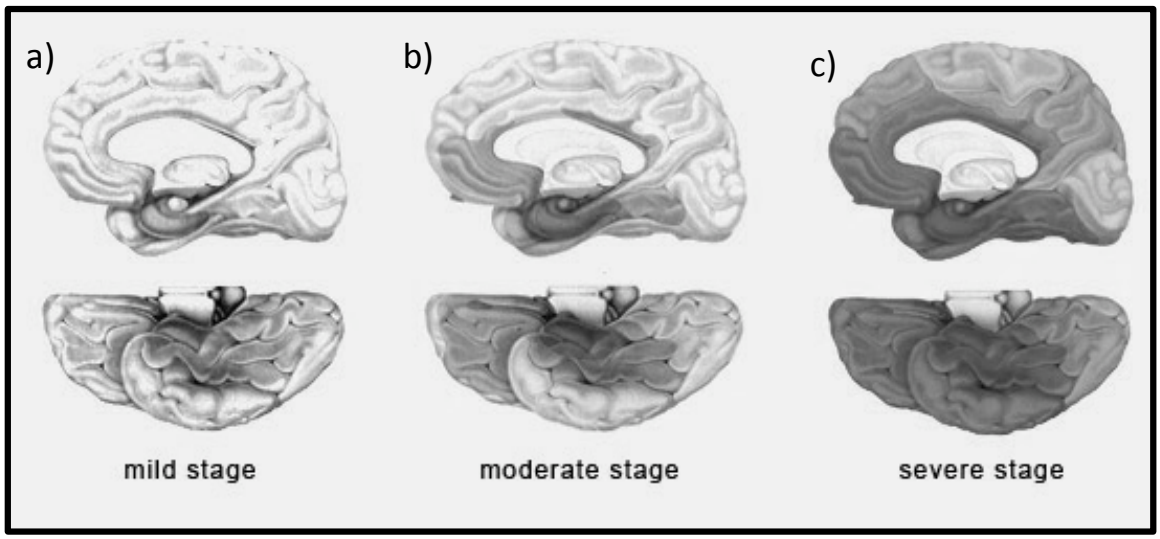

Figure 1.4. Progression of AD and brain deterioration as depicted by darker regions throughout the brain.

AD is the 6th leading cause of death in the United States (US). In addition to physical and emotional burden on the individual and their families, AD also presents a socio-economical problem. Currently in the US, there are ~4.7 million people over the age of 65 affected by AD with estimated Medicare and Medicaid costs of around $150 billion. This population will grow by 2050 to an estimated ~13.8 million leading to an increased cost of about $1.2 trillion, which will definitely impact socio-economically these national insurance institutions (Thies et al., 2013, Weuve et al., 2014). Treatment for AD does not exist, but pharmacological drugs can slow down clinical symptoms at the early stages of the disease. These costly pharmacological drugs mitigate the symptoms by enhancing

neurotransmission and brain connectivity but do not present a cure. Most of these drugs (e.g. donepezil, galatamine, rivastigmine, and tacrine) reduce the breakdown of acetylcholine, a neurotransmitter that preserves brain function. Others inhibit glutamine (e.g. memantine), another neurotransmitter that accumulates in high quantities in AD brains and has a toxic (Thies et al., 2013). While they may mitigate AD-related symptoms, these drugs are ineffective when enough brain deterioration or AD progression has occurred. Thus, emerging research is focusing on other alternatives that may prevent or slow-down the progression of AD. One promising and less costly alternative is aerobic exercise. Hence in this work, I investigated the relationship between aerobic exercise and brain health in the older population using *in-vivo* brain imaging techniques (e.g. structural and diffusion magnetic resonance imaging). In the next section, I will briefly cover these and other *in-vivo* imaging techniques that are currently being used in the understanding of AD.

1.3. IN-VIVO BRAIN IMAGING IN AD

In the past few decades, advances in neuroimaging technology made it possible to investigate *in-vivo* structural and functional connectivity of the brain. A variety of brain imaging techniques have contributed to a better understanding of Alzheimer's disease. Here, I will cover the most established neuroimaging techniques and describe its findings in Alzheimer's disease neuroimaging research.

1.3.1 Structural Magnetic Resonance Imaging (sMRI)

Structural MRI (sMRI) uses a strong magnetic field (usually 1.5-3 Tesla) to polarize

the angular momentums of hydrogen atoms along the direction of the magnetic field. When polarized, radio-frequency pulses are triggered in the MRI machine leading to shorter deviations of these angular momentums from the strong magnetic field. Eventually, these atoms will return in alignment with the strong magnetic field, generating a frequency signals that are perceived by a receiver coil and transformed to the spatial domain, generating an image with specific dimensions (Figure 2.4, Chapter 2). This 3-dimensional pixel dimension is known as voxels and this term is commonly used when *in-vivo* imaging is collected. Depending on the different tissues, these voxels will have different brightness intensities, allowing us to investigate regional volumetric changes of cortical and subcortical regions within the brain.

In AD, brain deterioration occurs at an accelerated rate than in age-matched healthy non-demented (Jack et al., 2002, Salat, 2011). This brain atrophy is thought to be a consequence of dendritic and neuronal loss. Individuals with AD have reduced volume in specific regions such as the medial temporal lobe, with the entorhinal cortex being the most atrophied and relevant region followed by the hippocampus, amygdala and parahippocampus (Colcombe et al., 2004, Erickson et al., 2009, Floel et al., 2010). Another early stage region of atrophy is the posterior cingulate. These regions present reduced volume even before clinical symptoms appear. One special regions is the hippocampus where its volume decreases at a rate of 3-5% per year(Barnes et al., 2009). However, as the disease progresses changes spread throughout the whole brain with decreases in cortical thickness and expansions of ventricular and sulcal volumes. sMRI has also been used as a marker of disease progression, as cerebral atrophy is closely correlated with cognitive dysfunction (Hua et al., 2008b). Due to the sensitivity of this methodology, sMRI is also

used to dissociate other non-AD related pathologies. For example, in early stage dementias, the reduction in hippocampal volume tends to be greater in AD than in patients with other dementias such as Lewy bodies dementia or vascular dementia. sMRI can also aid in identifying other non-demented related pathologies such as strokes, tumors, or hematomas (Cotman and Berchtold, 2002).

Another structural imaging technique is called diffusion tensor imaging (DTI, see Chapter 2). DTI aims to characterize the overall integrity of bundles of axons known as tracts that travel in specific directions (Alexander et al., 2007). This method applies small gradient radio-frequency pulses in specific directions to alter the diffusion of water molecules. If restricted movement is observed along a specific direction, then it reflects a healthy and densely packed axonal bundles. DTI is the principal imaging acquisition technique used during this dissertation and Chapter 2 will provide more detailed information regarding the acquisition methodology. Briefly in AD, a reduction of white matter integrity generally measured by decrease in anisotropy (or direction dependent) has been reported. When compared to healthy controls, AD and MCI patients showed widespread decrease in fractional anisotropy, a common measure of diffusion ranging from 1 (very anisotropic) to 0 (very isotropic) (Brun and Englund, 1986, Huang et al., 2007, Gold et al., 2010, Teipel et al., 2010, Reid and Evans, 2013, Sachdev et al., 2013, Zhang et al., 2014). More specifically, previous meta-analyses have shown decreased anisotropy in localized white matter tracts. Large effect sizes were found in the uncinate fasciculus, the posterior cingulum and the superior longitudinal fasciculus in individuals with AD compared to healthy non-demented individuals. Medium effect sizes were found in the genu and splenium of the corpus callosum, the anterior cingulum and other tracts relating

frontal and temporal regions (Sexton et al., 2011, Clerx et al., 2012).

1.3.2 Functional Magnetic Resonance Imaging (fMRI)

Functional MRI is another MRI imaging technique that takes advantage of the blood oxygenated level dependent (BOLD) signal, which increases the intensity and contrast of a voxel when specific tasks (e.g. cognitive or arithmetic tasks) are performed during the acquisition of the image. This acquisition technique is thought to reflect the integrated synaptic activity due to changes in blood flow, blood volume, and the blood oxyhemoglobin/deoxyhemoglobin ratio (Logothetis et al., 2001).

In patients with AD, fMRI research has shown a decrease in hippocampal activity during the encoding of new information (e.g. encoding tasks) (Griffin et al., 2009, Keihaninejad et al., 2013). Conversely, during encoding tasks previous research described increased activity in prefrontal regions, which might reflect a functional activity compensatory mechanism (Griffin et al., 2009, Joyner and Green, 2009, Marlatt et al., 2012). Event-related functional hyperactivity during memory trails suggests to happen early in AD (or during mild cognitive impairment [MCI]) maybe as a compensatory mechanism for impeding neuronal failure. However, in later stages of MCI, a loss of neuronal activity is present, similar to what it is found in AD patients (Johnson et al., 2012a). Previous reports also suggest that these event-related functional hyperactivities might predict rapid cognitive decline (Highley et al., 2002, Buckner et al., 2008, Sperling et al., 2014) and loss of hippocampal function (Catani et al., 2002). During fMRI acquisition, specific brain regions activate in a similar pattern (e.g. high intensity brightness in specific locations) and are investigated associatively like a network of brain regions. The most frequent brain network

studied in AD is known as the default mode network (DMN). This DMN includes the following brain regions: the medial temporal lobe, the medial prefrontal cortex, the posterior cingulate cortex, the ventral precuneus, and the medial-lateral and inferior parietal cortex. Previous reports showed hypoactivity in this DMN when AD patients were under investigation (Carro et al., 2001, Nestor et al., 2004, Buckner et al., 2008, Gaffan and Wilson, 2008). In the MCI group, functional hyperactivation was also found when examined the DMN (Buckner et al., 2008). fMRI can also be collected when participants do not perform any functional task during acquisition. This fMRI acquisition sequence is known as a resting state fMRI and could be used easily for clinical research as no special equipment or task is necessary. Impaired resting state functionality have also been found in AD and MCI studies (Trejo et al., 2001, Biessels et al., 2006, Voss et al., 2013a).

1.3.3 Fluorodeoxyglucose (FDG) PET

Fluorodeoxyglucose (FGD) positron emission tomography (PET) is another *in-vivo* imaging technique which uses a tracer to follow a biologically active molecule in the brain. The brain's source of energy is mainly glucose, and when utilized, higher synaptic activity is present. An analog glucose tracer known as fluorodeoxyglucose (18F) with a radioactive decay of ~20mins is introduced to the participants. This glucose tracer generates harmless gamma rays that decay and are detected by the PET receiving unit. During this detection, the PET machine generates an image that describes the contrast brain's glucose uptake and rate of metabolism activity. This methodology has been validated as a biomarker for overall brain metabolism.

In clinically affected AD patients, even though specific alterations on FGD PET

images have not been identified, altered hypometabolism is commonly present in specific regions (Cotman and Berchtold, 2002, Johnson et al., 2012a). Previous AD reports showed decreased metabolic activity in the posterior cingulate gyri, posterior midline cortices (precuneus), inferior regions of the parietal lobe (precuneus), postero-lateral and medial portions of the temporal lobe, and the hippocampus. As the disease progresses, reductions of metabolic activity involve more frontal regions until its hypometabolism covers the entire brain (Johnson et al., 2012a). This trajectory of hypometabolism is concurrent with cognitive function decline along the normal, preclinical, prodromal and established AD trajectory, with early impairment in the posterior cingulate cortex (Johansen-Berg and Rushworth, 2009). In relation to histopathological markers, even though amyloid deposition reaches a plateau region during the progression of AD, FGD PET images continue to decline. This decline in hypometabolism may explain a level of local toxicity (Tian et al., 2014a). To date, this is one of the most robust functional brain imaging techniques used to characterize changes in AD (Johnson et al., 2012a).

1.3.4 Fibrillar A-beta PET

Fibrillar A-beta PET is another type of PET imaging technique that uses different ligand tracers to bind into the fibrillary A-beta depositions in AD. The most common ligands include the 11C-labeled “Pittsburg Compound B (PiB)” and the F18 ligand (Nealey et al., 2014, Tian et al., 2014a). Previous reports have shown that these tracers bind specifically to AD-related amyloid pathology, which makes this technique specific to this type of pathology (Pihlajamaki et al., 2009). However, reports showed negative results when researchers investigated other non-AD pathologies such as prion amyloid (Raj et al.,

2012), pathologically confirmed alpha-synucleinopathy (Bach et al., 2014), or pure cases of taupathies related to semantic dementia (Johnson et al., 2012a). The most prominent regions for A-beta PET imaging include the precuneus, posterior cingulate, parieto-temporal, and frontal regions with relative sparing in the hippocampus. Previous studies have also found deposition of fibrillary A-beta in cognitively normal adults over the age of 70, perhaps suggesting a pre-diagnosis of the disease 10-15 years before clinical onset (Ashburner, 2007, Scharfman and Chao, 2013, Schwarz, 2013). In addition, previous reports showed that when using the PiB tracer, its measures did not correlate with memory assessments in established AD but it did in MCI and healthy older adults, which also suggests that A-beta deposition occurs well before the onset of the symptoms (Schaller, 1997, Ashburner, 2007, Onodera and Hicks, 2010). Additionally, at early AD stages of positive amyloid results it is yet very difficult to find a direct relationship between fibrillar A-beta PET and cognition stages of the participants.

1.4 EXERCISE AND BRAIN HEALTH

Maintaining an adequate exercise routine is one of the healthiest things anyone can do and can start at any time. In general terms, exercise improves your mood, boosts your energy, controls your weight, and prevents many health conditions and diseases. Routinely exercise can increase bone density, prevent falls (by increasing balance), metabolic syndrome, type-2 diabetes, depression, arthritis, and certain types of cancer (e.g. colon and breast cancer). In addition it prevents stroke and lowers the risk for cardiovascular disease by boosting your high-density lipoproteins (HDL) known as “good” cholesterol and

decreasing unhealthy triglycerides. Besides all these benefits, emerging evidence shows the benefits of exercise in cognition and structural brain health by boosting neurogenesis and other neuroprotective mechanisms (Kramer et al., 1999, van Praag et al., 2005, Van der Borght et al., 2009, Creer et al., 2010, Marlatt et al., 2012, Mustroph et al., 2012, Erickson et al., 2014).

Human studies of normal aging suggest that exercise may also protect against cognitive decline (Hill et al., 1993, Hassmen and Koivula, 1997, Kramer et al., 1999, Friedland et al., 2001, Barnes et al., 2003, Abbott et al., 2004). For example, a recent study showed that people who engaged in physical activity at any point in their lifetime were less likely to show cognitive impairments in adulthood (Middleton et al., 2010). In another 6.2-year follow-up study in older adults, it has been proven that exercise significantly reduced the rates of dementia on participants who exercise three or more times per week when compared to those who exercised fewer times (Larson et al., 2006). Another study also showed that exercise provides a 20% reduction risk of cognitive impairment equivalent to taking three years off age (Weuve et al., 2004). In specific cognitive domains, exercise appeared to have the largest effect size in executive functions followed by mental control, spatial tasks, and psychomotor speed (Colcombe and Kramer, 2003, Zarei et al., 2010, Zeineh et al., 2012, Ford et al., 2013, Lee et al., 2013, Voss et al., 2013b, Kirk-Sanchez and McGough, 2014, Leuze et al., 2014). Thus, for a better understanding of exercise physiology, in the following sections I will cover some exercise-related descriptions that are key to understand for a thorough understanding of this dissertation work.

1.4.1 Physical activity, exercise, and physical fitness

To better understand the effects of exercise, it is worth noting the differences

between three commonly interchangeable terms: physical activity, exercise, and physical fitness. Physical activity is defined as any bodily movement that requires the spending of metabolic energy. Sleep in considered a physical activity yet it demands very small amounts of energy when compared with other leisure activities such as sports, conditioning exercise or even household activities (e.g. home repair or cleaning). Exercise can be thought as a subclass of physical activity as it is defined as any bodily movement resulting in energy expenditure, but it is also a planned, structured, and repetitive activity. The main objective of any exercise is to maintain physical fitness components. Finally, physical fitness is a set of attributes that people have or achieve and is known as the ability to carry out daily tasks with vigor and alertness, without undue fatigue and with ample energy to enjoy leisure-time pursuits (Caspersen et al., 1985). Physical fitness includes five different health-related components: cardiorespiratory fitness, muscular endurance, muscular strength, body composition, and flexibility.

1.4.2 Energy demands in aerobic and non-aerobic exercise

In terms of fuel energy demand, exercise can be divided into two types: aerobic and non-aerobic exercise. The main difference between these exercise types is the presence of oxygen when producing chemical energy. Aerobic exercise needs oxygen in the release of energy molecules while non-aerobic exercise does not. In any type, the process of producing chemical energy begins with the ingestion of food. Differently from mechanical engines, the body cannot extract “heat” energy from the oxidation of foods. If so, our tissues will burst into flames, and our fluids will boil. Instead, the energy dynamics involve chemically splitting potential energy bonds found in carbohydrates, fats, and protein bonds

(McArdle et al., 2010). This process is dynamic and happens, as the body demands it.

The special carrier of free energy in the body is an energy-rich nucleotide compound called adenosine triphosphate (ATP). At the beginning of any exercise type, ATP and phosphocreatine (PCr) provide immediate energy to power muscle actions (e.g. start moving your legs for running). PCr is a molecule known to rapidly mobilize high-energy reserves in the skeletal muscle and brain. If the exercise continues after a few seconds, the body will require more energy to continue with the activity. Thus, another non-aerobic metabolic mechanism known as glycolysis is triggered to produce additional energy-rich ATP molecules. This process converts glucose into another organic compound known as pyruvate while releasing two molecules of ATP, the energy rich compound. Short-term non-aerobic exercise triggers this instantaneous energy production mechanism. Examples of non-aerobic exercise include weightlifting, football, or short distance sprinting. If the exercise continues for longer periods of time (e.g. aerobic exercise), then aerobic energy mechanisms are triggered. Here, aerobic energy production uses oxygen to generate a higher number of ATP molecules. The number of generated ATP molecules during aerobic glycolysis increased to 36-38 molecules of ATP per molecule of glucose. Most of these ATP molecules are released during the citric acid cycle (or Krebs cycle) that happens in the mitochondria, the engines of most eukaryotic cells. Some aerobic exercise examples included running, bicycling or swimming, and it usually include activities that last longer periods of time. During aerobic exercise, apparent physiological changes are experienced such as an increase in breathing leading to higher exchange rates of oxygen and CO_2. These physiological exchange gas ratios allow us to measure the aerobic fitness capacity of individuals. One of the most used measures is known as the maximum rate of oxygen

consumption (VO_2peak).

1.4.3 Maximum rate of oxygen consumption (VO_2peak)

Maximum rate of oxygen consumption (VO_2peak) during incremental aerobic exercise usually performed on a stationary treadmill measure the aerobic capacity of an individual. This test reflects the aerobic cardiorespiratory endurance of an individual, which is defined as the ability of the circulatory and respiratory system (e.g. heart, lungs, and blood vessels) to balance metabolic demands by supplying adequate fuel and eliminating fatigue products. This test is known as the maximal oxygen uptake or VO_2max. The units of this test can be expressed in liters per minute (L/min) or in milliliters of oxygen per kilogram of body mass per minute (mL/[kg*min]). This test is set up to be sufficiently long to exhaust the aerobic energy system.

The test begins when the participant starts running on a flat treadmill. As the test continues, the treadmill will increase in elevation at different graded levels. As the graded levels increase in elevation, the runner will consume more oxygen. During the first increases, oxygen consumption will increase rapidly. However, as steeper inclines and faster speeds increase, oxygen consumption increases will start to drop until it reaches a plateau region. This plateau region is known as the maximal consumption rate or VO_2max. Beyond this point, the oxygen utilization is disregarded, and energy transfer will occur due to non-aerobic glycolysis forming lactate acid accumulation (McArdle et al., 2010). Eventually, if exercise continues beyond the point of maximal oxygen intake, the runner will become exhaust and will not be able to continue.

1.4.4 Exercise, AD, and brain neuroplasticity

In relation to brain neuroplasticity, recent reports have shown the positive benefits of exercise and physical activity in animal and human models (Hayes et al., 2013, Voss et al., 2013b). The main advantage for the usage of animal models is the feasibility to invasively characterize pathological changes in the brain. However in regards to AD, it is difficult to choose a correct animal model because many animals do not develop this pathology despite achieving long life spans (Bartzokis, 2004). Canines are one attractive model because they suffer from naturally-occurring cognitive decline, similar to humans. Canines also develop deposition of amyloid plaques in their brains, which has an identical amino acid sequence as humans (Wheeler-Kingshott and Cercignani, 2009). Hence in this model, previous evidence suggests that exercise reduces age-related losses in cognitive function including learning and memory (Cotman and Berchtold, 2007, Wheeler-Kingshott and Cercignani, 2009). Other potential AD-related animal models extensively used are transgenic rodents (e.g. rats and mice). These animals have been genetically modified to include Alzheimer's disease DNA material. In these models, extensive evidence has shown that exercise enhances the production of different neurotrophic and anabolic factors (e.g. BDNF, VEGF, IGF-1, TrkB receptor), increased cognition and behavior (adaptation, learning and memory, executive functions, attention and processing speed), increased synaptic plasticity, brain structure, and neurogenesis (for a review (Voss et al., 2013b)).

In humans, it is more challenging to study the effects of exercise at the cellular level due to evident invasive limitations. Human studies are done either post-*mortem* or using *in-vivo* brain imaging technologies. *Post-mortem* analyses in patients with AD helped us to understand the pathology of the disease. However, to understand the effects of exercise in

this population using *post-mortem* analyzes can be very challenging. Thus, *in-vivo* non-invasively imaging techniques are currently under investigation. The main limitation with *in-vivo* imaging is the large macro-scale resolution that does not allow us to identify micro- or nano- cellular changes in the brain. Usually imaging voxel resolutions are in the millimeter scale and encompass millions of axons yet apparent differences can be identified (Concha, 2014, Walhovd et al., 2014).

Using structural magnetic resonance imaging (MRI), researchers have identified positive correlations between exercise, cognition, and brain health. For example, in a study of 165 nondemented older adults (Erickson et al., 2009), higher levels of aerobic fitness were associated with increased hippocampal volume, a subcortical brain region that plays an important role in memory and is also one of the first regions to be affected by AD. Another study found that after 6 months of aerobic fitness training in 59 healthy older adults, significant increases in brain's gray and white matter volume were found as a function of fitness training (Colcombe et al., 2006). Previous work also showed that higher levels of cardiorespiratory (CR) fitness in early AD are associated with larger whole brain volumes (Burns et al., 2008). More specifically, higher levels of CR fitness were related to regionally specific increases in gray and white matter volumes (Honea et al., 2009). In gray matter, these regions included the parietal and medial temporal cortices while white matter regions included regions along the inferior parietal cortex. In a longitudinal functional MRI study, higher levels of CR fitness showed a slower progression of AD and lower rates of atrophy in the medial temporal lobe (Vidoni et al., 2012a). A recent review also explored further the positive influence of CR fitness and brain plasticity in the brain (Hayes et al., 2013). Proposed exercise-related mechanisms in the brain include the

increased activation of neurotrophins (e.g. brain-derived neurotrophic factor [BDNF], insulin like-growth factor 1, [IGF-1] vascular endothelial growth factor [VEGF], and tyrosine kinase [TrkB]), exercise-induced increase in neuronal precursor cell activity, mediation survival of progenitor cells induced by exercise, induced exercise-related expression of dentate granule cells, and exercise-induced activation in neurotransmitter (e.g. cannabinoid signaling and serotonin) (Voss et al., 2013b). Here in this work, I expanded the investigation of exercise-related brain changes by characterizing the integrity of brain's white matter using novel techniques for processing diffusion-weighted images.

1.5 SUMMARY AND SPECIFIC AIMS

Evidence suggests that AD neurodegeneration in white matter occurs in the enthorinnal and prefrontal regions of the brain and with further extends in parietal, and occipital deterioration (Sullivan and Pfefferbaum, 2006, Davis et al., 2009, Barrick et al., 2010, Bennett et al., 2010, Burzynska et al., 2010, Teipel et al., 2010, Salat, 2011). Due to the ineffectiveness of pharmaceutical drugs to postpone or mitigate this brain deterioration, research is focusing on inexpensive alternative treatments such as including exercise on a weekly basis. High levels of exercise and fitness are associated with maintenance of brain's cortical volume across the lifespan, and a lower risk of progression for developing AD (Colcombe et al., 2003, Gordon et al., 2008, Honea et al., 2009, Erickson et al., 2010, Weinstein et al., 2012, Hayes et al., 2013). However, it is not clear whether exercise has a specific impact on white matter integrity and connectivity, especially in the AD population. In few white matter-exercise related studies, inconclusive results showed

positive correlations between aerobic fitness and white matter integrity in prefrontal, temporal (Marks et al., 2007, Johnson et al., 2012b) and medial regions (Honea et al., 2009, Johnson et al., 2012b, Tian et al., 2014b), while other studies did not show significant findings (Voss et al., 2012). Additionally, there is currently no longitudinal study that investigates the relation between exercise and white matter changes in the older population at early stages of AD. Thus, the *objective* of this work was to investigate the effects of exercise on white mater integrity using novel diffusion imaging methodologies.

Specific Aim 1 (Chapter 5): To assess the hypothesis that higher cardiorespiratory fitness is associated with higher levels of white matter integrity in individuals at early stages of AD (n=37). This cross-sectional investigation established a comparative analysis with current literature on how VO_2peak (maximal oxygen consumption), a marker of physical fitness, is positively associated with white matter integrity in the AD population (Marks et al., 2007, Marks et al., 2011, Johnson et al., 2012b).

Specific Aim 2: To assess the hypothesis that a longitudinal 26-week exercise intervention program will increase white matter integrity and connectivity in healthy older adults (n=10, 60 years and over, chapter 6) and older adults at early stages of AD (n=30, 65 years and over, chapter 7 and 8). In humans, a recent meta-analysis utilizing questionnaires and few interventional exercise programs found evidence that cardiorespiratory fitness links to neural integrity in older adults at risk of dementia mainly in prefrontal, temporal, and parietal regions (Hayes et al., 2013). Two diffusion imaging procedures were assessed during this specific aim. First, we investigated the changes in structural white matter integrity after the exercise intervention program in exercise-related tracts for the non-

demented cohorts (Chapter 6)) and AD-related tracts for the AD participants (Chapter 7,8). Secondly, we used a probabilistic tractography analysis to investigate whether exercise affect the structural connections between the thalamus to peripheral cortical regions (Chapter 8).

Chapter 2

From diffusion weighted imaging to the tensor calculation

2.1 A BRIEF INTRODUCTION TO DIFFUSION TENSOR IMAGING

Diffusion tensor imaging (DTI) is a magnetic resonance imaging (MRI) technique used to characterize the integrity of white matter tracts in the brain, by measuring the Brownian motion of water molecules (more details in the next subsection) (O'Donnell and Westin, 2011). This motion can be isotropic or anisotropic. Isotropic motion is the random movement of particles with no specific direction or constraints in its environment while anisotropic motion (or directional dependent, Figure 2a) is restricted to its environment. For example, the motion/spreading of an ink drop in cup of water is isotropic while a similar ink drop spilled on a texture surface (such as celery or textured wood) has a more anisotropic spreading as it follows the direction of the texture. The same principle is applied in the brain's white matter tissue using DTI in a 3-dimensional perspective. White matter in the brain consists of bundles of axons and glial supporting cells (oligodendrocytes and fewer astrocytes) that are white in appearance (hence its name "white matter"). These bundles of fibers are commonly known as tracts when travel in specific directions and when healthy, they provide an anisotropic environment. Hence in neurodegenerative (and others), we can investigate the integrity of this environment by calculating specific diffusion metrics that may modify the environment restrictive anisotropic characteristics (Hartline, 2008, Walhovd et al., 2014).

During the diffusion acquisition, gradient signals are triggered at specific locations, generating diffusion characteristics in specific three-dimensional planes. The locations of white matter tracts and its trajectory will modify the diffusion signal that is collected. For example, if the white matter tracts are aligned parallel to a specific diffusion gradient signal, a faster diffusion signal is acquired (e.g. higher intensity voxel). On the other hand,

slower diffusion motion or no diffusion (e.g. a darker voxel) might be collected if the gradient signal is applied perpendicularly to the direction of these tracts, as they act as a restricted diffusion environment. Hence, in deteriorated white matter tracts, perpendicular gradient fields to specific tracts may measure faster diffusion, which indicates a disruption of the environment directly affected by a disruption of these tracts (e.g. less myelinated axons, decreased in cell density, or obstruction due to abnormal deposits such as amyloid-beta plaques in the case of Alzheimer's disease) (Concha, 2014, Walhovd et al., 2014).

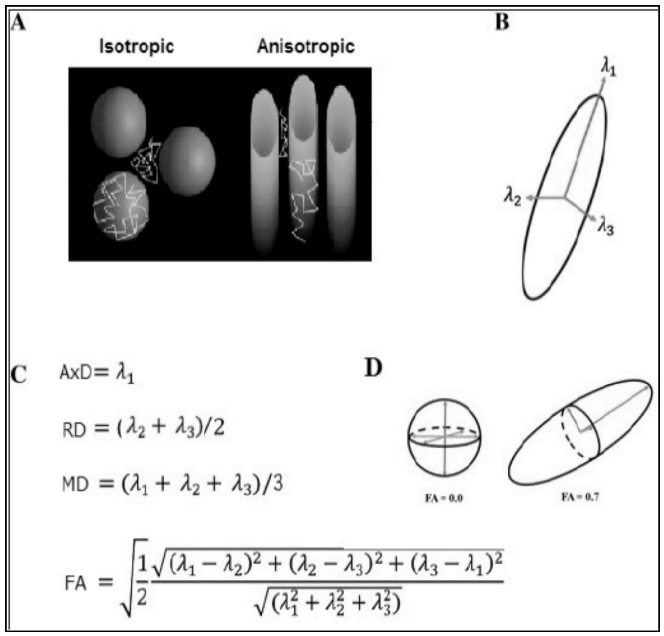

Figure 2.1. Part A) represents the isotropic and anisotropic diffusion while part B) shows the principal components of diffusion. Part C) depicts the most common algebraic diffusivity measurements and finally part D) represents the shape of diffusion behavior for fractional anisotropy values.

Diffusion imaging was introduced for clinical and research practice by Denis LeBihan in 1986 (Le Bihan et al., 1986) and a decade later in 1994, Peter Basser proposed the use of a 3x3 symmetric rotationally invariant tensor (Basser et al., 1994, Le Bihan et al., 2001), which describes the diffusion of water in an ellipsoid-like shape (Figure 2b) (O'Donnell and Westin, 2011). From this tensor calculation (given at each specific voxel), scalar metrics were derived using information from the three principal components of directions (or eigenvectors, Figure 2b).

For example, a scalar metric that measures the total diffusion is called mean diffusivity (MD) and is calculated by averaging the three rotationally invariant components of the diffusion tensor (Beaulieu, 2002, Sen and Basser, 2005). Another scalar diffusivity metric known as axial diffusivity (AxD) represents the principal component of diffusion (λ_1) with larger values representing faster diffusions. AxD is related to axonal injury both in ischemic and chemically induced white matter lesions (Song et al., 2003, Song et al., 2005). Radial diffusivity (RD) is another metric of the diffusion tensor and is calculated by averaging the two orthogonal components (λ_2 and λ_3) of the principal diffusion eigenvector. RD is associated with loss of myelination and cross-sectional axonal injury (Figure 2c) (Song et al., 2005). Fractional anisotropy (FA) is another widely used scalar metric of diffusion. FA measures the fraction of diffusion that is anisotropic by looking at the normalized variance of the eigenvalues of the tensor (Figure 2c). FA ranges from 0 (being the most isotropic) to 1 (being the most anisotropic or direction-dependent) (Le Bihan et al., 2001, Basser and Jones, 2002). It is also worth noting that although these diffusivity measures are sensitive to micro-structural changes during *in-vivo* imaging, a one-to-one relationship with cellular characteristics such as myelination quality, axonal or glial cell density cannot be characterized due to current imaging macro-scale resolution limitations (Jones et al., 2013a, Concha, 2014, Walhovd et al., 2014). Hence, these metrics provide a more global diffusion characteristic of its environment (e.g. brain's white matter) and investigators should be cautious when interpreting their results in a one-to-one relationship with cellular structures.

Recently, diffusion tensor imaging (DTI) has gained popularity making it one of the standard measurements to characterize white matter tissue in the brain. It is currently

used in different neurological diseases and as an additional tool for neuro-navigation in tumor resections (O'Donnell and Westin, 2011). Thus, in this chapter I will introduce the concepts of "self-diffusion", the theory behind magnetic resonance imaging acquisition and how diffusion weighted images are acquired. Finally, I will provide an analytical estimation of the diffusion tensor imaging that will eventually allow us to calculate the different scalar diffusivity measurements previously described.

2.2 FROM FICK'S LAW TO THE DIFFUSION TENSOR

2.2.1 Fick's law, Brownian motion, and Einstein's motion theory

Adolf Eugene Fick (Figure 2.2) was a German-born physician and physiologist that introduced the law of molecular diffusion currently known as Fick's Law in 1855. In this law, he explained the motion or diffusion of molecules from a high concentration region to a lower concentration region. Let's imagine we drop a droplet of colored dye into a 2-dimensional surface (e.g. on a table, or a liquid media). If no other action is taken to clean or stir the droplet, the droplet will slowly expand radially. This expansion is known as "mutual diffusion". Fick's law describes this process mathematically in the following equation:

Figure 2.2 Adolf Fick (Germany 1829-1901). Retrieved from (Gasson, 2014).

$$\boldsymbol{J} = -D \cdot \nabla\phi \qquad \text{[Eq 2.1]}$$

where the net flux **J** (mol /m^2·s) denotes the rate of particles moving (mol/s) in a specific area (e.g. m^2). The negative sign is arbitrary and denotes a "loss" of particles from high concentration regions to lower concentration regions, analogous on how high temperature

flows to colder regions. “D” denotes a constant value called the “diffusivity coefficient” (m^2/s). This diffusivity constant D is specific to the temperature environment, viscosity, and size of the specific particles. In room temperature, the values range from $0.6x10^{-9}$ to $2x10^{-9}$ m^2/s. In biological tissues, this values range from 10^{-11} to 10^{-10} m^2/s. Finally, $\nabla\phi$ denotes the amount of particles or concentration in a given dimension. The downwards triangle “∇" denotes the rate of change (or gradient) in the concentration of particles “ϕ" that is dependent on time and its given dimensions. For example in a 3-dimensional media using the Cartesian coordinates will look as follow:

$$\nabla\phi = \frac{\partial\phi}{\partial x} + \frac{\partial\phi}{\partial y} + \frac{\partial\phi}{\partial z} \qquad \text{[Eq. 2.2]}$$

Equation 2.1 (or Eq. 2.2 in a 3-dimensional Cartesian coordinate) describes the behavior of molecules when a countercurrent solute is added to a media (e.g. dropping a droplet on a surface) leading to an imbalance of particle concentrations. However, if we let the droplet sit for an extended period without changing any environmental factors (e.g. temperature or pressure), we will not see any apparent change in diffusion. At this stage, many will conclude that there is no diffusion in this media. However, even though on average the net flux of all particles can be neglected, another type of microscopically diffusion movement was observed known as the “self-diffusion” or “Brownian motion”.

Figure 2.3 Robert Brown (Scotland 1773 - 1858). Retrieved from (Wikipedia.org, 2014)

Robert Brown a Scottish botanist (Figure 2.3) first observed “self-diffusion” in 1828 when he studied pollen grains suspended in water under his microscope (Brown,

1828). He noticed that these grains moved randomly without any apparent cause. Many decades after Brown's experiment, Albert Einstein described a similar phenomenon that will present sufficient evidence for the atom discovery (Einstein, 1905). Einstein was unaware of Brown's experiment when we came to the following conclusion:

"… bodies of microscopically visible size suspended in a liquid will perform movement of such magnitude that they can be easily observed in a microscope." (Einstein, 1956).

To explain the "self diffusion" of particles, Albert Einstein used a probabilistic framework and reconciled Fick's Law and Brownian motion (Einstein, 1956). He introduced the "displacement distribution" concept as the likelihood or probability of a single particle to move a certain distance. In a Gaussian distribution, the likelihood of displacements is proportional to the diffusivity coefficient explained by Fick's Law as following:

$$\langle x^2 \rangle = 2 \cdot D \cdot t \qquad \text{[Eq. 2.3]}$$

Where $\langle x^2 \rangle$ denotes the mean-squared displacement of a particle, which is the most common statistical measure of spatial movement on a random motion. D denotes the constant coefficient diffusivity and t denotes the diffusion time. The probability of movements is related to its diffusivity coefficient D as shown in Figure 2.4. Additionally, these displacements are also influenced by the geometrical structure of the environment. Thus in biological tissues (e.g. the brain), we can detect and alter the displacements of these particles by applying a resonant frequency pulse, which is specific to water molecules (or hydrogen atoms) in the brain, which is covered in the next section.

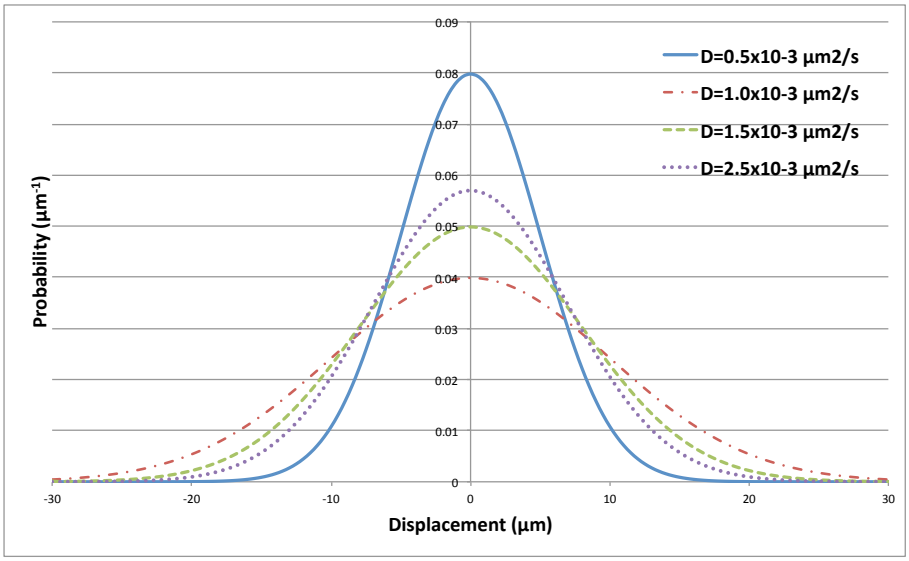

Figure 2.2 Representation of the Gaussian displacement distribution plots for various diffusion coefficients. Larger diffusion coefficients tend to have broader displacement probabilities suggesting an increase in diffusion mobility.

2.2.2 Magnetic resonance imaging (MRI)

Magnetic resonance imaging (MRI) was originally developed in the early 1950s in the US and the Soviet Union (Carr and Purcell, 1954, MacWilliams, 2003). This technique uses strong magnetic fields (usually 1.5-3 Tesla compared to Earth's magnetic field of 25-65 µTesla) to momentarily polarize the angular momentums of hydrogen atoms found in water molecules. Hydrogen is the most common element in the universe and also in our body, which is mainly composed of water (up to 60% or up to 85% in the brain) (Watson et al., 1980). These hydrogen atoms contain a single negatively charged electron and a positively charged proton. Interestingly under normal conditions, these atoms rotate within an arbitrary axis (known as precession); consequently in water (with abundant hydrogen atoms) they do not generate a total magnetization field. However, when a very strong magnetic field is applied to these atoms (such as the MRI powerful magnetic field), the precession of these atoms aligns along the direction of the magnetic field. Some

hydrogen atoms will be positively aligned in the direction of the magnetic field (high energy state) and others will align in the opposite direction (lower energy state, Figure 2.4b), generating an atom-specific magnetic dipole (thin arrow in Figure 2.4). The rotation frequency of these hydrogen atoms is known as the Larmor frequency:

$$\omega = \gamma \cdot B \qquad \text{[Eq. 2.4]}$$

which depends on the magnetic field “B” and gyromagnetic ratio "γ", a constant specific to the atomic nucleus. The Larmor frequency for the hydrogen atom is 42.58 MHz/Tesla.

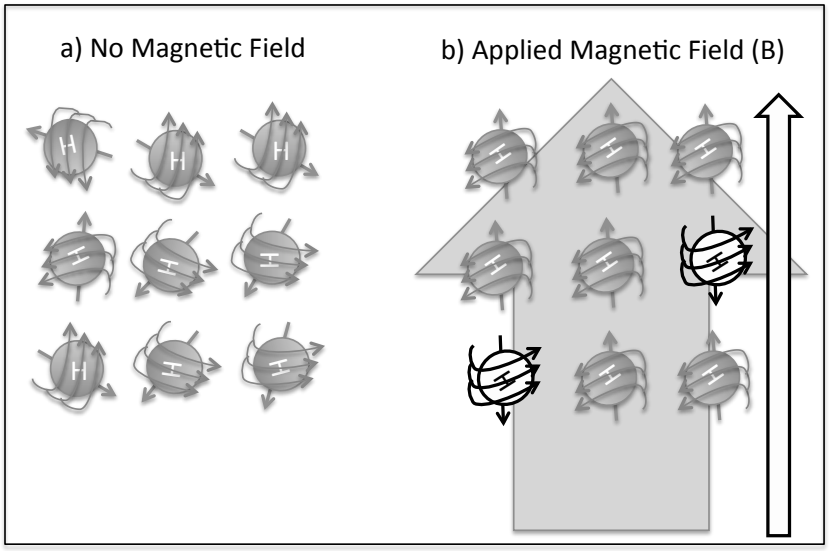

Figure 2.3. Part a) represents the arbitrary precession of the hydrogen atoms in the absence of a strong magnetic field. However when a strong magnetic field (thick orange arrow) is present (b), the hydrogen atoms precess along the direction of the magnetic field (high energy state depicted in filled circles) or oppositely to the magnetic field (low energy state depicted in open circles). The alignment of hydrogen atoms will produce an atom-specific magnetic dipole as shown in the think blue arrow.

This spinning rate (or Larmor frequency) is important because if a radiofrequency (rf) pulse at the Larmor frequency is triggered, it will modify momentarily the alignment of these atoms. This action will modify the total magnetic dipole generated by the alignment

of the hydrogen atoms. A good analogy to understand this concept is pushing a children's swing. If you push too fast or too slow, you will eventually stop the swing. However, if you push the swing at its swinging frequency (e.g. resonance frequency), you will increase the kinetic energy of the swing and accelerate it. Thus, after the strong magnetic field is triggered, a 90^{o} radiofrequency pulse at the Larmor frequency is generated which modifies the alignment of the atomic specific magnetic dipole momentarily. This pulse misaligns the hydrogen magnetic dipole from its previously parallel alignment to the strong magnetic force as it moves to the perpendicular direction in alignment with the radiofrequency pulse (Figure 2.5b). However, due to inhomogeneous effects of the MRI magnetic field and dipolar interactions some atoms rotate around its axis at a faster or slower rate. This phenomenon is called dephasing, and it's represented in figure 2.5c. Thus to reverse the dephasing anomaly, an additional 180^{o} rf pulse is applied (Figure 2.5d), leading to a better "pulsated signal" (Figure 2.5e). Eventually, these atoms will want to align again with the strong magnetic field (Figure 2.5f) and in doing so they generate an electrical current signal known as the T2 relaxation signal (e.g. due to changes in the electrical current generated by the atom specific magnetic field), which can be detected by a receiver antenna (MR coil) and generate an image. At a longer period of time, this perpendicular dipole moment depicted in figure 2.5f will align with the permanent strong MRI magnetic field (orange arrow in figure 2.4) and by doing so; it also generates another electrical current known as the T1 longitudinal relaxation sequence or T1 recovery. This echo signals are dependent on their environment. In the brain, different brightness images are depicted due to the different tissues s (e.g. gray matter, white matter, or cerebrospinal fluid).

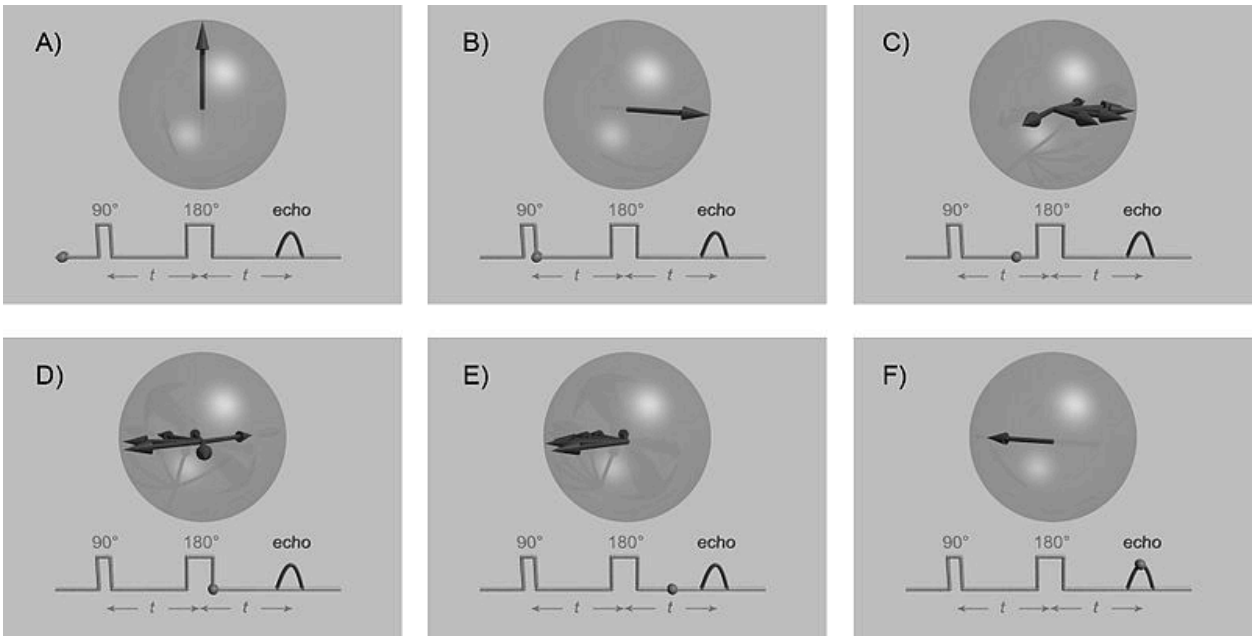

Figure 2.4 Part A depicts the magnetization dipole moment generated when all the hydrogen atoms are aligned to the strong magnetic field generated by the MRI machine. After a 90^0 radio-frequency pulse is triggered, this magnetic dipole will shift in the direction of the radiofrequency pulse (e.g. or perpendicular to the strong magnetic field, part B). At this moment, inhomogeneities occur and will slow down or speed up its precession rate of the dipole moment (known as dephasing", part c). Hence, another 180^o radiofrequency pulse is introduced (part b). Slower precession atoms will speed up and faster precession atoms will slow down (part e) and eventually a stronger perpendicular dipole moment is acquired (part f). T2 relaxation signals occur during the dephasing of these atoms (part c-e) while T1 recovery images are acquired after the perpendicular precession (part f) returns to its stable condition aligned with the strong magnetic field (part a).

2.2.3 From MRI to diffusion weighted images (DWI)

In addition to triggering the secondary 180^o rf pulse to improve the intensity of the T2 relaxation signal, in diffusion-weighted images the sensitivity of the MR signal is also dependent on the molecular diffusion within the boundaries of the biological tissue. In 1950, a physicist named Erwin Hahn described that the reduction of the MRI signal could be accounted by the translational diffusion of particles within an inhomogeneous magnetic field (Hahn, 1950). Four years later in 1954, Carr and Purcell proposed a mathematical and physical framework that permitted the measurement of signal that was reduced due to diffusivity motions (Carr and Purcell, 1954). Their idea involved adding another less strong

"magnetic field gradient", which would consequently modify the spinning of these particles as they would experience different magnetic fields depending on their locations. In this framework, they described that the Larmor frequency [Eq. 2.4] would vary not only due to the strength of the strong magnetic field (B), but also due to the strength and direction of a weaker gradient magnetic field "$\boldsymbol{G}$". Thus Eq 2.4 can be rewritten as

$$\omega = \gamma \cdot \boldsymbol{B_0} + \gamma \cdot \boldsymbol{G} \qquad \text{[Eq. 2.5]}$$

Intuitively, for a very short time τ', particles at a given position x in a particular time t will experience a magnetic field B_o + G, which will lead to a phase shift,

$$\phi(t) = -\gamma\big(\boldsymbol{B_0} + \boldsymbol{G}\, x(t)\big)\tau' \qquad \text{[Eq. 2.6]}$$

After a decade in 1965 Stejskal and Tanner introduced another technique that expanded the mathematical diffusion framework by Carr and Purcell (Stejskal and Tanner, 1965). They proposed to replace the additional weak gradient magnetic field by shorter pulsed duration gradients that can be triggered right after the rf pulses. With this idea, it was possible to identify the difference in duration between the gradient pulse time and the diffusion time right after the gradient pulses were signaled. So if we ignored the constant phase change due to the strong magnetic field Bo (omitting the first term in Eq. 2.6 for simplicity), we can characterize the net phase change due to the gradient direction by

$$\phi_i = -q \cdot \delta \cdot G \cdot x_i \ , \ \ where \ \ i = 1,2 \qquad \text{[Eq. 2.7]}$$

and x_i is the position of the particle during the first (i=1) and second (i=2) rf pulse. The gradient pulse duration is denoted by "δ" and the magnitude by "G", which are the same in

values for both rf pulses at 90° and 180°. However, the additional 180° reverses the phase change of the particles so the total aggregated phase change is described by:

$$\phi_2 - \phi_1 = -q \cdot \delta \cdot G\,(x_2 - x_1) \qquad \text{[Eq. 2.8]}$$

Clearly in the equation above (Eq. 2.8), if the particles in a specific position do not move (i.e. $x_1 = x_2$), the phase change will equal zero and the signal acquired will solely depend on the influence of the strong B_0 field (only the first term in Eq. 2.5). However, if the particles randomly move due to the additional weak field gradient "G", then $x_1 \neq x_2$ and the MRI receiving coil will detect and collect the decrease in signal. This reduction in signal can be described by the Stejskal-Tanner equation:

$$\frac{S_k}{S_o} = e^{[-\gamma^2 \cdot \boldsymbol{G}^2 \cdot \delta^2 \cdot d\left(\Delta - \frac{\delta}{3}\right)]}, \qquad \text{[Eq. 2.9]}$$

where S_o denotes the echo signal acquired without any additional pulsed gradient magnetic field, S_k denotes the echo signal acquired when a pulsed gradient magnetic field is triggered for a "δ" duration and a "G" magnetic field magnitude, γ denotes the gyromagnetic ratio, d is the diffusion coefficient while "Δ" denotes the time between the two rf pulses. Intuitively, the right side of Eq. 2.9 contains constant terms that can be grouped in a constant variable known as the "b" factor (more of this in the next section). The left side of Eq 2.9 contained our acquisition signals when specific gradient fields are introduced (S_k) or when there is no presence of a gradient field (S_o). Thus, to derive a rotationally invariant diffusion tensor, we need to combine a number of weak gradient fields and solve a system of equation. This tensor calculation is covered in the next sections.

2.2.4 From diffusion weighted Images to the Diffusion Tensor

To estimate the diffusion tensor, many diffusion gradient pulses (at least six) with different orientation locations are applied (Behrens et al., 2003b). Depending on the orientation of the magnetic field gradients and the anisotropy of the brain's biological tissues, some particles will maintain stationary along the strong magnetic pulse B. Other more isotropic particles that diffuse parallel to the magnetic gradient pulse will move, causing a random phase shift and decrease in echo signal (Eq. 2.8). Thus, the intensity of the pulsed gradient signal (S_k) and the original signal with no gradient pulses (S_o) are used to calculate the diffusion tensor (D) by solving the Stejskal-Tanner equation (Eq. 2.9) (Stejskal and Tanner, 1965, Kingsley, 2006a). For simplicity, we can arrange Eq. 2.9 as follow,

$$S_k = S_0 e^{-b\boldsymbol{g_k^T D g_k}} \qquad \text{[Eq. 2.10]}$$

Where S_k denotes the diffused signal at the specific "$\mathbf{g_k}$" gradient direction, "S_o" denotes the intensity of the signal with no pulse gradient field direction, and "b" is a constant known as the b-factor. This "b" constant combines the known coefficients in Eq. 2.9, which include the gyromagnetic values (γ) , the gradient magnetic pulse length (δ), the time between the initial rf pulse at 90^o and the second 180^o rf pulse (Δ), and the coefficient diffusivity value (d). In the adult brain, common b-factor values range between 600-1200 s/mm^2. Finally, "D" denotes the diffusion 3x3 symmetric tensor that needs to be calculated.

To calculate **"D"**, a minimum of 6 gradient diffusion weighted images are needed (S_k) and at least an image with no gradient direction (S_0). Usually to increase the signal to noise ratio, a few S_0 images are collected and the averaged signal is used in diffusion imaging. In clinical research, a higher number of diffusion-weighted images (S_k) are also

used for better diffusion motion estimations. In this chapter, we present an analytical solution for two diffusion weighted image acquisitions. The first example sequence contained 1 no diffusion weighted image and 6 diffusion weighted images and the second acquisition example contained 6 no diffusion-weighted images with 36 diffusion-weighted images.

Given the higher number of voxels and the complication of solving these systems of equations, most publications do not cover the estimation as it is generally done by non-commercial software packages. Thus, the aim of the following section is to solve analytically the diffusion tensor "D" given two different acquisition parameters. For simplicity the solutions are bounded to one specific voxel (a 3-dimensional pixel), which can repeatedly iterate in every voxel of the image. Matlab functions (MATLAB 2012a, The MathWorks Inc., Natick, MA, 2000)(MathWorks, 2005), and imaging tools (for extracting intensities at each voxel) were used during this procedure. At the end, I compared my results with one of the most reliable software packages that derived this tensor intrinsically (FSL) (Smith et al., 2004b, Woolrich et al., 2009). FSL is a comprehensive library of analysis tools for FMRI, MRI and DTI brain imaging data. FSL tools are written mainly by members of the Analysis Group, FMRIB, Oxford, UK. FSL runs on any operating system (OSX, Windows, or Linux) and most of the tools can be used from the command line and as GUIs ("point-and-click" graphical user interfaces) (Smith et al., 2004b, Woolrich et al., 2009).

2.2.5 Analytical implementation of the diffusion tensor

Case 1: The "H" approach for 6 DWIs: This first case represents the first sequence acquisition example with six gradient directions (S_k) images and a single non-diffusion image (S_0). Given the following gradient direction pulses and intensities with a b-value of 800 s/mm^2 in Table 2.1 and by denoting **"gk"** in the simplified Stejskal-Tanner equation (Eq 2.10) for a 3-dimensional domain,

$$\boldsymbol{g_k} = [G_x, G_y, G_z]^T \qquad \text{[Eq. 2.11]I}$$

And our unknown **"D"**:

$$\boldsymbol{D} = \begin{pmatrix} \boldsymbol{D_{xx}} & \boldsymbol{D_{xy}} & \boldsymbol{D_{xz}} \\ \boldsymbol{D_{yx}} & \boldsymbol{D_{yy}} & \boldsymbol{D_{yz}} \\ \boldsymbol{D_{zx}} & \boldsymbol{D_{zy}} & \boldsymbol{D_{zz}} \end{pmatrix} \qquad \text{[Eq. 2.12]}$$

We can solve and expand the simplified Stejskal-Tanner (Eq 2.10) in terms of **D**:

$$\frac{-ln\left(\frac{S_k}{S_0}\right)}{b} = \left(G_{xi}^2 D_{xx} + G_{yi}^2 D_{yy} + G_{zi}^2 D_{zz} + 2G_{xi}G_{yi}D_{xy} + 2G_{\square i}G_{zi}D_{xz} + 2G_{yi}G_{zi}D_{yz}\right)$$

[Eq. 2.13]

where the subscript "i" denotes each gradient direction pulse (in this case "i' will go from 1 to 6).

One approach to solve this system of equations is to use matrix algebra. Thus let express **D** as a six-element column vector, **Dv**:

$$\boldsymbol{Dv} = [\, D_{xx}, D_{yy}, D_{zz}, D_{xy}, D_{xz}, D_{yz}]^T \qquad \text{[Eq. 2.14]}$$

With a six-element row matrix **H** containing a large M x 6 matrix (derived from the normalized gradients g_{xi}, g_{yi}, and g_{zi}), where M in the number of gradient directions (in this case M=6 based of the diffusion weighted images for this example):

$$\boldsymbol{H} = \begin{pmatrix} G_{x1}^2 & G_{y1}^2 & G_{z1}^2 & 2G_{x1}G_{y1} & 2G_{x1}G_{z1} & 2G_{y1}G_{z1} \\ G_{x2}^2 & G_{y2}^2 & G_{z2}^2 & 2G_{x2}G_{y2} & 2G_{x2}G_{z2} & 2G_{y2}G_{z2} \\ & & & \vdots & & \\ G_{x6}^2 & G_{y6}^2 & G_{z6}^2 & 2G_{x6}G_{y6} & 2G_{x6}G_{z6} & 2G_{y6}G_{z6} \end{pmatrix} \qquad \text{[Eq. 2.15]}$$

Lastly, let's define a Y-matrix for the left side of equation [Eq. 2.13]:

$$\boldsymbol{Y} = \left(\frac{ln\frac{S_0}{S_1}}{b}, \frac{ln\frac{S_0}{S_2}}{b}, \ldots, \frac{ln\frac{S_0}{S_6}}{b} \right) \qquad \text{[Eq. 2.16]}$$

Thus we can express [Eq. 2.13] with the following 6 directions system of equation as:

$$\boldsymbol{Y} = \boldsymbol{H} \cdot \boldsymbol{Dv} \qquad \text{[Eq. 2.17]}$$

With only six diffusion weighted signals, there is an exact analytical solution for the tensor that can be solved using standard methods such as the Cramer's rule,(Kinglsey, 2006)

$$(\boldsymbol{H}^{-1}\boldsymbol{H}) \cdot \boldsymbol{Dv} = \boldsymbol{Dv} = \boldsymbol{H}^{-1} \cdot \boldsymbol{Y} \qquad \text{[Eq. 2.18]}$$

The analytical solution for Eq. 2.18 was computed in Matlab scripts (see Appendix A and B) and compared to the values calculates by FSL, a neuroimaging software tool.

Gradient Pulses	**Gradient direction pulses at**			**Voxel Intensity**
	G_X	G_Y	G_Z	
No diffusion image (So)	0	0	0	312
Gradient pulse 1 ($S_{k=1}$)	0.817324	-0.49673	-0.29196	206
Gradient pulse 2 (S_2)	0.465087	-0.03533	0.88456	129
Gradient pulse 3 (S_3)	0.820439	-0.31517	0.477018	174
Gradient pulse 4 (S_4)	-0.80334	0.593293	-0.05141	233
Gradient pulse 5 (S_5)	-0.15636	0.78899	-0.59418	154
Gradient pulse 6 (S_5)	-0.11253	-0.34483	-0.93189	187

Table 2.1. Representation of the six gradient directions and its specific intensities values at location x=66, y=64, and z=21 in MNI space.

Case 2 The "B" approach for >>6 DWIs: In this case, thirty-six gradient directions (S_k) and six normal no-gradient pulse images (S_0) were collected and the analytical solution is presented in this section using a different approach called the "B approach" due to its matrix derived definition. For calculations in >6 DWIs using the H approach, please refer to the following publication (Kingsley, 2006b).

In the previous case, we were able to solve for the equations with only 6 DWIs and 1 image with no diffusion. However, our tensor approximation might not be very accurate. For example, in cases where none of the six gradient direction pulses align with the anisotropic direction of a white matter fiber bundle, the 6 diffusion-weighted images will

fail to capture the ideal anisotropic diffusion motion. Additionally, shorter movements will be detected if these gradient pulse directions are slightly off the orientation of the brain tissue. On the other hand if these gradient pulses are applied perpendicular to the tissue, no movement will be detected. In the 3D space, a completely accurate model will be ideally derived if we collect infinitesimal number of diffusion weighted pulse directions. Though, due to our current technology this is impossible and thus we relay on higher number of gradient pulse directions. Currently, higher numbers of diffusion weighted pulse directions are collected (~40-60 DWIs instead of 6). However, even though the higher number of pulse gradients increases the chances of a better tensor estimation, it will also increase the acquisition time which may eventually lead to patient discomfort and movement while acquiring the signal. Thus depending on the study parameters (e.g. children tend to move more in longer acquisition durations), the researcher needs to specify an optimal acquisition protocol. Thus, for this analytical derivation example, I used 36 DWIs and 6 non-diffused images at a random specific voxel location (x=76, y=64 and z=21) as shown by Table 2.2.

So for this "B approach" lets denote a seven-element column vector with the first six row representing the six distinct tensor elements and the final row representing the "S_0" no diffusion signal,

$$\boldsymbol{\alpha} = [\, D_{xx}, D_{yy}, D_{zz}, D_{xy}, D_{xz}, D_{yz}, \ln(S_o)]^T \qquad \text{[Eq. 2. 19]}$$

When no diffusion images are collected, they are usually averaged to estimate a better no diffusion signal (depicted as S_0). This must be done when utilizing the H approach

to avoid errors in tensor calculations. However, in this approach they can either be combined or treated individually.

In addition to the "$\boldsymbol{\alpha}$" matrix, lets denote an individual "**b**" matrix [Eq. 2.20] (Kingsley, 2006a). These 6 terms include b_{xx}, b_{yy}, b_{zz}, $b_{xy}=b_{yz}$, $b_{xz}=b_{zx}$, and $b_{yz}=b_{zy}$ or in vector notation:

$$b_i = (\, b_{xxi}, b_{yyi}, b_{zzi}, 2b_{xyi}, 2b_{xzi}, 2b_{yzi}) \qquad \text{[Eq. 2. 20]}$$

where "i" denotes every individual diffusion weighed image (in this case, i=42). This **b** matrix could also be combined in a seven-row vector that involves the non-diffusion signal at the last column:

$$\boldsymbol{B_i} = (\, -b_{xxi}, -b_{yyi}, -b_{zzi}, -2b_{xyi}, -2b_{xzi}, -2b_{yzi}, 1) \qquad \text{[Eq. 2.21]}$$

If we expand the following vector, we get a Nx7 **B** matrix,

$$\boldsymbol{B} = \begin{bmatrix} -b_{xx1} & -b_{yy1} & -b_{zz1} & -2b_{xy1} & -2b_{xz1} & -2b_{yz1} & 1 \\ \vdots & \vdots & \vdots & \vdots & \vdots & \vdots & \vdots \\ -b_{xxN} & -b_{yyN} & -b_{z\square N} & -2b_{xyN} & -2b_{xzN} & -2b_{yzN} & 1 \end{bmatrix} \qquad \text{[Eq. 2.22]}$$

where N denotes the number of gradient directions (in our case N=36 gradient directions). Thus, to represent [Eq. 2.10] in term of **B** and $\boldsymbol{\alpha}$, we get a natural logarithm formulation that looks like this:

$$ln(S_i) = \ln(S_0) - \boldsymbol{b_i} : \boldsymbol{D} = \boldsymbol{B_i} \cdot \alpha \qquad \text{[Eq. 2.23]}$$

where ":" denotes the inner dot product and "**D**" represents the diffusion gradient tensor in [Eq. 2. 12]. We could also represent every signal intensity in this Nx1 matrix called **x:**

$$\boldsymbol{x} = \begin{pmatrix} ln(S_1) \\ ln(S_2) \\ \vdots \\ ln(S_N) \end{pmatrix} \qquad \text{[Eq. 2.23]}$$

Now because the Nx7 **B** matrix is not squared, we will need to calculate the Pseudo inverse of **B**, "$\mathbf{B}^{\Psi}$" as follow:

$$(\boldsymbol{B}^T\boldsymbol{B})^{-1}\boldsymbol{B}^T\boldsymbol{B}\boldsymbol{\alpha} = \boldsymbol{\alpha} = (\boldsymbol{B}^T\boldsymbol{B})^{-1}\boldsymbol{B}^T\boldsymbol{B}\boldsymbol{x} \qquad \text{[Eq. 2.24]}$$

$$(\boldsymbol{B}^T\boldsymbol{B})^{-1}\boldsymbol{B}^T = \boldsymbol{B}^{\Psi} \qquad \text{[Eq. 2.25]}$$

The calculation for $\boldsymbol{\alpha}$ could be done similar to the **H** method in Eq 2.8. The data points are treated as equal for the original signal intensities, however this will not be true for their logarithms. So if the signal intensities have the same variance, then the uncertainty in $\ln(S_i)$ is proportional to $1/S_i$. Thus, the least-square fit should give more weight to the $\ln(S_i)$ of high S_i and less weight to $\ln(S_i)$ of low S_i values. This is accomplished by modifying (Kinglsey, 2006) Eq. 2.25 as follows:

$$\boldsymbol{\alpha} = (\boldsymbol{B}^T\boldsymbol{\Sigma^{-1}}\boldsymbol{B})^{-1}(\boldsymbol{B}^T\boldsymbol{\Sigma^{-1}})\boldsymbol{x} \qquad \text{[Eq. 2.26]}$$

Where $\boldsymbol{\Sigma^{-1}}$ is a diagonal NxN matrix for the intensities whose elements are S_i^2/σ_i^2 (signal intensities squared divided by the variance of it):

$$\boldsymbol{\Sigma^{-1}} = \begin{pmatrix} \frac{S_1^2}{\sigma_1^2} & 0 & \dots & 0 \\ 0 & \frac{S_2^2}{\sigma_2^2} & \cdots & 0 \\ \vdots & \vdots & \ddots & \vdots \\ 0 & 0 & \dots & \frac{S_N^2}{\sigma_N^2} \end{pmatrix} \qquad \text{[Eq. 2.27]}$$

Thus, by computing [Eq. 2.26], we could estimate our tensor variables specified in [Eq. 2.19]. Additional programs used for comparison and algebra computations were shown in the Appendix.

2.2.6 Comparison with FSL DTI estimation

After calculating the diffusion tensor **D** analytically it is worth noting that slight differences in one of the most common packages used to evaluate DTI were found probably due to simplistic algorithms used to balanced high computational power and accuracy in the results. For the purpose of understanding the tensor derivations, I presented only the first stage analytical computation for DTI in a single voxel. However a normal MRI image includes millions of voxels and thus it will require more time and higher computer power demands to computes all voxels. Calculating the tensor on each voxel goes beyond this chapter as it is done in an iterative method. To put it in perspective, the imaging data collected during this work included 65 diffusion weighed images with ~80 million voxels. Thus, ~80 million matrices with 65x65 dimensions are necessary to derive the tensor maps for every participant image. Thus for simplicity throughout this work, I used the FSL toolbox (DTIFIT) to derive these calculations.

In this work, I presented the necessary background information to understand analytically the derivation of the diffusion tensor and this major components of diffusion. Throughout this work, I investigated the changes in diffusivity metrics derived from these components of diffusion. Thus, I believe I covered the objective of this chapter, which was to describe in a simple manner how these mathematical diffusion metrics are derived analytically to be used broadly in the neuroscience world.

Gradient Pulses	**Gradient direction pulses at**			**Voxel Intensity**
	G_X	G_Y	G_Z	
No diffusion image (So)	0.0000	0.0000	0.0000	312
No diffusion image (So)	0.0000	0.0000	0.0000	345
No diffusion image (So)	0.0000	0.0000	0.0000	317
No diffusion image (So)	0.0000	0.0000	0.0000	293
No diffusion image (So)	0.0000	0.0000	0.0000	318
No diffusion image (So)	0.0000	0.0000	0.0000	327
Gradient pulse 1 ($S_{k=1}$)	1.0000	0.0000	0.0000	206
Gradient pulse 2 ($S_{k=2}$)	0.8173	-0.4967	-0.2920	129
Gradient pulse 3 ($S_{k=3}$)	0.4651	-0.0353	0.8846	174
Gradient pulse 4 ($S_{k=4}$)	0.8204	-0.3152	0.4770	233
Gradient pulse 5 ($S_{k=5}$)	-0.8033	0.5933	-0.0514	154
Gradient pulse 6 ($S_{k=6}$)	-0.1564	0.7890	-0.5942	187
Gradient pulse 7 ($S_{k=7}$)	-0.1125	-0.3448	-0.9319	160
Gradient pulse 8 ($S_{k=8}$)	0.5180	0.8004	0.3017	196
Gradient pulse 9 ($S_{k=9}$)	0.8217	0.3191	0.4722	234
Gradient pulse 10 ($S_{k=10}$)	-0.1539	0.3004	-0.9413	203
Gradient pulse 11 ($S_{k=11}$)	-0.7541	-0.5437	-0.3684	212
Gradient pulse 12 ($S_{k=12}$)	-0.4413	-0.8974	0.0046	214
Gradient pulse 13 ($S_{k=13}$)	-0.3398	0.9397	-0.0389	124
Gradient pulse 14 ($S_{k=14}$)	0.3022	0.5148	0.8023	171
Gradient pulse 15 ($S_{k=15}$)	-0.0663	0.8784	0.4734	99
Gradient pulse 16 ($S_{k=16}$)	-0.3919	-0.6726	0.6277	188
Gradient pulse 17($S_{k=17}$)	0.4299	0.5884	-0.6848	169
Gradient pulse 18 ($S_{k=18}$)	0.2995	-0.6225	0.7231	212
Gradient pulse 19 ($S_{k=19}$)	0.4238	-0.5502	-0.7195	74
Gradient pulse 20 ($S_{k=20}$)	-0.6019	0.5992	0.5279	90
Gradient pulse 21 ($S_{k=21}$)	-0.0921	-0.2396	0.9665	141
Gradient pulse 22 ($S_{k=22}$)	-0.6430	-0.1081	0.7582	127
Gradient pulse 23 ($S_{k=23}$)	0.0444	-0.9530	0.2999	169
Gradient pulse 24 ($S_{k=24}$)	0.2644	0.9453	-0.1909	154
Gradient pulse 25 ($S_{k=25}$)	-0.6574	0.4606	-0.5964	232
Gradient pulse 26 ($S_{k=26}$)	-0.2388	-0.7826	-0.5750	150
Gradient pulse 27 ($S_{k=27}$)	-0.9671	0.0025	-0.2543	193
Gradient pulse 28 ($S_{k=28}$)	-0.6231	-0.1211	-0.7727	196
Gradient pulse 29 ($S_{k=29}$)	0.8189	0.0623	-0.5705	135
Gradient pulse 30 ($S_{k=30}$)	-0.8446	-0.4754	0.2464	197
Gradient pulse 31 ($S_{k=31}$)	0.6156	-0.7677	0.1780	155
Gradient pulse 32 ($S_{k=32}$)	0.3741	0.0276	-0.9270	116
Gradient pulse 33 ($S_{k=33}$)	0.8046	0.5638	-0.1865	195
Gradient pulse 34 ($S_{k=34}$)	-0.2403	0.3430	0.9081	122
Gradient pulse 35 ($S_{k=35}$)	0.2446	-0.9277	-0.2820	153
Gradient pulse 36 ($S_{k=36}$)	-0.9369	0.1259	0.3260	182

Table 2.2. Representation of the thirty-six gradient directions acquisition example with 6 no-diffusion images and its specific intensities values at location x=66, y=64, and z=21 in MNI space.

Chapter 3 Preface:

This chapter is my first published work on using neuroimaging data, more specifically using diffusion imaging data. Here, the goal was to identify changes in white matter integrity on different neurodegenerative diseases. We included four groups in this study, Parkinson's disease without dementia (PD), Parkinson's disease participants progressed into a Parkinson's with dementia (PDD), a group of participants at early stages of dementia (AD), and a healthy non-demented control group (CON). This work prepared me to understand the pathology of these diseases (Parkinson's disease and Alzheimer's disease), its structural changes in the brain, and the usage of neuroimaging diffusion tools to investigate these changes. This work also allowed me to understand the advantages and disadvantages of each DTI processing method that I applied in this chapter: a region of interest approach and a more global whole-brain tract-based spatial statistics (TBSS) approach. After the completion of the study, I decided to compare TBSS to a more tract-related methodology that I described as a tract-of-interest (TOI) approach, which will be covered in the next chapters.

Chapter 3

A comparative white matter study with Parkinson's disease, Parkinson's disease with dementia and Alzheimer's disease

3.1 ABSTRACT

Alzheimer's disease (AD) and Parkinson's disease (PD) are among the most common neurodegenerative disorders affecting older populations. AD is characterized by impaired memory and cognitive decline while the primary symptoms of PD include resting tremor, bradykinesia, and rigidity. In PD, when mild cognitive changes are frequent, the disease progresses to PD with dementia (PDD). PDD and AD are different in pathology although the differences in microstructural brain changes remain unknown. Thus, we used diffusion tensor imaging (DTI) to investigate white matter tract differences in individuals with AD (n=13), PD (n=12), PDD (n=9), and healthy non-demented controls (CON) (n=13). We used whole brain tract-based spatial statistics (TBSS) and a region of interest (ROI) analysis focused on the substantia nigra (SN). We found that individuals with PDD had more widespread white matter degeneration compared to PD, AD, and CON. Individuals with AD had few regional abnormalities in the anterior and posterior projections of the corpus callosum while PD and CON did not appear to have significant white matter degeneration when compared to other groups. ROI analyses showed that PDD had the highest diffusivity in the SN and were significantly different from CON. However, no significant ROI differences were found between CON, PD, or AD. In conclusion, global white matter microstructural deterioration is evident in individuals with PDD, and thus DTI may provide means to tease out pathological differences between these dementias.

3.2 INTRODUCTION

Aging is accompanied by alterations in physiological, functional, and structural biological changes in the brain. In older adults the most frequent neurodegenerative

disorder is Alzheimer's disease (AD) followed by Parkinson's disease (PD) (Schocke et al., 2002, Yoshikawa et al., 2004, de Lau and Breteler, 2006). AD is characterized by impaired memory and cognitive decline, roughly affecting 4.5 million people in the US (Thies et al., 2013) while PD is a movement disorder with primary motor features of rest tremor, bradykinesia and rigidity (de Lau and Breteler, 2006). The risk of developing dementia in PD (PDD) is reported to be as high as 70% with a 6-fold chance to develop dementia compared to age-matched controls (Aarsland et al., 2002, Burton et al., 2004). In PD, the loss of dopaminergic neurons in the substantia nigra is considered the hallmark neuropathological finding (Rudow et al., 2008, Zhan et al., 2012). Yet it is evident that in white matter, these pathological changes go beyond the basal ganglia, as shown by significant white matter deterioration in cortical and subcortical regions (Burton et al., 2004, Matsui et al., 2007a, Matsui et al., 2007b, Karagulle Kendi et al., 2008, Kamagata et al., 2012, Zheng et al., 2013).

In the last few decades, *in vivo* non-invasive techniques such as diffusion tensor imaging (DTI) have been developed to investigate white matter alterations in neurodegenerative diseases. DTI measures the orientation and direction of water molecules in neural tissue, and one of its functions is to characterize the integrity of white matter fibers (Basser et al., 1994, Le Bihan, 2003). However, diffusion imaging studies on individuals with PD have been inconsistent. Two studies reported a lack of white matter deficit when comparing PD to healthy elderly subjects (Yoshikawa et al., 2004, Hattori et al., 2012) while others found reduced white matter integrity by measures of fractional anisotropy (FA), mainly in the substantia nigra (Yoshikawa et al., 2004, Chan et al., 2007, Vaillancourt et al., 2009), the cingulum,(Kamagata et al., 2012), the thalamus and putamen,

and frontal and temporal cortices (Zhan et al., 2012). A study using a more global approach (tract-based spatial statistics [TBSS]) showed reduced FA in PD compared to CON mainly in superior and inferior pre/post central gyrus, posterior striatum and frontal white matter regions (Zhan et al., 2012).

Alterations in PDD white matter as evidenced by decreased FA have also been reported in a number of brain regions such as the corpus callosum (Kamagata et al., 2012), frontal, temporal, and occipital lobes (Matsui et al., 2007b, Hattori et al., 2012). Additional DTI studies also examined individuals with Lewy body dementia (LBD), a pathology similar to PDD where cognitive changes occur prior to parkinsonism or motor symptoms (Dodel et al., 2008). Hattori *et. al.* found that individuals with PDD and LBD both had decreased FA in posterior and anterior brain regions compared to controls (Hattori et al., 2012). Watson *et. al.* compared LBD and AD using DTI and found a reduced FA in LBD subjects compared to CON predominantly in parieto-occipital tracts with relative sparing in frontal brain areas. When compared to CON, AD participants showed a more widespread reduced FA in the frontal brain (Watson et al., 2012). Kantarci *et. al.* found decreased diffusivity mainly in the amygdala and the inferior longitudinal fasciculus (associated with visual hallucinations) when patients with DLB were compared to controls while AD were characterized with higher diffusivity in temporo-parietal regions (Kantarci et al., 2010).

Though recent studies have investigated white matter changes associated with various neurodegenerative diseases, to our knowledge limited studies have compared AD, PD, and PDD at the level of white matter microstructure changes. It is important to understand these differences, which will lead us to a better understanding of each pathology progression. Thus in this study, we aimed to characterize group differences in

white matter neural fibers using two diffusivity metrics: fractional anisotropy (FA) and mean diffusivity (MD). First, whole brain voxelwise analyses were performed using tract-based-spatial statistics (TBSS) in 4 groups: PDD, AD, non-demented PD, and healthy non-demented (CON). Secondly, we aimed to measure DTI markers of dopaminergic neuronal loss using a region of interest (ROI) analysis in the substantia nigra (SN). We hypothesized that the cohort with combined cognitive decline and impaired motor control (PDD) would show the most expansive global white matter degeneration compared to AD, PD and healthy aging individuals (CON).

3.3 METHODS

Demographics

A total of 48 participants were included in this study. Healthy elderly non-demented subjects (Clinical Dementia Rating [CDR], 0; n=13) and individuals with AD (CDR, 0.5; n=12, CDR, 1; n=2) were included from ongoing studies at the University of Kansas Alzheimer's Disease Research Center (Vidoni et al., 2012b). Diagnostic criteria for AD require the gradual onset and progression of impairment in memory and in at least one other cognitive and functional domains from the NINCDS-ADRDA criteria (McKhann et al., 1984b). The presence or absence of AD dementia and its severity if present, was determined using the CDR scale (Morris, 1993).

Individuals with PD and PDD were recruited from the Parkinson's Disease and Movement Disorder Center at the University of Kansas Medical Center. A neurologist specializing in movement disorders diagnosed all the idiopathic PD according to the United Kingdom Parkinson's Disease Society Brain Bank Criteria for diagnosis (Hughes et al.,

1992). Diagnostic criteria for PDD were based on recommendations from the Movement Disorder Society Task Force for level 1 testing (Dubois et al., 2007) and included tests from the Uniform Data Set (UDS) used by the national network of Alzheimer's disease centers (Weintraub et al., 2009). Extra pyramidal signs were assessed using the motor subscale of the Unified Parkinson's Disease Rating Scale (UPDRS).

Diffusion Imaging Acquisition

Diffusion weighted images were acquired in a 3.0 Tesla Allegra MRI scanner using single-shot echo-planar imaging sequences with a repetition time [TR]=1000ms and echo time [TE]=81ms. Diffusion gradients were applied in 36 directions with 2 b-values (b = 0 s/mm^2 and b= 800 s/mm^2). Sixty-eight 2-mm sections were acquired in at in-plane resolution of 128x128 with a 300mm field of view (FOV). The total image acquisition time was 12 min.

Tract-Based Spatial Statistics

We performed voxelwise analysis in FA and MD using tract-based spatial statistics (TBSS), part of the Functional Software Laboratory [FSL 4.1.9] (Smith et al., 2004a, Smith et al., 2006). First, FA and MD images were created by fitting a tensor model to the raw eddy corrected diffusion data using FMRIB's Diffusion Toolbox (FDT) and then brain-extracted using the Brain Extraction Tool [BET] (Smith, 2002). All subjects' FA/MD images were aligned into a common space target (FMRIB58_FA) using the nonlinear registration tool FNIRT (Andersson et al., 2007, Andersson et al., 2010), which used a b-spline representation of the registration warp field (Schnabel et al., 2001). After registration, a

mean FA image was created and thinned-out (at 0.2 threshold) to create a mean FA skeleton, which represents the centers of all tracts common to all the groups. Each subject's aligned FA/MD data were then perpendicularly projected onto the skeleton and the data was fed for voxelwise cross-subject statistics.

Statistical group differences among AD, PD, PDD and CON for FA and MD maps were performed using RANDOMISE, a TBSS statistical tool that computes non-parametric permutations using the generalized linear model (Winkler et al., 2014). We used a threshold-free cluster enhancement [TFCE] approach (Anderson and Robinson, 2001, Nichols and Holmes, 2002, Smith and Nichols, 2009) and set the number of permutations to 5,000 using age and gender as the confound regressors. We compared each group to each other. Significance values were reported at $p<0.05$ corrected. To discuss our results, we overlapped a white-matter probabilistic tractography atlas derived from the John Hopkins University (Wakana et al., 2007, Hua et al., 2008a). Fiber tract threshold criteria included a probability of existence greater than 0.7 with mention of no other secondary fibers in the skeleton location.

Region of Interest (ROI) Analysis

Substantia nigra ROI were drawn on each image using Fslview 3.1.8, part of the Oxford Center for Functional MRI of the Brain (FMRIB) software library. After identifying the slice where the substantia nigra (SN), red nucleus, and subthalamic nucleus were noticeable, we moved one slice ventral where the SN was visible. At this specific location, two raters (R.P. and R.R.) drew ROIs in the red-green-blue (RGB) principal diffusivity invariant eigenvector, using the green color as a reference for fibers in the SN traveling in the ventral-dorsal direction. Then, we extracted FA and MD from these ROIs (Figure 3.1).

The inter-class correlation for the ROI regions was 0.834 while intra-class correlations were 0.913 and 0.949 respectively. Additionally, a Bland-Altman analysis (Bland and Altman, 1986, Hanneman, 2008), was used to compare these values giving a mean difference of 0.03 percentage points with a 95% confidence interval between -0.13 and 0.064. For comparisons between groups, one-way analysis of variance (ANOVA) was performed using age and sex as covariates. All statistical analyses were performed using SPSS 20.0 (SPSS Inc, Chicago, IL) while setting our alpha to $p<0.05$ to avoid Type I error.

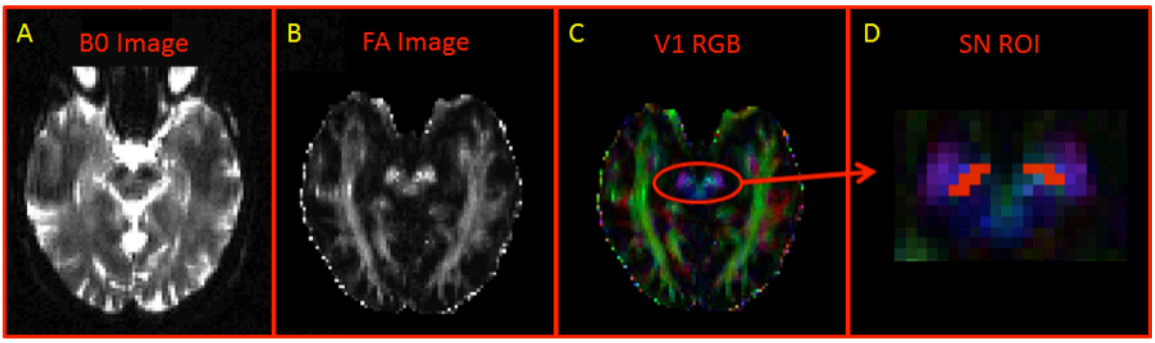

Figure 3.1._ Region of Interest (ROI) image representations in the substantia nigra (SN). (A) Shows the b_0 slice image with darker SN. (B) Shows the FA image with brighter SN. (C) Shows the principal eigenvectors in RGB color. (D) is a zoomed image of the region-of-interest with the mask denoted in red.

3.4 RESULTS

Demographics and clinical features

Table 3.1 shows the demographics data for the PD, PDD, AD, and CON groups. Education and MMSE were found to be significantly different among groups. Post-hoc analyses showed that PDD had a significantly lower mean education compared to CON ($p=0.002$), and the AD group ($p =0.003$). The PDD group also had a significantly lower MMSE than the AD, CON, and PD groups ($p<0.001$) while the AD group was significantly

lower than the CON (p =0.006) and the PD (p=0.016). UPDRS and disease duration was significantly higher in the PDD group when compared to the PD group (p <0.001).

	Control (n=13)	AD (n=14)	PD (n=12)	PDD (n=9)	P-Value	Post-hoc significance (LSD)
	Mean (SD)	Mean (SD)	Mean (SD)	Mean (SD)		
Age (yrs)	71.54 (7.45)	71.07 (7.32)	67.5 (4.01)	74.78 (5.12)	0.086	
Sex (M:F)	6:7	8:6	5:7	8:1	0.14	
Education (yrs)	16.77 (2.09)	16.64 (2.27)	15.33 (2.23)	13.67 (2.18)	0.007	CON, AD >PDD*
MMSE (max 30)	28.92 (1.32)	26.79 (2.45)	28.67 (1.44)	22.22 (2.17)	<0.001	CON, AD, PD>PDD** and CON >AD**
Total UPDRS	NA	NA	19.58 (7.10)	32.89 (5.86)	<0.001	PDD>PD**
Disease duration (years)	NA	NA	6.38 (4.19)	16.33 (6.92)	<0.001	PDD>PD**

NA= not applicable; n= number; SD = standard deviation *p< 0.01; **p< 0.001.
Table 3.1. Demographics and neuropsychological data of all subjects.

Region of Interest (ROI) Analysis

In our substantia nigra, we found a significant decrease in FA in the PDD group when compared to the CON group (p=0.004). We found that individuals with PDD also had increased mean diffusivity when compared to the CON group (p=0.011). There were no significant FA or MD differences between CON and AD, PD and AD, PDD and AD, PD and CON, or PD and PDD. Mean values and standard errors are shown in Figure 3.2.

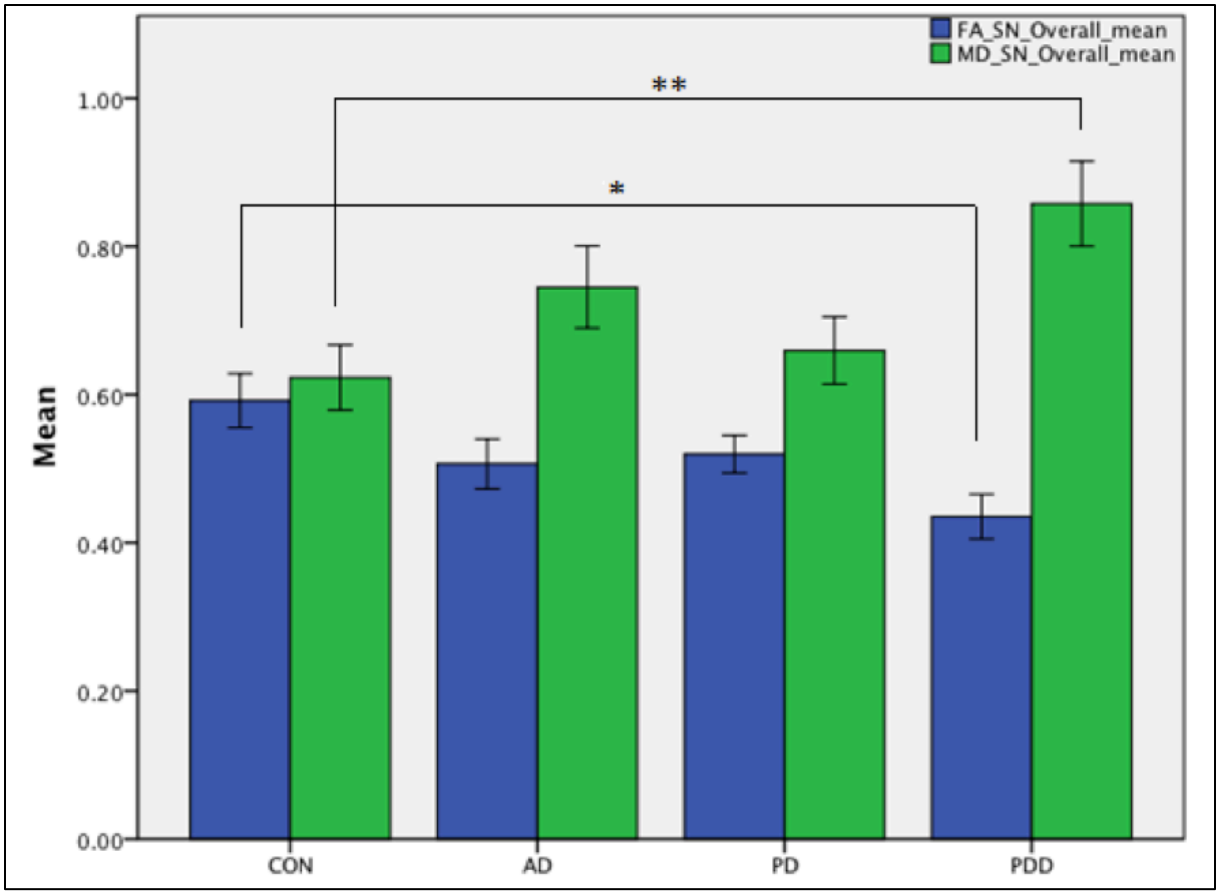

Figure 3.2. Substantia nigra ROI results after performing a one-way ANOVA with age and sex as covariated between each group. Overall mean diffusivity metrics across different groups: fractional anisotropy (blue) and mean diffusivity (green). Error bars denote ±1 standard error of the mean (SEM). Mean values for each group are CON (FAmean= 0.59, MDmean=0.62), AD (FAmean= 0.51 MDmean= 0.75), PD (FAmean= 0.52 MDmean= 0.67), and PDD (FAmean=0.44 MDmean=0.86). Stars denote significant results (in FA, CON>PDD at p=0.004*, and in MD, PDD>CON at p=0.01**).

Tract-Based Spatial Statistics

Non-parametric whole brain TBSS analyses were performed to compare group differences between PD, PDD, AD, and control groups on FA and MD. Significant results were divided in ten different probabilistic tracts (Mori and van Zijl, 2002). Significant group differences in specific white matter tract are depicted in Table 3.2 for FA and Table 3.3 for MD. Additionally, an image representation of the results are shown in Figure 3.3.

Fractional Anisotropy (FA)	CON > PDD		PD > PDD		AD > PDD		PD > AD	
	Left	Right	Left	Right	Left	Right	Left	Right
Anterior Thalamic Radiation	-	-	★	★	■	-	-	-
Corticospinal Tract	-	-	-	-	■	-	-	-
Forceps Major	★	★	-	-	■	■	■	-
Forceps Minor	■	■	★	★	-	■	-	■
Inferior fronto-occipital fasciculus	■	■	★	★	■	■	■	-
Inferior Longitudinal fasciculus	★	★	★	★	■	■	■	-
Superior longitudinal fasciculus	-	■	★	-	■	-	-	-
Uncinate fasciculus	■	-	★	-	■	-	-	■
Cingulum (hippocampus)	-	-	-	-	-	-	-	-
Cingulum (cingulate gyrus)	-	-	★	-	-	-	-	-

■._ denotes p<0.05. ★._ denotes p<0.01

Table 3.2. FA results for every group comparison on specific white matter tracts. Results were divided between left and right hemisphere. CON vs. AD and CON vs. PD did not show any significant differences and thus they were omitted from the table.

Mean Diffusivity (MD)	CON < PDD		PD < PDD		AD < PDD		PD < AD	
	Left	Right	Left	Right	Left	Right	Left	Right
Anterior Thalamic Radiation	■	■	■	■	★	★	-	-
Corticospinal Tract	■	★	■	■	★	★	-	-
Forceps Major	■	■	-	-	★	★	■	-
Forceps Minor	★	★	★	★	■	■	■	■
Inferior fronto-occipital fasciculus	★	★	★	★	★	★	-	-
Inferior longitudinal fasciculus	-	-	★	■	★	★	-	-
Superior longitudinal fasciculus	★	★	★	★	★	★	-	-
Uncinate fasciculus	★	★	★	■	★	■	■	-
Cingulum (hippocampus)	-	-	-	■	-	■	-	-
Cingulum (cingulate gyrus)	■	-	-	-	-	-	-	-

■._ denotes p<0.05. ★._denotes p<0.01

Table 3.3. MD results for every group comparison on specific white matter tracts. Results were divided between left and right hemisphere. CON vs. AD and CON vs. PD did not show any significant differences and thus they were omitted from the table.

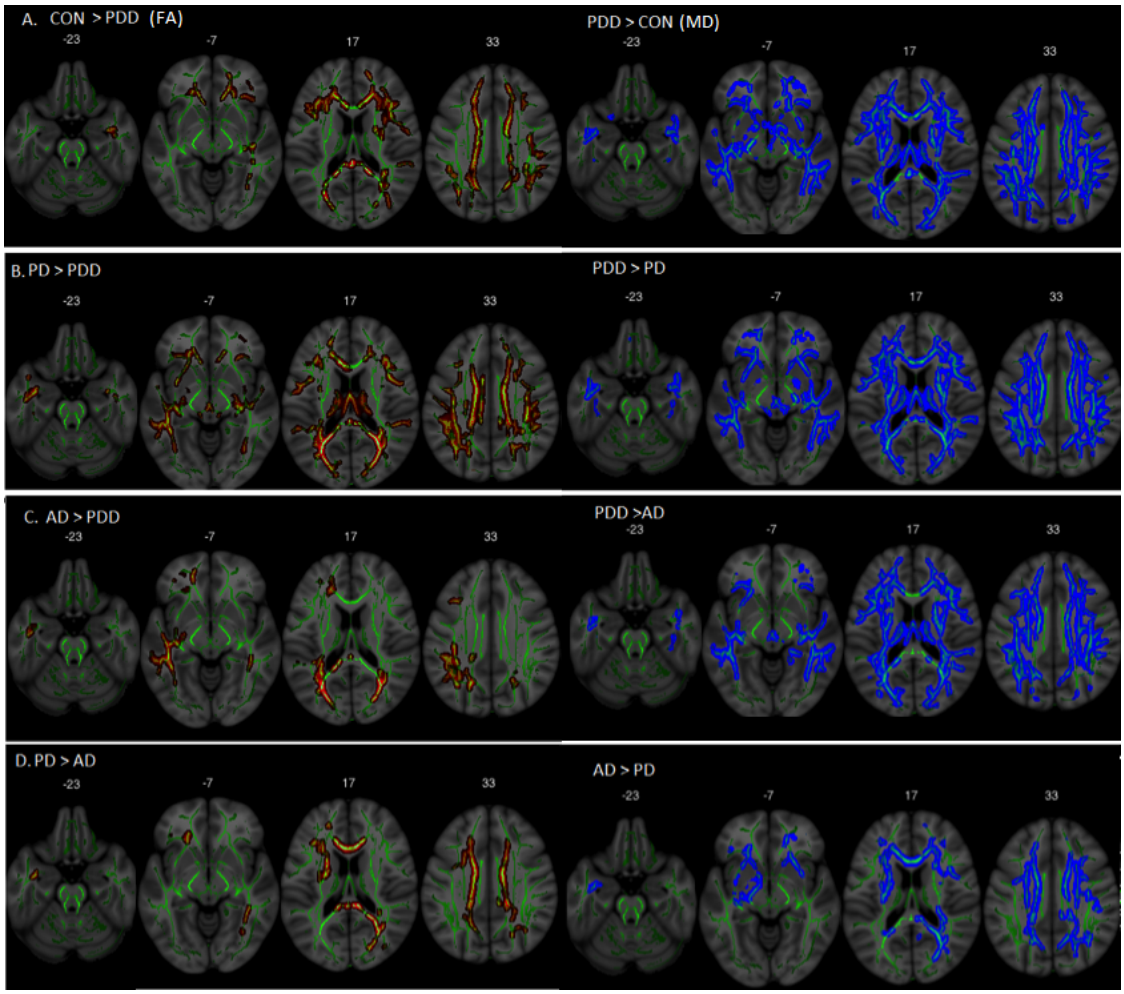

Figure 3.3. TBSS results for FA (in red) and MD (in blue). A) denotes higher diffusion in PDD when compared to CON, B) denotes lower diffusion in PDD when compared to PD, C) depicts lower diffusion in AD when compared to CON, and D) shows AD lower diffusion values when compared to PD. All images are displayed in a Montreal Neurological Institute (MNI) background (in grey) with the mean group skeleton superimposed (in green).

3.5 DISCUSSION

We characterized white matter integrity differences in AD, PD, PDD, and healthy non-demented controls using tract-based spatial statistics and ROI analyses in the substantia nigra. We found that the PDD group showed extensive global white matter degeneration when compared to PD, AD and healthy controls. In addition, we found that the AD group had lower diffusion in projection tracts of the corpus callosum (forceps minor and forceps major) when compared to PD. Our ROI analyses in the SN showed decreased

FA and increased MD in the PDD group when compared to controls. Though, no significant white matter changes were found in the SN when PD, AD, or non-demented control groups were compared. Hence, our findings suggest that individuals with PDD showed increased diffusion sensitive to our diffusivity metrics, which may be used as a potential tool for characterizing changes in the progression of this disease.

In the whole brain analysis, one of the tracts found to be deteriorated in PDD when compared with the control and AD group is the corticospinal tract (CST). Deterioration and injuries in this tract directly relate to motor weakness and rigidity leading to an impaired human gait (Barthelemy et al., 2011). However, we did not find any white matter deterioration differences in the CST when the PD group was compared to controls. A possible explanation could be that this cohort was in the early stages of PD ($UPDRS_{Mean}$= 19.58), and probably our diffusion metrics were not sensitive to detect early PD white matter deterioration. Additionally, diffusion of the inferior fronto-occipital fasciculus (IFOF), inferior longitudinal fasciculus (ILF), and superior longitudinal fasciculus (SLF) were significantly decreased in the PDD when compared to PD, AD, and controls. Even though the IFOF is poorly understood, it interconnects the frontal, temporal, and occipital lobes and its known to affect auditory and visual processing and neuro-motor functioning (Martino et al., 2010). The ILF provides a direct connection from occipital cortex to the temporal lobe (Kvickstrom et al., 2011, Gold et al., 2012). Anteriorly the ILF joins the uncinate fasciculus to relay information to the orbito-frontal cortex (Ashtari, 2012). Lesions in these ILF and SLF fibers have been related to thought disorders, visual emotion, and cognitive impairments (Makris et al., 2005, Chanraud et al., 2010). A recent investigation found similar results in the ILF explaining an association with visual

hallucinations (Kantarci et al., 2010). In AD, the SLF has shown to be significantly reduced bilaterally (Parente et al., 2008). The SLF has also been reported to control movement integrity, gait related functions, and early gait disturbances (Schmahmann et al., 2007, Scherder et al., 2011). Finally, we found that the uncinate fasciculus showed significant FA decrease in PDD and AD when compared to PD, and controls. The uncinate fasciculus interconnects the anterior temporal lobe, the amygdala, and hippocampus with the orbitofrontal cortex (Papagno et al., 2011). In AD, degeneration of the uncinate fasciculus has been associated as a secondary effect after grey matter atrophy (Damoiseaux et al., 2009) and along with the SLF, corpus callosum and cingulum are the fibers most affected with this pathology (Douaud et al., 2011, Scherder et al., 2011).

Our results also showed white matter integrity deterioration in the PDD group followed by a slight deterioration in the AD group mainly in white matter tracts that have been associated with cognitive decline and movement disorders. It may be that our PDD individuals were further along in their dementia progression than our AD individuals, who were at early stages of the disease. This may explain the significant differences between the PDD and the AD groups. We did not find global white matter deterioration in the PD group when compared to the healthy individuals, which is in agreement with the previous reports (Wiltshire et al., 2010, Hattori et al., 2012, Kamagata et al., 2012). However, another explanation could be the age differences between PD, AD and healthy elderly individuals, with PD being relatively younger. The decrease in white matter anisotropy could be related to increased age and not driven by a specific pathology (Salat, 2011).

In regards to the substantia nigra, we found abnormalities only in individuals with PDD. This finding is consistent with PD dopaminergic nigrostriatal system deterioration

where a greater number of neurons are lost (Hodaie et al., 2007). However, no differences were found when the PD group was compared to the healthy group. Previous ROIs investigations in the basal ganglia also failed to distinguish differences in FA and MD between PD and controls (Schocke et al., 2002, Yoshikawa et al., 2004, Chan et al., 2007). However, a recent study found reduced FA in the substantia nigra in early PD when compared to controls, with greater differences in the caudal region (Vaillancourt et al., 2009). A possible explanation for the lack of difference in our study is that microstructural white matter changes of dopaminergic neurons at early stages of PD may not be detectable with our diffusion acquisition. High resolution and specific imaging sequencing for regions of interest across the cortex could have helped identify white matter changes at these early stages of the disease that were not apparent with our diffusion acquisition parameters.

We did not find any significant abnormalities in white matter microstructure in the AD group when compared to healthy non-demented controls perhaps because the AD patients were in the early stages of the disease (mean MMSE = 26.79). The accumulation of amyloid beta in AD may lead to synaptic loss and degeneration (Braak and Braak, 1991b, Hardy and Selkoe, 2002). However at early stages of the disease, these aggregates may primarily damage the neuronal body of the axon, which compose mainly gray matter tissue. Hence, axonal body deterioration, which includes white matter tissue, may occur later in the disease even though other reports have disprove this hypothesis and believe that white matter deterioration might precede gray matter dysfunction (Brun and Englund, 1986, Sjobeck et al., 2006, Sachdev et al., 2013, Zhang et al., 2014). Previous studies that compared early stages of AD, later stages of AD, and healthy normal controls showed reduced white matter diffusion in AD, and to a lesser extent in mild cognitive impairment,

when compared to healthy controls (Zhuang et al., 2010, Shu et al., 2011), while others did not find any white matter changes in MCI or AD (Scola et al., 2010, Teipel et al., 2010).

Our primary limitation was the relatively small number of subjects in each disease group. Age differences between the younger PD and older PDD groups were also prominent and may have impacted the results, yet we controlled for age in our analyses. Moreover, even though TBSS aims to improve the sensitivity of subject registration and smoothing, it performs qualitative statistics in a normalized number of fibers, thus some pathological changes in each fiber may be disregarded due to the thinning out of the skeleton map. In addition, FA and MD might have been representing similar diffusivity metrics based on its analytical definition (Alexander et al., 2007, O'Donnell and Westin, 2011). FA is a measure of degree of diffusivity based ranging from 1 (very anisotropic) to 0 (very isotropic) while MD is an averaged metric of diffusion based on the three dimensional diffusivity components. In future studies we will consider other diffusion metrics such as radial diffusivity and/or axial diffusivity. Finally, this study is a cross-sectional study, and further investigation with longitudinal data could give us more insights on the progressive nature of each of these pathologies.

3.6 CONCLUSION

We found that individuals with Parkinson's disease dementia showed significant regional (substantia nigra) and global white matter deterioration when compared to non-demented individuals by means of fractional anisotropy and mean diffusivity. However, individuals at early stages of Alzheimer's disease and Parkinson's disease did not appear to have diffusivity changes when compared to non-demented elderly subjects using the

current DTI methodology. Even though our results suggest that DTI and TBSS may be sensitive to understand the progression of these pathologies (especially in PDD), additional larger and longitudinal studies could improve the ability to characterize whether DTI is sensitive enough to understand the changes and progression of white matter tract integrity in these pathologies.

Chapter 4 Preface:

After using diffusion imaging data to investigate changes in white matter integrity in Parkinson's disease and Alzheimer's disease neurodegenerative diseases (Chapter 3), I decided to compare the characteristics of two diffusion imaging methods: tract-based spatial statistics (TBSS) and tract-of-interest (TOI). The rationale for this study was that I noticed a lack of standardization in reporting diffusion imaging data in the literature, and I sought to identify a clear methodological approach for my consequent analyses. Diffusion imaging characterizes water diffusion within white matter tracts, a conduit of many white axonal fibers traveling together in parallel directions. These conduits cover many brain regions rather than being located at any one place. However, previous reports in diffusion imaging described significant results in whole white matter conduits (known as tract) if small cluster of voxels (3-dimensional pixels) reached significance at a specific brain region. However, these voxels do not cover the entire white matter conduit, which might lead to false positives interpretations when significant results are described in relation to specific regions rather than white matter tracts.

Hence, in this chapter I sought compared TBSS to an alternative *a-priori* tract-of-interest (TOI) approach where the main interest is to evaluate diffusivity measures in the whole white matter conduits (or specific white matter tracts). Here, I also discussed each method's advantages and limitations in relation to a large sample dataset (n=208). This older adult dataset encompassed healthy non-demented, participants diagnosed with Alzheimer's disease, and mild cognitive impairment.

Chapter 4

Diffusion tensor imaging and Alzheimer's disease: a comparison between two processing methods, tract-based spatial statistics (TBSS) and tract of interest (TOI)

4.1 ABSTRACT

Objective

Given no DTI methodological gold standard, we characterized and compared the ability of two diffusion tensor imaging (DTI) processing methods, tract-based spatial statistics (TBSS) and tracts of interest (TOI), to distinguish white matter differences in older healthy non-demented (ND), mild cognitive impairment (MCI), and Alzheimer's disease (AD) cohorts.

Methods

We analyzed cross-sectional DTI data from ND (n=57), MCI (n=67), and AD (n=37) participants enrolled in the Alzheimer's disease Neuroimaging Initiative (ADNI). We used diffusion imaging data and measures of fractional anisotropy (FA) and radial diffusivity (RD) to assess the integrity on white matter. Using TBSS analyses, we conducted whole brain analyses to test FA and RD group differences (ND vs. AD, ND vs. MCI, and MCI vs. AD). Similarly when we used TOI, we conducted parametric analyses in *a-priori* white matter tracts, previously related to AD.

Results

The TBSS results showed a widespread FA decline in the AD cohorts when compared to MCI and to a greater extent when compared to ND ($p<0.05$ corrected). No significant differences were found when MCI was compared to ND or in any RD group comparisons. The TOI method found significant group differences in both FA and RD measures, specifically in the splenium of the corpus callosum, cingulum, inferior fronto-occipital, and uncinate fasciculus.

Conclusion

Both TBSS and TOI identified overall FA decline as the disease severity progressed (AD>MCI>ND) but TBSS results were less tract specific and difficult to interpret in relation to white matter tracts. Additionally, TBSS failed to identify differences in RD while the results for RD in the TOI method were more sensitive than FA. Our study suggests that choosing different DTI methods may lead to different results, which may explain the variability in previous AD-related results. Thus, we encourage future studies to consider a more standardized and tract specific DTI methodology such as TOI. However, researchers should be aware that the TOI method is not sensitive to voxel-by-voxel analyses. Instead, it uses averaged diffusivity values throughout whole white matter tracts to perform statistics. Alternatively, we encourage researchers to understand the flaws TBSS may encounter, especially when non-FA images (eg. RD) are under investigation.

4.2 INTRODUCTION

Alzheimer's disease (AD) is a progressive neurodegenerative disease that disrupts cognition and affects one in nine people over 65 and one in three over the age of 85 (Thies et al., 2013). AD is typically considered a gray matter disease yet emerging *in vivo* neuroimaging studies demonstrated that white matter changes in AD might be independent or even precede grey matter deterioration (Bartzokis, 2004, Sachdev et al., 2013, Amlien and Fjell, 2014). Although *in-vivo* imaging studies do not provide a micro-scale cellular resolution, an indirect interpretation of integrity can be assessed using magnetic resonance imaging such as diffusion imaging and metrics of fractional anisotropy (FA) and radial diffusivity (RD). FA provides a degree of diffusivity orientation ranging

from 0 (perfectly isotropic) to 1 (perfectly anisotropic) and is related to overall white matter microstructural integrity while RD measures perpendicular diffusivity and reflects changes in axonal diameter and myelination (Song et al., 2003, Kingsley, 2006a, Alexander et al., 2011, O'Donnell and Westin, 2011). Hence, lower RD is related to increased white matter integrity. These diffusivity metrics represent intrinsic characteristics of white matter and have been widely used in AD as shown by previous reviews (Gold et al., 2012, Reid and Evans, 2013, Zhang et al., 2014) and meta-analysis reports (Sexton et al., 2011, Clerx et al., 2012). However due to inconsistent findings, there is still much debate where and when these changes occur in the progression of the disease. These inconsistencies worsen when studies include a mild cognitive group (MCI) (Damoiseaux et al., 2009, Acosta-Cabronero et al., 2010, Liu et al., 2011, Alves et al., 2012, Bosch et al., 2012, Mufson et al., 2012). MCI is defined as an early non-demented group with highly likelihood to develop AD. Though, not all MCIs develop AD (Zhuang et al., 2010). Thus in this study we wanted to investigate the differences between these groups and whether different diffusion imaging methods (TBSS or TOI) lead to similar or different results and conclusions.

One of the most common methods used in DTI is called tract-based spatial statistics (TBSS) (Smith et al., 2006). TBSS was established to overcome limitations that aroused when voxel-based morphometry (Eskildsen et al., 2014) were used to process DTI data. Originally, voxel-based morphometry methods were developed to investigate gray matter differences in T1 high-resolution structural images. However, when the usage of VBM methods extended to diffusion imaging space, it confounded limitations. Two main limitations included brain tissue misalignments and the arbitrary choice of smoothing kernels (Jones et al., 2005). When every subject's image is registered to a common

template, there is no guarantee that successful alignment occurs and that every voxel represents exactly the same spatial region in every subject (Friston and Ashburner, 2004). This problem aggravates in periventricular regions where non-white matter tissue (i.e. cerebrospinal fluid) may be registered as white matter, leading to partial volume effects. The arbitrary choice of smoothing is also problematic because there is no "correct amount" or a standard choice for a smoothing threshold. In smaller white matter tracts, where a mixed-tissue misalignment may occur, spatial smoothing will intensify this problem adding more variability to the images and eventually leading to biased results. To overcome these limitations, TBSS was implemented as a novel method that "thins out" major white matter tract conduits in every subject's DTI diffusivity measure (FA or RD) and projects its values into a mean common skeleton template. Then, statistical analyses (usually non-parametric permutations) are performed in these projections and the interpretations and results are based on this thinned-out skeletonized data.

While TBSS overcomes alignment and smoothing limitations found in VBM analyses, it engenders other flaws. First, the skeletonization step projects the highest 3-dimensional perpendicular diffusivity voxel value (e.g. FA) into its adjacent skeleton voxel location (Smith et al., 2006), which might create a favorable bias in thicker white matter regions versus thinner regions (Edden and Jones, 2011). Additionally, the skeleton creation reduces the information being derived from white matter tracts (Bach et al., 2014) and consequently the statistical analysis will only include those voxels with the highest FA values, omitting less anisotropic white matter information. Another limitation arises due to the misalignment biased that occurs when choosing a specific template before the skeletonizing step (Zalesky, 2011, Keihaninejad et al., 2012), which exacerbates with

longitudinal data (Keihaninejad et al., 2013). Finally and previously not reported is the lack of reporting results in a standard and concise manner. For example, many studies report small number of voxels within some white matter tracts (e.g. cingulum, corpus callosum, etc…) as significant only because the results slightly overlap with standard white matter atlases (Teipel et al., 2010, Liu et al., 2011, Alves et al., 2012, Bosch et al., 2012). Even though this description specifies particular brain regions, we believe that when reporting white matter tracts, the authors need to consider the entire continuous conduit (of the tract) rather than just smaller overlapping regions. Alternatively, you could report white matter differences representing brain locations (e.g. temporal, frontal, parieto-occipital) as previously done (Damoiseaux et al., 2009, Acosta-Cabronero et al., 2010) yet the results may be misleading. This lack of standardization when reporting white matter results makes it difficult to reproduce data, interpret results, and draw conclusions from similar diffusion imaging investigations. To overcome these limitations, others have used a different approach that deviates from a skeleton-derived TBSS analysis (Zheng et al., 2013). Instead of projecting highest DTI voxels values into a thinned out skeleton, the tract of interest (TOI) approach identified *a-priori* white matter tracts, averages the diffusivity measures (e.g. FA or RD), and feeds the mean values into a statistical program (e.g. SPSS) for further statistical analysis. This processing methodology allows the investigator to obtain overall diffusivity measures from specific *a-priori* white matter tracts rather than doing whole brain imaging analyses as performed by the processing pipeline of TBSS (FSL, 2013c).

Thus, the goal of this study was to characterize and compare group differences using two diffusivity metrics: TBSS and TOI. We evaluated data from a group of older adults diagnosed as ND, MCI, and AD. We expected the AD to have the lowest integrity in white

matter followed by the MCI and ND. We aimed to compare and discuss in relation to specific white matter tracts and explain whether the processing methodology may cofound interpretations.

4.3 METHODS

Sample

Baseline diffusion imaging data was obtained from the Alzheimer's disease Neuroimaging Initiative (ADNI, (ADNI, 2012)) on February 3rd, 2014. Our data included cross-sectional DTI images from older adults who were ND (n=57), MCI (n=67), and AD (n=37). ADNI was launched in 2003 by the National Institute of Aging (NIA), the National Institute of Biomedical Imaging and Bioengineering (NIBIB), the Food and Drug Administration (FDA), private pharmaceutical companies, and nonprofit organizations to sponsor an ongoing observational study, as a $60 million, 5-year public-private partnership. The primary goal of ADNI has been to test whether serial magnetic resonance imaging (MRI), positron emission tomography (PET), other biological markers, and clinical and neuropsychological assessment can be combined to measure the progression of mild cognitive impairment (MCI) and early Alzheimer's disease (AD). Its mission is to study the rate of change in cognition, brain structure, and biomarkers.

Clinical assessment

All the participants included in this study underwent standard clinical and neuropsychological examinations including the clinical dementia rating (CDR) (Morris, 1993), physical examination, laboratory procedures and neuropsychological tests at baseline, and follow-up intervals (6,12, and 24 months) to identify conversion between

diagnosis (ND to MCI, MCI to AD, ND to AD, or in the opposite direction). To assess cognitive measures, evaluations included the Mini-Mental State Examination (MMSE) (Folstein et al., 1975) and an 11-item Alzheimer's Disease Assessment Scale-cognitive scale (ADAS-cog) (Rosen et al., 1984). These and other standardized evaluation protocols are described specifically elsewhere (available online at (ADNI, 2013)). The ND group criteria consisted on having a MMSE scores between 24 and 30 (inclusive), a CDR score of 0, and no significant depression. MCI participants had a MMSE score between 24 and 30 (inclusive), a CDR score of 0.5, memory complains and objective memory loss. AD participants scored between 20 and 26 in the MMSE (inclusive), a CDR score of 0.5 or 1.0, and met criteria for probably AD based on the National Institute of Neurological Disorders and Stroke. To increase the diagnosis accuracy of the groups and the consistency of each clinical diagnosis, we excluded participants who converted between baseline and follow-up evaluations (n=12) or did not have follow-up interventions (n=23).

Neuroimaging

Baseline MRI was collected at 14 acquisition sites across North America with a repetition time [TR] ≈9000ms and echo time [TE] ≈62ms. Five non-diffusion images (b_0 = 0 s/mm^2) and 42 diffusion gradient directions ($b_{5\text{-}41}$= 1000 s/mm^2) were collected. Fifty-nine 2.7-mm axial slices were acquired in at in-plane resolution of 256x256mm with a 66-mm field of view (FOV). Visual checking was performed to exclude scans with excessive movement artifacts and poor quality. After manually inspecting one hundred and diffusion weighted images (35 excluded due to diagnosis conversion), we excluded twelve images due to substantial distortion (n=6) or bad quality acquisition (n=6).

Imaging Analysis

First, we performed similar pre-processing steps in TBSS and TOI using the FMRIB Software Library (FSL 5.0.4) (Smith et al., 2004a). We applied eddy current correction in all images to overcome small distortions and simple head motion by aligning the diffusion weighted images to the b_0 images. Next, the brain extraction tool (BET2) was applied to strip the brain from the skull, and diffusivity FA and RD maps were calculated using DTIFIT. Then, all the FA and RD images were non-linearly registered, aligned and transformed into a common 1x1x1mm standard MNI space template (FMRIB58_FA_1mm) using a non-linear registration tool FNIRT, which uses a b-spline representation of the registration map field, as part of the TBSS processing stream. The next procedures were divided based on each methodology.

For the TBSS analysis, we followed standard published procedures (Smith et al., 2006). The FA images from every subject were non-linearly registered, aligned, and transformed to a common template, which was thinned out to create a mean FA skeleton. This mean FA skeleton represents the center of all tracts common to the group. Then, each subject's aligned FA and RD data were projected onto the mean FA skeleton. These projections were done on every voxel in the skeleton by searching the highest FA value perpendicular to the skeleton. Once the highest voxel value location is found, it is assigned to the skeleton template location. In non-FA images (e.g. RD), the voxel location previously found in FA was projected into the skeleton. These projections were repeated on every subject's FA and the resulting projected skeletons from every subject were combined into a 4D skeleton image. This 4D skeleton image was thresholded to include tracts with FA

values higher than 0.2. Then, the resulting data was fed into voxelwise cross-subject statistics (Figure 4.1a).

For the TOI approach, we omitted the "skeletonizing" step. Instead, after all subject's diffusion space were co-registered to the standard MNI template; we applied a 2-mm smoothing kernel using FSLMATHS (FSL, 2013b), part of FSL. Next, to determine AD-related *a-priori* tracts, we extracted white matter tract binary masks from the Johns Hopkins University probabilistic white matter atlas previously registered to the common MNI space (Mori et al., 2005, Wakana et al., 2007, Hua et al., 2008a). These masks were generated using deterministic tractography and were thresholded to account for at least 0.25 probability of tract existence (Figure 4.1b). For every subject's FA or RD image, we "masked in" AD-related *a-priori* tracts (Figure 4.2). These tracts included the cingulum (CCG) (Zhang et al., 2007, Liu et al., 2011, Alves et al., 2012), the inferior fronto-occipital fasciculus (IFOF) (Alves et al., 2012, Bosch et al., 2012), the inferior longitudinal fasciculus (ILF) (Liu et al., 2011, Alves et al., 2012, Bosch et al., 2012), the uncinate fasciculus (UF) (Bosch et al., 2012, Zhang et al., 2014), and the corpus callosum (genu, body and splenium) (Stahl et al., 2007, Alves et al., 2012, Bosch et al., 2012). Average FA or RD values were computed on every tract bilaterally and feed into a statistical program for further statistical analyses.

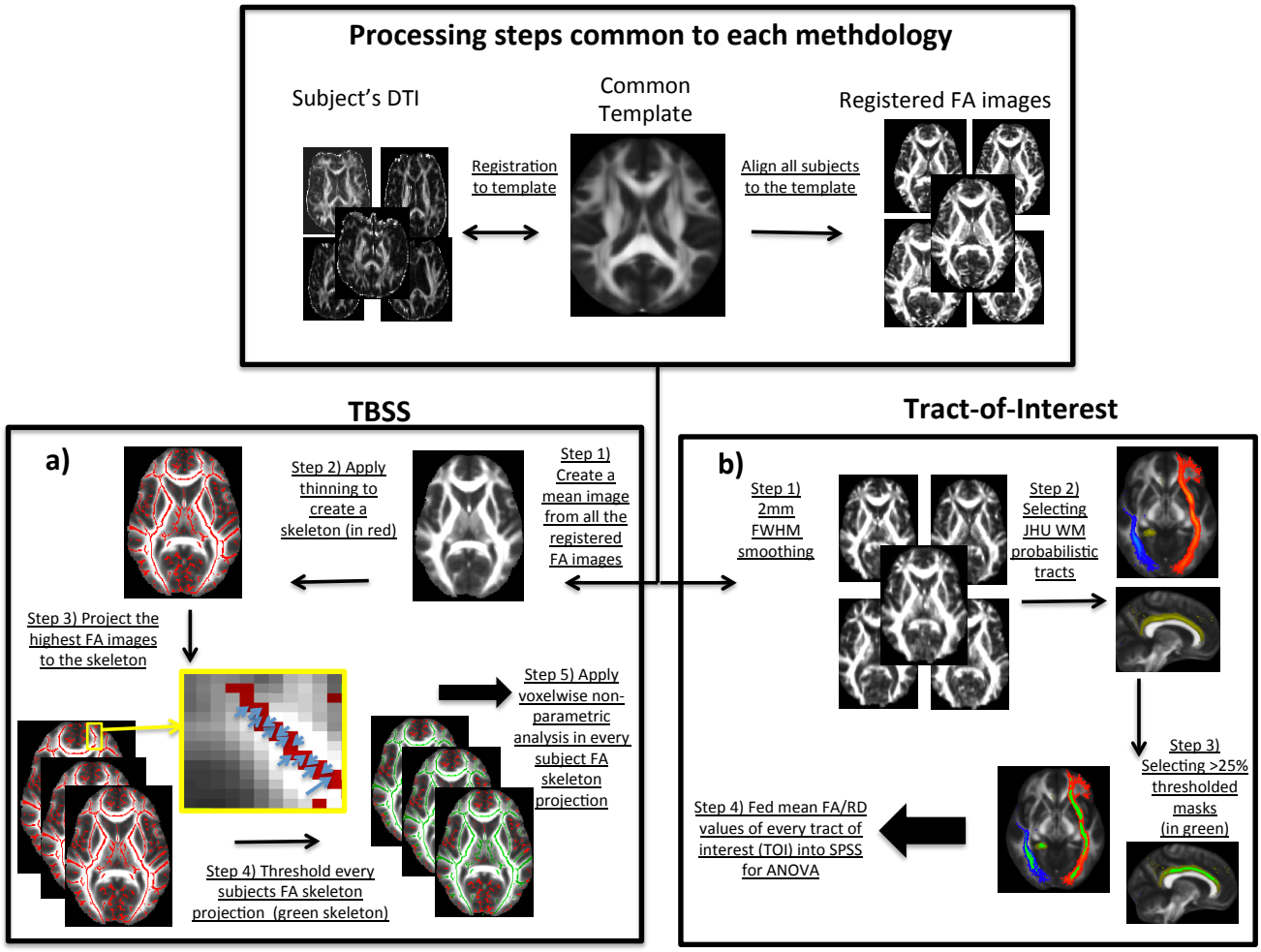

Figure 4.1. These diagrams depict step-by-step the two methodologies used during this investigation: a) tract-based spatial statistics (TBSS) and b) the tract-of-interest approach.

Statistical analysis

For demographics data, we conducted parametric analysis of variance (ANOVA) and chi-square (χ^2) tests to evaluate group differences. As appropriate, post-hoc analyses were conducted to identify differences between groups (ND vs. MCI, ND vs. AD, and MCI vs. AD) using the Fisher least significant difference (LSD) test.

For TBSS, we performed voxelwise non-parametric analyses using permutation-based statistical interference (Nichols and Holmes, 2002, Winkler et al., 2014, FSL, 2015).

To test group differences (ND vs. MCI, ND vs. AD, and MCI vs. AD) in FA and RD, we used the generalized linear model and include two-regressor models with age and gender as covariates. We set the number of permutations to 5000, reported significant results using the threshold-free cluster-enhancement (Smith and Nichols, 2009), and set our alpha (two-tailed) to 0.05 corrected for multiple comparisons.

For TOI, average FA/RD values on *a-priori* tracts were extracted and analyzed outside of imaging space using SPSS 22.0 (IBM Corp., Armonk, NY). To evaluate group mean differences, we conducted ANOVA tests on every tract unilaterally (left and right). When appropriate, post-hoc analyses were conducted using least square difference (LSD) tests to identify specific group differences (ND vs. MCI, ND vs. AD, and MCI vs. AD). We included gender and age as covariates and set our alpha (two-tailed) to 0.05 corrected.

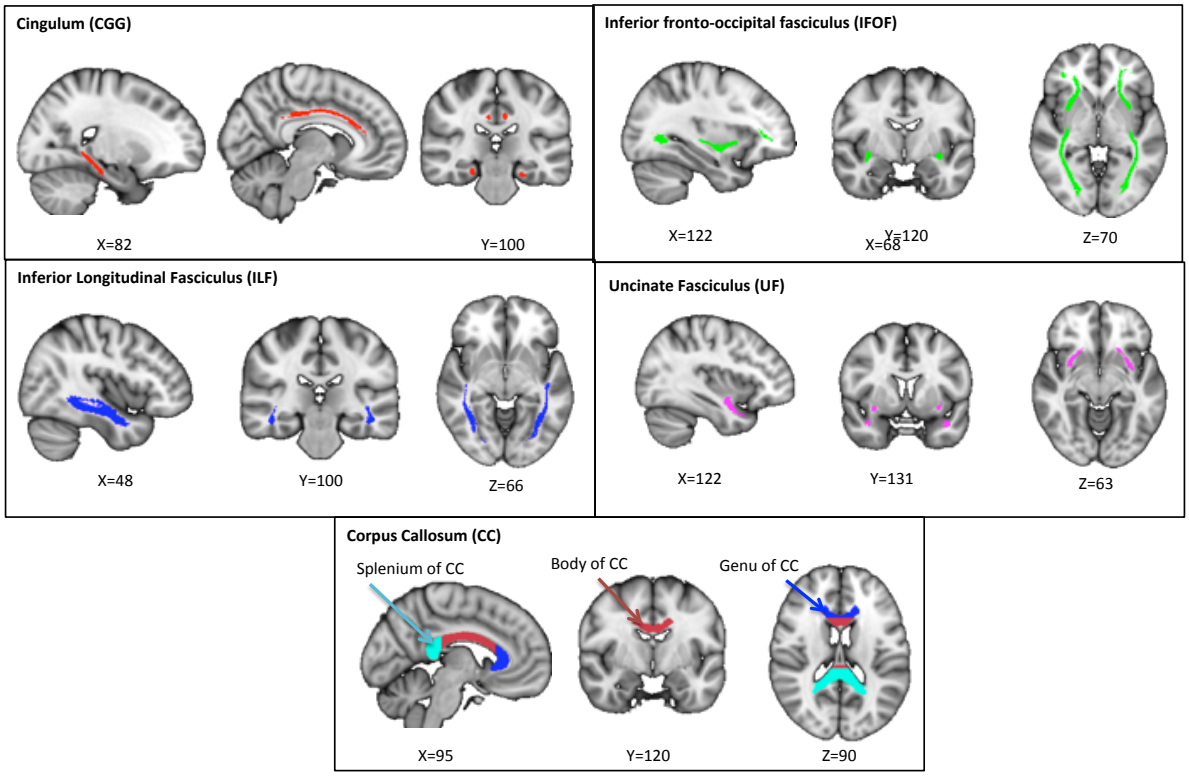

Figure 4.2. Representation of the *a-priori* white matter tracts, which include the cingulum (top left), the inferior fronto-occipital fasciculus (top right), the inferior longitudinal fasciculus (middle left), the uncinate fasciculus (middle right), and the corpus callosum (bottom) divided in the genu (blue), body (maroon), and splenium (light-blue).

4.4 RESULTS

Demographics

Participants' demographics are provided in Table 4.1. There were no differences in age, gender, or education across the diagnosis groups. The cognitive measurements were significantly different across groups with MMSE being highest in the ND, intermediate in the MCI and lowest in the AD ($p<0.001$). Post-hoc analyses for the CDR sum of boxes also showed higher values in AD, intermediate in the MCI, and lowest in ND.

	ND (n=57)]	**MCI** (n=67)	**AD** (n=37)	**p-value**	**Post hoc results**
Age	73.0 ± 5.7	73.6 ± 7.4	74.5 ± 8.5	0.609	-
Gender	24 M / 33 F	42 M / 25 F	22 M / 15 F	0.058	-
Education	16.2 ± 2.7	15.7 ± 2.8	15.3 ± 2.8	0.287	-
MMSE	28.7 ± 1.6	27.6 ± 1.7	23.2 ± 1.8	<0.001	ND>MCI>AD
CDR-SOB	0.05 ± 0.2	3.5 ± 0.7	4.6 ± 1.5	<0.001	ND<MCI<AD

Table 4.1. Participant's demographics divided by each group: non-demented (ND), mild cognitive impairment (MCI) and Alzheimer's disease (AD).

Tract-based Spatial Statistics

To investigate group differences (ND vs. AD, ND vs. MCI, AD vs. MCI), we performed whole brain group comparisons in the FA and RD skeleton maps. The ND group showed widespread and significantly higher FA values when compared to AD ($p<0.05$ corrected, Figure 4.3a). These locations include all the *a-priori* white matter major tracts specified in Figure 4.2 that travel within the frontal, temporal, parietal, and occipital lobes. No significant results were found in the opposite direction (ND<AD). Similarly, higher FA values were found when the MCI group was compared to the AD group but to a lesser

extent (p<0.05 corrected, Figure 4.3b). No significant differences were found in the opposite direction (MCI>AD) or when the ND group was compared to the MCI group.

For RD, we did not find any significant group differences. Though, there was a trend (p<0.08 corrected) of higher RD in AD when compared to ND only in the anterior fornix.

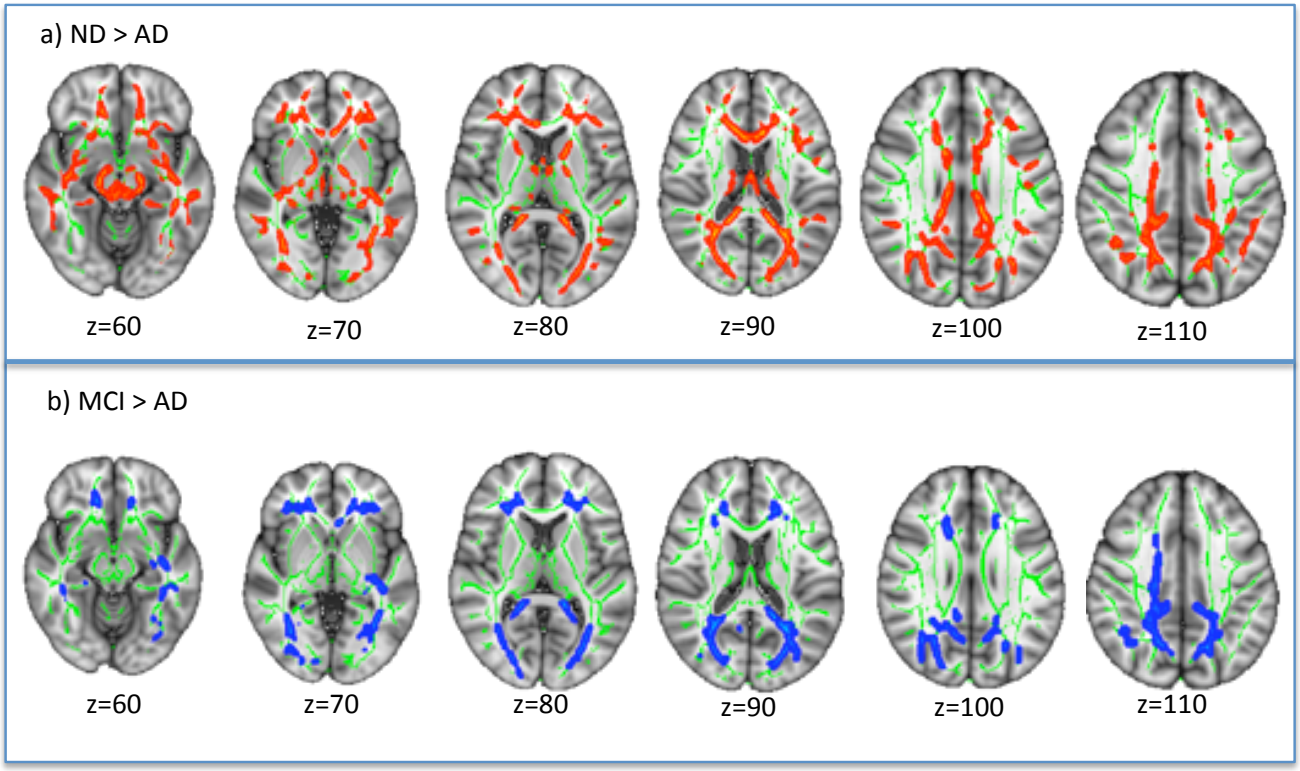

Figure 4.3. Significant group differences using TBSS in fractional anisotropy (FA) maps. Top row represents higher FA in ND when compared to AD (significant voxels were thickened in red using tbss_fill for better visualization). The bottom row represents higher FA (in blue) in MCI when compared to AD. No differences were found when ND was compared to MCI or in any of the radial diffusivity (RD) comparison tests (images not shown). Green depicts the mean FA skeleton overlapped in the MNI152 brain standard template (radiological orientation).

Tract of Interest Approach

To investigate group differences in averaged FA/RD values, we conducted analysis of variance and post-hoc analyses when appropriate in every *a-priori* white matter tract covarying for age and gender. When we examined FA values, significant results were found

in the splenium of the corpus callosum, bilaterally in the cingulum, inferior fronto-occipital fasciculus, and left uncinate fasciculus (Table 4.2). When examined RD values, all the *a-priori* TOI were significantly different between groups (Table 4.3).

	Fractional Anisotropy			ANOVA	
	ND	MCI	AD	p-value	Post-hoc
Corpus Callusom (CC-)					
CC-Genu	0.48	0.48	0.46	0.160	-
CC-Body	0.50	0.50	0.48	0.060	-
CC-Splenium	0.66	0.64	0.63	**0.001**	ND>AD
Cingulum (CCG-)					
CCG-L	0.40	0.39	0.37	**<0.001**	ND>AD, MCI>AD
CCG-R	0.37	0.37	0.35	**<0.001**	ND>AD, MCI>AD
Inferior fronto-occipital fasciculus (IFOF-)					
IFOF-L	0.40	0.39	0.39	**0.044**	ND>AD
IFOF-R	0.40	0.39	0.39	**0.048**	ND>AD
Inferior Longitudinal Fasciculus (ILF-)					
ILF-L	0.39	0.39	0.38	0.069	-
ILF-R	0.41	0.41	0.40	0.065	-
Uncinate Fasciculus (UF-)					
UF-L	0.37	0.36	0.36	**0.004**	ND>MCI, ND>AD
UF-R	0.36	0.35	0.35	0.175	-

Table 4.2. Group difference results for fractional anisotropy (FA) in *a-priori* tracts using the tract of interest approach.

	Radial Diffusivity			ANOVA	
	ND	MCI	AD	p-value	Post-hoc
Corpus Callusom (CC-)					
CC-Genu	0.97	0.96	1.03	**0.001**	ND<AD, MCI<AD
CC-Body	0.75	0.77	0.81	**0.001**	ND<AD, MCI<AD
CC-Splenium	0.49	0.51	0.55	**<0.001**	ND<MCI<AD
Cingulum (CCG-)					
CCG-L	0.63	0.65	0.70	**<0.001**	ND<MCI<AD
CCG-R	0.60	0.63	0.66	**<0.001**	ND<MCI<AD
Inferior fronto-occipital fasciculus (IFOF-)					
IFOF-L	0.65	0.67	0.69	**<0.001**	ND<MCI, ND<AD
IFOF-R	0.65	0.67	0.69	**0.001**	ND<MCI<AD
Inferior Longitudinal Fasciculus (ILF-)					
ILF-L	0.64	0.66	0.68	**<0.001**	ND<MCI<AD
ILF-R	0.61	0.62	0.64	**0.004**	ND<AD, MCI<AD
Uncinate Fasciculus (UF-)					
UF-L	0.68	0.72	0.77	**<0.001**	ND<MCI<AD
UF-R	0.66	0.69	0.75	**<0.001**	ND<MCI<AD

Table 4.3. Groups difference results for radial diffusivity (RD) in *a-priori* tracts using the tract of interest (TOI) approach.

TBSS vs. TOI comparison

For the purpose of comparing TBSS with TOI in terms of result interpretation, we calculated the percent overlap between the voxels located in the TBSS skeleton and each *a-priori* tract depicted in the TOI method (Figure 4.4d). We found small percent overlaps in every tract due to the "thinned-out" skeleton template used in TBSS. The lowest TBSS-TOI region overlap was found in the genu-CC (19.86% of the total *a-priori* tract mask) while the highest percentage overlap was found in the IFOF-R (30.13%).

In addition, we calculated the percent overlap of significant voxels depicted in TBSS with every tract in TOI (Figure 4.4e, Table 4.4). Since we only found significant TBSS results in the FA maps (and only in the ND vs. AD and MCI vs. AD comparison), we presented these overlaps in Table 4.4. As expected, we found higher significant result overlaps in the ND>AD comparison than in the MCI>AD comparison. The highest significant overlap was the left cingulum with 21.30% overlap (CCG-L in the ND-AD comparison) while the same tract showed the lowest percent overlap in the MCI-AD group comparison (0.73%). These

percent overlaps might be misleading when reporting results because the significant voxels in the skeleton represents a very small fraction of specific white matter tracts. That is, these results might not represent an overall integrity of the whole tract but smaller and regional (not tract specific) structural changes within the brain, which might be more suitable for describing anatomical or volumetric structural changes and not for specific tract-derived methods such as DTI.

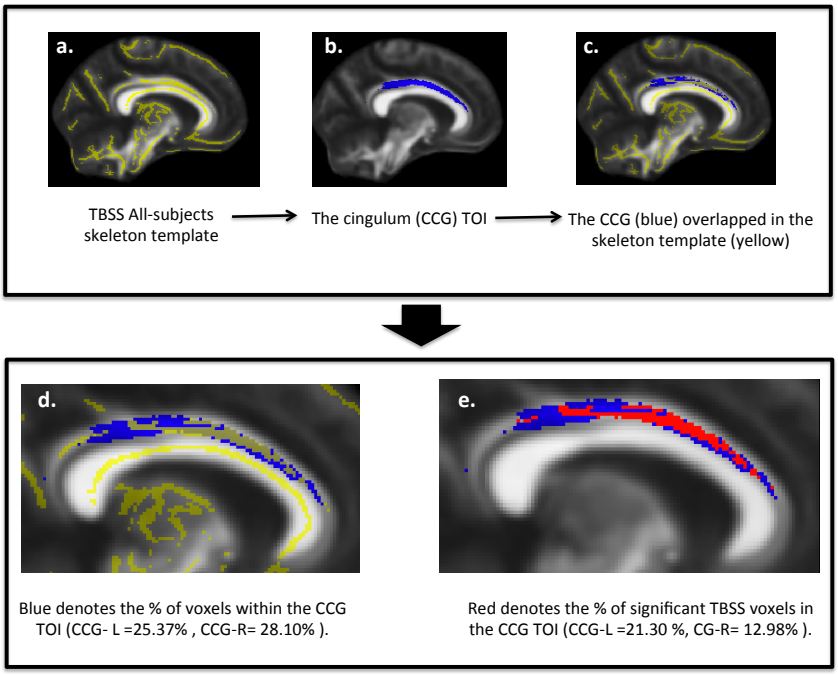

Figure 4.4. Overlapping descriptive representation of fractional anisotropy values in the cingulum using TBSS and TOI (ND>AD). The TBSS skeleton is depicted in yellow, blue depicts the *a-priori* tract of interest mask (the cingulum), and red denotes the overlapping significant voxels between the two methods.

	% TOI represented by the TBSS skeleton	% TOI represented by the significant TBSS voxels	
		ND > AD	MCI > AD
Corpus Callusom (CC-)			
CC-Genu	19.86%	11.11%	1.28%
CC-Body	22.89%	10.25%	0.77%
CC-Splenium	18.05%	10.81%	4.86%
Cingulum (CCG-)			
CCG-L	25.37%	21.30%	0.73%
CCG-R	28.10%	12.98%	7.11%
Inferior fronto-occipital fasciculus (IFOF-)			
IFOF-L	27.39%	14.79%	10.48%
IFOF-R	30.13%	13.28%	8.16%
Inferior Longitudinal Fasciculus (ILF-)			
ILF-L	27.62%	9.72%	4.26%
ILF-R	25.74%	10.20%	5.64%
Uncinate Fasciculus (UF-)			
UF-L	25.40%	15.65%	0.92%
UF-R	26.40%	11.48%	0%*

Table 4.4. Overlapping percentages between the cluster of voxels belonging to the TBSS skeleton and whole white matter TOI conduits (left column). The right columns indicate the significant voxels that overlap both methodologies (TBSS and TOI).

4.5 DISCUSSION

Currently there is no gold standard for processing and describing results using diffusion imaging data, thus the aim of this study was to characterize and compare the ability of two DTI processing methods: tract-based spatial statistics (TBSS) and tract of interest (TOI) to detect white matter differences between ND, MCI, and AD groups. Our objective was to identify whether different DTI data processing methods may account for inconsistent results when describing AD-related studies. We found that TBSS showed lower FA in AD group when compared to the ND group throughout the whole brain and to a lesser extent when compared to the MCI group. TBSS results also showed no significant differences when ND was compared to MCI nor in any RD group comparisons (ND vs. MCI, ND vs. AD, and MCI vs. AD) but with a marginal higher RD in the anterior fornix when AD was compared to ND ($p<0.08$ corrected). On the other hand, the TOI method found a

consistent white matter decline (AD<MCI<ND) when averaged FA and RD values were evaluated.

ND vs. AD

When examining FA, both TBSS and TOI showed a widespread white matter decline in the AD group when compared to the ND group. These results are consistent with previous findings (Damoiseaux et al., 2009, Acosta-Cabronero et al., 2010, Alves et al., 2012, Bosch et al., 2012) and indicate that different diffusion processing methodologies will provide similar results. However, the RD results differed among these methods. In TBSS, we did not find any group differences while TOI found higher RD in the AD group in all the *a-priori* white matter tracts. A possible explanation may be related to a peculiar flaw that TBSS has when projecting non-FA diffusion data into the skeleton. In the automated TBSS process, all the non-FA voxels (e.g. RD) that get projected into the skeleton are in the same location as the highest and perpendicular FA voxel location (Smith et al., 2006). Thus, the RD voxel values that get projected into the skeleton may contain arbitrary RD values (either higher or lower in diffusion characteristics) leading to a less inconsistent skeleton projection protocol. This will increase the variability when doing voxelwise statistical analyses because of unpredictable RD voxel value projections into the skeleton, which depend solely on FA information. Even though, FA and RD are proportional by definition, they describe different diffusion phenomena (Alexander et al., 2007, O'Donnell and Westin, 2011). Hence, we believe that this issue may account for inconsistent results previously reported in non-FA images when using TBSS (Acosta-Cabronero et al., 2010, Alves et al., 2012, Bosch et al., 2012).

To directly compare our FA results in both methodologies, we overlapped the TBSS significant voxels with the *a-priori* tract masks used in TOI (Figure 4.4, Table 4.4). We found very low percent overlaps as low as 9.72% in the left inferior longitudinal fasciculus and as high as 21.30% in the left cingulum. Thus, we believe that results describing white matter tract differences based on overlapping small cluster of voxels within specific white matter atlas may be inaccurate due to its very small percentage overlaps (up to 21.30%, in this case). Future DTI researchers who use TBSS or any whole brain imaging analysis should be aware of this and explicitly mention that the significant findings encompass only a projection or thinned-out overlap portion of a tract rather than reporting results in relation to whole white matter tracts. Alternatively, we suggest investigators to report their results in specific brain locations (e.g. temporal, frontal, occipital) rather than overlapping their findings within specific. Though this will not resolve the issue of standardizing white matter reports when using DTI, which is explicitly solved with the *a-priori* TOI methodology.

ND vs. MCI

In TBSS we did not find any significant results in FA nor RD, which are consistent with previous non-significant reports (Damoiseaux et al., 2009, Alves et al., 2012, Bosch et al., 2012, Teipel et al., 2012). In TOI, post-hoc analysis showed higher FA values only in the left uncinate fasciculus, which agrees with a previous report (Alves et al., 2012) and the large effect sizes of a meta-analysis report (Sexton et al., 2011). Interestingly, RD TOI results were significantly different in all the tracts, suggesting that RD is a more sensitive than FA for identifying white matter tract differences between these groups. However, these results differ from the TBSS as no RD group differences were found in any of the

group analyses. As previously discussed in TBSS, the variability of projecting arbitrary RD voxel values into the skeleton might lead to non-significant results, especially when comparing these since the MCI group is denoted as a transitional stage for higher likelihood of AD conversion. Thus, according to our results we believe that subtle micro-structural white matter changes may occur in the MCI group when compared to the ND and when using a "thinned-out" whole brain analyses with apparent non-FA projection flaws, this white matter integrity comparison may vanish.

MCI vs. AD

In TBSS, we found a widespread FA decline in the AD group when compared to the MCI but to a lesser extent than the ND-AD comparison. Similarly but more specific in TOI, post-hoc analyses showed that MCI presented higher FA values in the cingulum and uncinate fasciculus, which have been previously found in other reports (Zhang et al., 2007, Mielke et al., 2009, Liu et al., 2011). Even though both methods showed significant results, TBSS covers more brain locations than our *a-priori* TOI approach. One possibility for widespread results in TBSS is that in the FA skeleton, we are comparing the highest FA values that are projected into the skeleton. Thus, these results can be interpreted as an overall decline of the "highest FA" voxel values adjacent to the skeleton template but fails to report what happens with less anisotropic values that did not get projected into the common skeleton. Thus, this results suggests an overall FA decline in the AD group when compared to the MCI. In relation to RD, the TOI processing method showed to be more sensitive to white matter tract differences between AD and MCI. Post-hoc analyses showed that all the tracts have a significant higher RD in AD when compared to MCI. On the other hand, no changes were found with TBSS.

When comparing TBSS and TOI using our FA percentage overlap comparison, we found even smaller significant percent overlaps than in the ND-AD comparison due to lesser TBSS significant voxel regions. These percentage overlaps are as small as 1% in the left cingulum and as high as 10.48% in the left inferior fronto-occipital fasciculus. Again misleading information may be reported when TBSS results are overlapped with available white matter tract atlases. Interestingly, the tract with the lowest percentage overlap (the cingulum, 1%) showed a significant group difference in TOI. On the other hand, the highest percentage tract overlap (inferior fronto-occipital fasciculus) did not present significant differences in TOI. The inferior fronto-occipital fasciculus is one of the longest tracts that encompass many voxels and a possible explanation for significant findings in TBSS and not in TOI might be related to the statistical analysis used in TBSS. Our TBSS analysis performed non-parametric permutation-based statistical analyses (Winkler et al., 2014) in every voxel within a tract while TOI averages a specific diffusivity metric (either FA or RD) for each *a-priori* tract of interest. Thus, being the inferior fronto-occipital fasciculus one of the longest tracts, increased probability for false positive may occur when doing statistical comparison voxel-by-voxel as in the case of TBSS.

Final remarks

We found that when using diffusion-imaging data, differences between group populations can occur due to specific processing methods. In the case of TBSS this problem intensifies when non-FA measures (e.g. RD) are also under investigation. TBSS provides a more global and less tract-specific diffusion imaging methodology but it showed to be robust only for FA maps most likely due to its flaws when processing non-FA metrics (e.g. RD). Additionally when describing findings in TBSS, future investigators need to describe

clusters of significant voxels as belonging to a "portion" of a white matter tract or describe the location in relation to a more general description of brain regions rather than specifying whole white matter tracts. Alternatively, we suggest using *a-priori* hypotheses driven methods such as TOI. In this study, our *a-priori* TOI method showed lower diffusivity measures in relation to the progression stages of AD (AD<MCI<ND). This hypothesis driven method combines all the diffusivity voxel values (either FA or RD in this case) in relation to *a-priori* white matter tracts and averages an overall value, allowing a more standard description of the results. However, no voxel-by-voxel statistical analysis is performed deviating from whole brain exploratory analyses such as TBSS. Thus, future researchers need to make a concise decision on what method they should use based on the questions they want to answer. More exploratory processing methods (e.g. TBSS) might allow you to investigate broader regions yet it might increase the possibility for Type I error and might complicate the interpretation and description of the results. Alternatively, hypothesis-driven methods such as TOI can be used to explicitly describe results in relation to specific white matter tracts. However, these methods are more restrictive for exploratory whole brain analyses. It is also worth noting that in any diffusion processing methodology although diffusion imaging measures are sensitive to micro-structural changes *in-vivo*, a one-to-one relationship with cellular characteristics such as myelination quality, dendritic spine growth, axonal density, or glial cell density cannot be characterized due to the current imaging macro-scale resolution limitations (Concha, 2014, Walhovd et al., 2014).

Limitations

One limitation for comparing these methods is the different statistical analyses used for each method. While we performed non-parametric whole brain analyses using the general linear model in TBSS, we performed a parametric analyses of variance in our TOI method away from imaging space. However, the goal of this study was to characterize and discuss white matter differences between two completely different diffusion processing methods. Hence, alternating specific approaches to claim the usage of similar statistical analyses will deviate from each default diffusion processing methodology. It is also impossible to compare both methods with the same statistical analyses as whole brain TBBS uses non-parametric statistics in a voxels-by-voxel basis while TOI does statistics on averaged diffusivity values that contained many voxels belonging to a specific tracts. Non-parametric statistical comparisons could have been evaluated for the TOI method but we believe this deviates from a normal post-processing imaging protocol. Another limitations for both methods are the susceptibilities that arise when transformation the diffusion imaging data into a common MNI space. In relation to TBSS, these misalignments susceptibilities are intrinsically corrected by the thinning-out or skeletonizing processing step, as explained in the introduction and a previous report (Smith et al., 2006). However, these susceptibilities are not corrected when extracting *a-priori* masks in TOI based on the information of the atlas-based template. To overcome these limitations, we extracted white matter tracts from defined probabilistic atlases where the cores of these tracts were slightly thinned-out to include at least 0.25 probability of tract existence. We believe that this thresholding mitigates misalignment and smoothing mixed-tissue variations that may emerge at the edges of the *a-priori* TOI tracts. Another limitation in this study is the lack of

other diffusivity metrics such as axonal diffusivity (AxD) or mean diffusivity (MD). Our rationale for not using these metrics is the lack in interpretability in relation to our results. For example AxD represents the magnitude of highest diffusivity direction and previous Alzheimer's disease showed inconsistent reports with increased AxD (Acosta-Cabronero et al., 2010, Bosch et al., 2012) and others (Huang et al., 2007) showing decreased AxD in the AD group. In relation to MD, we believe it does not offer any additional information as its definition (the average of the three components of diffusion) is directly related to the calculation of FA, which is included in this study. Additionally, the increase of statistical analyses using other non-FA metrics would increase our error to encounter false positive results while decreasing an alpha for multiple comparison corrections. These diffusivity measures are also more biased to partial volume effects, crossing fibers, less anisotropic tissue, and its diffusion shape dependency (e.g. oblate, elongated cigars shape, and low diffusion spherical shapes might present similar axial diffusivity and mean diffusivity values).

4.6 CONCLUSION

We characterized and compared the ability of two DTI processing methods TBSS and TOI to differentiate white matter differences (by measures of FA and RD) in ND, MCI, and AD cohorts. Both methods reported lower FA in the AD group when compared to MCI and ND. However, TBSS did not find any RD differences between groups. This may be due to limitations found when processing and projecting non-FA (e.g. RD) values to FA-dependent skeletons. On the other hand in the TOI method, RD was more sensitive than FA in capturing diffusivity group differences in specific white matter tracts. However,

researchers should be aware of the information each diffusivity metric described and how it is processed within each method.

Hence, our results indicate that different DTI processing methods may explain inconsistent findings previously reported in relation to this pathology. For future white matter tract-specific investigations we suggest the use of TOI as it provides an *a-priori* driven hypothesis and a better interpretation of the results in relation to specific tracts. However, TOI might not be suitable when exploratory whole-brain analyses are under investigation. In this case, TBSS is a more feasible candidate yet future researchers should be aware that significant findings might be prone to Type I/II errors based on its voxel-by-voxel analysis, or when non-FA metrics (e.g. RD) are under investigation. Additionally when reporting results in TBSS, researchers should be aware that smaller cluster of significant regions cannot account for conclusions based on whole white matter tract conduits as previously been described because it might only represent a small portion of the white matter conduit.

Chapter 5 Preface:

This chapter presents the results of my first work using diffusion imaging and an *a-priori* tract-of-interest approach to characterize the effects of aerobic exercise. It extends my progress on understanding diffusion imaging and applying a hypothesis driven method to describe results in a more organized and scientifically sounded way, with results being described in relation to specific *a-priori* white matter tracts.

During this investigation we evaluated the associations between higher measures of cardiorespiratory level (by performing maximal oxygen test [VO_2peak]) and white matter tract integrity by measures of fractional anisotropy and radial diffusivity. Previous studies have shown positive relations between preserved white matter tract integrity and higher cardiorespiratory fitness levels but only in healthy non-demented cohorts. Studies in Alzheimer's disease populations lack the usage of diffusion tensor imaging to evaluate associations with cardiorespiratory fitness levels. Here, I expanded previous work done in the University of Kansas Alzheimer's Research Center beyond volumetric and functional connectivity.

Chapter 5

Cardiorespiratory fitness and white matter integrity in early Alzheimer's disease

5.1 ABSTRACT

Objective:

To investigate the relationship between cardiorespiratory (CR) fitness and the brain's white matter tract integrity using diffusion tensor imaging (DTI) in the Alzheimer's disease (AD) population.

Methods:

We recruited older adults in the early stages of AD (n=37; CDR=0.5 and 1) and collected cross-sectional fitness and diffusion imaging data. We examined the association between CR fitness (peak oxygen consumption [VO_2peak]) and fractional anisotropy (FA) in AD-related white matter tracts using two processing methods: a tract-of-interest approach and tract-based spatial statistics (TBSS). If results were significant, we also evaluated the association of CR fitness with subsequent diffusivity metrics (radial diffusivity [RD], mean diffusivity [MD], and axial diffusivity [AxD]). Similarly, we also evaluated whether cognitive scores were associated with preservation of white matter tract integrity.

Results:

The tract-of-interest approach showed that higher VO_2peak was associated with preserved white matter integrity in FA in the right inferior fronto-occipital fasciculus ($p=0.035$, $r=0.36$). We did not find a significant correlation using TBSS, though there was a trend for increased white matter integrity with higher VO_2peak measures ($p<0.01$ uncorrected). In relation to cognitive scores, none of our analyses reached significance yet we found a trend for increased processing speed with higher FA in the left inferior fronto-occipital fasciculus.

Conclusion:

Our findings indicate that higher CR fitness levels in early AD participants may be related with preserved white matter integrity in the progressed deterioration of AD. However to draw stronger conclusions, we encourage other investigators to explore further the relationship between CR fitness and white matter integrity in AD.

5.2 INTRODUCTION

Alzheimer's disease (AD) is a neurodegenerative disease and the most common cause of dementia. AD affects one in nine people over the age of 65 and one in three over the age of 85 (Thies et al., 2013). To date, there is no cure and post-mortem (Brun and Englund, 1986, Braak and Braak, 1991b) and *in-vivo* neuroimaging reports showed brain deterioration in AD as the disease progresses (Thompson et al., 2003, Sexton et al., 2011, Burggren and Brown, 2014). Current contemporary pharmacological treatments have also proven largely ineffective in attenuating AD-related brain degeneration. Thus, increasing research is focusing on lifestyle changes that could possibly mitigate this progressed deterioration. For instance, a growing hope is to include exercise as a daily activity, which improves one's overall cardiorespiratory (CR) fitness levels, and with that, brain health (Colcombe et al., 2006, Boots et al., 2014, Erickson et al., 2014).

In healthy older adults, higher levels of CR fitness are associated with a variety of benefits in the brain, namely preserved overall brain volume, hippocampal volume, white matter integrity, cognition, and overall brain health (Colcombe et al., 2003, Marks et al., 2007, Erickson et al., 2009, Johansen-Berg and Rushworth, 2009, Marks et al., 2011, Johnson et al., 2012b, Petersen and Posner, 2012). In the AD population, higher levels of CR

fitness have been associated with preserved brain volume (Burns et al., 2008, Petersen and Posner, 2012). More specifically, higher CR fitness levels have been associated with increased gray and white matter volumes in the parietal and medial temporal cortices (Honea et al., 2009, Tian et al., 2014a). However to our knowledge in the AD population, there has been no research associating CR fitness levels with diffusion tensor imaging (DTI) metrics on brain's white matter integrity.

DTI is a structural magnetic resonance imaging technique that characterizes the diffusivity of water molecules. In white matter, the movement of these molecules is anisotropic as it's mainly composed of axonal bundles and supportive glial cells that travel through specific directions (Walhovd et al., 2014). Disruption in these white matter tracts occurs during the aging process and may accelerate in the AD population (Salat, 2011). Previous DTI investigations on CR fitness in healthy non-demented cohorts showed that increased CR fitness is associated with preserved white matter integrity in frontal and temporal regions (Voss et al., 2012, Tian et al., 2014a). Moreover, relationships between increased levels of CR fitness and white matter tracts have been identified in the cingulum (Marks et al., 2007, Marks et al., 2011), uncinate fasciculus (Marks et al., 2007), and corpus callosum (Johnson et al., 2012b). However, there have been no DTI studies on CR fitness in individuals with AD. Thus in this study we characterized the relationship of CR fitness with white matter integrity using two DTI methods, an *a-priori* tract-of-interest approach and tract-based spatial statistics (TBSS) (Smith et al., 2006), The *a-priori* tract-of-interest method allows us to quantify the integrity of specific AD-related white matter tracts while TBSS allows for a global whole brain voxel-wise analysis.

5.3 METHODS

Sample

This study took place at the University of Kansas Alzheimer's Disease Center (KU ADC) as part of the Alzheimer's Disease Exercise Program Trial (ADEPT). For this investigation, we collected preliminary baseline data from individuals (n=40) enrolled in an ongoing aerobic exercise trial (Vidoni et al., 2012b). The final baseline sample included 37 sedentary older adults in the earliest stages of AD (CDR 0.5; n= 23, CDR 1; n= 14) after removing individuals due to substantial imaging distortion (n=1) or bad quality acquisition (n=2). Institutionally approved informed consent was obtained before enrollment. Additionally, this trial excluded individuals who have significant neurological diseases other than AD which include: major psychiatric disorders, major depression (Geriatric Depression Scale > 5), clinically-evident stroke or systemic infection, myocardial infarction or significant cardiovascular or respiratory disease, history of cancer in the last 5 years, current or past history of drug or alcohol abuse, insulin-dependent diabetes mellitus, and significant pain or musculoskeletal disorder that would limit exercise.

Clinical assessment

A clinician performed physical and neurological examinations and assessed each participant using a semi-structured interview given to the participant and a collateral source (e.g. participant's spouse or child). Medications, past medical history, family history, education, and demographic information were collected from the collateral source. Diagnostic classification was made at a consensus conference attended by neurologists, neuropsychologists, and nurse practitioners of the University of Kansas Alzheimer's Disease Center. Diagnostic criteria for AD included the gradual onset and progression of an

impairment in memory and at least one other cognitive and functional domain (NINCDS-ADRDA criteria) (McKhann et al., 1984a). The Clinical Dementia Rating (CDR) determined the severity of dementia (Morris, 1993). Only participants with a diagnosis of probable AD or who were classified with mild cognitive impairment likely due to probable AD with a Global CDR of 0.5 (very mild) or 1.0 (mild dementia) were included in the study. A battery of neuropsychological tests was also administered to each participant by trained psycometricians. Then, these scores were normalized using the uniform data set (UDS) previously described (Shirk et al., 2011) and divided into 5 cognitive domains (memory, attention, speed, executive function, and language) for further analysis.

CR fitness assessment

CR fitness was measured by peak oxygen consumption (VO_2peak [ml/kg/min]) during a graded treadmill exercise test using a Cornell modified Bruce protocol (Hollenberg et al., 1998, Burns et al., 2008). Each participant was asked to start walking on a treadmill while the speed and incline increased progressively. Only individuals who achieved a respiratory exchange ratio (RER) ≥ 1.0 were included in the study. Oxygen consumption was averaged over 15-second intervals, and the highest measurement was considered VO_2peak (Anderson et al., 2011, Vidoni et al., 2012b).

Neuroimaging

Magnetic resonance imaging (MRI) was collected at baseline within three weeks of the CR fitness assessment. The session included a high-resolution T1 image that was used for anatomic localization and to assess for gross anatomical differences with a high gray-white matter contrast (MPRAGE; 1x1x1mm voxels; TR = 2500, TE = 4.38, TI = 1100, FOV 256 x 256 with 18% oversample, 1mm slice thickness, flip angle 8 degrees). In addition, a

diffusion weighted sequence was designed to provide optimal results for this analysis while minimizing scanner duration for the participant. The diffusion weighted acquisition used a Siemens 3.0 Tesla Skyra MRI with a repetition time (TR)= 1000ms and echo time (TE)=90ms. Diffusion gradients were applied in 65 directions (b_0= 0 s/mm^2 and $b_{1\text{-}64}$= 1000 s/mm^2). Seventy-five 2-mm sections were acquired in at in-plane resolution of 128x128 with a 300mm field of view (FOV).

Imaging Analysis

We processed the diffusion weighted images using the FMRIB Software Library (FSL 5.0.4) (Smith et al., 2004a). The remaining 37 images were eddy-current corrected for small distortions and simple head motion by alignment of the diffusion weighted images to the b_0 image. Next, a brain extraction tool (BET2) was applied to strip the brain from the skull, and diffusivity FA, RD, MD, and AxD measures were calculated using DTIFIT and FSLMATHS, part of the FSL toolbox. FA provides a measure of degree of anisotropic diffusion ranging from 0 (perfectly isotropic) to 1 (perfectly anisotropic) and is related to an overall measurement of white matter microstructural integrity (Alexander et al., 2011). RD is a measure of perpendicular diffusivity and reflects changes in axonal diameter and myelination (Song et al., 2005). MD measures an overall measure of diffusion by averaging the three orthogonal components of diffusion while AxD measures the magnitude of diffusion in the principal diffusion direction (Alexander et al., 2007).

For the *a-priori* tract-of-interest method, each diffusivity measure was non-linearly registered, aligned, and transformed into a common 1x1x1mm standard MNI space template (FMRIB58), following the initial steps of TBSS processing pipeline before and skipping the skeletonizing step (Smith et al., 2006). Next, we performed a 2-mm smoothing

using FSLMATHS and to determine AD-related *a-priori* tracts, we extracted white matter binary tract masks from the Johns Hopkins University (JHU) probabilistic atlas after being registered to the common MNI space (Mori et al., 2005, Hua et al., 2008a). The following tracts previously reported to be associated with AD (Figure 5.1) were included and divided by hemisphere: the cingulum (CCG) (Xie et al., 2005, Zhang et al., 2007, Burzynska et al., 2010, Liu et al., 2011, Zhang et al., 2014), the inferior fronto-occipital fasciculus (IFOF) (Gold et al., 2010, Teipel et al., 2010, Alves et al., 2012), the superior longitudinal fasciculus (SLF) (Liu et al., 2011, Sexton et al., 2011, Alves et al., 2012, Bosch et al., 2012), and the uncinate fasciculus (UF) (Liu et al., 2011, Sexton et al., 2011, Bosch et al., 2012). For every subject's FA and subsequent diffusivity metric (e.g. RD, MD, or AxD), we then "masked in" every tract, included only voxels thresholded at FA values higher than 0.2, and calculated an averaged diffusivity value on every tract. Hence, every participant contained an overall diffusivity value for every tract, which was consequently fed into a statistical program for further statistical analysis.

In addition to the tract-of-interest method, we also performed a TBSS analysis (Smith et al., 2006). First, we created FA images by fitting the tensor model to the raw diffusion data using FDT, part of FSL. After brain extraction, all subject's FA data were aligned into a common MNI space using nonlinear transformations (Andersson et al., 2007). Next, all subject's FA data were thinned out to create a mean FA skeleton which represents the center of all the tracts common to the group. Then, each subject's diffusivity metrics were projected into this skeleton and thresholded to include only voxel with FA values higher than 0.2. The resulting data was fed into RANDOMISE, a tool for non-parametric permutation inference on neuroimaging data (Winkler et al., 2014). Similar to

the tract-of-interest approach, FA was the primary diffusivity metric with subsequent measures of RD, MD, and AxD.

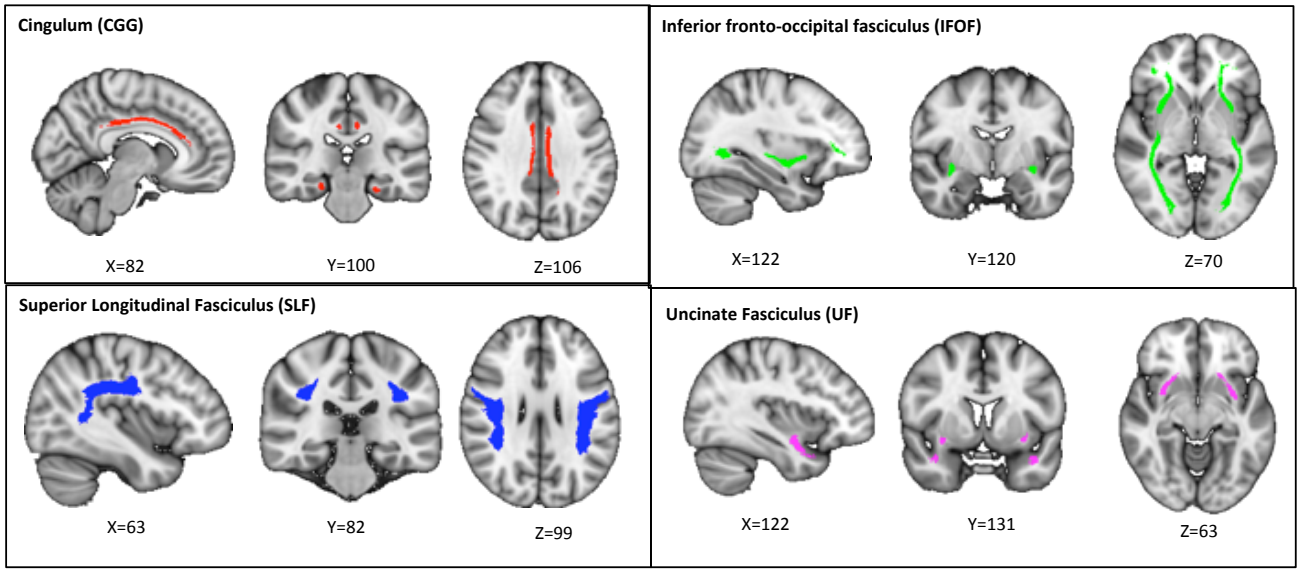

Figure 5.5. AD-related *a-priori* white matter tracts: the cingulum (red, top left), the inferior fronto-occipital fasciculus (green, top right), the superior longitudinal fasciculus (blue, bottom blue), and the uncinate fasciculus (pink, bottom right). Tract representation is shown using the standard MNI brain in radiological orientation.

Statistical analysis

For the tract-of-interest approach, statistical analyses were conducted using SPSS 22.0 (IBM Corp., Armonk, NY). As our primary diffusivity measure, we tested partial correlations of FA values with VO_2peak on every *a-priori* tract-of-interest, controlling for age and gender. A total of 8 correlation comparisons were performed splitting our *a-priori* tracts by hemisphere (left and right). These planned comparisons were carefully selected and are focused only in a few scientifically sensible comparisons. Thus, we do not correct for multiple comparisons, set our alpha to 0.05 and, treated each non-overlapping *a-priori* tract-of-interest as an independent analysis, as previously suggested (Keppel and Wickens, 2004). For whole brain TBSS analyses, we performed non-parametric analyses using permutation based statistical inference known as randomise, which is part of FSL (Winkler

et al., 2014). We assessed linear correlations between VO_2peak and FA (our primary diffusivity metric) controlling for age and gender and set the number of permutations to 5000 using threshold-free-cluster-enhancement. We set our alpha to be 0.05 corrected. Subsequent similar analyses were performed in the other diffusivity metrics (RD, MD, and AxD). To determine the relationship between cognition and white matter integrity, we also performed partial correlations (correcting for age and gender) of the diffusivity measure in the *a-priori* white matter tracts with mean z-scores of the uniform neuropsychological data set (UDS) stratified in 5 cognitive categories: memory, attention, speed, executive function, and language (Shirk et al., 2011).

5.4 RESULTS

Demographics

Table 5.1 summarizes the demographics, physical, and CR fitness characteristics of the 37 participants included in the final analysis.

	Mean (STDEV)
Demographics	
Age (n=37)	72.35 (7.9)
Female (#,%)	14 (37.8)
MMSE	25.6 (3.3)
CDR Global = 0.5 (#,%)	25 (67.6)
CDR Sum of Boxes	3.4 (1.5)
Education (years)	15.4 (3.6)
Fitness and Body measures	
BMI	26.9 (4.1)
Lean Mass (kg)	47.6 (10.2)
VO_2peak (ml/kg/min)	21.6 (5.1)

Table 5.1. Participants' demographics and fitness characteristics.

CR fitness and white matter integrity

In the tract-of-interest analysis, we found a significant correlation between increased FA and higher VO_2peak lateralized to the right inferior fronto-occipital fasciculus (r=0.358, p=0.035), after controlling for age and gender (Table 5.2, Figure 5.2). We did not find significant correlations with VO_2peak and MD, RD, or AD, however there was a trend for decreased RD with higher VO_2peak in the right cingulum (r=-0.315, p=0.065) and the right inferior fronto-occipital fasciculus (r=-0.313, p=0.067) (Table 5.3).

White matter tract:	Fractional Anisotropy
Cingulum	
Left	0.48 (0.04)
Right	0.42 (0.04)
Inferior Fronto Occipital Fasciculus	
Left	0.41 (0.03)
Right	0.41 (0.03)*
Superior Longitudinal Fasciculus	
Left	0.41 (0.03)
Right	0.41 (0.03)
Uncinate Fasciculus	
Left	0.39 (0.03)
Right	0.40 (0.03)

Table 5.2. Averaged fractional anisotropy values for every *a-priori* white matter tract (SD).
* denotes p<0.05 during the partial correlation of FA with VO_2peak analysis.

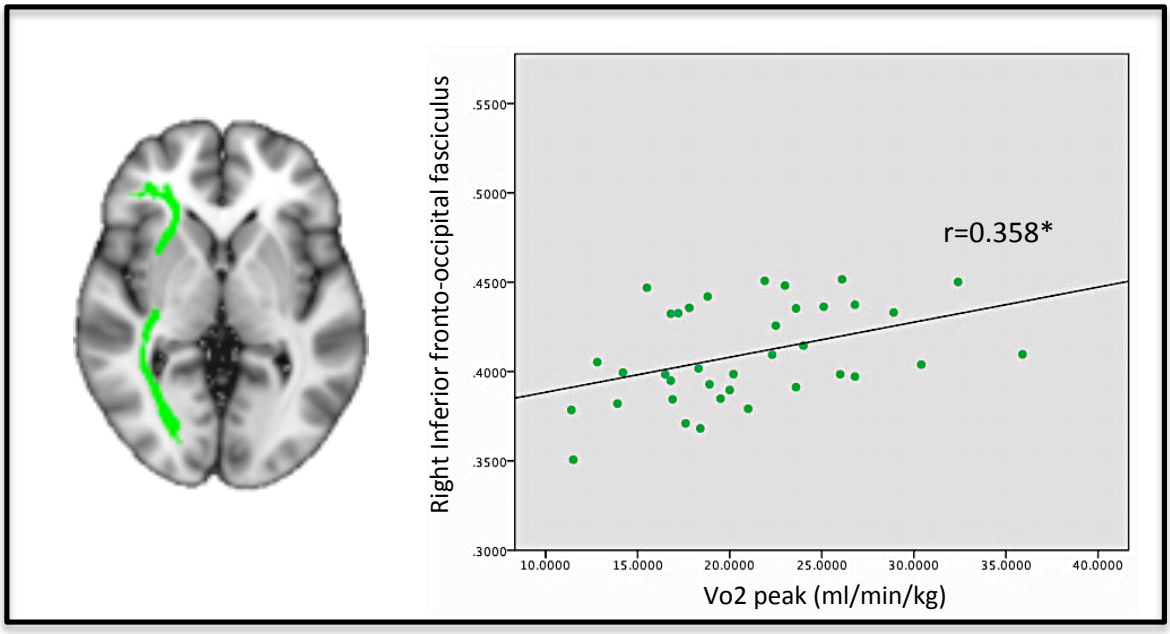

Figure 5.2 Linear fit plot for VO_2peak and fractional anisotropy (FA) in the right inferior fronto-occipital fasciculus (green), a white matter tract that passes through the frontal, temporal, and occipital lobe. The tract-of-interest is overlaid on a T1 MNI template. * denotes p<0.05 and orientation is radiological (left is right).

The TBSS analysis did not show any significant partial correlations of the diffusivity metrics (FA, RD, MD, or AxD) with VO_2peak at a statistical threshold of p<0.05 corrected. However as an exploratory measure at an uncorrected threshold of p<0.01, a positive association of FA values with VO_2peak were visible more predominantly in the right hemisphere with sparse regions in the left side (Figure 5.3).

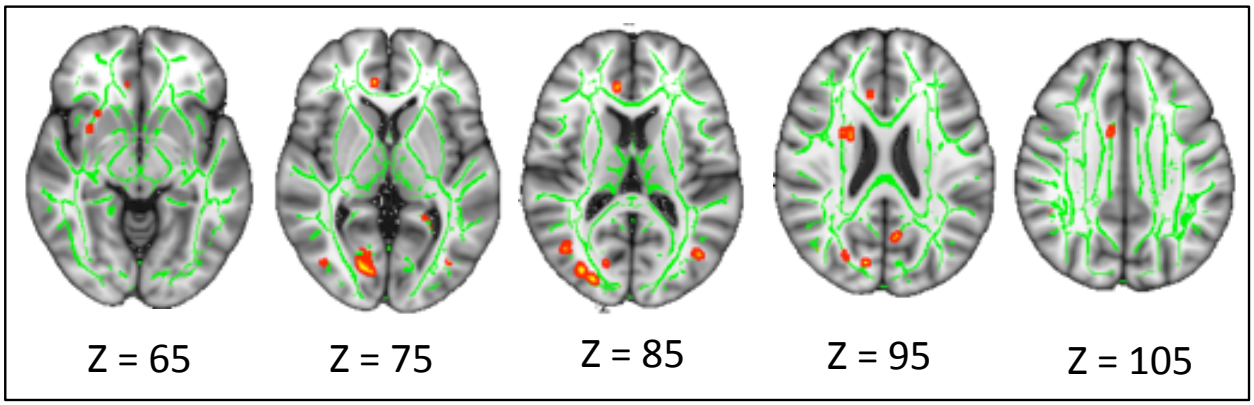

Figure 5.3. TBSS results associating FA with VO_2peak. Red regions depicts thickened results at p<0.01 uncorrected overlapped in the green skeleton and the MNI template.

Cognitive Measures

None of the cognitive measures were significantly associated with any diffusivity metric, however there was a trend for a positive relationship of increased processing speed with higher FA in the IFOF on the left hemisphere (p=.092, r=.293).

White matter tract:	Radial Diffusivity	Mean Diffusivity	Axial Diffusivity
Cingulum			
Left	0.55 (0.06)	0.76 (0.05)	1.20 (0.05)
Right	0.59 (0.06)$^{+}$	0.76 (0.04)	1.13 (0.05)
Inferior Fronto Occipital Fasciculus			
Left	0.69 (0.08)	0.88 (0.07)	1.27 (0.06)
Right	0.70 (0.07)$^{+}$	0.89 (0.06)	1.29 (0.06)
Superior Longitudinal Fasciculus			
Left	0.55 (0.06)	0.88 (0.07)	1.18 (0.06)
Right	0.59 (0.06)	0.88 (0.07)	1.19 (0.06)
Uncinate Fasciculus			
Left	0.55 (0.06)	0.9 (0.09)	1.25 (0.08)
Right	0.59 (0.06)	0.88 (0.07)	1.23 (0.07)

Table 5.3. Subsequent correlations of other diffusivity metrics (SD) on every tract-of-interest. $^{+}$denotes p<0.07.

5.5 DISCUSSION

In participants in the early stages of AD, we found that higher levels of CR fitness were associated with increased white matter integrity in a tract that travels from the occipital region to the temporal lobe. This tract is known as the inferior fronto-occipital fasciculus and the findings were lateralized to the right hemisphere. To our knowledge, this is the first study to demonstrate an association between CR fitness and white matter tract integrity in older adults in the early stages of AD. Thus we encourage future research in AD to explore these findings further to compare and validate our results.

Cardiorespiratory fitness impacts brain health in a variety of ways. In animal models, previous studies showed that aerobic exercise attenuated age-related decreases in hippocampal neurogenesis, potentially delayed the onset of AD, reduced amyloid beta deposition and pro-inflammatory cytokines, and enhanced levels of brain-derived

neurotropic factors (for a review, (Voss et al., 2013b)). In humans, higher CR fitness levels were associated with better cognition, decreased risk for early AD and preserved brain volumes (Hayes et al., 2013). We have previously identified a relationship between CR fitness and larger brain volumes in individuals with early AD (Burns et al., 2008), more specifically in the parietal and medial temporal lobes (Honea et al., 2009). Furthermore, in a longitudinal analysis we found that increased CR fitness over two years was related to lower rates of medial temporal atrophy (Vidoni et al., 2012a). Now we expanded our investigation beyond volume, using diffusion imaging.

Recent diffusion imaging studies in non-demented individuals found positive associations with higher VO_2peak levels and preserved white matter integrity in the cingulum (Marks et al., 2007, Marks et al., 2011), the uncinate fasciculus (Marks et al., 2007), and along the frontal regions of the brain (Voss et al., 2012). However and to our knowledge none of these reports identified a relationship of higher CR fitness levels and preserved white matter integrity in the inferior fronto-occipital fasciculus, the significant finding in this AD-specific study. This tract is known to be one of the longest white matter bundles in the brain connecting parts of the occipital, temporal, and frontal lobes, thus making it difficult to isolate when conducting whole brain white matter analyses integrity (e.g. TBSS). Hence to overcome this problem, we performed an *a-priori* tract-of-interest approach. The exact role for this tract is still under debate, but previous studies have shown that the integrity of this tract deteriorates with AD (Alves et al., 2012, Bosch et al., 2012, Yu et al., 2014). However, this specific tract does not present the strongest AD-related white matter deterioration. Other tracts such as the superior longitudinal fasciculus, the cingulum, and the uncinate fasciculus have a stronger AD-related

deterioration association as shown by large effect sizes in a previously published meta-analysis report (Sexton et al., 2011). Thus, a possible interpretation for our findings is that higher levels of CR fitness might act as a neuro-protective mechanism for slowing down the progression of AD, especially in white matter tracts that have not been fully compromised. Though, the neuro-protective effects of higher CR fitness levels may also occur in early-deteriorated tracts (e.g. the superior longitudinal fasciculus, the cingulum, and the uncinate fasciculus) but in healthy non-demented adults with no symptoms of AD, as previously described (Marks et al., 2007, Marks et al., 2011, Voss et al., 2012, Tseng et al., 2013). However to draw more valid conclusions, we encourage other researchers to explore further this question in a larger sample while including participants with wider range of CR fitness levels because our sample only included sedentary early AD participants with lower CR fitness levels.

Another interesting finding is that our result was lateralized to the right hemisphere. Only one other CR fitness report specified a left lateralized finding in the cingulum (Marks et al., 2011), while others did not report any hemispheric lateralization (Johnson et al., 2012b, Voss et al., 2012, Tian et al., 2014b). Another study also suggested that cortical degeneration in AD occurs faster in the left hemisphere, but mainly in gray matter (Thompson et al., 2003). However, a meta-analysis indicated no differences in white matter integrity between hemispheres among non-demented, mild cognitive impairment, and AD groups (Sexton et al., 2011). Supporting our right lateralized results, a previous DTI study showed that FA values in the right splenium and genu mediated cognitive tasks in healthy older adults (Madden et al., 2009). Though in our study, we did not find any cognitive relationships with increased integrity in the *a-priori* tracts-of

interest. Thus more studies are needed to explore hemispheric dominance further in regards to the relationship between CR fitness, white matter, and the possible relationships with cognition.

In regards to the diffusion imaging processing methodology, we performed TBSS analyses to compare our results with previous published work in non-demented participants (Johnson et al., 2012b, Voss et al., 2012, Gons et al., 2013) but our results did not show any significant results. While TBSS is the most commonly used analysis technique, its method is limited to a skeletonized white matter evaluation, which represents only the highest and perpendicular FA voxel intensities projected along each voxel within the skeleton (Bach et al., 2014). These and other TBSS considerations have been previously reported elsewhere (Zalesky, 2011, Keihaninejad et al., 2013, Bach et al., 2014). Hence, we also performed *a-priori* tract-of-interest analyses, which allowed us to quantify diffusivity metrics on specific tracts previously implicated in AD (Sexton et al., 2011, Alves et al., 2012, Bosch et al., 2012, Zhang et al., 2014). However, the tract-of-interest analysis may also be susceptible to partial volume effects, given enlarged ventricles and atrophy, which are common in older adults with early AD. Hence to overcome these limitations, we only included voxels with higher anisotropy values (FA > 0.2) and reduced our tract masks to include only voxels with a higher probability of existence based of the white matter probabilistic atlas (Hua et al., 2008a).

Within other limitations of this study is the lack of a non-demented control group because this investigation was conducted with preliminary baseline data from individuals enrolled in an ongoing aerobic exercise trail. Non-demented controls could have helped identify the effects of CR fitness on brain's white matter integrity independent of the AD

pathology, and future studies should include both groups. We also did not have individuals with a broader range of dementia severity, thus we could not tested for a relationship of disease progression or severity with fitness-related diffusion change. Additionally, we only recruited participants that are sedentary as determined by a telephone assessment of physical activity (Mayer et al., 2008, Vidoni et al., 2012b). A wider range of participants (sedentary and active) would have ideally added a better statistical estimation of the AD population. Another limitation is that we did not control for white matter lesions (WMLs) because we did not collect high contrast FLAIR images. However after inspecting every image for noticeable WMLs, we also performed a threshold criterion to only include voxels with FA values higher than 0.2. This criterion would ideally exclude highly isotropic voxels, which may be contaminated due to unperceived WMLs. Finally, we need to acknowledge that during the *a-priori* tract-of-interest approach we did not correct for multiple comparisons. Even though we recognize that this statistical setup has a higher chance of making Type I errors, we believed that this extra statistical power is acquired based on a carefully planned *a-priori* hypothesis driven experiment.

5.6 CONCLUSION

We assessed the relationship of CR fitness with white matter integrity in individuals with early-stage AD. We found a positive association between CR fitness levels and white matter integrity in the right inferior fronto-occipital fasciculus, independent of age and gender. These results suggest that increased CR fitness might positively affect white matter integrity even after the onset of Alzheimer's disease. To our knowledge, this is the first diffusion imaging study in the AD population that aims to characterize the association

between CR fitness levels and white matter tract integrity. Thus, we encourage future investigations on this matter so we can draw stronger conclusions on the neuro-protective effects of exercise and higher CR fitness in white matter and brain health.

Chapter 6 Preface:

Aerobic exercise activity may improves brain health, however, there are a lack of interventional studies quantifying the level of exercise needed to undergo neuro-protective change. Thus, the aim of this chapter was to investigate the effects of different exercise dose intensities on *a-priori* exercise-related gray matter regions and white matter tracts. However, due to the small sample size with longitudinal imaging exercise data (n=10) I could not statistically evaluate group differences in the 4 exercise groups, and as a complementary alternative, I investigated the relationships between total exercise duration and changes in volumetric gray matter cortical segmentations and diffusivity measures of white matter tracts.

Chapter 6

A longitudinal assessment of brain neuroplasticity and exercise intensity in healthy older adults: a 26-week exercise intervention study.

6.1 ABSTRACT

Objective

To investigate the effects of different aerobic exercise doses on brain's gray matter structures and white matter tracts on healthy non-demented older adults who underwent a 26-week aerobic intervention program.

Methods

At baseline and follow-up, brains imaging data, cardiorespiratory measures and exercise time duration were assessed in healthy non-demented older adults (CDR = 0, n=10, age_{mean}= 73.2). Brain imaging data included structural gray matter cortical segmentations and white matter diffusivity measures (fractional anisotropy [FA] and radial diffusivity [RD]) collected at baseline and follow-up. Similarly, cardiorespiratory fitness (CR) levels were measured by peak oxygen consumption based on body weight (VO_2peak [ml/kg/min]) before and after the intervention program. We also collected exercise time duration, which indicated the total amount of minutes an individual exercised in the entire intervention program. We evaluated the associations of longitudinal volumetric and diffusion imaging changes with changes in VO_2peak and total exercise duration using partial correlations and controlling for age and scanner type.

Results

We did not find any significant correlations between changes in gray matter volumes or white matter diffusivity metrics (FA or RD) and changes in VO_2peak ($p>0.05$). In relation to exercise time duration, longer durations were positively associated with decreased measures of RD in the genu of the corpus callosum ($r=-0.85$, $p=0.01$), denoting

preservation of white matter tract integrity. Conversely, a decrease in RD was also associated with longer durations in the right cingulum ($r=0.75$, $p=0.03$).

Conclusion

Our findings indicate that longer duration of aerobic exercise may be neuro-protective for specific white matter tracts such as the genu of the corpus callosum. Conversely, increased aerobic exercise duration was also associated with increased RD in the right cingulum, probably denoting age-related or disease-related deterioration. However due to our small sample size and the lack of exercise dose-intensity evaluations, we encourage others to investigate this matter so better conclusion can be made in relations to exercise dose intentisy and brain health.

6.2 INTRODUCTION

Age-related brain deterioration is associated with cognitive decline in older populations leading to increased risk for neurodegenerative diseases such as Alzheimer's disease (Hedden and Gabrieli, 2004). By 2050, the number of older adults (65 years and over) will increase almost 3-fold, from 524 million people (8% of the world's population) to 1.5 billion (representing 16% of the world's population) (Hebert et al., 2013, Pallin et al., 2014). Thus, strategic treatments are needed to slow down cognitive decline, improve brain health, and consequently quality of life. A potential alternative treatment is to maintain a healthy lifestyle with the inclusion of routinely aerobic exercise. Besides the general benefits of exercise to improve general health (e.g. reduce cardiovascular risks, reduce morbidity, and mortality) (Haskell et al., 2007), exercise has been previously associated with improved cognition and preserved brain health (see reviews (Hayes et al.,

2013) and (Voss et al., 2013b)). In older adults, meta-analysis reports showed that physical activity improves cognitive domains such as processing speed, executive function, and memory (see reviews (Colcombe and Kramer, 2003, Smith et al., 2010, Erickson et al., 2014)). Interestingly age-related gray matter volumes (Colcombe et al., 2006, Erickson et al., 2010, Floel et al., 2010, Gow et al., 2012) and white matter diffusivity metrics (Marks et al., 2011, Gow et al., 2012, Johnson et al., 2012b, Voss et al., 2012, Tian et al., 2014a) are also positively associated with higher exercise activity. However, the exercise dose intensity sufficient to affect brain structure remains unknown with only few studies reporting findings in this matter (Erickson et al., 2010, Ruscheweyh et al., 2011). Hence, giving the lack of interventional studies to distinguish the effects of exercise dose intensity in the brain, the aim of the study was to characterize the influence of three interventional aerobic exercise routines, representing 50%, 100%, and 150% of the recommended dose on brain structure. For older adults, current recommendations suggest performing moderate-intensity exercise for a minimum of 30 mins, five days a week or a vigorous-intensity activity for 20 mins on three days per week (Nelson et al., 2007). However, the effects of different exercise doses on brain's neuroplasticity remained unknown.

Thus, we hypothesize that previously exercise related gray matter regions (precuneus, parahippocampal, entorhinal, caudal middle frontal, caudal anterior cingulate, rostral anterior cingulate, rostral middle frontal, superior parietal) and white matter tracts (corpus callosum, cingulum, superior longitudinal fasciculus, and uncinate fasciculus) may have a positive relationship with longer exercise time durations.

6.3 METHODS

Participants

As part of the trail of exercise on aging and memory program (TEAM; https://clinicaltrials.gov/, NCT01129115), we randomized sedentary healthy older adults (65 years of age and older) without cognitive impairment into a 26-week randomized control trail of aerobic exercise (treadmill walking). Based on the recommendations from the American College of Sports and Medicine (ACSM) (Nelson et al., 2007), we randomly assigned the participants in four groups with specific exercise dose intensities: no exercise (controls, n=25), 75 minutes per week (n=25), 150 minutes per week (n=27), and 225 minutes per week (n=24). The goal of the exercise trail was to keep the exercise intensity consistent across groups while altering the exercise dose by duration. Clinical assessments, cardiorespiratory fitness, and functional health were measured at baseline and post-intervention. Unfortunately due to funding limitations, our brain imaging acquisition at baseline and follow-up was assessed only in 10 participants (controls=3, 75min/week=5, 150min/week=1 , 225 min/week=1).

Clinical assessment

After obtaining informed consent approved by the University of Kansas Medical Center Institutional Review Board (#11883) in potential participants, clinicians performed a full physical and neurological examination, a review of past medical history, and assessed the exclusion of dementia using the Clinical Dementia Rating (CDR) (Morris, 1993, Vidoni et al., 2012b). For the inclusion criteria, participants had to be at least 65 years of age, sedentary or underactive, free of cognitive impairment of any etiology and possess adequate vision and hearing to participant in cognitive testing (Mayer et al., 2008). In

addition, participants should not be insulin-dependent and were without recent history (<2 years) of major cardiorespiratory, musculoskeletal or neuropsychiatric impairment.

Intervention

For the exercise intervention groups, participants were instructed not to start or stop new regular physical activity for the duration of the study. The control group was also asked not to change their previous physical activity. Exercisers began their aerobic exercise activity at their nearest Young Men's Christian Association of Greater Kansas City (YMCA) location under the guidance of personal trainers (Vidoni et al., 2012b). All intervention groups were set a goal of 60 minutes at week 1 with increases of 21 mins. per week until they achieved their allocated exercise duration routine (e.g. 75, 150, or 225 min/week) over 3-5 days a week. An exercise notebook was provided to log their weekly activity, exercise intensity, and the exercise daily duration. Exercise intensity was prescribed as a target heart zone based on a percentage of heart rate reserve (HRR) above resting heart rate. During the first 4 weeks, the target heart rate zone was 40-55% of HRR. In weeks 5-18, the target zone was 50-60% of HRR and during weeks 19-26, the target heart rate was 60-75% of HRR. We selected a 26-week intervention period to maximize physiological adaptation without overburdening participants and based on the recommendations of previous reports (Colcombe et al., 2006, Ruscheweyh et al., 2011).

Physical activity assessment

Physical activity assessments were measured by peak oxygen consumption based on body weight (VO_2peak [ml/kg/min]), a direct measurement of cardiorespiratory fitness, during a graded treadmill exercise test using a Cornell modified Bruce protocol for older adults (Hollenberg et al., 1998, Burns et al., 2008). The participants were asked to start

walking on a treadmill while the speed and incline increased progressively. Only individuals who achieved a respiratory exchange ratio (RER) ≥ 1.0 were included in this evaluation. If the participant did not achieve an RER of 1.0, the test was repeated on a different day. Oxygen consumption was averaged over 15-second intervals and the highest measurement was considered VO_2peak. The collection of these data and other anthropomorphic measures are explained in more detailed in a previous publication (Vidoni et al., 2012b).

Neuroimaging

Magnetic resonance images were collected at baseline within 3 weeks of the CR fitness assessment in a Siemens 3.0 Tesla Skyra MRI machine. The session included a high-resolution T1 MPRAGE image for anatomic localization and gray matter segmentations (MPRAGE; 1x1x1mm voxels; TR = 2500, TE = 4.38, TI = 1100, FOV 256 x 256 with 18% oversample, 1mm slice thickness, flip angle 8 degrees). In addition, diffusion weighted images were collected using a repetition time (TR)= 1000ms and echo time (TE)=90ms. Diffusion gradients were applied in 65 directions (b_0= 0 s/mm^2 and $b_{1\text{-}64}$= 1000 s/mm^2). Seventy-five 2-mm sections were acquired in at in-plane resolution of 128x128 with a 300mm field of view (FOV).

Imaging Analysis

Cortical FreeSurfer Segmentation

After manually checking every T1 MPRAGE structural image, we performed a longitudinal volumetric segmentation using "recon-all" as part of the FreeSurfer software suite (FreeSurfer 5.2.3) for imaging analysis. The technical details of these procedures are described in prior publications (Dale and Sereno, 1993, Dale et al., 1999, Fischl and Dale,

2000, Fischl et al., 2001, Fischl et al., 2004, Han et al., 2006, Jovicich et al., 2006). Briefly, this procedure included an automated Talairach transformation, and segmentations of the white matter and deep gray matter volumetric structures based on a surface-based stream (Fischl et al., 2002, Fischl et al., 2004). Due to its computationally intensive procedure, we submitted our imaging segmentation to the high performance computing batch system at the Information and Telecommunication Technology Center (ITTC), which is part of The University of Kansas.

Once the segmentations were completed for every image, we extracted the volumetric measures of cortical areas previously related to exercise and exercise intensity (Erickson et al., 2010, Ruscheweyh et al., 2011, Braskie et al., 2014, Coelho et al., 2014). These segmentations included the left and right measures of the precuneus, parahippocampal, enthorinnal, caudal middle frontal, caudal anterior cingulate, rostral anterior cingulate, rostral middle frontal, and superior parietal cortices (Figure 6.1). Then, volumetric percent changes ($100*[T_{follow\text{-}up} - T_{baseline}]/T_{baseline}$) were calculated and fed to SPSS for statistical evaluations.

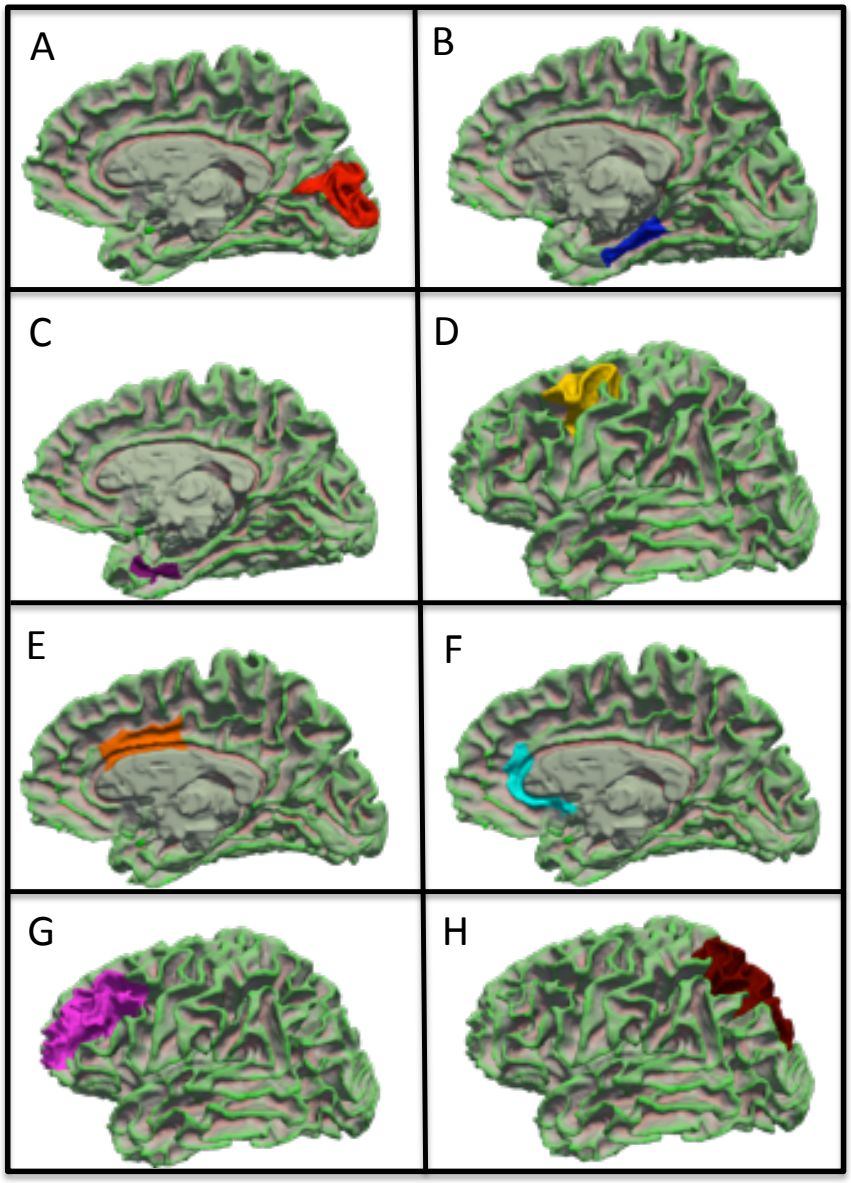

Figure 6.1. Volumetric region of interest segmentations overlaid in a green cortical template. The following cortices are: the precuneus (red, A), parahippocampal (blue, B), enthorinal (purple, C), caudal middle frontal (yellow, D), caudal anterior cingulate (orange, E), rostral anterior cingulate (turquoise, F), rostral middle frontal (pink, G), and superior parietal (brown, H) cortices.

Diffusion Tensor Tract-of-Interest (TOI)

We pre-processed the diffusion weighted images using the FMRIB Software Library neuro-imaging tools (FSL 5.0.4) (Smith et al., 2004a). After manually inspecting our diffusion weighted images, we applied eddy current correction for small distortions and simple head motion, by alignment the diffusion weighted images to the non-diffusion b_0

image. Next, brain extraction tool (BET2) was applied to strip the brain from the skull, and diffusivity FA and RD images were calculated using DTIFIT. As suggested by a recent article in relation to longitudinal data, interpolation asymmetries might arise when co-registering and resampling follow-up images to their baseline images. Hence, the choice of a halfway co-registration method will result in an unbiased template towards any single point (Keihaninejad et al., 2013). So as previously suggested, for every participant we linearly registered the baseline and follow-up images to a halfway registration point, using FLIRT and MIDTRANS, which are part of the FSL tools (Jenkinson and Smith, 2001, Jenkinson et al., 2002). Then, we non-linearly registered, aligned, and transformed every image to a most representative template using diffeomorphic transformations (Avants et al., 2011) and the ANTs registration tools (e.g. buildtemplateparallel.sh), as previously suggested (Schwarz et al., 2014). Next, we warped the most representative template into the MNI space and deformed all previously co-registered images to the common 1x1x1mm standard MNI space template (FMRIB58_FA_1mm). At this stage, we created a mean FA image, skeletonized it, and we finally projected all subject's FA data onto a mean skeleton as stated in steps 3 and 4 for the tract-based spatial statistics processing pipeline (Smith et al., 2006).

Then we overlapped the skeletonized image to particular *a-priori* white matter tracts. To do so, we generate our white matter *a-priori* tracts-of-interest (TOI) masks from the Johns Hopkins University probabilistic white matter atlas (Mori et al., 2005). We believe this approach is more tract-specific and has the advantage of explicitly showing results in relation to specific whole conduits of white matter tracts. We included the following tracts because they have been reported as being positively associated with exercise: corpus callosum, cingulum, superior longitudinal fasciculus, and uncinate

fasciculus (Marks et al., 2011, Gow et al., 2012, Johnson et al., 2012b, Tian et al., 2014a) (Figure 6.2). Average FA and RD values were computed from every skeleton voxel that overlapped specific tract at baseline and follow-up (Figure 6.3). Additionally percent change FA/RD measure were calculated ($100*[T_{follow\text{-}up}-T_{baseline}]/T_{baseline}$) and fed into SPSS for further statistical analysis.

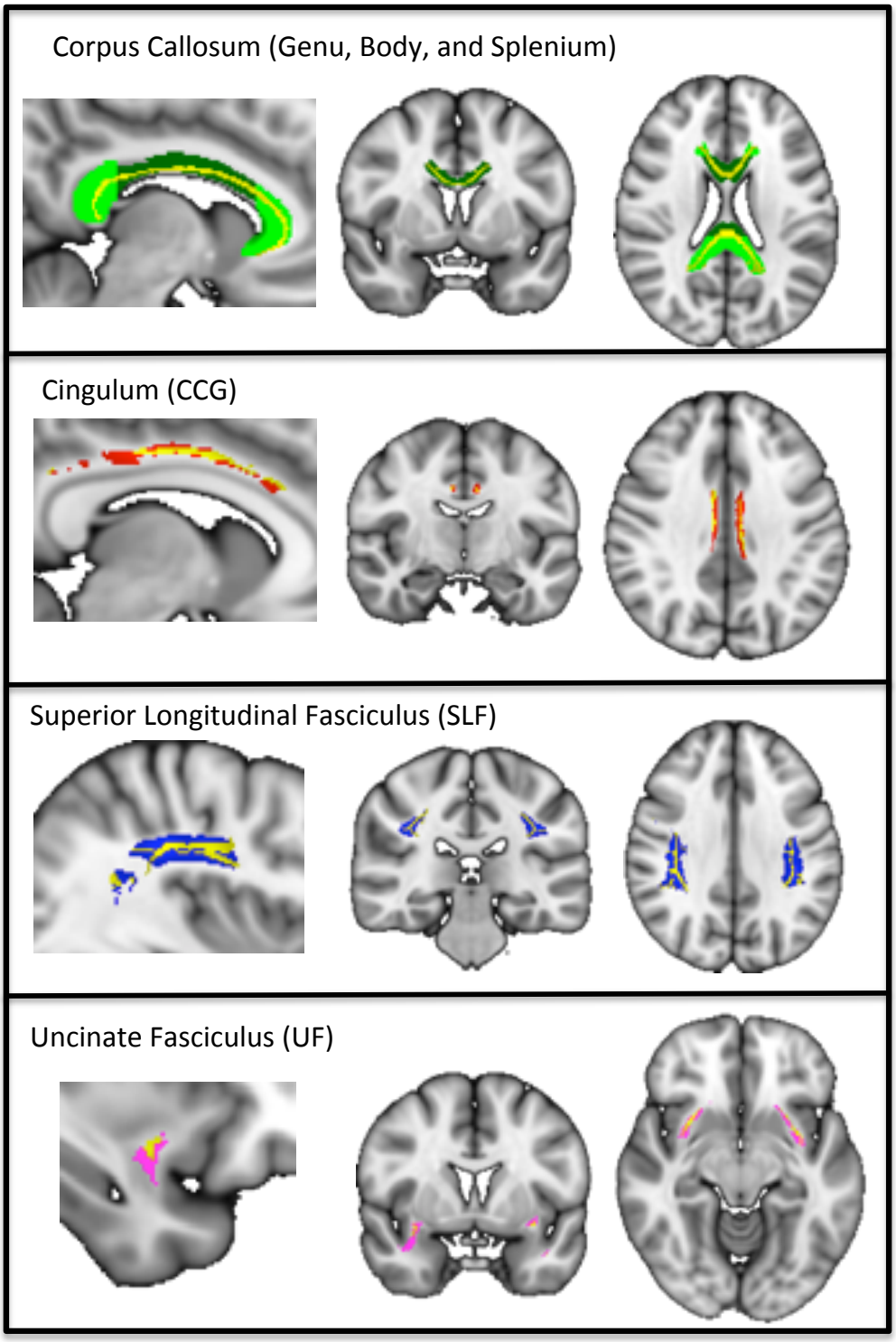

Figure 6.2. Representation of *a-priori* white matter tracts. Tracts are shown in green (corpus callosum divided into the posterior [splenium], medial [body], and anterior [genu] region), red (cingulum), blue (superior longitudinal fasciculus), and pink (uncinate fasciculus). Skeletons are shown in yellow overlaying the JHU tracts of interest.

Statistical analysis

Statistical analyses were conducted using SPSS 22.0 (IBM Corp., Armonk, NY). We performed partial correlations (controlling for age ad scanner type) of VO_2peak changes with percent volume changes (for volumetric FreeSurfer segmentations) or with percent FA/RD changes (for DTI data). Then, to investigate the relationship of brain health with total exercise duration, we performed partial correlation analyses (controlling for age and scanner type) of total exercise duration (higher intensity exercise participants will have higher exercise dose intensity) with percent volumetric changes in gray matter or FA/RD on every *a-priori* region or tract. We set our alpha (two-tailed) to 0.05.

6.4 RESULTS

Participants Demographics

Sample and fitness measures are shown in Table 6.1. No significant group differences (exercisers vs. controls) were found when controls were compared to the exercise group except for the percent VO_2peak change (p=0.012).

	Control	Exercise (all intensities)	All Groups
Sample Characteristics			
N (female)	3 (2)	7 (6)	10 (8)
Baseline Age (SD)	67.33 (1.5)	75.71 (6.3)	73.2 (6.6)
Baseline MMSE (SD)	29.33 (0.6)	29.57 (0.8)	29.5 (0.7)
Baseline BMI (SD)	25.2 (3.1)	26.9 (4.1)	26.5 (3.7)
Fitness Measures			
Baseline VO_2peak (ml/kg/min)	25 (5.4)	22.6 (2.9)	23.3 (3.7)
VO_2peak change (%)	-0.67 (1.3)	1.73 (0.9)	0.92 (1.6)*
Baseline Lean Mass (SD, units???)	42.42 (6)	39.1 (3.6)	40.09 (4.4)
Exercise Duration (hrs)	-	94.89 (50)	-
Lean Mass Change (%)	-1.4 (5.2)	6.1 (6.5)	3.7 (0.1)

Table 6.1. Participant's demographics. * denotes significant difference between groups (p<0.05).

FreeSurfer Cortical Segmentations

For every gray matter cortical segmentation, we performed partial correlations of longitudinal volumetric changes with the changes in VO_2peak and exercise duration, controlling for age. The results of our partial correlations are depicted in Table 6.2. In relation to VO_2peak and total exercise duration, none of our percent cortical volumes reached significance (p>0.05).

% Volumetric change:	% change in VO_2peak		Exercise Duration	
	r	p-value	r	p-value
PreCuneus				
Left	0.42	0.3	0.28	0.5
Right	0.41	0.32	0.33	0.42
Parahippocampal				
Left	-0.26	0.54	-0.5	0.2
Right	-0.06	0.88	-0.33	0.43
Enthorinnal				
Left	-0.3	0.47	-0.62	0.1
Right	0.49	0.22	-0.26	0.53
Caudal Middle Frontal				
Left	0.08	0.84	0.35	0.4
Right	0.28	0.5	0.57	0.14
Caudal Anterior Cingulate				
Left	-0.16	0.71	-0.07	0.88
Right	0.01	0.99	-0.22	0.6
Rostral Anterior Cingulate				
Left	0.47	0.25	0.34	0.41
Right	0.27	0.52	-0.4	0.33
Rostral Middle Frontal				
Left	0.63	0.09	0.53	0.18
Right	0.39	0.34	0.28	0.51
Superior Parietal				
Left	0.5	0.21	0.38	0.35
Right	0.42	0.3	0.52	0.19

Table 6.2. Participant's partial correlations (controlling for age) of all the *a-priori* FreeSurfer segmentations with the fitness measures (VO_2peak and exercise duration). * denotes significant (p<0.05).

White Matter Integrity

Partial correlations of percent FA/RD changes with changes in VO_2peak and exercise duration were performed, controlling for age. When percent FA changes were correlated with VO_2peak, none of the *a-priori* white matter tracts reached significance ($p>0.05$, Table 6.3). However, we found that participants with longer exercise durations showed a significant decreased in percent RD change in the genu of the corpus callosum ($r=-0.85$, $p=0.01$, Table 6.4, Figure 6.4), denoting preservation of white matter tract integrity. On the other hand, a significant increase in percent RD change in the right cingulum was also correlated with longer exercise duration ($r=0.75$, $p=0.03$, Table 6.4, Figure 6.3).

% change in VO_2peak	% change in Fractional Anisotropy		% change in Radial Diffusivity	
	r	p-value	r	p-value
Corpus Callosum				
Genu	0.2	0.64	-0.32	0.44
Body	-0.01	0.99	-0.23	0.58
Splenium	0.13	0.75	-0.53	0.17
Cingulum				
Left	0.01	0.98	-0.27	0.52
Right	0.29	0.48	0.07	0.88
Superior Longitudinal Fasciculus				
Left	0.28	0.5	0.09	0.84
Right	0.2	0.64	0.51	0.2
Uncinate Fasciculus				
Left	0.18	0.68	-0.21	0.61
Right	0.07	0.87	0.6	0.12

Table 6.3. Depicts partial correlation analyses of percent changes in FA and RD metrics with percent change in VO_2peak, controlling for age.

Total exercise duration	% change in Fractional Anisotropy		% change in Radial Diffusivity	
	r	p-value	r	p-value
Corpus Callosum				
Genu	-0.46	0.26	**-0.85**	**0.01***
Body	-0.48	0.23	-0.55	0.16
Splenium	-0.29	0.48	-0.43	0.29
Cingulum				
Left	-0.41	0.31	-0.48	0.23
Right	-0.35	0.4	**0.75**	**0.03***
Superior Longitudinal Fasciculus				
Left	-0.46	0.25	0.07	0.87
Right	-0.38	0.36	-0.2	0.64
Uncinate Fasciculus				
Left	-0.38	0.35	0.12	0.77
Right	-0.61	0.11	0.29	0.49

Table 6.4. depicts partial correlation analyses of percent changes in FA and RD with total exercise duration, controlling for age. * denotes $p<0.05$

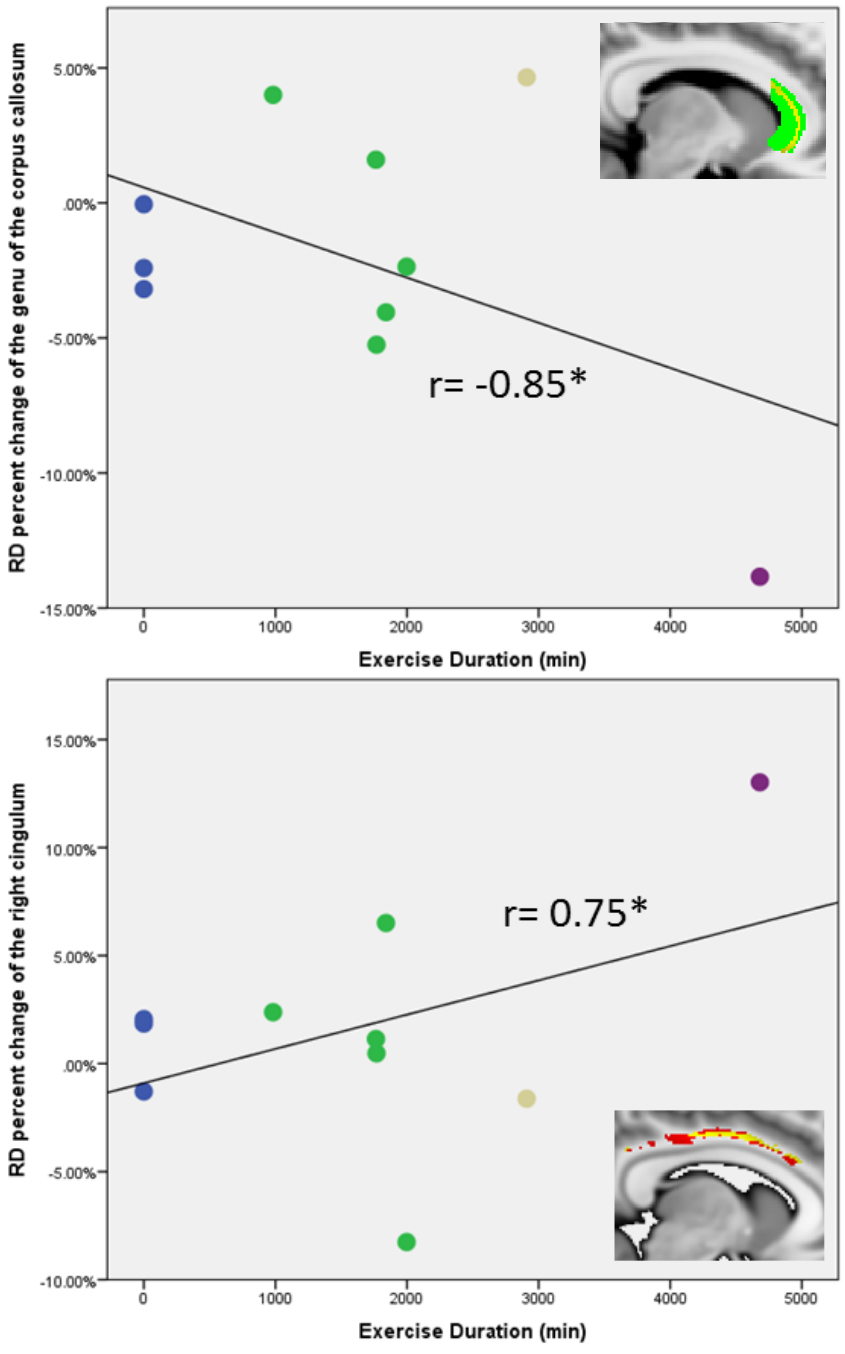

Figure 6.3. Scatter plots representing the associations of total exercise duration and RD percent change in the genu of the corpus callosum (top row) or the right cingulum (bottom row). The color dots classify each participants exercise dose: blue denotes the control participants; green denotes 75 mins/week, yellow 150 min/week, and purple 225 mins/week. The regression linear plot depicts all the dots with no color discrimination. * denotes $p<0.05$.

6.5 DISCUSSION

The aim of this study was to characterize changes in gray matter segmentations and white matter integrity in healthy non-demented subjects who participated in an aerobic 26-week exercise intervention program with different intensity doses. We performed analyses in regions previously associated with physical activity in gray cortical segmentations (Colcombe et al., 2006, Erickson et al., 2010, Floel et al., 2010, Gow et al., 2012) and white matter tracts (Marks et al., 2011, Gow et al., 2012, Johnson et al., 2012b, Voss et al., 2012, Tian et al., 2014a). Due to our small sample size we were not able to perform tests to evaluate different exercise dose intensities. Alternatively, we evaluated partial correlations of volumetric or diffusivity longitudinal changes with longitudinal percent changes of VO_2peak and total exercise time duration. After intervention, we did not find any significant associations of percent changes of cortical volumes with changes in VO_2peak. Similarly, no significant correlations were found in percent cortical volume changes and exercise time duration. In relation to white matter tract integrity, we did not find any significant correlations of diffusivity longitudinal changes (FA or RD) with changes in VO_2peak. However, we found that decreased percent RD changes in the genu of the corpus callosum were associated with longer exercise, denoting an increased preservation of white matter integrity. On the contrary, an increased in percent RD changes were also correlated with longer exercise duration in the genu of the corpus callosum.

The neuro-protective mechanisms related to physical activity and brain preservation have been previously identified in animal models. These mechanisms include cardiovascular, metabolic, and neurotrophic effects (Barber et al., 2012, Voss et al., 2013b). Increased cerebral blow flow, acetylcholine and arterial pressure have also been previously

found in walking animal models (Nakajima et al., 2003). Additionally, physical activity has shown to be 40% more protective for the cardiovascular system than predicted risk factors such as blood lipids, hypertension, or diabetes (Joyner and Green, 2009). Previous animal reports have shown that physical activity upregulates different growth factors in the hippocampus such as insulin-like growth factor 1 (IGF-1) (Carro et al., 2001, Trejo et al., 2001), vascular endothelial growth factor (VEGF) (Tang et al., 2010) and overexpression of brain-derived neurotrophic factor (BDNF) proteins (Griffin et al., 2009, Marlatt et al., 2012). Recently, serum levels for BDNF, IGF-1 and VEGF were also investigated in older adult participants who underwent a 1-year aerobic exercise program. These researchers showed that only in the exercise group, the connectivity between the parahippocampus and the middle temporal gyrus was associated with increased BDNF, IGF-1 and VEGF serum levels (Voss et al., 2013a).

In humans, our results can be compared with other reports that investigated the relationship between high exercise intensity and preservation of brain health. For example, a 9-year follow-up exercise study divided its participants in 4 groups according to the self-reported number of walking blocks (Erickson et al., 2010). They reported that the highest quartile group with higher number of walking blocks showed greater gray matter volumes in all their specified regions (precentral gyrus, supplementary motor area, precuneus, and hippocampus) when compared to the their control group. However, no differences were reported when the other lower 3 quartiles were compared. Due to its observational nature and a single neuroimaging time-point (9 years subsequent to self reported physical activity questionnaire), they were unable to conclude that physical activity caused preservation of gray matter volume. Another 6-month longitudinal study examined three groups of older

adults who participated in different physical activities stratified into no exercise, Nordic walking (medium-intensity exercise), and gymnastics (low-intensity exercise) (Ruscheweyh et al., 2011). These researchers showed that high-intensity exercise was not required to achieve increases in memory performance yet no exercise group differences were reported in relation to increased gray matter volume. Instead, they showed a positive association of increased physical activity with greater volumes in many cortical regions with the cingulate and the prefrontal cortices being the most significant.

When we investigated the associations between the changes in cortical segmentations and total exercise duration, we did not find any regions that reached significance. However, when we compared the associations between the integrity of the *a-priori* white matter tracts and total exercise duration, we found an association of preserved white matter tract integrity (decreased RD percent change) in the genu of the corpus callosum with longer exercise time durations. Previous reports that investigated the relationship of physical activity and white matter tract integrity have found preserved integrity in this tract (Johnson et al., 2012b) and also others (e.g. the cingulum and uncinate fasciculus) (Marks et al., 2007, Marks et al., 2011). However, the relationship with physical activity dose intensity and white matter tract integrity has not yet been investigated. To our knowledge, this is the first study that investigated the effects of longer exercise durations in white matter tracts. Interestingly and contrary to previous publications, we also found a decreased in white matter integrity in the right cingulum (increased RD) with longer exercise durations. One explanation for this finding could be the concurrent age-related brain deterioration that may be affecting our participants. One interesting observations is that most of the participants with higher increases in RD in the right

cingulum appeared to have subtle decreases in cognitive changes (e.g MMSE at baseline is higher than at follow-up). The cingulum is also a white matter tract that deteriorates earlier in neurodegenerative diseases such as AD (Zhang et al., 2007, Zhang et al., 2014), thus this negative finding may reflect early tract deterioration due to progressed aging or earlier symptoms of AD. Though, we believe this explanation might be speculative rather than justifiable due to our small sample size and the lack of comparable reports. Hence, we encourage further investigations with higher number of participants and different exercise dose intensities to investigate further the mechanism on how different exercise dose intensities might affect the structural changes in the brain.

The results and interpretations from our study should be evaluated within the context of its strengths and limitations. Our biggest limitation is the small neuroimaging sample data, which did not permit us to compare the different exercise doses. Hence, we investigated the associations between longitudinal brain changes and total exercise duration, a directly related measure of exercise dose. We believe this investigation described preliminary results but not conclusive in regards of the exercise dose intensity. Another limitation in relation to exercise duration is the variability of physical activity outside the exercise intervention facilities. It may be possible that participants with higher doses of exercise might unintentionally decrease their physical activity due to fatigue cause by this new activity even though there were advised against doing so. Finally, it is worth noting the limitations with processing imaging data using voxelwise morphology processing steps, especially in longitudinal data sets (e.g. partial volume effects, unbiased longitudinal templates or registrations). Thus to overcome these limitations in relation to neuroimaging, we applied the most up to date suggested methodologies previously

published for structural gray matter segmentations (Reuter et al., 2010, Reuter and Fischl, 2011, Reuter et al., 2012) and white matter registrations (Avants et al., 2011, Keihaninejad et al., 2012, Keihaninejad et al., 2013, Schwarz et al., 2014).

6.6 CONCLUSION

In healthy non-demented older adults who underwent a 26-week exercise intervention, we found that longer exercise duration was associated with changes in white matter tract integrity especially in the genu of the corpus callosum. On the contrary in the right cingulum, longer exercise durations were associated with increased transverse diffusivity (e.g. RD), which may not reflect neuroprotective exercise effects but maybe a stronger age-related or disease-related deterioration. Thus, we believe that similar large sample investigations are needed to explore further the neuroplasticity of the brain based on different aerobic exercise intensity doses.

Chapter 7 Preface:

In healthy older adults, evidence has shown that white matter integrity is positively associated with higher levels of cardiorespiratory fitness. However, few studies have investigated the effects of aerobic exercise, a direct regulator of cardiorespiratory fitness, in the Alzheimer's disease population. Previous work done at the University of Kansas Alzheimer's Disease Center showed increased brain volume in gray and white matter regions associated with higher cardiorespiratory fitness levels. To continue with this investigation, in this chapter I examined changes in white matter using diffusion imaging data in a sample of Alzheimer's disease participants who underwent a 26-week longitudinal aerobic exercise intervention.

This chapter explored the effects of aerobic exercise in longitudinal white matter diffusivity changes and its relations with changes in cardiorespiratory fitness, total exercise duration, and cognitive measures.

Chapter 7

The effects of aerobic exercise on brain's white matter integrity in the Alzheimer's disease population: a 26-week intervention study

7.1 ABSTRACT

Objective:

To investigate the effects of aerobic exercise on brain's white matter tract integrity after a 26-week intervention program in Alzheimer's disease (AD) older adults.

Methods:

Older adults with early AD (n=29; CDR=0.5 and 1) were randomized in two groups: an aerobic exercise (treadmill walking) and a non-aerobic control group (stretching and toning). As indicators of longitudinal changes in white matter integrity, we calculated percent changes of diffusivity metrics in AD-related *a-priori* white matter tracts. Then, we evaluated longitudinal diffusivity group differences (aerobic vs. non-aerobic) on every tract. Additionally, for each group (aerobic or non-aerobic), we conducted partial correlation analyses (controlling for baseline age and CDR sum of boxes) of longitudinal diffusivity changes with changes in cardiorespiratory fitness (CR) levels, exercise duration, and changes in cognitive tests.

Results:

Group comparisons (aerobic vs. non-aerobic) showed no significant differences in the longitudinal diffusivity metrics ($p>0.15$). When evaluating correlation analyses, the aerobic exercise group had no significant association of VO_2peak changes with changes in diffusivity measures ($p>0.1$). However in the non-aerobic control group, decreased FA percent change was associated with increased changes in VO_2peak in the left inferior fronto-occipital fasciculus ($r=-0.62$, $p=0.02$). Longer aerobic exercise durations were also marginally associated with preserved white matter integrity in the splenium of the corpus callosum ($r_{FA}=0.56$, $p_{FA}=0.08$) and the right cingulum ($r_{FA}=0.56$, $p_{FA}=0.06$) while the non-

aerobic group showed decreased FA in the right uncinate fasciculus with increased changes in VO_2peak (r_{FA}=-0.6, p_{FA}=0.03). In relation to cognition, changes in executive function were improved in the aerobic group when compared to the non-aerobic (F=5.88, p=0.024). Additionally, only the aerobic exercise group showed that increased changes in mean cognitive scores were associated with preserved white matter in the genu of the corpus callosum (r_{FA}=0.59, p_{FA}=0.046) and marginally in the left cingulum (r_{FA}=0.57, p_{FA}=0.056).

Conclusion:

Even though we did not find any significant group differences in diffusivity metrics, we found that (only in the aerobic exercise group) longer exercise durations and mean cognitive measures were positively associated with preserved white matter tract integrity in AD-related white matter tracts. Hence, longer aerobic exercise activity may benefit the preservation of specific white matter tracts even after the onset of Alzheimer's disease yet further research is needed to validate our results.

7.2 INTRODUCTION

Alzheimer's disease (AD) is a neurodegenerative disorder affecting cognition and accelerated brain deterioration. Currently there is no cure for the disease and costly pharmacological treatments have proven ineffective because none of the treatments slow down or stop the disease. Instead, these pharmacological treatments excite the amount of neurotransmitters in the brain which improves cognition but are only effective at the earlier stages of the disease (Thies et al., 2013). Thus, increasing attention has been given to non-pharmacological treatments such as aerobic exercise, which may provide a low cost alternative to slow down the progression of AD. Evidence in animal and human studies

have shown the neuro-protective effects of aerobic exercise in mitigating AD brain deterioration. In animal models, one of the earlier reports showed that exercise increases brain-derived neurotropic factor (BDNF), a growth factor neurotrophin that support the function and survival of many neurons (Neeper et al., 1995). Then, additional studies showed that exercise also improves neuronal survival (Wu et al., 2008), neurogenesis (van Praag et al., 1999, Van der Borght et al., 2009, Creer et al., 2010, Marlatt et al., 2012, Mustroph et al., 2012), and cell proliferation (van Praag et al., 1999, van Praag et al., 2005, Wu et al., 2008, Van der Borght et al., 2009).

In humans, it is more challenging to study the effects of exercise at the cellular level due to current *in-vivo* imaging technical limitations. Nonetheless, interventional studies in larger non-cellular resolution scales (~mm) using magnetic resonance imaging (MRI) techniques have identified positive correlations between exercise, cognition, and brain health. For example, in a study of 165 nondemented older adults (Erickson et al., 2009), higher levels of aerobic fitness by measures of maximum oxygen consumption (VO_2peak) were associated with increased hippocampal volume, a subcortical brain region that plays an important role in memory and is one of the first brain regions affected in AD. Another study also found that after 6 months of aerobic fitness training in 59 healthy older adults, brain's gray and white matter volumes increased as a function of fitness training (Colcombe et al., 2006). Gray matter regions included areas of the dorsal anterior cingulate cortex, supplementary motor area, and middle frontal gyrus while white matter regions included the anterior portion of the corpus callosum known as the genu of the corpus callosum. These positive relationships between exercise and brain health are also in accordance with previous work done in the early AD population at the University of Kansas Alzheimer's

Disease Center the early AD population (Burns et al., 2008, Honea et al., 2009, Vidoni et al., 2012a).

In the early AD, researchers previously showed that higher levels of cardiorespiratory fitness were associated with larger whole brain volumes (Burns et al., 2008). More specifically, they found that higher levels of cardiorespiratory fitness were related to regionally specific increases in gray and white matter volumes. In gray matter, these regions included the parietal and medial temporal cortices while white matter regions included the inferior parietal cortices (Honea et al., 2009). Longitudinally using functional connectivity, they found that higher levels of cardiorespiratory fitness showed a slower progression of AD and lower rates of atrophy in the medial temporal lobe (Vidoni et al., 2012a). Here in this chapter, we expanded our investigation by characterizing the integrity of brain's white matter in early AD after a 26-week aerobic exercise intervention program using diffusion imaging.

Diffusion imaging is a magnetic resonance imaging technique that measures the displacement of water molecules by applying magnetic field gradient pulses (Le Bihan et al., 2001). Thus, the use of this technique is more meaningful in tissues that have anisotropic or directional dependent characteristics such as white matter in the brain. White matter is composed of healthy myelinated axons that travel together in bundles known as tracts. These tracts travel along specific directions and are densely packed, thus restricting the mobility of these water molecules while providing efficient brain connectivity. However, the integrity of these healthy tracts deteriorates with aging and accelerates with AD (Sexton et al., 2011, Gold et al., 2012, Sachdev et al., 2013). These white matter integrity changes can be investigated by derived diffusion tensor imaging (DTI)

metrics such as fractional anisotropy (FA), radial diffusivity (RD), axial diffusivity (AxD), and mean diffusivity (MD). FA describes the degree of diffusion-related anisotropy ranging from 0 (perfectly isotropic) to 1 (perfectly anisotropic) and is related to overall white matter microstructural integrity (Alexander et al., 2011, O'Donnell and Westin, 2011). RD measures perpendicular diffusion and reflects changes in axonal diameter and myelination density (Song et al., 2005). AxD measures the magnitude of diffusion in the principal direction while MD reflects an overall measure of diffusion by averaging the three orthogonal components of diffusion (Alexander et al., 2007).

To date, only few publications have shown the effects of exercise and cardiorespiratory fitness on white matter integrity using diffusion imaging and only in healthy non-demented (ND) cohorts. In these reports, only one 1-year ND longitudinal study showed that the aerobic exercise group was associated with increased FA mainly in prefrontal and temporal regions yet no significant results were reported (Voss et al., 2012). On the other hand cross-sectional studies showed that higher CR was associated with increased white matter integrity in the corpus callosum (Johnson et al., 2012b), cingulum (Marks et al., 2007), and uncinate fasciculus (Marks et al., 2007, Marks et al., 2011). Thus the goal of this study is to characterize and compare longitudinal changes in white matter integrity after a 26-week aerobic exercise intervention program in older adults at early stages of AD. Hence, we evaluated longitudinal diffusivity changes in *a-priori* white matter tracts previously related to AD (Sexton et al., 2011, Alves et al., 2012, Bosch et al., 2012) and aerobic exercise (Marks et al., 2007, Marks et al., 2011, Johnson et al., 2012b). Longitudinal group differences in white matter tract integrity and changes in cardiorespiratory fitness were evaluated. Additionally, we also evaluated the association of

these diffusivity longitudinal changes with changes in cardiorespiratory fitness, exercise intervention duration, and cognitive scores.

7.3 METHODS

Sample

The study took place at the University of Kansas Alzheimer's Disease Center (KU ADC) as part of the Alzheimer's disease Exercise Program Trial (ADEPT, #11969, NTC01128361). For this investigation, we collected longitudinal data from individuals enrolled in an ongoing aerobic exercise (n=15) or non-aerobic control (n=14) intervention program for 26 weeks. The final sample data included 29 sedentary older adults (60 years and older) in the earliest stages of Alzheimer's disease (baseline CDR=0.5, n=21 and CDR=1, n=8). In addition to a full physical and neurological examination, enrollees were assessed using a semi-structured interview given to the participant and a collateral source (e.g. participant's spouse or child). Medications, past medical history, family history, education, and demographic information were collected from the collateral source. The ongoing intervention program excluded individuals who had significant neurological diseases other than AD which included major psychiatric disorders, major depression (Geriatric Depression Scale > 5), clinically-evident stroke or systemic infection, myocardial infarction or significant cardiovascular or respiratory disease, history of cancer in the last 5 years, current or past history of drug or alcohol abuse, insulin-dependent diabetes mellitus, and significant pain or musculoskeletal disorder that would limit exercise. Institutionally approved informed consent was obtained before enrollment.

Clinical assessment

Diagnostic clinical classification was made at a consensus conference attended by neurologist, neuropsychologists and nurse practitioners of the University of Kansas Alzheimer's Disease Center. Diagnostic criteria included the gradual onset and progression of impairment in memory and in at least one other cognitive or functional domain based on the NINCDS-ADRDA criteria (McKhann et al., 1984a). The Clinical Dementia Rating (CDR) determined the severity of dementia (Morris, 1993). At baseline, only participants with AD or mild cognitive impairment likely due to AD and a Global CDR of 0.5 (very mild) and 1.0 (mild dementia) were included in the study. The CDR protocol has shown a 93% diagnostic accuracy for AD and has shown reliability in discriminating those with mild cognitive impairment, who have early-stage AD (Storandt et al., 2006, Burns et al., 2008).

In addition to the CDR protocol dementia, a battery of full neuropsychological tests were given to each participant and estimated cognitive uniform data sets (UDS) z-scores were calculated based on sex, age, and/or education (Shirk et al., 2011). Then, we divided these z-scored in five different cognitive domains: a mean score (UDSmean), memory (UDS_mem), attention (UDS_att), processing speed (UDS_speed), executive function (UDS_ef), and language (UDS_lang).

Intervention program

Early onset AD participants were randomized on a one-to-one basis to either an aerobic exercise group (e.g. walking on a treadmill) or a non-aerobic control group (e.g. stretching and toning). The randomization procedure used block randomization within each stratum defined by age (<75 years vs. >= 75 years old) and gender to ensure the groups were matched across variables. The intervention began within thirty days of

completion of the screening and baseline evaluations. In addition to neuroimaging data, cardiorespiratory fitness and anthropometric measures were collected at baseline and follow-up. Detailed information for the exercise and control group activities can be found in a previous publication (Vidoni et al., 2012b).

Aerobic group

Trained exercise personnel lead all sessions three non-consecutive days per week for 26 weeks in a local exercise facility most convenient for the participant. To be included in the final analysis, AD subjects were required to attend at least 80% (62 of the 78 sessions) of the aerobic exercise sessions during the course of the study. The aerobic training consisted primarily of walking on a treadmill with a 5-minute warm-up session and a 5-minute cool down period. Exercise routines were spread over 3-5 days per week with no more than 35 minutes per day for a desired duration time of 155 minutes per week. Exercise intensity was monitored and increased from 40 to 75% of heart rate reserve (HRR) during the progression of the study. During weeks 1-4, the heart rate zone was set to 40-55%, week 5-18 to 50-65% HRR, and week 19-26 to 60-75 of the HRR.

Non-aerobic control group

As proposed by previous publications (Colcombe and Kramer, 2003, Colcombe et al., 2003, Voss et al., 2012, Hayes et al., 2013), stretching and toning were used as a control non-aerobic activity intervention. These participants had a similar schedule and balance of cofounding variables such as attention, social interactions, and other unknown variables that might influence the result. An experienced and trained exercise instructor ran these sessions three days a week at the local exercise facility. The activities included axial and

appendicular stretching and toning exercises, seated exercises on a large diameter exercise ball, and modified versions of Tai Chi and yoga for older adults (Vidoni et al., 2012b).

CR fitness and total exercise duration

CR fitness evaluation

CR fitness was measured before and after the 26-week intervention program by peak oxygen consumption VO_2peak (ml/kg/min) during a graded treadmill exercise test using a Cornell modified Bruce protocol (Hollenberg et al., 1998, Burns et al., 2008). The participants were asked to start walking on a treadmill while the speed and incline increased progressively. Only individuals who achieved a respiratory exchange ratio (RER) ≥ 1.0 were included in this evaluation. Oxygen consumption was averaged over 15-second intervals and the highest measurement was considered VO_2peak.

Total Exercise Duration

In addition to VO_2peak measures, we provided each participant an exercise log and a Polar hear rate monitor, which were kept at the exercise facility to record their weekly activity for duration and intensity (for the aerobic exercise group) or duration and activity (for the control group). Certified personal trainers assisted the participants with Polar monitors, how to keep their heart rate zone and how to retrieve the session data from the watch to record on the exercise log. Data were recorded at the end of each session. After the intervention program was concluded, a total exercise intervention duration time for each participant was calculated by adding up all the recorded exercise minutes. We used this measurement to report adherence and to quantify the total exercise duration (in minutes) that each participant conducted during our intervention program.

Neuroimaging

Neuroimages were collected at baseline and follow-up within 3 weeks of the cardiorespiratory fitness assessment. The session included a high-resolution T1 image for anatomic localization and to assess for gross anatomical differences with a high gray-white matter contrast (MPRAGE; 1x1x1mm voxels; TR = 2500, TE = 4.38, TI = 1100, FOV 256 x 256 with 18% oversample, 1mm slice thickness, flip angle 8 degrees). Additionally, a diffusion weighted imaging sequence was also acquired and designed to provide optimal acquisition parameters while minimizing scanner duration for the participant. Due to an MRI scanner replacement during our recruitment process, two DTI sequences were acquired. The first DTI sequence (n= 16) was acquired in a Siemens 3.0 Tesla Allegra MRI scanner using single-shot echo-planar imaging sequences with a repetition time [TR]=1000ms and echo time [TE]=81ms. Diffusion gradients were applied in 36 directions (b_0=0 s/mm^2 and b_1=800 s/mm^2). The second diffusion imaging acquisition (n=13) used a Siemens 3.0 Tesla Skyra with a repetition time (TR)= 1000ms and echo time (TE)=90ms. Diffusion gradients were applied in 65 directions (b_0 = 0 s/mm^2 and $b_{1\text{-}64}$= 1000 s/mm^2). Seventy-five 2-mm sections were acquired in at in-plane resolution of 128x128 with a 300mm field of view (FOV) in both DTI acquisitions. To maintain longitudinal differences consistent, baseline and follow-up sequences for every participant were acquired in the same scanner, using either the Allegra or the Skyra MRI scanner. Previous investigations have shown the feasibility of using multi-site DTI collection for analysis (Teipel et al., 2012, Nir et al., 2013) and no differences between participants' age, gender or VO_2peak were found between scanners. Therefore, we combined both DTIs sequences in our analysis.

Imaging Analysis

We pre-processed the diffusion imaging sequence using the FMRIB Software Library neuro-imaging tools (FSL 5.0.4) (Smith et al., 2004a). After manually inspecting our diffusion weighted images, we applied eddy current correction for small distortion and simple head motion, by alignment the diffusion weighted images to the b_0 image. Next, brain extraction tool (BET2) was applied to strip the brain from the skull, and diffusivity FA and RD map images were calculated using DTIFIT. As suggested by a recent article (Keihaninejad et al., 2013), interpolation asymmetries might arise when resampling the follow-up images to the baseline images. Therefore for every image in every participant, first we linearly registered the baseline and follow-up images to a halfway registration point, using FLIRT and MIDTRANS, which are part of the FSL tools. Hence, the choice of a halfway registration would result in an unbiased template towards any single point. Then, we non-linearly registered, aligned, and transformed every image to a common 1x1x1mm standard MNI space (FMRIB58_FA_1mm) as suggested in the TBSS pipeline protocol (Smith et al., 2006), but we omitted the skeletonizing step. Instead, a 2-mm smoothing procedure was applied to each image using FSLMATHS.

To generate the white matter *a-priori* masks, we registered the Johns Hopkins University probabilistic white matter atlas (Mori et al., 2005, Hua et al., 2008a) to the MNI space and masked-in all the voxels that belong to our specific *a-priori* white matter tracts. Then, average diffusivity values (FA, RD, AxD, ad MD) were calculated in every tract-of-interest for every participant at baseline and follow-up. Finally, for every subject averaged percent changes of our diffusivity metrics ($[Timepoint_{follow\text{-}up}\text{-}Timepoint_{baseline}]/ Timepoint_{baseline}$) were fed into SPSS 22.0 for statistical analyses.

The following tracts previously reported to be associated with AD and exercise (Figure 7.1) were included and divided by hemisphere: the corpus callosum (split in the genu, body and splenium) (Sexton et al., 2011, Alves et al., 2012, Bosch et al., 2012, Johnson et al., 2012b), the cingulum (CCG) (Xie et al., 2005, Marks et al., 2007, Zhang et al., 2007, Liu et al., 2011, Marks et al., 2011, Zhang et al., 2014) the inferior fronto-occipital fasciculus (IFOF) (Gold et al., 2010, Teipel et al., 2010, Alves et al., 2012), the superior longitudinal fasciculus (SLF) (Teipel et al., 2010, Liu et al., 2011, Sexton et al., 2011, Alves et al., 2012, Bosch et al., 2012), and the uncinate fasciculus (UF) (Marks et al., 2007, Damoiseaux et al., 2009, Liu et al., 2011, Sexton et al., 2011, Bosch et al., 2012). We believe this approach allows us to investigate specific tracts and we can report our results in relation to whole white matter conduits rather than small clusters of significant voxels as previously described (Damoiseaux et al., 2009, Voss et al., 2012, Gons et al., 2013). We believe that reporting white matter tract when small significant voxels showed significance may be misleading and may increase the probability of Type I error due to probable regions that might be located in crossing fibers or at the edges of white matter, where other less anisotropic media (e.g. gray matter or cerebrospinal fluid) may contaminate the results.

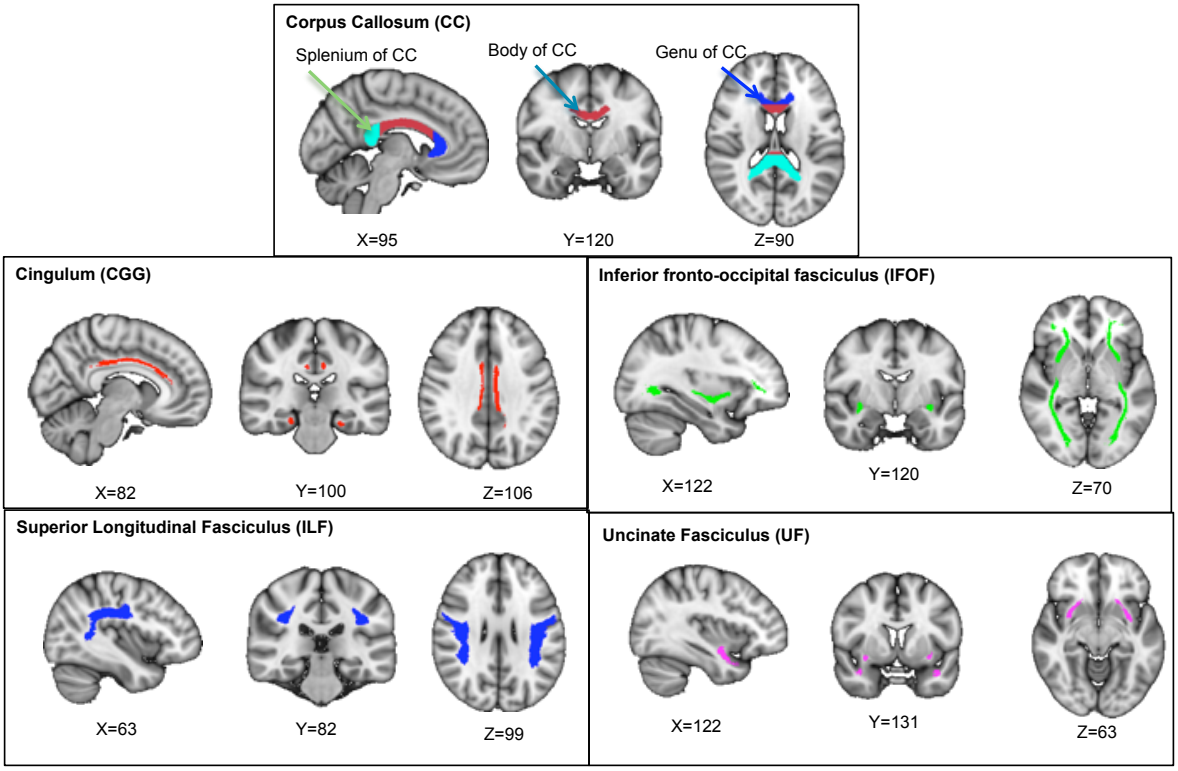

Figure 7.1. AD and exercise-related *a-priori* white matter tracts. These tracts include the corpus callosum (genu in blue, body in maroon, and splenium in light blue), the cingulum (red), the inferior fronto-occipital fasciculus (green), the superior longitudinal fasciculus (blue), and the uncinate fasciculus (pink). Tract representation is shown using the standard MNI brain and radiological orientation.

Statistical analysis

Statistical analyses were performed using SPSS 22.0 (IBM Corp., Armonk, NY). Demographics and physical characteristics were tested using parametric analyses (analysis of variance) or non-parametric analysis (chi-square) when appropriate.

To evaluate the longitudinal effects of aerobic (vs. non-aerobic), we conducted univariate group difference analyses controlling for baseline age and CDR sum of boxes (CDRsob). We believe that age affects the exercise physiological demands on our participants. Similarly, to account for disease progression we controlled for CDR sum of boxes as the disease directly relates to brain atrophy and cognitive decline (Sperling et al., 2014). Longitudinal group differences on every *a-priori* white matter tract were

investigating by calculating percent FA changes ([$FA_{follow\text{-}up}$-$FA_{baseline}$]/$FA_{baseline}$). If results were significant, subsequent percent diffusivity changes were evaluated in other non-FA diffusivity metrics (e.g. RD, AxD, or MD). Similarly we calculated longitudinal changes in VO_2peak ($VO_2peak_{follow\text{-}up}$– $VO_2peak_{baseline}$) and cognitive UDS scores and examined group differences using the similar univariate model.

We also examined the association of changes in CR fitness with white matter tract integrity. To do so on each group separately (aerobic or non-aerobic), we conducted partial correlations of changes in VO_2peak with changes in the diffusivity measures, controlling for baseline age and CDRsob. Additionally, we assessed the effects of total exercise intervention duration using partial correlations of total exercise duration with percent changes in the diffusivity measures (split by intervention group). Finally, to examine association of cognitive changes with changes in white matter integrity we conducted partial correlations of all the longitudinal changes in UDS scores with the diffusivity measures in every *a-priori* white matter tract (Table 7.1). We set our alpha to 0.05.

7.4 RESULTS

Demographics

Table 7.1 summarizes the subject's baseline demographics, physical, and CR fitness characteristics of the 29 participants included in the final analysis. Six participants were excluded because they did not reach our criteria for maximal exercise testing (n=3) or had abnormal diffusivity changes (n=3). We did not find significant differences between our intervention groups (aerobic vs. non-aerobic) in age, MMSE, BMI, VO_2peak, change in VO_2peak or intervention adherence (Table 7.1).

	Aerobic	Non-aerobic	p-value
N (female)	14(4)	15(5)	0.55
Age (SD)	73.4 (7.2)	70.8 (7.1)	0.34
MMSE (SD)	26.6 (3.4)	25.5 (2.9)	0.36
BMI (SD)	28 (2.9)	27.7 (4.4)	0.89
VO_2peak (ml/kg/min)	21.1 (4.2)	23.1 (6.0)	0.31
VO_2peak change	1.6 (2.0)	-0.3 (2.3)	0.09
Intervention Adherence (% minutes attended)	94.4%	86.5%	0.12

Table 7.1. Participant's baseline demographics, physical and fitness characteristics.

Group differences in white matter tract integrity

To assess the effects of aerobic exercise on every *a-priori* white matter tract, we conducted univariate analysis of variance (aerobic vs. non-aerobic) on percent FA changes controlling for age and CDRsob. We did not find any significant differences in percent FA (Table 7.2) thus no subsequent non-FA diffusivity analyses were conducted in this group difference comparison.

			Fractional Anisotropy		
			% change (mean)	Std. Deviation	p-value
Corpus Callosum	Body	CTL	-1.36	3.07	0.29
		150	-2.12	2.40	
	Genu	CTL	-1.62	2.79	0.52
		150	-2.12	2.92	
	Splenium	CTL	-1.11	3.36	0.53
		150	-1.34	2.88	
Cingulum (CCG-)	Left	CTL	-1.97	3.15	0.87
		150	-1.74	2.40	
	Right	CTL	-1.16	3.85	0.26
		150	-1.62	2.95	
Inferior Fronto-occipital fasciculus	Left	CTL	-1.03	2.86	0.23
		150	-1.85	2.36	
	Right	CTL	-1.11	2.77	0.33
		150	-2.01	2.93	
Superior Longitudinal Fasciculus	Left	CTL	-1.11	3.08	0.50
		150	-1.32	2.67	
	Right	CTL	-0.14	3.21	0.53
		150	-0.71	2.62	
Uncinate Fasciculus	Left	CTL	-1.50	3.12	0.58
		150	-1.66	2.96	
	Right	CTL	-1.40	3.34	0.15
		150	-2.70	3.23	

Table 7.2. Percent FA group differences (aerobic vs. non-aerobic) on every *a-priori* white matter tract. CTL denotes the non-aerobic group and 150 denotes the aerobic group.

Cardiorespiratory fitness and white matter tract integrity

To evaluate whether longitudinal changes of CR fitness affects changes in white matter integrity, we conducted partial correlations of changes in VO_2peak with percent FA changes on every *a-priori* white matter tract. These analyses explored whether an increased in CR fitness due to an intervention exercise program has an effect in white matter tract integrity. Thus, we split our results by intervention group: aerobic or non-aerobic control. No significant correlations were found for the aerobic exercise group but we found a marginally increased FA with increased VO_2peak in the genu of the corpus callosum (r=0.52, p=0.09, Table 7.3). On the other hand in the non-aerobic control group, increased changes in VO_2peak were associated with decreased FA only in the left inferior fronto-occipital fasciculus (r=-0.64, p=0.02, Table 7.3). However, subsequent analyses in this tract showed no significant correlations (r_{RD}=0.45, p_{RD}=0.15; r_{MD}=0.47, p_{MD}=0.11; r_{AxD}=0.29, p_{AxD}=0.33).

Fractional Anisotropy		Aerobic		Non-aerobic	
		r	p-value	r	p-value
Corpus Callosum	Body	0.20	0.54	-0.45	0.13
	Genu	0.52	0.09	-0.19	0.53
	Splenium	0.42	0.17	-0.37	0.22
Cingulum (CCG-)	Left	0.29	0.37	-0.38	0.20
	Right	0.12	0.72	-0.30	0.32
Inferior Fronto-occipital fasciculus	Left	0.30	0.34	**-0.64**	**0.02**
	Right	0.32	0.31	-0.14	0.65
Superior Longitudinal fasciculus	Left	0.32	0.32	-0.38	0.20
	Right	0.26	0.41	0.02	0.96
Uncinate Fasciculus	Left	0.02	0.95	-0.40	0.18
	Right	-0.33	0.29	-0.50	0.08

Table 7.3. Partial correlations of changes in VO_2peak with percent FA changes split by exercise group (aerobic or non-aerobic) and controlling for baseline age and CDRsob.

Total exercise duration and white matter tract integrity

To evaluate the effects of total exercise duration, we conducted partial correlation analyses of total exercise duration with longitudinal percent FA changes. Again, we split our results by intervention group: aerobic exercisers or non-aerobic controls. In the aerobic exercise group, we found that longer intervention times were marginally correlated with increased FA change in the right cingulum (r=0.56, p=0.06, Table 7.4). Subsequent non-FA diffusivity analyses in this tract also indicated white matter preservation (decreased in diffusivity measures) with longer exercise durations (r_{RD}=-0.75, p_{RD}=0.01; r_{MD}=-0.75, p_{MD}=0.01; r_{AxD}=-0.66, p_{AxD}=0.02). On the other hand, the non-aerobic control group showed decreased FA with longer exercise duration only in the right uncinate fasciculus (r=-0.6, p=0.03, Table 7.4). However, subsequent non-FA diffusivity partial correlation analyses in the non-aerobic right uncinate fasciculus were not significant (r_{RD}=0.10, p_{RD}=0.76; r_{MD}=0.04, p_{MD}=0.91; r_{AxD}=-0.13, p_{AxD}=0.66).

Fractional Anisotropy		Aerobic		Non-aerobic	
		r	P-Value	r	P-Value
Corpus Callosum	Body	0.33	0.30	-0.19	0.54
	Genu	0.50	0.10	-0.16	0.59
	Splenium	0.52	0.08	-0.11	0.72
Cingulum (CCG-)	Left	0.51	0.09	-0.34	0.26
	Right	**0.56**	**0.06**	-0.14	0.66
Inferior Fronto-occipital fasciculus	Left	0.42	0.18	-0.13	0.67
	Right	0.42	0.17	-0.25	0.42
Superior Longitudinal fasciculus	Left	0.49	0.10	-0.23	0.46
	Right	0.49	0.11	-0.51	0.07
Uncinate Fasciculus	Left	0.30	0.35	-0.28	0.36
	Right	-0.07	0.83	**-0.60**	**0.03**

Table 7.4. Partial correlations of total exercise duration with percent FA changes split by exercise group (aerobic or non-aerobic) and controlling for baseline age and CDRsob.

Group differences in cognition

To evaluate the effects of aerobic exercise in cognition, we conducted univariate analyses (aerobic vs. non-aerobic) in the longitudinal changes of the UDS scores (Table 7.5). We found that only the UDS executive function showed increased percent changes in the aerobic exercise group when compared to the non-aerobic control group ($UDS\_ef\_change_{Aerobic}$= 1.17, $UDS\_ef\_change_{Non\text{-}aerobic}$=-0.34, p=0.03).

		N	% change (Mean)	Std. Deviation	p-value
UDS_Mean_change	CTL	11	-0.05	0.38	0.74
	150	14	0.05	0.28	
UDS_Memory_change	CTL	12	0.27	0.89	0.83
	150	14	0.38	0.63	
UDS_Attention_change	CTL	12	0.06	0.44	0.07
	150	14	-0.28	0.43	
UDS_Speed_change	CTL	12	-0.06	0.62	0.41
	150	14	-0.24	1.18	
UDS_ExectiveFunction_change	**CTL**	**11**	**-0.34**	**1.06**	**0.03**
	150	**14**	**1.17**	**2.04**	
UD_Language_change	CTL	12	-0.25	0.60	0.58
	150	14	-0.02	0.86	

Table 7.5. Longitudinal group differences (aerobic vs. non-aerobic) in all the UDS cognitive scores.

Cognition and white matter tract integrity

To evaluate the association of cognitive scores with white matter tract integrity, we conducted partial correlations of longitudinal changes in UDS scores with longitudinal percent FA changes. Again, we split our results by intervention group: aerobic exercisers or non-aerobic controls. In the aerobic exercise group, we found that in the genu of the corpus callosum increased mean UDS scores were significantly correlated with increased FA percent change (r=0.57, p=0.046, Table 7.6). Subsequent diffusivity measures supported this finding with decreased diffusivity only in the RD metric (r_{RD}=-0.73, p_{RD}=0.01; r_{MD}=-0.34, p_{MD}=0.29; r_{AxD}=-0.32, p_{AxD}=0.31). Additionally, an increased in FA percent changes in

left cingulum was marginally associated with increased UDS mean (r=0.57,p=0.054, Table 7.6). However, subsequent diffusivity analyses were not significant (r_{RD}=-0.30, p_{RD}=0.35; r_{MD}=-0.21, p_{MD}=0.52; r_{AxD}=-0.12, p_{AxD}=0.72). In the non-aerobic control group, none of our partial correlation analyses were significant (p>0.05, Table 7.7).

EXERCISE (n=14)		UDS Mean	UDS Memory	UDS Attention	UDS Speed	UDS Executive Function	UDS Language
		r	r	r	r	r	r
Corpus Callosum	Body	0.48	0.00	0.14	0.35	-0.15	0.10
	Genu	**0.59***	0.27	0.08	0.14	-0.08	0.38
	Splenium	0.44	0.04	-0.01	0.28	-0.15	0.20
Cingulum (CCG-)	L	**0.57**$^{+}$	0.21	0.20	0.26	-0.05	0.04
	R	0.51	-0.11	0.14	0.41	-0.11	-0.05
Inferior Fronto-occipital fasciculus	L	0.48	0.10	0.23	0.32	-0.06	0.05
	R	0.45	0.12	0.07	0.28	-0.34	0.26
Superior Longitudinal fasciculus	L	0.36	-0.02	0.14	0.42	-0.25	0.14
	R	0.42	-0.10	0.05	0.30	-0.29	0.09
Uncinate Fasciculus	L	0.39	-0.12	0.15	0.37	-0.40	0.08
	R	0.15	-0.39	0.33	0.23	-0.16	-0.35

Table 7.6. Partial correlation coefficients in the aerobic exercise group when changes in UDS scores were correlated with percent FA changes on every white matter tract. * denotes significant findings (p<0.05). $^{+}$ denotes a marginally significant finding (p=0.054)

Non-aerobic (n=12)		UDS Mean	UDS Memory	UDS Attention	UDS Speed	DS Executive Functio	UDS Language
Corpus Callosum	Body	0.24	0.09	0.13	-0.15	-0.29	0.26
	Genu	0.14	0.02	-0.02	-0.19	0.05	-0.07
	Splenium	0.00	-0.15	-0.17	-0.38	0.00	-0.07
Cingulum (CCG-)	L	0.19	0.05	0.05	-0.19	-0.13	0.18
	R	-0.09	-0.34	-0.18	-0.35	-0.05	0.21
Inferior Fronto-occipital fasciculus	L	-0.02	-0.17	-0.02	0.04	-0.55	0.12
	R	-0.18	-0.44	-0.31	0.03	0.02	0.01
Superior Longitudinal fasciculus	L	-0.10	-0.17	-0.15	-0.33	-0.20	-0.15
	R	0.08	0.07	0.13	-0.33	-0.19	-0.07
Uncinate Fasciculus	L	0.10	-0.15	-0.05	-0.30	0.32	0.16
	R	0.04	-0.09	-0.04	-0.38	0.01	0.03

Table 7.7. Partial correlation coefficients in the non-aerobic control group when changes in UDS scores were correlated with percent FA changes on every white matter tract. * denotes significant findings (p<0.05).

7.5 DISCUSSION

In this study we wanted to investigate the effects of a 26-week aerobic exercise program on brain's white matter tract integrity in older adults at the earlier stages of AD. We conducted statistical analyses using scalar metrics of diffusion (FA, RD, AxD, and MD) on *a-priori* white matter tracts previously disrupted in early AD (Sexton et al., 2011, Alves

et al., 2012, Bosch et al., 2012) and/or associated with fitness related studies (Marks et al., 2007, Marks et al., 2011, Johnson et al., 2012b, Voss et al., 2012, Tseng et al., 2013, Tian et al., 2014b). First, we investigated longitudinal group differences (aerobics vs. non-aerobic) on longitudinal changes of white matter integrity, VO_2peak, and cognitive UDS scores. Second on each intervention group separately, we investigated if changes in cardiorespiratory fitness levels, intervention duration, or changes in UDS scores were associated with changes in white matter tract integrity.

Aerobic vs. non-aerobic exercise on brain's white matter integrity

After the conclusion of the 26-week intervention program, we examined the differences in percent diffusivity changes between the aerobic exercise and the non-aerobic control group on specific *a-priori* white matter tracts. We did not find any significant differences in percent diffusivity changes between groups. Our results are consistent with a previous 1-year longitudinal DTI study performed in healthy older non-demented adults (Voss et al., 2010). These authors did not find any significant differences in the aerobic group when compared to the stretching group but described a marginal group difference effect in the prefrontal regions. It is also worth noting that these authors used a different diffusion imaging processing methodology (TBSS) and a sample of non-demented older adults. A possible explanation for our null results may be that concurrent white matter deterioration due to aging (Salat, 2011) and more drastically due to AD (Chua et al., 2008, Sexton et al., 2011, Gold et al., 2012), which might affect and conflict with concurrent positive effects of aerobic exercise activity on the brain's white matter integrity (Hayes et al., 2013), leading to non-significant results.

Another possibility for our null findings could be that our *in-vivo* diffusion imaging acquisition was not sensitive enough to identify the effects of aerobic exercise after 26 weeks, especially in early AD participants. Even though in our study, we failed to distinguish neuro-protective mechanisms, positive mechanisms might have been triggered at the cellular level as supported by previous *post-mortem* animal studies (see review (Voss et al., 2013b)). At the cellular level, animal models have shown that long-term exercise (e.g. 2 months) increased neuronal spine density in the enthorinal cortex and CA1 pyramidal cells (Stranahan et al., 2007). Also animal models who run for prolonged times have shown to improve neuronal survival (Wu et al., 2008), increased neurogenesis (van Praag et al., 1999, Van der Borght et al., 2009, Creer et al., 2010, Marlatt et al., 2012, Mustroph et al., 2012), and increased cell proliferation (van Praag et al., 1999, van Praag et al., 2005, Wu et al., 2008, Van der Borght et al., 2009). Thus, subtle neuroprotective mechanisms might be occurring but it may be undetectable with our current diffusion imaging acquisition. Though it is worth noting that a one-to-one relationship with cellular characteristics such as myelination quality, axonal density, or glial cell density cannot yet be characterized with any *in-vivo* imaging modality (e.g. diffusion imaging) due to our current imaging macro-scale resolution limitations (Concha, 2014, Walhovd et al., 2014). Hence, longer exercise programs or larger sample studies might be needed to investigate further these neuro-protective mechanisms especially when using *in-vivo* neuroimaging tools.

To our knowledge, this is the first longitudinal diffusion imaging study investigating the effects of aerobic exercise in the early AD population. Our results are in accordance with only one other interventional study previously published in non-demented adults (Voss et al., 2012) and contradicts with volumetric studies (Colcombe et al., 2006, Liu-

Ambrose et al., 2010, Ruscheweyh et al., 2011, Vidoni et al., 2012a). Hence given the lack of AD-related diffusion imaging studies, it is difficult to draw conclusions about the protective mechanisms of aerobic exercise on brain's white matter tract integrity. Thus, there is a need for more research to understand how aerobic exercise may mitigate the evident white matter deterioration due to aging and AD.

The effects of CR fitness in white matter integrity

We did not find any significant associations of longitudinal changes in VO_2peak with changes in white matter tract integrity. These results disagreed with previous whole brain cross-sectional (Burns et al., 2008) and regional (Colcombe et al., 2003, Colcombe et al., 2006, Honea et al., 2009, Vidoni et al., 2012a) volumetric analyses. Similarly, our results diverged with previous diffusion imaging cross-sectional studies in non-demented participants (Marks et al., 2007, Marks et al., 2011, Johnson et al., 2012b). To our knowledge only one other longitudinal diffusion imaging report (in healthy non-demented older adults) described a marginally positive association of aerobic exercise intervention and preserved white matter integrity in prefrontal and temporal regions yet none of the regions reached significance (Voss et al., 2012). Additionally, this study used a composite CR fitness measure (using a graded maximal test [VO_2peak] and a Rockport walk test), which differs from our direct measurement of CR fitness based only in VO_2peak, making it difficult to compare our results. In our study, we also recruited sedentary AD participants that reported an average baseline VO_2peak (ml/kg/min) below the 20^{th} percentile (See Table 7.1) according to the American College of Sports Medicine guidelines (Medicine, 2009). Our study sample did not cover the entire percentile fitness range but only the

lowest and less fitted population due to the mandatory sedentary criteria during the screening selection process. In addition, this intervention was given to sedentary early AD, which might have a more challenging goal when performing the maximal oxygen consumption evaluation. Hence, our tests may not be reflecting an accurate measure of physiological strain but exhaustion due to novel physiologic demands, especially prior to the intervention program. However to overcome this limitation, we only included those participants who reached a respiratory exchange ratio of 1.0 during the CR fitness test.

Another explanation for our null findings might be explained by the diffusion processing method used during this investigation. Here, we averaged a specific diffusion value of the entire white matter tract rather than looking at voxel-by-voxel differences, as previously done (Voss et al., 2012, Gons et al., 2013, Tseng et al., 2013). Subtle changes may appear in smaller regions surrounding specific white matter tracts but when averaged values were calculated for an overall assessment of specific white matter tracts, these changes may increase in variance and may affect reaching significance. Though, these subtle changes in smaller voxels could be describing image-processing flaws that might not be related to the actual white matter micro-structural changes (e.g. image co-registrations, partial volume effects or crossing fibers). In previous diffusion imaging reports (only in healthy older adults), they found that white matter integrity has a positive association with CR fitness (Marks et al., 2007, Marks et al., 2011, Johnson et al., 2012b, Voss et al., 2012). However, these results were reported in smaller brain regions using regions-of-interest (not whole white matter tract conduits) or "thinned-out" voxelwise statistical methodologies (TBSS), which we believe may bring inconsistencies and limitations when

describing and discussing study specific results in relations to specific white matter tracts (see Chapter 2).

Longer aerobic exercise is associated with preserved white matter integrity

To investigate the effects of total exercise duration in white matter integrity, we conducted partial correlation analyses of percent change diffusivity measures with total intervention duration. In the aerobic exercise group, we found that the participants who spent more time exercising had an increased percent change in FA in the right cingulum and preserved diffusivity in subsequent diffusivity analyses (RD, MD, AxD). The cingulum has previously found to be one of the earliest tracts to deteriorate in early AD (Xie et al., 2005, Zhang et al., 2007, Sexton et al., 2011, Sachdev et al., 2013, Amlien and Fjell, 2014, Zhang et al., 2014) and have previously shown a positive association with CR fitness (Marks et al., 2007, Marks et al., 2011) in older non-demented cohorts. It may be possible that more vulnerable white matter tracts in AD receive the most benefit for an exercise intervention program especially during longer periods of exercise. Another possibility for our results is that participants who aerobically exercised longer times might have a better willingness to slow down the progression of AD leading to improvement in other co-found factors (e.g. lower depression, lower stress, increased mood, etc…) that may be facilitate triggering neuro-protective aerobic exercise-related mechanisms.

On the other hand in the non-aerobic control group, we found a decreased FA in the right uncinate fasciculus with longer exercise duration yet subsequent diffusivity measures were non-significant. The uncinate fasciculus connects the anterior temporal lobe with the lateral orbitofrontal cortex (Catani et al., 2002, Papagno et al., 2011). This tract is larger in

the right hemisphere (Highley et al., 2002) and even though its role remains unknown, the uncinate fasciculus is considered to be part of the limbic system and its function is critical to emotion and memory with a role in formation and retrieval of memories (Nestor et al., 2004, Gaffan and Wilson, 2008). Additionally, previous meta-analyses reports showed large effects on this tract when AD where compared to ND and MCI (Sexton et al., 2011). Thus, decreased FA in the non-aerobic controls might be reflecting AD-related brain deterioration progression, as this cohort group was not exposed to aerobic exercise.

Hence, these findings suggest that longer aerobic exercise durations may have a moderating effect in slowing down the progressed deterioration of white matter tracts due to AD. To our knowledge this is the first diffusion study in older AD and even though our results are partially in accordance with previously published results in animal models (Adlard et al., 2005, E et al., 2014) and other *in-vivo* imaging reports (Honea et al., 2009, Marks et al., 2011, Johnson et al., 2012b, Vidoni et al., 2012a), we encourage future research to investigate this matter in larger interventional studies with longer intervention times and different exercise intensity doses.

Aerobic exercise might slow down cognitive changes

To investigate the effects of aerobic exercise in cognition, first we examined group differences in cognitive UDS scores and found that executive function was significantly improved in the aerobic exercise group when compared to the non-aerobic control group. Supporting our finding, a previous meta-analyses report found that fitness training increased cognitive performance regardless of cognitive tasks, training methods or participant's characteristics, being executive function the domain with the highest fitness

training benefit (Colcombe and Kramer, 2003). Another meta-analytic review also aimed to assess the effects of aerobic exercise training on neurocognitive performance (Smith et al., 2010). They found that aerobic exercise was associated with improvements in attention, processing speed, executive function and memory. These and other reports describing the effects of aerobic exercise in cognition and executive functions are described in a recent review (Erickson et al., 2014).

In addition to group differences in cognitive UDS scores, we also examined the association of longitudinal changes in UDS scores with changes in white matter tract integrity. We only found significant associations of increased mean cognitive UDS scores in the aerobic exercise group with preserved diffusivity in the genu of the corpus callosum and marginally preserved in the left cingulum. These tracts are previously related to deteriorate early in AD (Sexton et al., 2011, Alves et al., 2012, Fjell et al., 2014, Zhang et al., 2014) and have neuro-protective effects with aerobic exercise (Marks et al., 2011, Johnson et al., 2012b). Thus, our positive findings in these tracts (the genu of the corpus callosum and the cingulum) suggest that a relation between micro-structural integrity of specific white matter tracts might lead to increased cognition. To our knowledge this is the first diffusion imaging study in early AD that investigated cognitive measures after an aerobic exercise intervention. Thus, we encourage future work on aerobic exercise, cognition, and brain plasticity to apply this and other analyses to investigate the structural connections of the brain (e.g. connectomics or tractography, more in chapter 8).

7.6 CONCLUSION

After a 26-week exercise intervention program in Alzheimer's disease participants, we investigated the structural diffusivity changes in white matter tract integrity and its association with cardiorespiratory fitness, exercise intervention duration, and cognitive UDS scores. While we did not find any group differences in white matter diffusivity measures or changes in cardiorespiratory fitness, we found an increased in UDS executive function (in the aerobic group when compared to the non-aerobic controls) after the exercise intervention. Additionally, longitudinal changes in white matter integrity were positively and marginally associated with longer exercise duration in the aerobic group in the right cingulum and the splenium of the corpus callosum. Similarly, the aerobic group showed marginally increased mean UDS scores with preserved diffusivity in the left cingulum and genu of the corpus callosum. Hence, even though we did not find group differences in longitudinal white matter changes, we believe that underlying mechanisms might be occurring at microstructural levels as manifested by a positive white matter tract preservation with longer exercise duration and increased cognitive scores. To our knowledge, this is the first interventional investigation in the AD population, so a need for future studies with longer exercise times, different exercise doses, and higher number of participants are strongly recommended.

Chapter 8 Preface:

In this chapter, I characterized the structural integrity of thalamo-cortical connections and classified each subthalamic nuclei in early Alzheimer's disease (AD) participants who underwent a 26-week aerobic exercise intervention program using probabilistic tractography and a classification target algorithm. The thalamus is a subcortical structure that filters incoming information from the peripheral body to the cerebral cortex. In Alzheimer's disease evidence of thalamic deterioration is inconclusive yet this structure acts as a gateway for relaying information to higher functioning cortical regions. This cortical region is also involved in executive function and other cognitive domains that are affected in AD yet its association with aerobic exercise is unknown. Thus, in this chapter I decided to explore further the effects of aerobic exercise in this structure, its connectivity to cortical regions, and its nuclei subdivision based on its likelihood of connection and by using a classification target algorithm. To investigate the effects of aerobic exercise in these thalamo-cortical connections, I compared percent change diffusivity and volumetric measures between groups (aerobic vs. non-aerobic). Additionally, after classifying every subject's subthalamic segmentations before and after intervention, I also calculated percent volumetric changes on every subthalamic nuclei and investigated the effects of aerobic exercise in these subdivisions.

Chapter 8

Aerobic exercise and thalamo-cortical connectivity in the Alzheimer's disease population: a 26-week exercise intervention study

8.1 ABSTRACT

Objective:

To investigate the effects of an aerobic intervention exercise program in thalamo-cortical connections using connectivity-based subthalamic segmentations and probabilistic tractography in sedentary older adults with early Alzheimer's disease (AD).

Methods:

Early AD participants (Clinical Dementia Rating [CDR] = 0.5 or 1) were randomized into a 26-week exercise intervention group, either an aerobic exercise group (treadmill walking, n= 16) or a non-aerobic control group (stretching and toning, n= 14). In addition to anthropometric measures, we collected magnetic resonance images (T1 and diffusion-weighted images) at baseline and follow-up. We performed probabilistic tractography using the thalamus as our seed region and seven cortical gyri as our target regions: cingulate, frontal, occipital, parietal, post-central, pre-central, and the temporal gyrus. Then, we conducted analyses of variance to test group differences (aerobic vs. non-aerobic) in these thalamo-cortical probabilistic connections using longitudinal percent changes in diffusivity metrics (fractional anisotropy [FA] and radial diffusivity [RD]). Finally, for every participant we subdivided their thalamus into seven sub-regions using connectivity-based seed classification algorithms. These algorithms classify the voxels of the thalamus (our seed region) according to the target cortical region that shows the highest probability of connection. Then for every participant, we calculated a longitudinal percent change differences in these volumetric classifications and assessed percent change group differences (aerobic vs. non-aerobic control). For every comparison, we used the univariateanalyses of variance controlling for age and gender and setting our alpha to 0.05.

Results:

We did not find any significant volumetric or diffusivity changes when characterizing the volumetric and diffusivity changes in the thalamo-cortical connections ($p>0.05$). However in our classification-based algorithm after a 26-week intervention program, the aerobic exercise group had increased thalamo-cortical connectivity to the right cingulate gyrus (2.67% vs -0.91%, $p=0.029$) and decreased connectivity to the left post-central gyrus (-1.12% vs 0.34, $p=0.041$) when compared to changes in the non-aerobic control group.

Conclusion

Using diffusion imaging tractography analyses, we found that 26 weeks of aerobic exercise is associated with dynamic changes in thalamo-cortical connectivity, suggesting that aerobic exercise even may modify thalamo-cortical brain connectivity after the onset of AD.

8.2 INTRODUCTION

The thalamus is an oval-shaped deep gray matter subcortical structure located in the dorsal portion of the diencephalon (Figure 8.1). Its primary function is to convey almost all sensory input information (other than olfaction) to the cerebral cortex. This structure acts as a "gatekeeper" of information to the cerebral cortex as it prevents or enhances the passage of information to the cortical regions, depending on the behavior state of the person. Almost all the information received by the cerebral cortex coming from the environment or by the body's internal receptors comes through the thalamus

(Casagrande et al., 2005). Due to its prominent role on relaying information to the cerebral cortex, this structure has a remarkably large number of pathways with many nuclei devoted to different thalamo-cortical connections. These nuclei can be divided in four main groups: anterior, medial and median, ventral anterior, and ventral posterior thalamus (Figure 8.1).

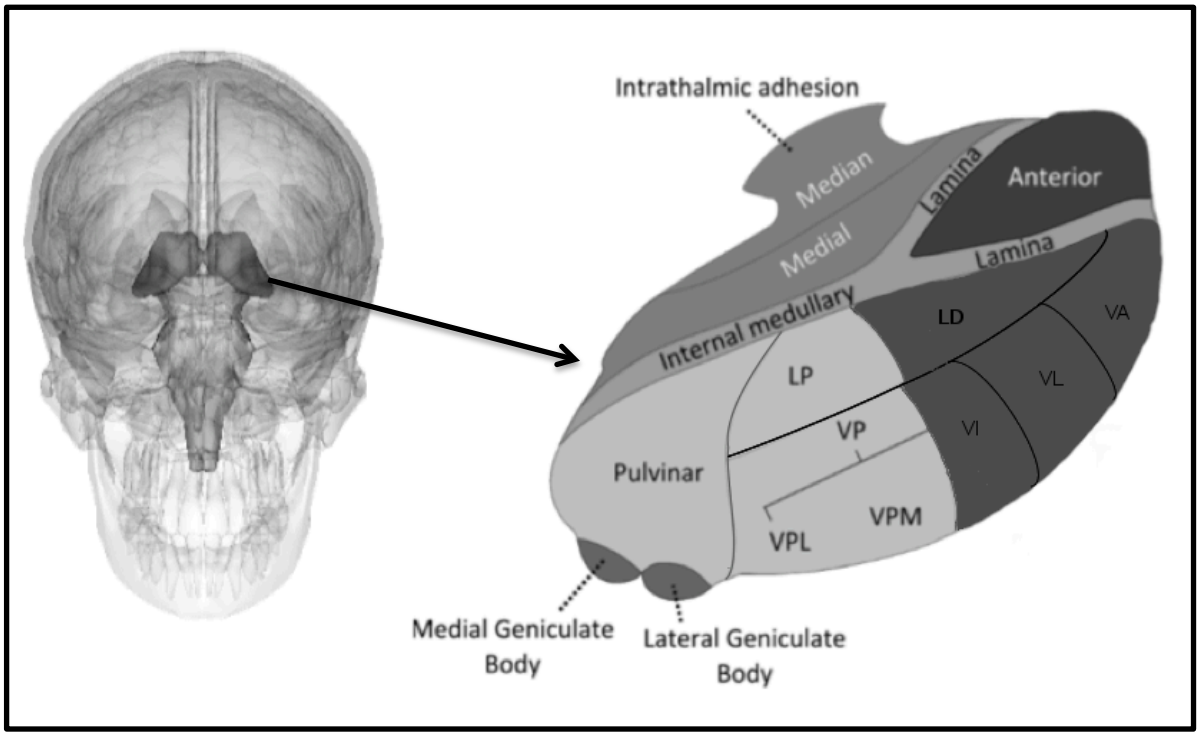

Figure 8.1. The thalamus and its four main nuclei groups: anterior (darkest), ventral anterior (darker), medial and median (light), and ventral posterior (lightest). L = lateral V=ventral, P=posterior, M = medial, A = anterior, I=Inferior.

The anterior group consists of only one nucleus and while its role is unknown, it is thought to participate in memory and emotion as it involves the limbic system and it is inter-connected with the cingulate and frontal gyri (FitzGerald et al., 2011). The medial/median nuclei group is connected to the entire prefrontal cortex. Its role is also unknown but it functions have been related to memory, cognition, judgment and mood

(FitzGerald et al., 2011). The ventral anterior group contains many nuclei and can be subdivided in the ventral anterior, ventral lateral and ventral posterior nuclei. The ventral anterior and ventral lateral nuclei are related to motor control, and carry information from the basal ganglia and cerebellum to the motor cortex. The ventral posterior group carries somatosensory information to the cortex. Finally, the posterior group contains the medial geniculate body, the lateral geniculate body and the pulvinar. The medial geniculate body is related to the auditory pathway as it receives information from the inferior colliculus (which carries auditory information from both ears) and projects it to the primary auditory cortex, located in the superior dorsal part of the temporal lobe (Brodmann areas 41 and 42). The lateral geniculate body is a complex structure where optic nerve axons terminate, and thus it is related to the visual system (Banich and Compton, 2010). The pulvinar is the largest nucleus in the thalamus and the most developed in humans yet its function is still very unknown. This nucleus might be involved in some aspects of visual perception or attention with occasional reports of language deficits after damage (Nolte, 2009).

These thalamo-cortical nuclei and their connections have been extensively characterized in non-human animals (Jones et al., 1985). However in humans, the characterization of these connections is very limited. One method to study thalamo-cortical connections includes the injection of fluorescent dyes *post-mortem,* which allows the tracing of each pathways. However, this method limits its characterization to small distances in the tenths of millimeters (Mufson et al., 1990, Onodera and Hicks, 2010). Dissection and histological analysis of major tracts have also been investigated but on a relatively small number of patients (Mufson et al., 1990, Onodera and Hicks, 2010)). Thus, this old method has now been replace with i*n-vivo* diffusion imaging techniques (Onodera

and Hicks, 2010, Ford et al., 2013, Leuze et al., 2014). *In-vivo*, we can characterize these thalamo-cortical connections using magnetic resonance diffusion imaging and probabilistic tractography algorithms (Behrens et al., 2003a). Diffusion imaging characterizes the diffusion of water molecules, which may be restricted to a specific media. For example, the thalamo-cortical connections in the brain are composed of axonal bundles that provide efficient structural connectivity between the thalamus and the cortical areas. These bundles will also restrict the movement of water along its specific direction thus providing a sensitive measure of diffusivity and an indirect measure of connectivity (e.g. anisotropic diffusion will be proportional to higher white matter tract integrity) that can be used to trace and characterize the structural integrity of these connections.

Two types of algorithms to trace diffusion tensor imaging been developed in the past decades: streamline tractography and probabilistic tractography. Streamline tractography is a more conventional technique that propagates from a seed mask (e.g. the thalamus) to a specific target in a single direction on a voxel-by-voxel projection basis and by using specific and high certainty fiber direction information (Jones et al., 1999). This high certainty fiber direction information is constrained by local voxel diffusivity thresholds and is limited to connections near gray matter where its isotropic diffusion is generally beyond the local diffusivity threshold. On the other hand, probabilistic tractography (Behrens et al., 2003b) propagates similarly to streamline tractography but instead of propagating in a single direction or being limited to a local diffusion threshold, this methodology estimates local probability propagation functions in every voxel that might connect the seed region to its target. Thus, this technique is not dependent on local diffusion thresholds and can fully propagate into more isotropic regions (e.g. gray matter),

providing a more comprehensive characterization of the specific thalamo-cortical connections. This technique has previously been used to describe the thalamo-cortical connections *in-vivo* to compare results with animal models (Behrens et al., 2003a), reflect variation in functional properties (Johansen-Berg et al., 2007), in early detection of AD (Zarei et al., 2010, Lee et al., 2013), or in other neuro-related diseases such as primary progressive aphasia (Galantucci et al., 2011). Here, we used this technique to evaluate thalamo-cortical changes in early stage AD older adults who underwent an aerobic exercise intervention program. To our knowledge, this is the first investigation that studies the effects of aerobic exercise in thalamo-cortical connectivity. We hypothesize that the integrity and probability of these thalamo-cortical connections may dynamically change to compensate for thalamo-cortical connections that get disrupted at early stages of AD.

8.3 METHODS

Sample

For this investigation, we collected data from sedentary individuals who agreed to enroll in an ongoing aerobic exercise trial. The final sample data included 30 sedentary older adults (60 years and older) in the earliest stages of AD (CDR, 0.5; n=21, CDR, 1; n=9). The ongoing exercise trial study excluded individuals who have significant neurological diseases other than AD, major psychiatric disorders, major depression (Geriatric Depression Scale > 5), clinically-evident stroke or systemic infection, myocardial infarction or significant cardiovascular or respiratory disease, history of cancer in the last 5 years, current or past history of drug or alcohol abuse, insulin-dependent diabetes mellitus, and

significant pain or musculoskeletal disorder that would limit exercise. Institutionally approved informed consent was obtained before enrollment.

Clinical assessment

In addition to a full physical and neurological examination, enrollees were assessed using a semi-structured interview given to the participant and a collateral source (e.g. participant's spouse or child). Medications, past medical history, family history, education, and demographic information were collected from the collateral source. Diagnostic classification was made at a consensus conference attended by neurologist, neuropsychologists and nurse practitioners of the University of Kansas Alzheimer's Disease Center and by using consensus diagnostic criteria for AD: gradual onset and progression of impairment in memory and in at least one other cognitive and functional domain (NINCDS-ADRDA criteria) (McKhann et al., 1984a). The Clinical Dementia Rating (CDR) determined the severity of dementia (Morris, 1993). Only participants with AD or mild cognitive impairment likely due to AD and a Global CDR of 0.5 (very mild) and 1.0 (mild dementia) were included in the study. The evaluation protocol has shown a diagnostic accuracy for AD of 93%, and has shown reliability in discriminating those with mild cognitive impairment, who have early-stage AD (Storandt et al., 2006, Burns et al., 2008).

Intervention program

Early onset AD participants were randomized on a one-to-one basis to an aerobic exercise group (walking on a treadmill) or a non-aerobic control group (non-aerobic activities). The randomization procedure used block randomization within each stratum defined by age (<75 years vs. >= 75 years old) and gender to ensure the groups were matched across variables. The intervention began within thirty days of completion of the

screening and baseline evaluations. CR fitness and anthropometric measures were collected at baseline and follow-up. Detailed information for the exercise and control group activities can be found in a previous publication (Vidoni et al., 2012b).

Aerobic Intervention

Trained exercise personnel lead all sessions three non-consecutive days per week for 26 weeks in a local exercise facility most convenient for the participant. To be included in the final analysis, AD subjects were required to attend at least 80% (62 of the 78 sessions) of the aerobic exercise sessions during the course of the study. The aerobic training consisted primarily of walking on a treadmill with a 5-minute warm-up session and a 5-minute cool down period. Exercise routines were spread over 3-5 days per week with no more than 35 minutes per day. Exercise intensity was monitored and increased from 40 to 75% of heart rate reserve (HRR) during the progression of the study. Weeks 1-4, heart rate zone was set to 40-55%, week 5-18 to 50-65% HRR, and week 19-26 to 60-75 HRR. The exercise duration time was set to 155 minutes per week.

Control non-aerobic intervention

As proposed by previous publications (Colcombe and Kramer, 2003, Colcombe et al., 2003, Vidoni et al., 2012b, Voss et al., 2012, Hayes et al., 2013), stretching and toning were used as a control non-aerobic intervention. These participants had a similar schedule and balance of cofounding variables such as attention, social interactions, and other unknown variables that might influence the result. An experienced and trained exercise instructor ran these sessions three days a week at the local exercise facility. The activities included axial and appendicular stretching and toning exercises, seated exercises on a large diameter exercise ball, and modified versions of Tai Chi and yoga for older adults. Certified

personal trainers were provided with a schedule of specific exercises and verbal instructions to assist every participant.

Neuroimaging

Magnetic resonance imaging was collected at baseline and follow-up within 3 weeks of the CR fitness assessment. The session included a high-resolution T1 image for anatomic localization, region-of interest segmentation, and to assess for gross anatomical differences with a high gray-white matter contrast (MPRAGE; 1x1x1mm voxels; TR = 2500, TE = 4.38, TI = 1100, FOV 256 x 256 with 18% oversample, 1mm slice thickness, flip angle 8 degrees). A diffusion weighted sequence was also acquired and designed to provide optimal acquisition parameters while minimizing scanner duration for the participant. Due to MRI scanner replacement during our recruitment process, two diffusion imaging sequences were acquired. The first DTI sequence ($n_{\text{baseline and follow up}}$= 14x2=28) was acquired in a Siemens 3.0 Tesla Allegra MRI scanner using single-shot echo-planar imaging sequences with a repetition time [TR]=1000ms and echo time [TE]=81ms. Diffusion gradients were applied in 36 directions (b_0 = 0 s/mm^2 and b_1= 800 s/mm^2). The second diffusion imaging acquisition ($n_{\text{baseline and follow up}}$= 16x2=32) used a Siemens 3.0 Tesla Skyra with a repetition time (TR)= 1000ms and echo time (TE)=90ms. Diffusion gradients were applied in 65 directions (b_0 = 0 s/mm^2 and b_1= 1000 s/mm^2. Seventy-five 2-mm sections were acquired in at in-plane resolution of 128x128 with a 300mm field of view (FOV) in both DTI acquisitions. To maintain longitudinal differences consistent, baseline and follow-up sequences for every participant were acquired in the same scanner, using either the Allegra or the Skyra MRI scanner. No differences between participants' age, gender or VO_2peak

were found between scanners. Therefore, we combined both diffusion imaging sequences in our analysis.

Imaging Analysis

T1 image segmentation

After manually checking every T1 MPRAGE structural image, we performed volumetric segmentation using the FreeSurfer image analyses suite (FreeSurfer 5.2.3). The technical details of these procedures are described in prior publications (Dale and Sereno, 1993, Dale et al., 1999, Fischl and Dale, 2000, Fischl et al., 2001, Fischl et al., 2004, Han et al., 2006, Jovicich et al., 2006). This procedure includes an automated Talairach transformation, and cortical and subcortical segmentations of white matter and gray matter structures based on a surface-stream imaging stream (Fischl et al., 2002, Fischl et al., 2004). Once the imaging-processing pipeline is finished, we extracted bilaterally (left and right) the baseline and follow-up volumetric segmentations of the thalamus (our seed region) and the following cortical regions: cingulate, frontal, occipital, parietal, post-central, pre-central, and temporal (our target regions). We used these segmentations as our seed and target masks during our probabilistic tractography analyses (Figure 8.2).

Pre-processing diffusion images

After manually inspecting our diffusion weighted images, we applied eddy current correction for small distortions and simple head motion, by alignment the diffusion weighted images to the b_0 image. Next, brain extraction tool (BET2) was applied to strip the brain from the skull, and diffusivity metrics (fractional anisotropy [FA] and radial diffusivity [RD]) were calculated for the posterior analyses. Once the diffusion weighted images were eddy current corrected, we submitted our images and their dependencies to

run probabilistic tractography algorithm to run in the high performance computing system (FSL, 2013a).

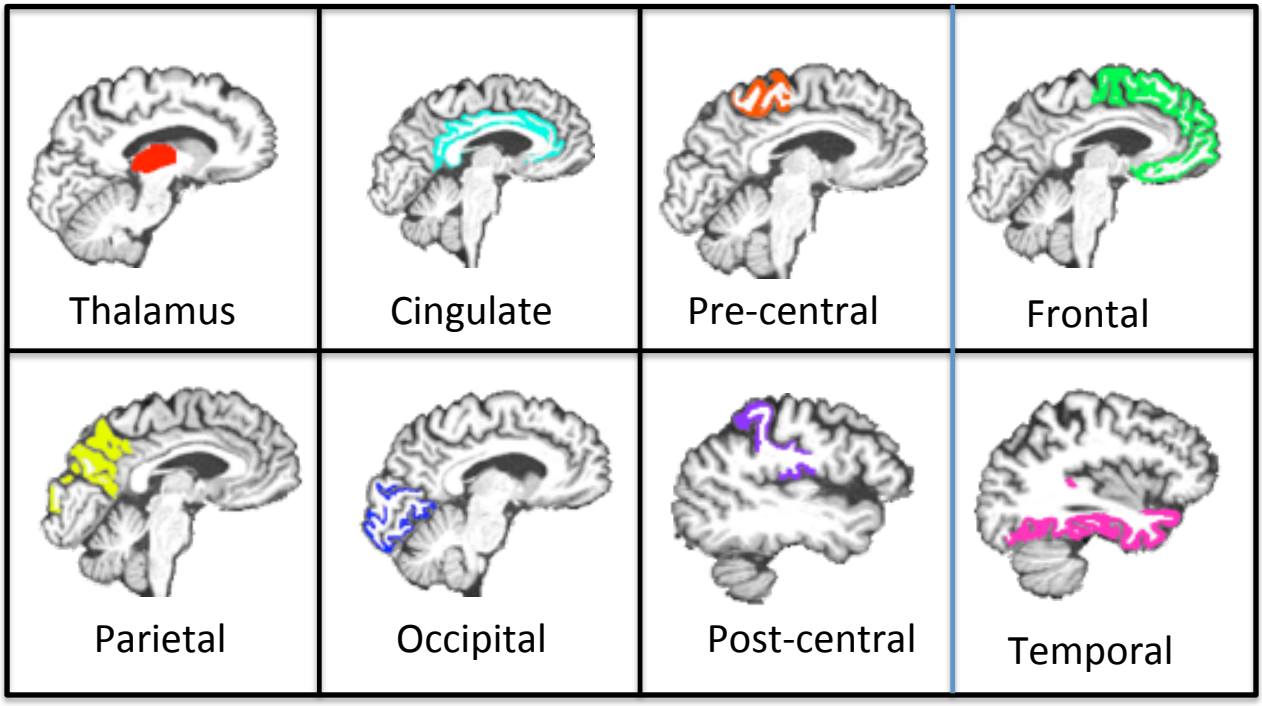

Figure 8.2. A representation of the seed mask (the thalamus in red) and target masks (highlighted in different colors according to its locations). These masks are overlapped into a specific participant's atructural space using the FreeSurfer segmentations.

Probabilistic tractography

On every participant's diffusion imaging data, we executed BEDPOSTX (FMRIB's Bayesian Estimation of Diffusion Parameters Obtained using Sampling Techniques) (Behrens et al., 2003b, Behrens et al., 2007) using the high performance computing cluster at The University of Kansas Information and Telecommunication Technology Center (ITTC). BEDPOSTX uses intrinsic information about multiple diffusion gradient angles to formulate orientation distribution functions (ODF) on every voxel thus creating all the necessary dependencies (e.g. probability distribution functions on every voxel) to run

probabilistic tractography. Next, we ran probabilistic tracking using PROBTRACKX (Behrens et al., 2007).

During this PROBTRACKX procedure, the algorithm repetitively samples a streamline projection from every voxel in the seed region to its target destination using the probabilistic distribution functions generated during BEDPOSTX. By tracing its seed-to-target projections multiple times, PROBTRACKX is able to build up connectivity distribution maps between the seed and the target region. All these procedures were performed in diffusion space for every participant using the thalamus as the seed region and target region. Thus, for every participant this process was repeated 14 times (7 for each hemisphere) at baseline and follow-up to cover all the target masks (or cortical regions). The analyses were done on unilateral in every hemisphere masking the contralateral hemisphere to avoid inter-hemisphere tracking connectivity. Additionally, we also masked other non-related structures such as the cerebellum, the midbrain, and the brain ventricles from each person's unique ventricle FreeSurfer segmentation.

We generated 5000 streamline samples from our seed region, with a maximum of 2000 steps with a length of 0.5 mm and a curvature threshold of 0.2. In this study, we used the thalamus as our seed region and the seven cortical regions as our target regions (separately), which were generated from the T1 image and using the FreeSurfer segmentations. Hence, since our FreeSurfer segmentations were not in diffusion space, we used FLIRT (FMRIB's linear registration tool) to transform these segmentations from structural space to its appropriate intra-subject diffusion space.

Structural connectivity diffusivity measures

To characterize the structural integrity of the thalamo-cortical connections, once the probabilistic tractography analyses were finished we applied a 15% threshold of maximum connectivity value to include only those voxels with highest likelihood of being connected to the seed region. This threshold criterion differs from a total streamline thresholded as previously reported, which directly accounts for inter-subject variability (Johansen-Berg et al., 2007). Instead as we are looking to pre- and post- intervention changes, our threshold criteria accommodates for individual differences in connectivity values for each tract while maximizing tract size and quality, as previously reported (Bennett et al., 2011). After we applied our threshold criteria at baseline and follow-up, we extracted the average FA/RD value on each thalamo-cortical connection (Figure 8.4), calculated an average FA/RD percent changes ($100*[Timepoint_{pos} - Timepoint_{pre}]/Timepoint_{pre}$) and fed this value into SPSS for further statistical analyses.

Classification Targets

After our seven probabilistic tractography analyses were conducted (thalamus-to-every-cortical-region) in every participant separately, we characterized the connectivity likelihood for every voxel in the thalamus to our 7 cortical target regions. To do so, we used the classification target approach provided by FSL. This algorithm quantifies the connectivity values on every voxel in the seed mask (e.g. the thalamus) with respect to all the 7 target connectivity projections. Then, it classifies and sub-divides (according to its connectivity) each voxel within the thalamus to one of the 7 cortical targets according to maximum likelihood of thalamo-cortical connectivity (Figure 8.3) (Behrens et al., 2003a). We then calculated the volume (on a voxel basis) of these sub-thalamic divisions before

and after the exercise intervention program, we measured a percent change ([$Timepoint_{pos}$ – $Timepoint_{pre}$]/$Timepoint_{pre}$), and fed this values into SPSS on every participant for further statistical analyses.

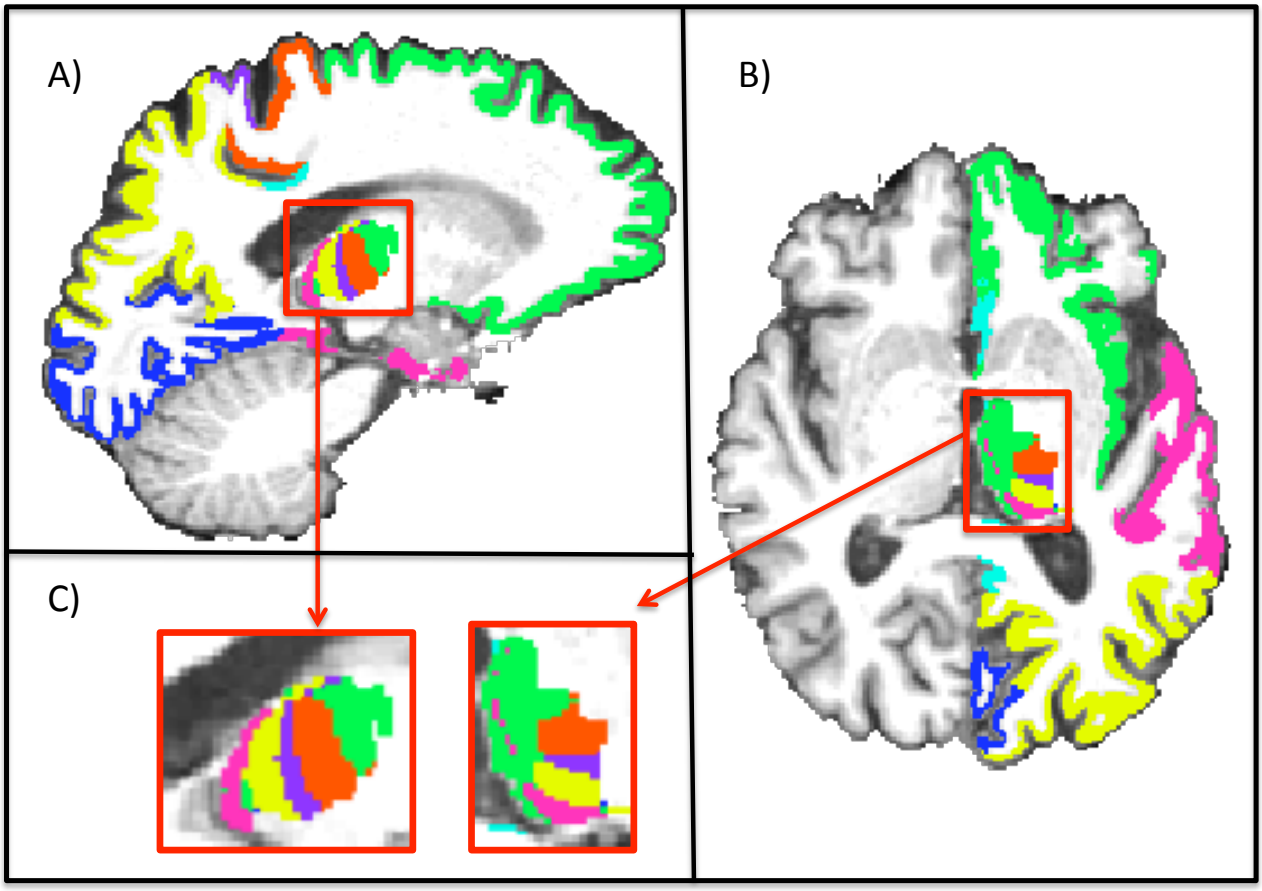

Figure 8.3. Subthalamic connectivity-based segmentations created by the classification target algorithms. The colored maps in the thalamus represent the highest connectivity likelihood to the cortical regions: frontal (green), precentral (orange), postcentral (purple), parietal (yellow), occipital (blue), and temporal (pink). Sagittal (A) and axial (B) views are represented with zoomed-in thalamus segmentations (C) for a specific participant.

Statistical analysis

Statistical analyses were conducted using SPSS 22.0 (IBM Corp., Armonk, NY). Parametric analysis of variance (ANOVA) and chi-square tests were used to evaluate group differences in clinical and demographic characteristics.

To test group differences (aerobic vs. non-aerobic) on longitudinal thalamo-cortical diffusivity metrics, we conducted similar ANOVA analyses in the percent FA/RD changes ($100*[T_{pos} - T_{pre}]/T_{pre}$), controlling for age, gender, and scanner type.

For the classification target algorithm, we quantified and classified the thalamus volumes into seven sub-regions according to its highest projection likelihood to the cortical targets. We classified each thalamic volume (left and right) for every participant before and after the intervention. Then, for every participant we calculated percent volumetric classification difference between pre and post intervention ($100*[T_{pos} - T_{pre}]/T_{pre}$). To compare the differences between aerobic exercise and non-aerobic controls, we then conducted univariate analyses on the percent changes between pre and post intervention ($[T_{pos} - T_{pre}]/T_{pre}$) for every thalamo-cortical sub-region using age, gender and scanner type as covariates. For all analyses, we set our alpha to 0.05.

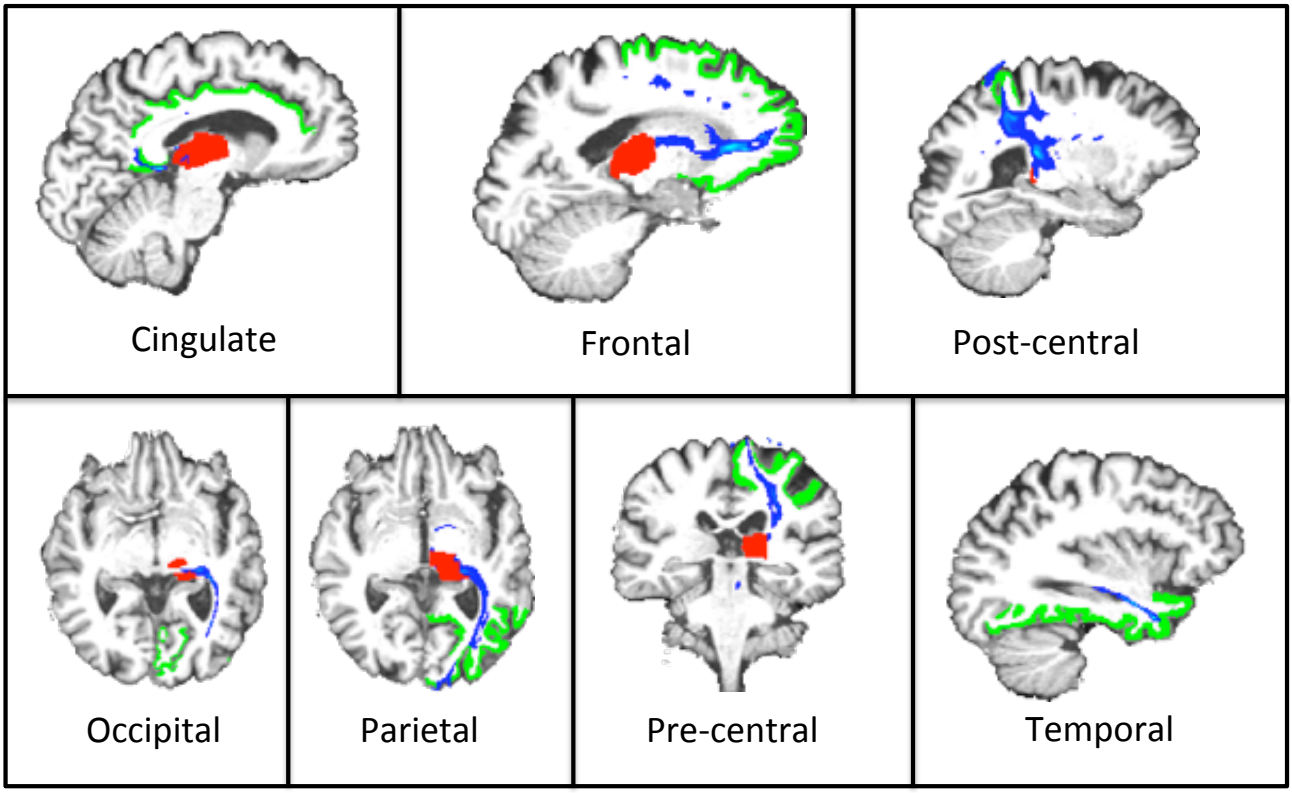

Figure 8.4 Thalamo-cortical connections thresholded at 15% of highest connectivity (in blue) from the specific thalamic seed (in red) and the different cortical target masks (in green) overlapped in a participants' FreeSurfer structural space.

8.4 RESULTS

Demographics

Table 8.1 summarizes the subject's baseline demographics, physical, and CR fitness characteristics of the 30 participants included in the study. We did not find any significant group differences (aerobic vs. non-aerobic) in gender, age, intervention adherence, and baseline MMSE, BMI, or VO_2peak. However, the aerobic exercise group presented a significantly higher change in VO_2peak ($100*[T_{post} - T_{pre}]/T_{pre}$) when compared to the non-aerobic control group.

	All groups	Aerobic	Non-aerobic	p-value
N (female)	30 (10)	14 (4)	16 (6)	0.45
Age (SD)	71.5 (6.7)	72.5 (6.4)	70.43 (7.2)	0.41
Baseline MMSE (SD)	26.1 (3.3)	26.7 (3.6)	25.5 (3.0)	0.34
Baseline BMI (SD)	28.2 (3.7)	28.4 (3.0)	28.0 (4.5)	0.81
Baseline VO_2peak (ml/kg/min)	21.9 (5.3)	20.5 (4.3)	23.6 (5.91)	0.11
VO_2peak change (%)	0.45 (2.1)	1.3 (1.8)	-0.54 (2.0)	**.014***
Intervention Adherence (% minutes attended)	91.6%	86.3%	96.7%	0.06

Table 8.1 Participant's demographics, physical, and fitness characteristics.

Diffusivity measures of the thalamo-cortical connections

We investigated group differences (aerobic vs. non-aerobic) in longitudinal diffusivity percent changes (FA and RD) of the thalamo-cortical structural connections (Figure 8.4, in blue). We did not find any significant results in the FA nor the RD percent measures (Table 8.2 and 8.3). Though, our data showed a trend for increased percent FA changes in thalamo-cortical connections in the aerobic exercise group when compared to decreased FA in the non-aerobic controls (Table 8.2, last column). Similarly, a trend (not significant) for lower RD percent changes were found in the aerobic exercise group when compared to the non-aerobic controls (Table 8.3).

Averaged FA values	Aerobic Exercise (n=16)		Non-aerobic Control (n=14)		Group diff.
	Pre	% diff	Pre	% diff	%change (p>0.1)
Cingulate-%					
Left	0.38 (0.08)	-0.93 (11.91)	0.36 (0.08)	-5.48 (19.24)	4.55
Right	0.42 (0.05)	1.38 (7.63)	0.040 (0.05)	-1.92 (10.58)	3.3
Frontal-%					
Left	0.41 (0.03)	1.54 (8.68)	0.42 (0.03)	-3.62 (7.79)	5.16
Right	0.41 (0.03)	0.99 (4.13)	0.42 (0.03)	-1.24 (4.59)	2.23
Occipital-%					
Left	0.46 (0.03)	-0.52 (7.76)	0.45 (0.05)	-4.41 (11.92)	3.89
Right	0.45 (0.05)	-2.16 (5.68)	0.46 (0.04)	-4.26 (10.11)	2.1
Parietal-%					
Left	0.44 (0.04)	-0.24 (5.38)	0.44 (0.05)	-2.21 (8.33)	1.97
Right	0.46 (0.04)	-0.25 (5.65)	0.44 (0.05)	-1.33 (8.15)	1.08
Post-central-%					
Left	0.45 (0.04)	2.11 (8.48)	0.44 (0.06)	-1.73 (8.41)	3.84
Right	0.46 (0.04)	1.63 (4.58)	0.43 (0.05)	0.3 (7.74)	1.33
Pre-central-%					
Left	0.46 (0.04)	0.09 (5.27)	0.47 (0.05)	-2.81 (6.45)	2.9
Right	0.46 (0.05)	1.84 (4.73)	0.46 (0.04)	-0.8 (5.83)	2.64
Temporal-%					
Left	0.33 (0.04)	5.07 (16.21)	0.34 (0.03)	-4.17 (13.98)	9.24
Right	0.33 (0.04)	4.68 (14.6)	0.32 (0.02)	-1.04 (8.51)	5.72

Table 8.2. Averaged fractional anisotropy measures before (pre-) intervention split by intervention groups. % diff denotes the averaged percent differences before and after intervention. Group diff %change denotes the group differences between percent changes in the exercise group compared to the non-aerobic controls.

Averaged RD values	Aerobic Exercise (n=16)		Non-aerobic Control (n=14)		Group diff.
	Pre	% diff	Pre	% diff	%change
Cingulate-%					
Left	0.85 (0.22)	3.97 (13.63)	0.89 (0.27)	20.95 (43.28)	-16.98
Right	0.73 (0.1)	-2.9 (12.93)	0.79 (0.15)	2.06 (17.82)	-4.96
Frontal-%					
Left	0.68 (0.07)	-0.69 (8.84)	0.65 (0.07)	6.3 (12.52)	-6.99
Right	0.67 (0.06)	-2.12 (8.13)	0.63 (0.06)	3.29 (5.52)	-5.41
Occipital-%					
Left	0.64 (0.07)	-0.08 (9.14)	0.65 (0.09)	16.07 (37.16)	-16.15
Right	0.69 (0.12)	1.15 (7.48)	0.65 (0.08)	6.45 (15.01)	-5.30
Parietal-%					
Left	0.64 (0.06)	-0.32 (7.53)	0.63 (0.08)	7.35 (19.08)	-7.67
Right	0.63 (0.05)	-0.12 (7.35)	0.64 (0.09)	3.63 (10.61)	-3.75
Post-central-%					
Left	0.64 (0.07)	-1.1 (9.26)	0.66 (0.12)	2.21 (15.57)	-3.31
Right	0.64 (0.05)	-1.72 (10.27)	0.69 (0.1)	0.52 (9.26)	-2.24
Pre-central-%					
Left	0.6 (0.06)	0.89 (9.15)	0.6 (0.08)	4.51 (8.57)	-3.62
Right	0.61 (0.05)	-2.91 (8.53)	0.62 (0.08)	2.81 (6.21)	-5.72
Temporal-%					
Left	0.95 (0.14)	-3.68 (13.93)	0.91 (0.11)	7.94 (25.19)	-11.62
Right	0.93 (0.14)	-3.71 (16.87)	0.95 (0.08)	2.78 (9.97)	-6.49

Table 8.3. Averaged radial diffusivity measures before (pre-) intervention split by intervention groups. % diff denotes the averaged percent differences before and after intervention. Group diff %change denotes the group differences between percent changes in the exercise group compared to the non-aerobic controls.

Sub-thalamic volumetric classification

To evaluate the effects of aerobic exercise in subthalamic volumes, we conducted group difference analyses (aerobic vs. non-aerobic) in the longitudinal volumetric changes of the whole thalamus and its subdivisions based on its likelihood for thalamo-cortical connectivity (Figure 8.3c). For the whole thalamus, we did not find any group differences or longitudinal difference in any of the groups (Table 8.4, first row). When evaluating volumetric thalamic subdivisions, we found that the exercise group had a significant increase in subthalamic volume that projects to the right cingulate gyrus when compared to the non-aerobic controls (2.67% vs -0.91%, p=0.029). On the other hand, we found a significant decrease in the subthalamic volume that projects to the left post central gyrus in the aerobic exercise group when compared to the non-aerobic controls (-1.12% vs 0.34%, p=0.041). All the other longitudinal subthalamic volumetric changes did not show significant differences between groups.

Table 8.4. Connectivity-based volumetric segmentations of the subthalamic volume before (pre) intervention. % diff denotes the percent difference after the intervention program. * denotes p<0.05.

	Aerobic Exercise (n=16)		Non-aerobic Control (n=14)		Group % diffences
	Pre	% diff	Pre	% diff	p-value
Thalamus Volume - cm^3					
Left	6.61 (1.0)	-1.06 (2.0)	6.48 (0.7)	-0.61 (1.8)	0.91
Right	6.92 (0.9)	-0.85 (1.0)	6.90 (0.7)	-0.78 (1.9)	0.48
Cingulate-%					
Left	5.61 (10.3)	0.95 (4.4)	4.03 (9.9)	-0.12 (2.4)	0.07
Right	3.62 (4.8)	2.66 (6.3)	1.78 (2.6)	-0.91 (1.7)	**0.03***
Frontal-%					
Left	43.85 (7.7)	0.29 (5.8)	49.22 (8.9)	1.8 (12.8)	0.83
Right	49.43 (7.8)	2.43 (4.4)	51.42 (9.0)	4.49 (9.3)	0.48
Occipital-%					
Left	1.92 (1.6)	0.59 (3.3)	1.8 (3.2)	0.43 (1.7)	0.87
Right	1.36 (1.5)	0.39 (2.4)	1.22 (1.5)	-0.01 (1.9)	0.63
Parietal-%					
Left	12.76 (5.0)	1.06 (4.9)	12.02 (5.0)	-2.12 (4.9)	0.14
Right	15.77 (4.6)	-1.01 (3.5)	12.8 (5.6)	-2.49 (6.6)	0.61
Post-central-%					
Left	4.60 (2.8)	-1.12 (2.1)	3.9 (2.3)	0.34 (2.2)	**0.04***
Right	4.16 (1.9)	0.32 (1.7)	3.58 (2.0)	-0.36 (2.5)	0.39
Pre-central-%					
Left	12.65 (3.7)	-0.57 (2.8)	12.16 (2.6)	-0.44 (2.3)	0.77
Right	12.37 (3.3)	-1.35 (1.7)	14.55 (4.5)	-0.66 (2.3)	0.36
Temporal-%					
Left	4.60 (2.8)	0.95 (8.6)	16.7 (8.8)	-0.37 (8.7)	0.89
Right	12.38 (5.9)	-3.12 (4.5)	13.46 (7.2)	-0.58 (5.4)	0.15

8.5 DISCUSSION

In this study, we investigated the effects of an interventional aerobic exercise program in thalamo-cortical connections and subthalamic volumes in a cohort of Alzheimer's disease patients. Hence, to evaluate group differences (aerobic vs. non-aerobic), we used diffusion imaging data, probabilistic tractography, and a classification target algorithm. First, we did not find any significant changes when we evaluated group differences in the thalamo-cortical diffusivity measures. Though, we found a trend for increased white matter preservation (decreased diffusivity) in the aerobic exercise group when compared to the non-aerobic control group. Second, we applied a classification target algorithm to investigate changes in subthalamic volume according to its likelihood of connectivity to 7 cortical regions (the cingulate, the frontal, the occipital, the parietal, the

post-central, the precentral and the temporal gyri). In the aerobic exercise group (compared to the non-aerobic control group), we found a longitudinal increase in the subthalamic volume that is connected to the right cingulate gyrus and a decreased in volume to the subthalamic region that connects the thalamus with the left post-central gyrus. To our knowledge, this is the first AD interventional study that explored the effects of aerobic exercise in thalamo-cortical connections.

In AD, brain atrophy is considered a marker of impaired functioning as the brain deteriorates long before clinical symptoms start to appear (Jack et al., 2010, Johnson et al., 2012a, Douaud et al., 2013). Neuroimaging studies have shown brain atrophy in gray matter regions (more specifically in medial temporal, frontal, and hippocampus regions) (Thompson et al., 2003) and in white matter tracts (more specifically in the uncinate fasciculus, the cingulum, the superior longitudinal fasciculus, and the corpus callosum) (Sexton et al., 2011, Clerx et al., 2012). In relation to thalamic atrophy and thalamo-cortical connections, *post-mortem* studies have been controversial due to inconsistent results (Braak and Braak, 1991a, Paskavitz et al., 1995). In *port-mortem* studies, the anterior thalamus nucleus is thought to be most affected in AD (Braak and Braak, 1991a). This nucleus connects directly to the hippocampus via the fornix, which is one of the earliest structures to be affected in AD (Oishi and Lyketsos, 2014). Additionally, the pulvinar part of the thalamus also connects to the hippocampus via the pulvinar tract (Zarei et al., 2010). On the other hand, *in-vivo* volumetric analyses have found decreased volumes in the thalamus when AD participants were compared to healthy older adults (de Jong et al., 2008, Zarei et al., 2010). The thalamus and brain regions including the precuneus, posterior cingulate cortex, frontal gyrus, and precentral gyrus have also shown decreased functional

connectivity in early AD when compared to non-demented controls (Wang et al., 2012, Zhou et al., 2013).In another age-related (age range between 20 and 74) diffusion imaging study, researchers found a significant age-related decrease in thalamo-cortical connections to the frontal lobe, a region that plays a crucial role in different cognitive domains including executive function, processing speed, and working memory (Hughes et al., 2012). Recent tractography-based analyses also showed that the atrophy of the dorsal-medial region of the thalamus in AD participants might have corresponded to changes in connectivity with the anterior temporal cortex and posterior hippocampus (Zarei et al., 2010). Here, we expanded the results of thalamo-cortical structural changes in AD before and after the effects of an aerobic exercise intervention program. To our knowledge, this is the first study of this type.

We found that the longitudinal thalamo-cortical connections to the right cingulate gyrus increased in the aerobic exercise group when compared to the non-aerobic control group. Similarly, we found that the thalamo-cortical connections to the left post-central gyrus decreased in the aerobic exercise group when compared to the non-aerobic control. These results suggest that the thalamo-cortical connections are dynamic and might change in response to environmental factors such as exercising for 26 weeks. The cingulate cortex received inputs from the thalamus and projects them to the enthorinnal cortex via the cingulum (Wyss and Van Groen, 1992). Both the cingulum (Xie et al., 2005, Zhang et al., 2007, Sexton et al., 2011, Sachdev et al., 2013) and the enthorinnal cortex (Janke et al., 2001, Thompson et al., 2001, Scharfman and Chao, 2013) are affected earlier in AD. Thus, it might be possible that AD-related disruption also occurred in thalamo-cortical connections that project to the cingulate gyrus. If this holds true, then our results indicate that AD-

related thalamo-cortical connections that get disrupted earlier due to AD (e.g. thalamo-to-cingulate connection), might be positively compensated by neuro-protective aerobic exercise mechanisms (see review (Voss et al., 2013a)), which is reflected in our results. Consequently, another less AD-related thalamo-cortical connection may diminish its connectivity as reflected by our decreased change in thalamo-cortical connection to the left post-central gyrus. However, the interpretation of our results are limited to our single study as no other thalamo-cortical connectivity studies have evaluated the effects of exercise in this older population.

However, previous studies have shown the positive effects of aerobic exercise or cardiorespiratory fitness in gray matter regions (Colcombe and Kramer, 2003, Colcombe et al., 2003, Colcombe et al., 2006, Burns et al., 2008, Erickson et al., 2009) and white matter tracts (Marks et al., 2007, Marks et al., 2011, Johnson et al., 2012b, Voss et al., 2012, Gons et al., 2013, Tian et al., 2014a). Additionally, meta-analysis reports showed that physical activity improves cognitive domains such as processing speed, executive function, and memory (see reviews (Colcombe and Kramer, 2003, Smith et al., 2010, Erickson et al., 2014)). In the Alzheimer's disease populations, we have found a positive relationship between CR fitness and brain atrophy in gray and white matter regions using structural volumetric analyses (Burns et al., 2008, Honea et al., 2009) and functional imaging connectivity (Vidoni et al., 2012a). Hence in this work, we expanded our investigation on the effects of aerobic exercise in the thalamus, and its thalamo-cortical connections.

One of the major limitations in our study is the different diffusion imaging sequence acquired during our intervention program. To minimize this limitation, we collected pre and post intervention data for all the participants who in the same scanner (either the Allegra or the Skyra) and we also conducted statistical analyses on percent change differences while controlling for scanner type. Another limitation is the small sample size in our analyses, which might increase the variance among our thalamo-cortical diffusivity and subthalamic volumetric measures. However a trend for preserved white matter integrity was found in the exercise group when compared to the non-aerobic control group. We believe that future studies with higher number of participants and an adequate diffusion acquisition sequences will allow us to characterize further the effects of aerobic exercise in AD after an aerobic exercise intervention.

8.6 CONCLUSION

After a 26-week aerobic exercise intervention program in older adults at the earlier stages of AD, we characterized longitudinal group differences in diffusivity metrics of thalamo-cortical connections and subthalamic volumes using diffusion imaging data. We found that after the exercise program, participants who underwent aerobic exercise had increased subthalamic volume connected to the right cingulate gyrus and decreased subthalamic volume connected to the left post-central gyrus. These findings suggest that the thalamo-cortical projections are dynamic and might change due to neuro-protective factors such as aerobic exercise. A compensation mechanism might be triggered with aerobic exercise that might allow a higher connectivity in AD-related disrupted regions (e.g. cingulate gyrus) while undercompensating its connectivity in less AD-involved regions

(e.g. post-central gyrus) yet further research should be done to investigate this matter further since (to our knowledge) this is the first study of its kind.

Preface Chapter 9

The main purpose of this work was to evaluate and apply novel diffusion imaging methods to characterize the effects of aerobic exercise activity on brain neuroplasticity. More specifically, I aimed to evaluate the effects of exercise in the integrity of the brain's white matter fiber bundles. This work focused on the older adult population with emphasis on participants who were diagnosed with early stage Alzheimer's disease. In this chapter, I discussed a brief summary of my findings, *in-vivo* imaging considerations and clinical considerations for researchers new to the field, future directions and a final conclusion of my work.

Chapter 9

Summary of findings, recommendations, future directions, and final remarks

9.1 Summary of findings

Chapter 3. *A comparative white matter study with Parkinson's disease, Parkinson's disease with dementia and Alzheimer's disease.*

The objective of this study was to investigate group differences in white matter integrity in Parkinson's disease (PD), Parkinson's diseases with dementia (PDD), Alzheimer's disease (AD), and a healthy control group (CON). This chapter was my first completed manuscript and allowed me to understand better the neuro-pathology and deterioration progression of two very common neurodegenerative diseases: Alzheimer's disease and Parkinson's disease. In addition, it allowed me to understand in depth the application of *in-vivo* neuroimaging techniques to characterize changes of white matter micro-structural integrity using diffusion imaging data. This study also expanded my knowledge on the different advantages and disadvantages of two common diffusion imaging methods: a region-of-interest (ROI) approach and whole brain tract-based spatial statistic (TBSS). At the conclusion of this work, I was able to combine these two diffusion imaging processing methods and I introduced a more white matter tract specific method (e.g. looking at changes based on white matter tracts rather than localized brain regions, see Chapter 4). Results showed whole brain deterioration in the PDD group when compared to the CON, PD, and AD group. Additionally, the AD group also showed global but in less extend white matter deterioration when compared to the PD group, which had significantly younger participants than the other groups.

Chapter 4. *Diffusion tensor Imaging and Alzheimer's disease: a comparison between two processing methods, tract-based spatial statistics and tract of interest*

This chapter focused on a methodological comparison between the most widely used diffusion imaging method known as tract-based spatial statistics (TBSS) and an *a-priori* tract-of-interest approach. Here I presented a tract-of-interest approach that overcomes some limitations of whole brain imaging analyses such as TBSS. I also wanted to investigate whether different diffusion imaging methods would change significant results in the progression of AD. Hence, in this chapter I processed a large dataset from the Alzheimer's Disease Neuroimaging Initiative (ADNI, n=208), a worldwide project that provides extensive clinical and neuroimaging data for the prevention and treatment of AD. I characterized and compared the integrity of white matter by means of diffusion among three groups of older adults: a healthy non-demented group, an Alzheimer's disease group, and a mild cognitive impairment (MCI) group, the latter being a transitional stage of non-demented populations with a higher likelihood to develop to AD (Mufson et al., 2012). The goal of this chapter was to use a large sample of older adults (with and without dementia) to compare and characterize the results of the *a-priori* tract-of-interest approach with TBSS for future consequent diffusion analyses. In TBSS, we found a widespread FA decline in the AD cohorts when compared to MCI and to a greater extent when compared to ND ($p<0.05$ corrected). No significant differences were found when MCI was compared to ND or in any RD group comparisons. In TOI, we found significant group differences in both FA and RD measures, specifically in the splenium of the corpus callosum, the cingulum, the inferior fronto-occipital, and the uncinate fasciculus.

At the conclusion of this study, I argued for the use of an *a-priori* tract-of-interest approach as it showed more descriptive results at specific *a-priori* whole white matter conduits (or tracts). In whole brain volume analyses (e.g. TBSS), clusters of significant voxels might describe deterioration only on parts of these white matter conduits. Hence, the results and interpretations should be described in relation to brain regions rather than white matter tracts, as they do not specify whole conduit white matter tract deterioration.

Chapter 5*. Cardiorespiratory fitness and white matter integrity in Alzheimer's disease*

Previous evidence indicates that exercise and physical activity have positive effects in slowing down the evident age-related brain deterioration. In white matter, only few reports (Marks et al., 2011, Johnson et al., 2012b, Voss et al., 2012, Gons et al., 2013, Chaddock-Heyman et al., 2014, Tian et al., 2014a) have shown this positive association but none have reported this in the Alzheimer's disease population. Thus, Chapter 5 aims to compare the relationship between cardiorespiratory fitness levels, a direct measure of physical activity, and white matter tract integrity in a sample of early stage Alzheimer's disease participants. I evaluated these associations in specific *a-priori* white matter tracts that deteriorate earlier in Alzheimer's disease. Additionally, I performed whole brain tract-based spatial statistics to look at relationships across the whole brain. The cross-sectional sample included older adults at the earlier stages of Alzheimer's disease (n=37). I evaluated partial correlations controlling for age and gender in fractional anisotropy, our primary diffusivity metric. If significant results were found, subsequent analyses were performed in other diffusivity metrics (radial diffusivity, mean diffusivity, and axial diffusivity). A positive correlation with preserved diffusivity and higher cardiorespiratory

fitness was found in a tract that connects temporal, occipital, and frontal cortices (e.g. inferior fronto-occipital fasciculus). Hence, our results suggest that increased CR fitness might positively affect white matter integrity even after the onset of Alzheimer's disease.

***Chapter 6**. A longitudinal assessment of brain neuroplasticity and exercise intensity in healthy older adults: a 26-week exercise intervention study*

To date, it is still uncertain the amount of exercise activity (or exercise dose intensity) needed to affect positively the neuroplasticity of the brain. Thus, to continue my investigation on the effects of exercise and brain health, in this chapter I aimed to explore the relationship between different exercise doses and brain structural differences using *a-priori* AD-related cortical gray matter regions and white matter tracts. The sample data consisted of healthy non-demented cohorts who underwent a longitudinal intervention program at different exercise doses (75 mins/week, 150 mins/week, 225 mins/week) and a control group. However, due to the small longitudinal sample (n=10) I was unable to investigate the differences between exercise doses. Instead, I performed partial correlation analyses to test whether total exercise duration of the intervention program was related to volumetric percent changes of gray matter or diffusivity changes of white matter integrity. Additionally, I evaluated the association of volumetric and diffusivity percent changes with changes in cardiorespiratory fitness. I found that none of the *a-priori* volumetric changes in cortical volumes were associated with changes in VO_2peak. However, I found an association of preserved white matter integrity in the genu of the corpus callosum with longer exercise duration, supporting the idea that higher exercise activity might lead to preserved white matter tract integrity. Conversely I found a decrease in integrity of the cingulum with

longer exercise time duration, which may be explained by the AD-related progression of the disease. However, based on our sample size our results might be speculative rather than conclusive thus we encourage future researchers to explorer further the amount of exercise dose intensity that might positively affect brain health.

Chapter 7.*The effects of aerobic exercise on brain's white matter integrity in the Alzheimer's disease population: a 26-week intervention program*

Due to the lack of interventional longitudinal studies in the Alzheimer's disease population on the effects of exercise in brain health (especially in white matter), I investigated the effects of a 26-week exercise intervention program on brain's white matter integrity. The sample data included early Alzheimer's disease participants (n=29) who underwent clinical, exercise, and neuroimaging evaluations at baseline and follow-up. I evaluated changes in diffusivity measures of *a-priori* white matter tracts and performed statistical longitudinal group difference analyses between the aerobic exercise group and the non-aerobic control group. Additionally for each group, I performed correlation analyses of percent diffusivity measures (fractional anisotropy and radial diffusivity) with percent changes in maximal oxygen consumption rates (VO_2peak), total intervention duration, and cognitive scores. No significant longitudinal group differences were found in white matter tract integrity or in changes of VO_2peak. However, the exercise group showed an increase in cognitive executive function when compared to the non-aerobic control group. Additionally only in the aerobic exercise group, longer exercise duration and mean cognitive scores were significantly associated with preserved white matter tract integrity after controlling for age and CDRsob. The results suggest that increased in cognition is

associated with preservation of white matter tract integrity yet the effects of physical fitness and exercise duration are inconclusive. I believe that future research with longer exercise intervention programs and a higher number of participants will allow us to explore further the neuro-protective mechanisms of aerobic exercise in this AD population who are at higher risk for accelerated white matter deterioration.

Chapter 8. *Aerobic exercise and thalamo-cortical connectivity in the Alzheimer's disease population: a 26-week exercise intervention study*

Evidence of exercise affecting cortical gray matter structures and white matter connectivity was covered in the previous chapters (chapter 5-7) of this work. In relation to the neuroprotective effect of aerobic exercise, this final chapter characterized the effects of aerobic exercise in structural thalamo-cortical connections and subthalamic volumes. The thalamus is a subcortical structure that acts as a relay station to filter all incoming information before directing it to cerebral cortex (Jones et al., 1985, Banich and Compton, 2010, FitzGerald et al., 2011). Being a highly interconnected subcortical structure to cortical regions that deteriorate in AD, I believe it is necessary to investigate whether the neuro-protective effects of aerobic exercise will affect this structure and its connections. Hence, I investigated whether a 26-week exercise intervention program can dynamically modify white matter thalamo-cortical connections and subthalamic volumes that precede cortical-to-cortical connectivity. The importance of this finding is to elucidate our understanding of the AD progression in the brain. I hypothesized that if higher functional networks (cortico-to-cortico) are disrupted in AD and that exercise might provide a neuro-protective effect, then lower functional incoming networks (thalamo-cortical) may also be

positively affected by strengthening those thalamo-cortical connections that are prone to disruption. I characterized the thalamo-cortical connections between an initial seed mask (e.g. the thalamus) and final target masks (e.g. seven cortical connections) using measures of diffusivity (e.g. fractional anisotropy and radial diffusivity). Additionally, I characterized and classified the different subthalamic nuclei based on the higher likelihood of connection to one of out target regions using a classification target algorithm. All these measures were evaluated before and after the intervention program in early Alzheimer's disease participants who underwent either aerobic (n=15) or non-aerobic (n=14) exercise training. I compared longitudinal group differences (aerobic exercise vs. non-aerobic controls) in diffusivity metrics for the thalamo-cortical connections and volumetric changes in the subthalamic nuclei. No group differences (aerobic vs. non-aerobic) were found in the thalamo-cortical connections. However in the aerobic exercise group, I found an increase in volume to the subthalamic region that connects to the right cingulate gyrus and a decrease in volume to those voxels that connect to post-central gyrus when compared to the non-aerobic control. These results suggests that aerobic exercise might dynamically change the thalamo-cortical connectivity to strengthen those connections that might have been deteriorated earlier in Alzheimer's disease. To our knowledge, this is the first probabilistic tractography analysis evaluating the effects of aerobic exercise in these thalamo-cortical connections. Thus, we encourage other researcher to investigate further so more valid conclusions can be drawn.

9.2 *IN-VIVO* IMAGING CONSIDERATIONS

Since the early 1980s neuroscience-related publications have increased exponentially (Jones et al., 2013b). The reason for this growth is related to the usage of advanced *in-vivo* magnetic resonance imaging (MRI, structural and functional imaging) to understand the behavior, functionality, and plasticity of the brain. Hence, there is a need to understand adequately the information these *in-vivo* images describe in relation to the neurobiology of the brain. In this section I will briefly describe some general considerations I believe every neuroscientist should consider before working with neuroimaging data.

First when acquiring *in-vivo* neuroimaging resonance data, researchers should be aware of the current limitations regarding the magnetic resonance imaging resolution (usually ~1-2 mm^3) and understand that a one-to-one relationship with cellular characteristics (usually in the μm) is complex as they offer a broader macroscopic picture of the neurobiology of the brain. For example in the case of white matter, diffusion imaging does not describe the characteristics of single myelinated axons but rather a macroscopic larger picture of the diffusion of water molecules constrained or unconstrained by thousands of axons traveling together in similar directions (Walhovd et al., 2014). If the density or myelination of these axons and supportive glial cells significantly changes due to some independent factor (e.g. age, gender, or aerobic exercise), then overall changes in diffusion are reflected and can be assessed by diffusion metrics (such as fractional anisotropy). However, the exact relationship between diffusion metrics and the underlying neurobiology is complex and difficult to interpret (Amlien and Fjell, 2014, Concha, 2014).

Another important consideration for all newcomers acquiring diffusion weighted images is the extent that motion artifacts during the scanning sequence could aggravate the

process of calculating diffusivity metrics. Thus, it is crucial to adapt a sequence based on your sample population (e.g. kids tends to move more than adults) while maintaining adequate acquisition duration and optimal parameters that will minimize the signal-to-noise ratio. This is very important when additional MRI sequences (e.g. fMRI, sMRI, spectroscopy, etc...) that lengthen the acquisition time are simultaneously collected in the same MRI session. In the case of diffusion imaging, the higher the number of gradient directions, the longer the sequence and the better estimation metrics you can get (Chapter 2), yet motion artifacts can greatly impact these calculations. However as technology gets better, more optimal acquisition parameters are currently being developed with shorter acquisition durations and improved metric estimations (e.g. DSI, HARDI, q-ball reconstruction) (Tuch, 2004, Poupon et al., 2008, Lee et al., 2014, Wilkins et al., 2014). Once the diffusion weighted images are acquired, the researcher should also consider the different limitations that arise when processing diffusion imaging data (Chapter 2). It is always imperative to inspect and quality check every single diffusion weighted image because single artifacts can cause detrimental effects when processing diffusion weighted images.

In relation to diffusion imaging data, there are two common approaches for exploring diffusion characteristics, you can either do group-wise statistical analyses (Chapter 5-7) or tractography analyses (chapter 8) (O'Donnell and Westin, 2011). During group-wise statistical analyses, usually tensor-based diffusivity metrics (e.g. fractional anisotropy or radial diffusivity)(O'Donnell and Westin, 2011) are calculated and fed into common group-wise statistical protocols (e.g. tract-based spatial statistics or DARTEL) (Smith et al., 2006, Ashburner, 2007). Considerations during these processing pipelines are

related to spatially transforming every image into a common space so a voxel-by-voxel statistical analysis is investigated. These implications are similar to what will happen in structural MRI images yet it might exacerbate the artifacts as diffusion imaging deals with diffusivity metrics previously calculated from a rotationally invariant tensor rather than volumetric measures. Thus, one of most common limitations for diffusion imaging is partial volume effects (e.g. investigating a phantom white matter tissue that belongs to gray matter or cerebrospinal fluid) as white matter tends to be less reliable in spatial location than gray matter. The reason for this problem is that white matter is in close proximity to ventricles that tend to enlarge as brain tissue atrophies especially in our sample of older adults with or without dementia (Braak and Braak, 1991b). This issue will affect pre-registration and post-registration misalignments as previously discussed (Edden and Jones, 2011, Zalesky, 2011). Additionally, to transform every subject's diffusion imagin into a common space, a "most representative" template should be chosen. Again, artifacts when transforming every diffusion image to a less group-specific but common template might add undesirable noise into the analysis. To overcome this limitation, different study specific templates are considered and other methodological reports are currently investigating strategies to improve inter-subject common template registrations (Keihaninejad et al., 2012, Schwarz et al., 2014). This problem exacerbates even further when longitudinal data is under investigation. To overcome this problem, a previous publication for example suggested a mid-point transformation in the intra subject images (Keihaninejad et al., 2013). Thus, throughout my work, I cautiously processed and used previous considerations when doing group-wise statistical analysis.

The second approach for using diffusion-imaging data is diffusion tractography, which can itself be divided into streamline tractography or probabilistic tractography. Streamline tractography uses the principal direction of diffusion and other diffusivity parameters (e.g. curvature or angle of diffusion, step length, step size) to generate a single tract conduit via voxel-by-voxel traveling from a seed mask to a specific target mask. Similarly, probabilistic tractography uses a seed and target mask but instead of generating a single connection, it creates a probabilistic map of projection based on the probability of diffusion on every anisotropic voxel. The main advantage of probabilistic tractography is its ability to create probabilistic conduits while streamline tractography only generates a single conduit, and will terminate if it reaches isotropic voxels that are most common in gray matter or cerebrospinal fluid. For either tractography method, the higher number of gradient directions (higher number of diffusion weighted images), the better estimation of diffusion you can achieve. However, the most known problem with diffusion data is when the conduit reaches a point of crossing fibers. At this point for example, streamline tractography might stop as crossing fiber voxel diffusion values tend to be isotropic anad may not reflect a specific white matter bundle direction. Thus, future investigators need to be aware of this problem and try to avoid these regions either by masking out potential crossing fiber regions or by using alternative sample strategies and methodologies to overcome these problems (Jensen et al., 2014, Lee et al., 2014, Wilkins et al., 2014). Finally, caution should be taken when interpreting the diffusion imaging results in either methodology. The researchers should to be aware of what the actual results are describing in relation to the brain, white matter integrity, and connectivity. Diffusivity measures such as fractional anisotropy or radial diffusivity for example, only offer information regarding

the diffusion direction dependency in a voxel either by looking at the degree of anisotropy (fractional anisotropy) or at the transverse diffusion (radial diffusivity). Thus, throughout this work I cautiously described our results based on the diffusivity metrics and not into a one-to-one relationship to neuronal characteristics (e.g. axonal bundle connectivity, increase density of myelination or supportive glial cells). However, it is important to recognize that these neuronal characteristics may be driven these diffusivity changes (Walhovd et al., 2014). Similarly, tractography analyses might cofound these spatial resolution limitations yet I believe that as technology advances (e.g. Moore's law (Schaller, 1997)), a future time will come where very high *in-vivo* imaging resolution will allow us to make comparable and more specific cellular characteristics.

9.3 OLDER ADULT EXERCISE-RELATED CONSIDERATIONS

During this work, the main objective was to characterize *in-vivo* the effects of aerobic exercise activities in older adult populations with and without memory problems. Here, I will describe some important considerations that should be taken into account when working with this population. First, it is worth noting that these clinical sedentary participants have beginning memory problems so special care should be taken when collecting neuroimaging data or evaluating the participants during the exercise tests. Therefore before collecting imaging data, at the day of the scan we met again with the participant and described carefully the imaging scanning procedure. Additionally, we evaluated their performance in cognitive tasks (if any) to be performed during specific scanning sequences (e.g. functional task-based imaging sequences). If the participants felt uncomfortable with these tasks, we decided to exclude these sequences from the data

collection. In relations to exercise evaluations, we adapted specific cardiorespiratory fitness tests for older populations, as their physiological demands might deviate from normal standardized fitness tests for younger populations (Hollenberg et al., 1998, Burns et al., 2008). Additionally, during the intervention program we carefully provided, a variety of YMCA facilities, so the participants can perform their weekly exercise activity in a conformable environment with reduced commuting time and increased accessibility. We believed this improved the adherence interventions rate and a more successful conclusion of our study.

Second, when working with older adult populations it is worth considering the implications of concurrent age-related deterioration or higher risk for other related diseases. Age-related deterioration in white matter occurs in every older adult (Bartzokis, 2011) thus in all our analyses we carefully control for this cofounding variable. Additionally, controlling for another cofounding variable that relates to the progression of the disease could also be an ideal strategy. To do so, we controlled for neurocognitive scores (e.g. CDR sum of boxes, Chapter 7-8) yet it is worth noting that its use might not be practical if a wide range of progression does not exist between our participants. Older adult populations are also at higher risk for other related diseases that may or may not impact white matter. Therefore, clinicians may perform a careful screening before enrolling participants to identify other diseases that will affect neurodegeneration independent of AD pathology. Strokes, tumors, cardiovascular disease, psychiatric disorders, myelin disorders, and other non AD-related dementias (e.g. Lewy bodies or vascular dementia) are some examples of disorders that might affect brain deterioration (Fields, 2008).

Finally, it is also worth considering the experimental statistical setup. In brain imaging, statistical tests could be performed using *a-priori* hypotheses (e.g. region-of-interest or tract-of-interest) or doing whole brain exploratory analyses. Throughout this work, I proposed using *a-priori* hypotheses by selecting specific white matter tracts that were related to exercise (Chapter 5) or AD-related deterioration (Chapter 6-8). I believe that this approach is more specific and allows us to provide an elegant scientific interpretation of our results based on better-planned experiments. However, we also included whole brain exploratory analyses (e.g. TBSS) to compare our results with current literature and confirm our *a-priori* evaluations. These exploratory analyses are also worth considering as they may identify regions (or tracts) that were previously not hypothesized yet caution should be taken due to an increase chance for detecting false positives.

9.4 FUTURE DIRECTIONS

After the conclusion of this work, I believe I have a better understanding of age-related and Alzheimer's disease brain deterioratin and how I can apply *in-vivo* neuroimaging techniques (such as diffusion imaging) to characterize structural changes in the brain. Additionally, I have gained much experience on how to combine my technical and scientific views to be able to develop hypotheses in different fields that include human physiology, neurobiology of disease, exercise science, and neuroscience.

Future work as part of my expertise might include the application of additional *in-vivo* neuroimaging techniques (e.g. structural and functional MRI, FDG PET, amyloid-PET, etc) to explore further the neuroplasticity of the brain and the neuro-protective effects of aerobic exercise. A very interesting approach would be to combine structural and

functional imaging data to performed more specific tractography analyses. For example, using structural volumetric data (T1 MPRAGE images), we could identify specific subcortical structures that are vulnerable to AD (e.g. hippocampus). Then using specific cognitive tasks during functional imaging sequences, we could identify brain regions with hyper- or hypo- activity similar to our region of interest (e.g. hippocampus), which may denote a similar pattern of connectivity. Hence, we could use probabilistic tractography to identify the patterns of connectivity and the integrity of these structural connections. This example gets more interesting if we collect longitudinal data since we could explore further the dynamic connectivity adaptation of these structural networks when an environmental factor is under investigation (e.g. aerobic exercise). Similarly, we could add PET imaging data to further classify our participants either by being amyloid negative or positive (in the case of amyloid-related ligands) or use poorly metabolic regions (in the case of metabolic ligands) as demarcations of poor brain connectivity. These future directions get even more interesting when machine learning classification target algorithms (e.g. independent component analysis, support vector machines) are added to the analyses.

Alternatively, I can also apply these methods to other sample populations where brain alterations due to pathology or developmental processes can be detected. For example, I believe that AD-related degeneration is a consequence of a poorly connected brain, a topic that is recently emerging (Bartzokis, 2011, Filley, 2012, Sachdev et al., 2013, Amlien and Fjell, 2014, Zhang et al., 2014). That being said, I believe that white matter deterioration might precede gray matter disruption yet not enough currently evidence points towards this inclination. One of the possible reasons might be due pioneering volumetric imaging results that provided the ground basis of AD-related results for *in-vivo*

imaging when more novel techniques (e.g. diffusion imaging) were not yet evaluated. Having said this, my future direction would be to investigate further my hypothesis in the neurodevelopmental process of the brain. As previously stated (Seung, 2012), we come to the world with our genes (similar to our dealt playing cards in a poker game). Then it's up to the environment to succeed on it by creating completely different brain connections. Hence, as the brain adapts to the new environment some brain connections strengthen or other weakens based on the adaption of every individual in their earlier years where many more white matter connections are present than in a fully developed adult brain. I believe that a similar but reversive process happens in the brains of older adults. Thus, my future direction would be to identify why this happens using advanced *in-vivo* neuro-imaging tools and a greater age range of individuals from childhood all the way to older adults. My goal for my future is to understand the neurobiological mechanisms of the brain, how it allows us to learn and remember processes, and how disease or lifespan development could change the behavior of this very complex organ.

9.5 FINAL REMARKS

The work presented in this dissertation provided an *in-vivo* approach to investigate the effects of aerobic exercise in white matter tract integrity after a supervised exercise intervention program. After the conclusion of this work, I was able to understand different concepts such as exercise physiology, neurodegenerative pathologies, and brain imaging tools that allowed me to address and characterize this topic. More specifically, I investigated and gained a broader understanding on the neuroprotective effects of aerobic exercise in the neuroplasticity of the brain, especially in white matter integrity. The results

reported here provided some insights on how increased aerobic exercise activity might lead to neuro-protective mechanisms that could be identify with white matter diffusivity metrics in early AD. However, due to our current MRI limitations I was not able to identify a one-to-one relationship with cellular or molecular mechanisms that might explain these neuro-protective mechanisms. Instead, a more global macro-scale picture of these changes was investigated and supported by animal and *post-mortem* studies (see review (Voss et al., 2013b)).

To summarize our key findings using *in-vivo* diffusion imaging techniques, I believe that aerobic exercise may provide a neuro-protective effect for the evident white matter deterioration occurring either by age-related changes or specific to the AD pathology. These neuro-protective mechanisms are also localized in specific white matter fibers, as shown by our *a-priori* tract-of-interest findings. In non-demented individuals the tracts that present a neuro-protective effects are those who are more susceptible to age-related deterioration (e.g. cingulum, uncinate fasciculus, or corpus callosum). On the other hand, the AD participants are also benefited from this neuro-protective effect yet the locations of these tracts differ. These tracts have not previously been identified in healthy exercise related studies (e.g. inferior fronto-occipital fasciculus) and due to the lack of AD-exercise related studies in white matter; we could not compare our results with others. However, one interpretation is that age-related tracts (e.g. cingulum, uncinate fasciculus, or corpus callosum) that are also disrupted earlier in AD (Sexton et al., 2011, Clerx et al., 2012) might not benefit completely with aerobic exercise since these tracts are already deteriorated even though subtle changes in cognition may or may not appear. However, I believe that aerobic exercise might trigger a neuro-protective response to other tracts where disease-

related deterioration has not fully affected them (e.g. inferior fronto-occipital fasciculus). However to validate this hypothesis, further research with longitudinal aerobic exercise trails should be performed in a wider range of AD and healthy non-demented participants.

As a final neurobiological mechanism hypothesis related to age-related white matter deterioration, I believe that this event occurs due to an abnormal and focal supply of metabolic energy leading to disruption in brain connectivity and eventually loss of brain mass. In relation to white matter and myelin (which makes up to ~50% of white matter (Miller et al., 2012)), myelination occurs in a protracted and localized manner, denoting that the development and production of myelin lasts for a long time and in different regions of the brain (Bartzokis, 2004, Haroutunian et al., 2014). This late-myelination production and maintenance peaks at the fifth decade and from there it declines as aging increases (Kemper, 1994, Bartzokis et al., 2001). However to counteract this myelin dysfunction, energy demands for optimal neurotransmission increases up to 500 fold (Hildebrand et al., 1993) yet there isn't an abundant increase in energy supply. Another example is the energy demands for oligodendrocytes, which are two to three-fold higher than other brain cells (Connor and Menzies, 1996). These cells produce and maintain myelin in the brain and are also the only cells in the brain responsible to synthetize cholesterol *de novo* (Bartzokis, 2004). Cholesterol in myelin sheaths promotes a closer membrane-to-membrane contact leading to tightly packed myelin and efficient brain connectivity (by providing an adequate electro-chemical insulation and faster neuro-transmission). In the aged brain the content of cholesterol is also highest in myelin (Saher et al., 2005). However as age increases, this tightly packed myelin sheaths and oligodendrocytes may be disturbed by byproducts age-

related levels of toxicity (e.g. increased iron levels (Power et al., 2002), excitotoxicity (Alonso, 2000), hypoperfusion (Kurumatani et al., 1998), or nitric oxide (Merrill et al., 1993)) or increased genetic risk factors that may disrupt cholesterol-related metabolism (e.g. Apoliprotein E4 allele variant) (Sadigh-Eteghad et al., 2012). Thus, I believe that age-related energy disruption may initiate a cascade of inefficient brain connectivity and neurodegeneration. However counteracting this deleterious effect, the neuroprotective mechanisms of aerobic exercise might slow down this cascade of inefficient brain connectivity. The neuroprotective mechanisms of aerobic exercise include the increased levels of neurotrophins (e.g. BDNF, IGF-1, VEGF, TrkB receptor), increase long-term potentiation, enhance neurogenesis, and increase levels of proteins associated with synaptic plasticity (see review (Voss et al., 2013b)). In this work, I tried to capture these findings using *in-vivo* diffusion imaging technology yet I believe that future studies combining multi-imaging analyses (sMRI, fMRI and DTI) will elucidate further the understanding of brain neuro-plasticity, its biological mechanisms, and its effects in aerobic exercise in the aging and Alzheimer's disease population. As a previously stated, "if the brain was so simple we could understand it, we would be so simple that we couldn't" yet a I am a strong believer that a time will come when we will fully understand the brain and based on our exponential growth in this field, this future is not far.

APPENDIX A

Matlab scripts generated to analytically calculate the diffusion tensor

%A.1 – Functions used to calculate the simple 6 direction diffusion tensor

```
%Function to make the F Matrix:
function [Y] = makeY(S)
%Include intensity at b=0
sizeS=size(S);
Ya=S(2:sizeS(1));
Y=log(312./Ya)/800;
```

```
%Function to make the H Matrix:
function [H] = makeH(GsWithB0s)
%Include vector 0 0 0!!!
%Getting rid og b=0 parameter since its not important
sizeGsWithB0s=size(GsWithB0s);
%Check how many 0s are in the function and remove them from
gradients
count=0; %index that will account for gradient with no zero
for i=1:sizeGsWithB0s(1)
    if ((GsWithB0s(i,1) ==0 && GsWithB0s(i,1) ==0) &&
GsWithB0s(i,3) == 0)
        count=count+1;
    end
end
% Gs with no zero gradients
Gs=GsWithB0s(count+1:sizeGsWithB0s(1),:);
sizeGs=size(Gs);
%Initializing H for the variables...
H=ones(sizeGs(1),6);
for i=1:sizeGs(1)
    %For exmaple H1=[Gx^2 Gy^2 Gz^2 2GxGy 2GxGz 2GyGz]
%same for all the other directions...
H(i,1)=Gs(i,1)^2;
H(i,2)=Gs(i,2)^2;
H(i,3)=Gs(i,3)^2;
H(i,4)=2*Gs(i,1)*Gs(i,2);
H(i,5)=2*Gs(i,1)*Gs(i,3);
H(i,6)=2*Gs(i,2)*Gs(i,3);
end
```

%A.2 – Matlab script that calls the dependent functions in A.1 to calculate the diffusion tensor from the 6 diffusion weighted images

```
%Importing gradient directions
```

```
Gs=importdata('../bvecs');
Gs6=importdata('bvecs6');
%Importing intensities at the followed directions
s=importdata('../VoxelIntensities_x76_y64_z21.txt');
s6=importdata('Intensities.txt');
%Making Y matrix Nx1, where N is the number of intensities at
each gradient
Y6=makeY(s6);
H6=makeH(Gs6);
H=makeH(Gs);

%Check size of H
sizeH=size(H);
sizeH6=size(H6);

%Here is where we will determine the result of our Dtensor
% using either

%Cramer's rule for a perfect solution or the least square
% methods if N>6

%Using Cramer's rule to determine the Deff=D if the matrix is
% 6x6, meaning the exact number of directions needed.

    %H Approach!!
    Dh6=inv(H6)*Y6;
    %B Approach!!
    B6=makeB(Gs6);
    X6=makeX(s6);
    SIGMA6=makeSIGMA(s6);
    Db6All=inv(B6'*SIGMA6*B6)*(B6'*SIGMA6)*X6;
    Db6=Db6All(1:size(Db6All)-1);

%Here we wil be using the least square methods to approximate
% out D tensor components and thus using the B approach

    %B Approach!!
    B=makeB(Gs);
    X=makeX(s);
    SIGMA=makeSIGMA(s);
    DbAll=inv(B'*SIGMA*B)*(B'*SIGMA)*X;
    Db=DbAll(1:size(DbAll)-1);

%Computing the Eigevalues
Egs=makeEgs(Db);
Egs6=makeEgs(Db6);

%Computing the Eigenvectors. Ez are arbitrary an arbitrary
```

```
% number for z directions so we can compare our results to the
% program we used.
Ez =[ 0.697466 -0.521337 0.491680];
Ez6 =[ -.9333942 0.162498 0.318351];
Evs=makeEvs(Egs,Db,Ez);
Evs6=makeEvs(Egs6,Db6,Ez6);

%Computing the markers used in DTI
FAMD=makeMarkers(Egs);
FAMD6=makeMarkers(Egs6);
```

A.2 – Functions used to calculate the simple 6 direction diffusion tensor

Function to make the F Matrix:

```
function [Y] = makeY(S)
%Include intensity at b=0
sizeS=size(S);
Ya=S(2:sizeS(1));
Y=log(312./Ya)/800;
```

Function to make the H Matrix:

```
function [H] = makeH(GsWithB0s)
%Include vector 0 0 0!!!
% Getting rid og b=0 parameter since its not important
sizeGsWithB0s=size(GsWithB0s);
%Check how many 0s are in the function and remove them from
  gradients

count=0; %index that will account for gradient with no zero
for i=1:sizeGsWithB0s(1)
    if ((GsWithB0s(i,1) ==0 && GsWithB0s(i,1) ==0) &&
GsWithB0s(i,3) == 0)
        count=count+1;
    end
end
% Gs with no zero gradients
Gs=GsWithB0s(count+1:sizeGsWithB0s(1),:);
sizeGs=size(Gs);
%Initializing H for the variables...
H=ones(sizeGs(1),6);
for i=1:sizeGs(1)
    %For exmaple H1=[Gx^2 Gy^2 Gz^2 2GxGy 2GxGz 2GyGz]
%same for all the other directions...
```

```
H(i,1)=Gs(i,1)^2;
H(i,2)=Gs(i,2)^2;
H(i,3)=Gs(i,3)^2;
H(i,4)=2*Gs(i,1)*Gs(i,2);
H(i,5)=2*Gs(i,1)*Gs(i,3);
H(i,6)=2*Gs(i,2)*Gs(i,3);
end
```

A.3 Functions used to calculate the simple 6+ direction diffusion tensor

%Function to make the X Matrix:

```
%Rodrigo Perea
%EECS 700 Project: Implementation of X
%Objective: Implements X with the given input:
%Intensities= intenstity at each specific level.
% Output:
% X=ln(Intensities)
%This equations come from part III of Kingsley 2005
% "Introduction to DTI Mathematics Part II: Tensors,
%  Rotations, and Eigenvectors.

%making Eigenvectors:
function [X] = makeX(Intensities)
X=log(Intensities);
```

Function to make the B Matrix:

```
%Rodrigo Perea
%Implementation of the B matrix.
%Objective: This function will accept gradient directions w
%           b=0 intensities making a matrix GsWithB0s(Nx3)
%           and the corresponding intensities eps (Nx1) and D %
tensor in a and will output a B matrix.

%This equations come from part III of Kingsley 2005
%"Introduction to DTI Mathematics Part II: Tensors, Rotations, %
and Eigenvectors


%making Eigenvectors:
function [B] = makeB(GsWithB0s)
sizeGsWithB0s=size(GsWithB0s);
% %Check how many 0s are in the function and remove them from
gradients
```

```
%------------------COMMENT BEGIN
% count=0 %index that will account for gradient with no zero
% for i=1:sizeGsWithB0s(1)
%     if ((GsWithB0s(i,1) ==0 && GsWithB0s(i,1) ==0) &&
GsWithB0s(i,3) == 0)
%         count=count+1;
%     end
% end
%------------------COMMENT END

sizeGsWithB0s=size(GsWithB0s);
Gs=GsWithB0s;
% Gs=GsWithB0s(2:sizeGsWithB0s(1),:);

sizeGs=size(Gs);
%Initializing H for the variables...
B=ones(sizeGs(1),6);

for i=1:sizeGs(1)
    %For exmaple H1=[Gx^2 Gy^2 Gz^2 2GxGy 2GxGz 2GyGz]
%same for all the other directions...
B(i,1)=-800*Gs(i,1)^2;
B(i,2)=-800*Gs(i,2)^2;
B(i,3)=-800*Gs(i,3)^2;
B(i,4)=-800*2*Gs(i,1)*Gs(i,2);
B(i,5)=-800*2*Gs(i,1)*Gs(i,3);
B(i,6)=-800*2*Gs(i,2)*Gs(i,3);
B(i,7)=1;
end
```

Function to make the Σ^{-1} Matrix:

```
%Rodrigo Perea
%Objective: Implements capital sigma with the given input:
% Intensities= intensity at each specific level.
% This equations come from part III of Kingsley 2005 "
% Introduction to DTI
%Mathematics Part II: Tensors, Rotations, and Eigenvectors.

%making Eigenvectors:
function [SIGMA] = makeSIGMA(Intensities,B)
% Creating a covariance matrix and multiply it by a identity
function of
% same length
sizeI=size(Intensities);

%Making the covariance Squared
Cov=diag(cov(Intensities));%.*eye(sizeI(1),size(2));
CovSquare=Cov.^2;
```

```
%Making the intensities Square
IntSquare=Intensities.^2;


% Making SIGMA
SIG=IntSquare./CovSquare;
% And diagonalizing SIGMA....
SIGMA=diag(SIG);
```

A.4 Functions for post processing (eigenvalues, eigenvectors and diffusion markers)

```
%Function to calculate the eigenvalues
function [eigenvalues] = makeEgs(Donecolumn)
%This equations come from part II of Kingsley 2005
% "Introduction to DTI Mathematics Part I: Tensors, Rotations,
% and Eigenvectors.

%Making a 6x1 matrix into a 3x3 matrix
D=ones(3,3);
D(1,1)=Donecolumn(1);
D(1,2)=Donecolumn(4);
D(1,3)=Donecolumn(5);
D(2,1)=D(1,2);
D(2,2)=Donecolumn(2);
D(2,3)=Donecolumn(6);
D(3,1)=D(1,3);
D(3,2)=D(2,3);
D(3,3)=Donecolumn(3);

%Preprocessed contants that will be used to calculate evals and
evecs
I1= D(1,1)+D(2,2)+D(3,3);
I2= D(1,1)*D(2,2)+D(2,2)*D(3,3)+D(3,3)*D(1,1)-
(D(1,2)^2+D(1,3)^2+D(2,3)^2);
I3= D(1,1)*D(2,2)*D(3,3)+2*D(1,2)*D(1,3)*D(2,3)-
(D(3,3)*D(1,2)^2+D(2,2)*D(1,3)^2+D(1,1)*D(2,3)^2);
v=(I1/3)^2-I2/3;
s=(I1/3)^3-I1*I2/6+I3/2;
theta=acos(s/v^(3/2))/3;

%Calculating the eigenvalues
lambda1=I1/3+ 2*v^(1/2)*cos(theta);
lambda2=I1/3- 2*v^(1/2)*cos(pi/3+theta);
lambda3=I1/3- 2*v^(1/2)*cos(pi/3-theta);
```

```
eigenvalues(1)=lambda1;
eigenvalues(2)=lambda2;
eigenvalues(3)=lambda3;

%Function to calculate the following eigenvectors
%Rodrigo Perea
%Objective: This function will accept eigenvalues (3x1) and D
% tensor in a(6x1) column and output a 3x1 Eigenvector array.

%This equations come from part II of Kingsley 2005
% Introduction to DTI Mathematics Part I: Tensors, Rotations,
% and Eigenvectors making Eigenvectors:


% Egs = Eigenvalues previous calculated.
% D=diffusion tensor calculated with as 6x1 column
% Ez= arbitraty values for the eigenvalue Ez

function [Evs] = makeEvs(Egs,Donecolumn,Ez)
 %Variables for Egs:
%The tensor model converted in a 3x3 matrix:
D(1,1)=Donecolumn(1);
D(1,2)=Donecolumn(4);
D(1,3)=Donecolumn(5);

D(2,1)=D(1,2);
D(2,2)=Donecolumn(2);
D(2,3)=Donecolumn(6);

D(3,1)=D(1,3);
D(3,2)=D(2,3);
D(3,3)=Donecolumn(3);
for i=1:3
A(i)=D(1,1)-Egs(i);
B(i)=D(2,2)-Egs(i);
C(i)=D(3,3)-Egs(i);
end
%
for i=1:3
Evs(i,1)=Ez(i)*(D(1,2)*D(2,3)-B(i)*D(1,3))/(A(i)*B(i)-D(1,2)^2);
Evs(i,2)=Ez(i)*(D(1,2)*D(1,3)-A(i)*D(2,3))/(A(i)*B(i)-D(1,2)^2);
Evs(i,3)=Ez(i);
end

Function to calculate the principal component markers for
diffusion in the brain. This helped on verifying our correct
calculation and compare them with FSL, the imaging software the
automates all the entire process.
%Rodrigo Perea
```

```
%EECS 700 Project: Implementation B matrix.
%Objective: This function will the processed eigenvalues and
will output
% two main important markers, FA, MD.

%This equations come from part III of Kingsley 2005
"Introduction to DTI
%Mathematics Part II: Tensors, Rotations, and Eigenvectors.
%making Eigenvectors:

function [Markers] = makeMarkers(Egs)
%Computing the MD
MD=mean(Egs);
%Computing the FA
e1=Egs(1);
e2=Egs(2);
e3=Egs(3);
FA=sqrt((3*(e1-MD)^2+(e2-MD)^2+(e3-MD)^2)/(2*(e1^2+e2^2+e3^2)));
Markers(1)=FA;
Markers(2)=MD;
```

REFERENCES

Aarsland D, Laake K, Larsen JP, Janvin C (2002) Donepezil for cognitive impairment in Parkinson's disease: a randomised controlled study. Journal of neurology, neurosurgery, and psychiatry 72:708-712.
Abbott RD, White LR, Ross GW, Masaki KH, Curb JD, Petrovitch H (2004) Walking and Dementia in Physically Capable Elderly Men. JAMA: The Journal of the American Medical Association 292:1447-1453.
Acosta-Cabronero J, Williams GB, Pengas G, Nestor PJ (2010) Absolute diffusivities define the landscape of white matter degeneration in Alzheimer's disease. Brain : a journal of neurology 133:529-539.
Adlard PA, Perreau VM, Pop V, Cotman CW (2005) Voluntary exercise decreases amyloid load in a transgenic model of Alzheimer's disease. The Journal of neuroscience : the official journal of the Society for Neuroscience 25:4217-4221.
ADNI (2012) Alzheimer's Disease Neuroimaging Initiative. vol. 2015.
ADNI (2013) Welcome from the ADNI principal investigator. vol. 2015.
Alexander AL, Hurley SA, Samsonov AA, Adluru N, Hosseinbor AP, Mossahebi P, Tromp do PM, Zakszewski E, Field AS (2011) Characterization of cerebral white matter properties using quantitative magnetic resonance imaging stains. Brain connectivity 1:423-446.
Alexander AL, Lee JE, Lazar M, Field AS (2007) Diffusion tensor imaging of the brain. Neurotherapeutics : the journal of the American Society for Experimental NeuroTherapeutics 4:316-329.
Alonso G (2000) Prolonged corticosterone treatment of adult rats inhibits the proliferation of oligodendrocyte progenitors present throughout white and gray matter regions of the brain. Glia 31:219-231.
Alves GS, O'Dwyer L, Jurcoane A, Oertel-Knochel V, Knochel C, Prvulovic D, Sudo F, Alves CE, Valente L, Moreira D, Fubetaer F, Karakaya T, Pantel J, Engelhardt E, Laks J (2012) Different patterns of white matter degeneration using multiple diffusion indices and volumetric data in mild cognitive impairment and Alzheimer patients. PloS one 7:e52859.
Amlien IK, Fjell AM (2014) Diffusion tensor imaging of white matter degeneration in Alzheimer's disease and mild cognitive impairment. Neuroscience.
Anderson HS, Kluding PM, Gajewski BJ, Donnelly JE, Burns JM (2011) Reliability of peak treadmill exercise tests in mild Alzheimer disease. The International journal of neuroscience 121:450-456.
Anderson MJ, Robinson J (2001) Permutation tests for linear models. Australian & New Zealand Journal of Statistics 43:75-88.
Andersson J, Jenkinson M, Smith S (2010) Non-linear registration, aka Spatial normalisation. 2007. FMRIB technical report TR07JA2. Available from: www. fmrib. ox. ac. uk/analysis/techrep.
Andersson JLR, Jenkinson M, Smith S (2007) Non-linear optimisation. FMRIB Analysis Group Technical Reports: TR07JA02 from www fmrib ox ac uk/analysis/techrep.
Ashburner J (2007) A fast diffeomorphic image registration algorithm. NeuroImage 38:95-113.
Ashtari M (2012) Anatomy and functional role of the inferior longitudinal fasciculus: a search that has just begun. Developmental medicine and child neurology 54:6-7.

Avants BB, Tustison NJ, Song G, Cook PA, Klein A, Gee JC (2011) A reproducible evaluation of ANTs similarity metric performance in brain image registration. NeuroImage 54:2033-2044.
Bach M, Laun FB, Leemans A, Tax CM, Biessels GJ, Stieltjes B, Maier-Hein KH (2014) Methodological considerations on tract-based spatial statistics (TBSS). NeuroImage 100:358-369.
Banich MT, Compton R (2010) Cognitive neuroscience: Cengage Learning.
Barber SE, Clegg AP, Young JB (2012) Is there a role for physical activity in preventing cognitive decline in people with mild cognitive impairment? Age and ageing 41:5-8.
Barnes DE, Yaffe K, Satariano WA, Tager IB (2003) A Longitudinal Study of Cardiorespiratory Fitness and Cognitive Function in Healthy Older Adults. Journal of the American Geriatrics Society 51:459-465.
Barnes J, Bartlett JW, van de Pol LA, Loy CT, Scahill RI, Frost C, Thompson P, Fox NC (2009) A meta-analysis of hippocampal atrophy rates in Alzheimer's disease. Neurobiology of aging 30:1711-1723.
Barrick TR, Charlton RA, Clark CA, Markus HS (2010) White matter structural decline in normal ageing: a prospective longitudinal study using tract-based spatial statistics. NeuroImage 51:565-577.
Barthelemy D, Grey MJ, Nielsen JB, Bouyer L (2011) Involvement of the corticospinal tract in the control of human gait. Progress in brain research 192:181-197.
Bartzokis G (2004) Age-related myelin breakdown: a developmental model of cognitive decline and Alzheimer's disease. Neurobiology of aging 25:5-18; author reply 49-62.
Bartzokis G (2011) Alzheimer's disease as homeostatic responses to age-related myelin breakdown. Neurobiology of aging 32:1341-1371.
Bartzokis G, Beckson M, Lu PH, Nuechterlein KH, Edwards N, Mintz J (2001) Age-related changes in frontal and temporal lobe volumes in men: a magnetic resonance imaging study. Archives of general psychiatry 58:461-465.
Basser PJ, Jones DK (2002) Diffusion-tensor MRI: theory, experimental design and data analysis - a technical review. NMR in biomedicine 15:456-467.
Basser PJ, Mattiello J, LeBihan D (1994) Estimation of the effective self-diffusion tensor from the NMR spin echo. Journal of magnetic resonance Series B 103:247-254.
Beaulieu C (2002) The basis of anisotropic water diffusion in the nervous system - a technical review. NMR in biomedicine 15:435-455.
Behrens TE, Berg HJ, Jbabdi S, Rushworth MF, Woolrich MW (2007) Probabilistic diffusion tractography with multiple fibre orientations: What can we gain? NeuroImage 34:144-155.
Behrens TE, Johansen-Berg H, Woolrich MW, Smith SM, Wheeler-Kingshott CA, Boulby PA, Barker GJ, Sillery EL, Sheehan K, Ciccarelli O, Thompson AJ, Brady JM, Matthews PM (2003a) Non-invasive mapping of connections between human thalamus and cortex using diffusion imaging. Nature neuroscience 6:750-757.
Behrens TE, Woolrich MW, Jenkinson M, Johansen-Berg H, Nunes RG, Clare S, Matthews PM, Brady JM, Smith SM (2003b) Characterization and propagation of uncertainty in diffusion-weighted MR imaging. Magnetic resonance in medicine : official journal of the Society of Magnetic Resonance in Medicine / Society of Magnetic Resonance in Medicine 50:1077-1088.

Bennett IJ, Madden DJ, Vaidya CJ, Howard DV, Howard JH, Jr. (2010) Age-related differences in multiple measures of white matter integrity: A diffusion tensor imaging study of healthy aging. Human brain mapping 31:378-390.
Bennett IJ, Madden DJ, Vaidya CJ, Howard JH, Jr., Howard DV (2011) White matter integrity correlates of implicit sequence learning in healthy aging. Neurobiology of aging 32:2317 e2311-2312.
Biessels GJ, Staekenborg S, Brunner E, Brayne C, Scheltens P (2006) Risk of dementia in diabetes mellitus: a systematic review. Lancet neurology 5:64-74.
Bland JM, Altman DG (1986) Statistical methods for assessing agreement between two methods of clinical measurement. Lancet 1:307-310.
Boots EA, Schultz SA, Oh JM, Larson J, Edwards D, Cook D, Koscik RL, Dowling MN, Gallagher CL, Carlsson CM, Rowley HA, Bendlin BB, LaRue A, Asthana S, Hermann BP, Sager MA, Johnson SC, Okonkwo OC (2014) Cardiorespiratory fitness is associated with brain structure, cognition, and mood in a middle-aged cohort at risk for Alzheimer's disease. Brain imaging and behavior.
Bosch B, Arenaza-Urquijo EM, Rami L, Sala-Llonch R, Junque C, Sole-Padulles C, Pena-Gomez C, Bargallo N, Molinuevo JL, Bartres-Faz D (2012) Multiple DTI index analysis in normal aging, amnestic MCI and AD. Relationship with neuropsychological performance. Neurobiology of aging 33:61-74.
Braak H, Braak E (1991a) Alzheimer's disease affects limbic nuclei of the thalamus. Acta neuropathologica 81:261-268.
Braak H, Braak E (1991b) Neuropathological stageing of Alzheimer-related changes. Acta neuropathologica 82:239-259.
Braskie MN, Boyle CP, Rajagopalan P, Gutman BA, Toga AW, Raji CA, Tracy RP, Kuller LH, Becker JT, Lopez OL, Thompson PM (2014) Physical activity, inflammation, and volume of the aging brain. Neuroscience 273:199-209.
Brown R (1828) A Brief Account of Microscopical Observations Made... on the Particles Contained in the Pollen of Plants, and on the General Existence of Active Molecules in Organic and Inorganic Bodies.
Brun A, Englund E (1986) A white matter disorder in dementia of the Alzheimer type: a pathoanatomical study. Annals of neurology 19:253-262.
Buckner RL, Andrews-Hanna JR, Schacter DL (2008) The brain's default network: anatomy, function, and relevance to disease. Annals of the New York Academy of Sciences 1124:1-38.
Burggren A, Brown J (2014) Imaging markers of structural and functional brain changes that precede cognitive symptoms in risk for Alzheimer's disease. Brain imaging and behavior 8:251-261.
Burns JM, Cronk BB, Anderson HS, Donnelly JE, Thomas GP, Harsha A, Brooks WM, Swerdlow RH (2008) Cardiorespiratory fitness and brain atrophy in early Alzheimer disease. Neurology 71:210-216.
Burton EJ, McKeith IG, Burn DJ, Williams ED, O'Brien JT (2004) Cerebral atrophy in Parkinson's disease with and without dementia: a comparison with Alzheimer's disease, dementia with Lewy bodies and controls. Brain : a journal of neurology 127:791-800.

Burzynska AZ, Preuschhof C, Backman L, Nyberg L, Li SC, Lindenberger U, Heekeren HR (2010) Age-related differences in white matter microstructure: region-specific patterns of diffusivity. NeuroImage 49:2104-2112.
Carr HY, Purcell EM (1954) Effects of diffusion on free precession in nuclear magnetic resonance experiments. Physical Review 94:630.
Carro E, Trejo JL, Busiguina S, Torres-Aleman I (2001) Circulating insulin-like growth factor I mediates the protective effects of physical exercise against brain insults of different etiology and anatomy. The Journal of neuroscience : the official journal of the Society for Neuroscience 21:5678-5684.
Casagrande VA, Guillery RW, Sherman SM (2005) Cortical function: A view from the thalamus: Gulf Professional Publishing.
Caspersen CJ, Powell KE, Christenson GM (1985) Physical activity, exercise, and physical fitness: definitions and distinctions for health-related research. Public health reports 100:126-131.
Catani M, Howard RJ, Pajevic S, Jones DK (2002) Virtual in vivo interactive dissection of white matter fasciculi in the human brain. NeuroImage 17:77-94.
Chaddock-Heyman L, Erickson KI, Holtrop JL, Voss MW, Pontifex MB, Raine LB, Hillman CH, Kramer AF (2014) Aerobic fitness is associated with greater white matter integrity in children. Frontiers in human neuroscience 8:584.
Chan LL, Rumpel H, Yap K, Lee E, Loo HV, Ho GL, Fook-Chong S, Yuen Y, Tan EK (2007) Case control study of diffusion tensor imaging in Parkinson's disease. Journal of neurology, neurosurgery, and psychiatry 78:1383-1386.
Chanraud S, Zahr N, Sullivan EV, Pfefferbaum A (2010) MR diffusion tensor imaging: a window into white matter integrity of the working brain. Neuropsychology review 20:209-225.
Chua TC, Wen W, Slavin MJ, Sachdev PS (2008) Diffusion tensor imaging in mild cognitive impairment and Alzheimer's disease: a review. Current opinion in neurology 21:83-92.
Clerx L, Visser PJ, Verhey F, Aalten P (2012) New MRI markers for Alzheimer's disease: a meta-analysis of diffusion tensor imaging and a comparison with medial temporal lobe measurements. Journal of Alzheimer's disease : JAD 29:405-429.
Coelho FG, Vital TM, Stein AM, Arantes FJ, Rueda AV, Camarini R, Teodorov E, Santos-Galduroz RF (2014) Acute aerobic exercise increases brain-derived neurotrophic factor levels in elderly with Alzheimer's disease. Journal of Alzheimer's disease : JAD 39:401-408.
Colcombe S, Kramer AF (2003) Fitness effects on the cognitive function of older adults: a meta-analytic study. Psychological science 14:125-130.
Colcombe SJ, Erickson KI, Raz N, Webb AG, Cohen NJ, McAuley E, Kramer AF (2003) Aerobic fitness reduces brain tissue loss in aging humans. The journals of gerontology Series A, Biological sciences and medical sciences 58:176-180.
Colcombe SJ, Erickson KI, Scalf PE, Kim JS, Prakash R, McAuley E, Elavsky S, Marquez DX, Hu L, Kramer AF (2006) Aerobic exercise training increases brain volume in aging humans. The journals of gerontology Series A, Biological sciences and medical sciences 61:1166-1170.
Colcombe SJ, Kramer AF, Erickson KI, Scalf P, McAuley E, Cohen NJ, Webb A, Jerome GJ, Marquez DX, Elavsky S (2004) Cardiovascular fitness, cortical plasticity, and aging.

Proceedings of the National Academy of Sciences of the United States of America 101:3316-3321.
Concha L (2014) A macroscopic view of microstructure: Using diffusion-weighted images to infer damage, repair, and plasticity of white matter. Neuroscience 276C:14-28.
Connor JR, Menzies SL (1996) Relationship of iron to oligodendrocytes and myelination. Glia 17:83-93.
Cotman CW, Berchtold NC (2002) Exercise: a behavioral intervention to enhance brain health and plasticity. Trends in neurosciences 25:295-301.
Cotman CW, Berchtold NC (2007) Physical activity and the maintenance of cognition: learning from animal models. Alzheimer's & dementia : the journal of the Alzheimer's Association 3:S30-37.
Creer DJ, Romberg C, Saksida LM, van Praag H, Bussey TJ (2010) Running enhances spatial pattern separation in mice. Proceedings of the National Academy of Sciences of the United States of America 107:2367-2372.
Dale AM, Fischl B, Sereno MI (1999) Cortical surface-based analysis. I. Segmentation and surface reconstruction. NeuroImage 9:179-194.
Dale AM, Sereno MI (1993) Improved Localizadon of Cortical Activity by Combining EEG and MEG with MRI Cortical Surface Reconstruction: A Linear Approach. Journal of cognitive neuroscience 5:162-176.
Damoiseaux JS, Smith SM, Witter MP, Sanz-Arigita EJ, Barkhof F, Scheltens P, Stam CJ, Zarei M, Rombouts SA (2009) White matter tract integrity in aging and Alzheimer's disease. Human brain mapping 30:1051-1059.
Darwin C (1872) On the Origin of Species by Means of Natural Selection 6th edition. Page reference to reprint edition, 1963. New York: Heritage Press.
Davis SW, Dennis NA, Buchler NG, White LE, Madden DJ, Cabeza R (2009) Assessing the effects of age on long white matter tracts using diffusion tensor tractography. NeuroImage 46:530-541.
de Jong LW, van der Hiele K, Veer IM, Houwing JJ, Westendorp RG, Bollen EL, de Bruin PW, Middelkoop HA, van Buchem MA, van der Grond J (2008) Strongly reduced volumes of putamen and thalamus in Alzheimer's disease: an MRI study. Brain : a journal of neurology 131:3277-3285.
de Lau LM, Breteler MM (2006) Epidemiology of Parkinson's disease. Lancet neurology 5:525-535.
Dodel R, Csoti I, Ebersbach G, Fuchs G, Hahne M, Kuhn W, Oechsner M, Jost W, Reichmann H, Schulz JB (2008) Lewy body dementia and Parkinson's disease with dementia. Journal of neurology 255 Suppl 5:39-47.
Douaud G, Jbabdi S, Behrens TE, Menke RA, Gass A, Monsch AU, Rao A, Whitcher B, Kindlmann G, Matthews PM, Smith S (2011) DTI measures in crossing-fibre areas: increased diffusion anisotropy reveals early white matter alteration in MCI and mild Alzheimer's disease. NeuroImage 55:880-890.
Douaud G, Menke RA, Gass A, Monsch AU, Rao A, Whitcher B, Zamboni G, Matthews PM, Sollberger M, Smith S (2013) Brain microstructure reveals early abnormalities more than two years prior to clinical progression from mild cognitive impairment to Alzheimer's disease. The Journal of neuroscience : the official journal of the Society for Neuroscience 33:2147-2155.

Dubois B, Burn D, Goetz C, Aarsland D, Brown RG, Broe GA, Dickson D, Duyckaerts C, Cummings J, Gauthier S, Korczyn A, Lees A, Levy R, Litvan I, Mizuno Y, McKeith IG, Olanow CW, Poewe W, Sampaio C, Tolosa E, Emre M (2007) Diagnostic procedures for Parkinson's disease dementia: recommendations from the movement disorder society task force. Movement disorders : official journal of the Movement Disorder Society 22:2314-2324.

E L, Burns JM, Swerdlow RH (2014) Effect of high-intensity exercise on aged mouse brain mitochondria, neurogenesis, and inflammation. Neurobiology of aging 35:2574-2583.

Edden RA, Jones DK (2011) Spatial and orientational heterogeneity in the statistical sensitivity of skeleton-based analyses of diffusion tensor MR imaging data. Journal of neuroscience methods 201:213-219.

Einstein A (1905) Über die von der molekularkinetischen Theorie der Wärme geforderte Bewegung von in ruhenden Flüssigkeiten suspendierten Teilchen. Annalen der physik 322:549-560.

Einstein A (1956) Investigations on the Theory of Brownian Motion, reprint of the 1st English edition (1926). Dover, New-York.

Erickson KI, Leckie RL, Weinstein AM (2014) Physical activity, fitness, and gray matter volume. Neurobiology of aging 35 Suppl 2:S20-28.

Erickson KI, Prakash RS, Voss MW, Chaddock L, Hu L, Morris KS, White SM, Wojcicki TR, McAuley E, Kramer AF (2009) Aerobic fitness is associated with hippocampal volume in elderly humans. Hippocampus 19:1030-1039.

Erickson KI, Raji CA, Lopez OL, Becker JT, Rosano C, Newman AB, Gach HM, Thompson PM, Ho AJ, Kuller LH (2010) Physical activity predicts gray matter volume in late adulthood: the Cardiovascular Health Study. Neurology 75:1415-1422.

Eskildsen SF, Coupe P, Fonov VS, Pruessner JC, Collins DL, Alzheimer's Disease Neuroimaging I (2014) Structural imaging biomarkers of Alzheimer's disease: predicting disease progression. Neurobiology of aging.

Fields RD (2008) White matter in learning, cognition and psychiatric disorders. Trends in neurosciences 31:361-370.

Filley CM (2012) White matter dementia. Therapeutic advances in neurological disorders 5:267-277.

Fischl B, Dale AM (2000) Measuring the thickness of the human cerebral cortex from magnetic resonance images. Proceedings of the National Academy of Sciences of the United States of America 97:11050-11055.

Fischl B, Liu A, Dale AM (2001) Automated manifold surgery: constructing geometrically accurate and topologically correct models of the human cerebral cortex. IEEE transactions on medical imaging 20:70-80.

Fischl B, Salat DH, Busa E, Albert M, Dieterich M, Haselgrove C, van der Kouwe A, Killiany R, Kennedy D, Klaveness S, Montillo A, Makris N, Rosen B, Dale AM (2002) Whole brain segmentation: automated labeling of neuroanatomical structures in the human brain. Neuron 33:341-355.

Fischl B, van der Kouwe A, Destrieux C, Halgren E, Segonne F, Salat DH, Busa E, Seidman LJ, Goldstein J, Kennedy D, Caviness V, Makris N, Rosen B, Dale AM (2004) Automatically parcellating the human cerebral cortex. Cerebral cortex 14:11-22.

FitzGerald MJT, Gruener G, Mtui E (2011) Clinical neuroanatomy and neuroscience: Elsevier Health Sciences.
Fjell AM, McEvoy L, Holland D, Dale AM, Walhovd KB, Alzheimer's Disease Neuroimaging I (2014) What is normal in normal aging? Effects of aging, amyloid and Alzheimer's disease on the cerebral cortex and the hippocampus. Progress in neurobiology.
Floel A, Ruscheweyh R, Kruger K, Willemer C, Winter B, Volker K, Lohmann H, Zitzmann M, Mooren F, Breitenstein C, Knecht S (2010) Physical activity and memory functions: are neurotrophins and cerebral gray matter volume the missing link? NeuroImage 49:2756-2763.
Folstein MF, Folstein SE, McHugh PR (1975) "Mini-mental state". A practical method for grading the cognitive state of patients for the clinician. Journal of psychiatric research 12:189-198.
Ford AA, Triplett W, Sudhyadhom A, Gullett J, McGregor K, Fitzgerald DB, Mareci T, White K, Crosson B (2013) Broca's area and its striatal and thalamic connections: a diffusion-MRI tractography study. Frontiers in neuroanatomy 7:8.
Friedland RP, Fritsch T, Smyth KA, Koss E, Lerner AJ, Chen CH, Petot GJ, Debanne SM (2001) Midlife recreational activity inversely associated with Alzheimer's disease risk. Proc Natl Acad Sci 98:3440-3445.
Friston KJ, Ashburner J (2004) Generative and recognition models for neuroanatomy. NeuroImage 23:21-24.
FSL (2013a) FMRIB's Diffusion Toolbox - FDT v2.0. vol. 2015.
FSL (2013b) Fslutils. vol. 2015.
FSL (2013c) TBSS/UserGuide. vol. 2015.
FSL (2015) Randomise. vol. 2015.
Gaffan D, Wilson CR (2008) Medial temporal and prefrontal function: recent behavioural disconnection studies in the macaque monkey. Cortex 44:928-935.
Galantucci S, Tartaglia MC, Wilson SM, Henry ML, Filippi M, Agosta F, Dronkers NF, Henry RG, Ogar JM, Miller BL, Gorno-Tempini ML (2011) White matter damage in primary progressive aphasias: a diffusion tensor tractography study. Brain : a journal of neurology 134:3011-3029.
Gasson A (2014) Contact Lens History. vol. 2015.
Gold BT, Johnson NF, Powell DK, Smith CD (2012) White matter integrity and vulnerability to Alzheimer's disease: preliminary findings and future directions. Biochimica et biophysica acta 1822:416-422.
Gold BT, Powell DK, Andersen AH, Smith CD (2010) Alterations in multiple measures of white matter integrity in normal women at high risk for Alzheimer's disease. NeuroImage 52:1487-1494.
Gons RA, Tuladhar AM, de Laat KF, van Norden AG, van Dijk EJ, Norris DG, Zwiers MP, de Leeuw FE (2013) Physical activity is related to the structural integrity of cerebral white matter. Neurology 81:971-976.
Gordon BA, Rykhlevskaia EI, Brumback CR, Lee Y, Elavsky S, Konopack JF, McAuley E, Kramer AF, Colcombe S, Gratton G, Fabiani M (2008) Neuroanatomical correlates of aging, cardiopulmonary fitness level, and education. Psychophysiology 45:825-838.
Gow AJ, Bastin ME, Munoz Maniega S, Valdes Hernandez MC, Morris Z, Murray C, Royle NA, Starr JM, Deary IJ, Wardlaw JM (2012) Neuroprotective lifestyles and the aging brain: activity, atrophy, and white matter integrity. Neurology 79:1802-1808.

Griffin EW, Bechara RG, Birch AM, Kelly AM (2009) Exercise enhances hippocampal-dependent learning in the rat: evidence for a BDNF-related mechanism. Hippocampus 19:973-980.
Hahn EL (1950) Spin echoes. Physical Review 80:580.
Han X, Jovicich J, Salat D, van der Kouwe A, Quinn B, Czanner S, Busa E, Pacheco J, Albert M, Killiany R, Maguire P, Rosas D, Makris N, Dale A, Dickerson B, Fischl B (2006) Reliability of MRI-derived measurements of human cerebral cortical thickness: the effects of field strength, scanner upgrade and manufacturer. NeuroImage 32:180-194.
Hanneman SK (2008) Design, analysis, and interpretation of method-comparison studies. AACN advanced critical care 19:223-234.
Hardy J, Selkoe DJ (2002) The amyloid hypothesis of Alzheimer's disease: progress and problems on the road to therapeutics. Science 297:353-356.
Haroutunian V, Katsel P, Roussos P, Davis KL, Altshuler LL, Bartzokis G (2014) Myelination, oligodendrocytes, and serious mental illness. Glia 62:1856-1877.
Hartline DK (2008) What is myelin? Neuron Glia Biology 4:153-163.
Haskell WL, Lee IM, Pate RR, Powell KE, Blair SN, Franklin BA, Macera CA, Heath GW, Thompson PD, Bauman A, American College of Sports M, American Heart A (2007) Physical activity and public health: updated recommendation for adults from the American College of Sports Medicine and the American Heart Association. Circulation 116:1081-1093.
Hassmen P, Koivula N (1997) Mood, physical working capacity and cognitive performance in the elderly as related to physical activity. Aging-Clinical and Experimental Research 9:136-142.
Hattori T, Orimo S, Aoki S, Ito K, Abe O, Amano A, Sato R, Sakai K, Mizusawa H (2012) Cognitive status correlates with white matter alteration in Parkinson's disease. Human brain mapping 33:727-739.
Hayes SM, Hayes JP, Cadden M, Verfaellie M (2013) A review of cardiorespiratory fitness-related neuroplasticity in the aging brain. Frontiers in aging neuroscience 5:31.
Hebert LE, Weuve J, Scherr PA, Evans DA (2013) Alzheimer disease in the United States (2010-2050) estimated using the 2010 census. Neurology 80:1778-1783.
Hedden T, Gabrieli JD (2004) Insights into the ageing mind: a view from cognitive neuroscience. Nature reviews Neuroscience 5:87-96.
Highley JR, Walker MA, Esiri MM, Crow TJ, Harrison PJ (2002) Asymmetry of the uncinate fasciculus: a post-mortem study of normal subjects and patients with schizophrenia. Cerebral cortex 12:1218-1224.
Hildebrand C, Remahl S, Persson H, Bjartmar C (1993) Myelinated nerve fibres in the CNS. Progress in neurobiology 40:319-384.
Hill RD, Storandt M, Malley M (1993) The impact of long-term exercise training on psychological function in older adults. J Gerontol 48:12-17.
Hodaie M, Neimat JS, Lozano AM (2007) The dopaminergic nigrostriatal system and Parkinson's disease: molecular events in development, disease, and cell death, and new therapeutic strategies. Neurosurgery 60:17-28; discussion 28-30.
Hollenberg M, Ngo LH, Turner D, Tager IB (1998) Treadmill exercise testing in an epidemiologic study of elderly subjects. The journals of gerontology Series A, Biological sciences and medical sciences 53:B259-267.

Honea RA, Thomas GP, Harsha A, Anderson HS, Donnelly JE, Brooks WM, Burns JM (2009) Cardiorespiratory fitness and preserved medial temporal lobe volume in Alzheimer disease. Alzheimer disease and associated disorders 23:188-197.
Hua K, Zhang J, Wakana S, Jiang H, Li X, Reich DS, Calabresi PA, Pekar JJ, van Zijl PC, Mori S (2008a) Tract probability maps in stereotaxic spaces: analyses of white matter anatomy and tract-specific quantification. NeuroImage 39:336-347.
Hua X, Leow AD, Parikshak N, Lee S, Chiang MC, Toga AW, Jack CR, Jr., Weiner MW, Thompson PM, Alzheimer's Disease Neuroimaging I (2008b) Tensor-based morphometry as a neuroimaging biomarker for Alzheimer's disease: an MRI study of 676 AD, MCI, and normal subjects. NeuroImage 43:458-469.
Huang J, Friedland RP, Auchus AP (2007) Diffusion tensor imaging of normal-appearing white matter in mild cognitive impairment and early Alzheimer disease: preliminary evidence of axonal degeneration in the temporal lobe. AJNR American journal of neuroradiology 28:1943-1948.
Hughes AJ, Ben-Shlomo Y, Daniel SE, Lees AJ (1992) What features improve the accuracy of clinical diagnosis in Parkinson's disease: a clinicopathologic study. Neurology 42:1142-1146.
Hughes EJ, Bond J, Svrckova P, Makropoulos A, Ball G, Sharp DJ, Edwards AD, Hajnal JV, Counsell SJ (2012) Regional changes in thalamic shape and volume with increasing age. NeuroImage 63:1134-1142.
Jack CR, Jr., Dickson DW, Parisi JE, Xu YC, Cha RH, O'Brien PC, Edland SD, Smith GE, Boeve BF, Tangalos EG, Kokmen E, Petersen RC (2002) Antemortem MRI findings correlate with hippocampal neuropathology in typical aging and dementia. Neurology 58:750-757.
Jack CR, Jr., Knopman DS, Jagust WJ, Shaw LM, Aisen PS, Weiner MW, Petersen RC, Trojanowski JQ (2010) Hypothetical model of dynamic biomarkers of the Alzheimer's pathological cascade. Lancet neurology 9:119-128.
Janke AL, de Zubicaray G, Rose SE, Griffin M, Chalk JB, Galloway GJ (2001) 4D deformation modeling of cortical disease progression in Alzheimer's dementia. Magnetic resonance in medicine : official journal of the Society of Magnetic Resonance in Medicine / Society of Magnetic Resonance in Medicine 46:661-666.
Jenkinson M, Bannister P, Brady M, Smith S (2002) Improved optimization for the robust and accurate linear registration and motion correction of brain images. NeuroImage 17:825-841.
Jenkinson M, Smith S (2001) A global optimisation method for robust affine registration of brain images. Medical image analysis 5:143-156.
Jensen JH, Helpern JA, Tabesh A (2014) Leading non-Gaussian corrections for diffusion orientation distribution function. NMR in biomedicine 27:202-211.
Johansen-Berg H, Della-Maggiore V, Behrens TE, Smith SM, Paus T (2007) Integrity of white matter in the corpus callosum correlates with bimanual co-ordination skills. NeuroImage 36 Suppl 2:T16-21.
Johansen-Berg H, Rushworth MF (2009) Using diffusion imaging to study human connectional anatomy. Annual review of neuroscience 32:75-94.
Johnson KA, Fox NC, Sperling RA, Klunk WE (2012a) Brain imaging in Alzheimer disease. Cold Spring Harbor perspectives in medicine 2:a006213.

Johnson NF, Kim C, Clasey JL, Bailey A, Gold BT (2012b) Cardiorespiratory fitness is positively correlated with cerebral white matter integrity in healthy seniors. NeuroImage 59:1514-1523.
Jones DK, Knosche TR, Turner R (2013a) White matter integrity, fiber count, and other fallacies: the do's and don'ts of diffusion MRI. NeuroImage 73:239-254.
Jones DK, Simmons A, Williams SC, Horsfield MA (1999) Non-invasive assessment of axonal fiber connectivity in the human brain via diffusion tensor MRI. Magnetic resonance in medicine : official journal of the Society of Magnetic Resonance in Medicine / Society of Magnetic Resonance in Medicine 42:37-41.
Jones DK, Symms MR, Cercignani M, Howard RJ (2005) The effect of filter size on VBM analyses of DT-MRI data. NeuroImage 26:546-554.
Jones EG, Steriade M, McCormick D (1985) The thalamus: Plenum Press New York.
Jones OD, Wagner AD, Faigman DL, Raichle ME (2013b) Neuroscientists in court. Nature reviews Neuroscience 14:730-736.
Jovicich J, Czanner S, Greve D, Haley E, van der Kouwe A, Gollub R, Kennedy D, Schmitt F, Brown G, Macfall J, Fischl B, Dale A (2006) Reliability in multi-site structural MRI studies: effects of gradient non-linearity correction on phantom and human data. NeuroImage 30:436-443.
Joyner MJ, Green DJ (2009) Exercise protects the cardiovascular system: effects beyond traditional risk factors. The Journal of physiology 587:5551-5558.
Kamagata K, Motoi Y, Abe O, Shimoji K, Hori M, Nakanishi A, Sano T, Kuwatsuru R, Aoki S, Hattori N (2012) White matter alteration of the cingulum in Parkinson disease with and without dementia: evaluation by diffusion tensor tract-specific analysis. AJNR American journal of neuroradiology 33:890-895.
Kantarci K, Avula R, Senjem ML, Samikoglu AR, Zhang B, Weigand SD, Przybelski SA, Edmonson HA, Vemuri P, Knopman DS, Ferman TJ, Boeve BF, Petersen RC, Jack CR, Jr. (2010) Dementia with Lewy bodies and Alzheimer disease: neurodegenerative patterns characterized by DTI. Neurology 74:1814-1821.
Karagulle Kendi AT, Lehericy S, Luciana M, Ugurbil K, Tuite P (2008) Altered diffusion in the frontal lobe in Parkinson disease. AJNR American journal of neuroradiology 29:501-505.
Keihaninejad S, Ryan NS, Malone IB, Modat M, Cash D, Ridgway GR, Zhang H, Fox NC, Ourselin S (2012) The importance of group-wise registration in tract based spatial statistics study of neurodegeneration: a simulation study in Alzheimer's disease. PloS one 7:e45996.
Keihaninejad S, Zhang H, Ryan NS, Malone IB, Modat M, Cardoso MJ, Cash DM, Fox NC, Ourselin S (2013) An unbiased longitudinal analysis framework for tracking white matter changes using diffusion tensor imaging with application to Alzheimer's disease. NeuroImage 72:153-163.
Kemper TL (1994) Neuroanatomical and neuropathological changes during aging and dementia.
Keppel G, Wickens TD (2004) Design and analysis : a researcher's handbook. Upper Saddle River, N.J.: Pearson Prentice Hall.
Kinglsey P (2006) Introduction to diffusion tensor imaging mathematics: Part III. Tensor calculation, noise, simulations, and optimization. Concepts Mag Res A, 28A 155-179.

Kingsley PB (2006a) Introduction to diffusion tensor imaging mathematics: Part II. Anisotropy, diffusion‐weighting factors, and gradient encoding schemes. Concepts in Magnetic Resonance Part A 28:123-154.
Kingsley PB (2006b) Introduction to diffusion tensor imaging mathematics: Part III. Tensor calculation, noise, simulations, and optimization. Concepts in Magnetic Resonance Part A 28:155-179.
Kirk-Sanchez NJ, McGough EL (2014) Physical exercise and cognitive performance in the elderly: current perspectives. Clinical interventions in aging 9:51-62.
Kramer AF, Hahn S, Cohen NJ, Banich MT, McAuley E, Harrison CR, Chason J, Vakil E, Bardell L, Boileau RA, Colcombe A (1999) Ageing, fitness and neurocognitive function. Nature 400:418-419.
Kurumatani T, Kudo T, Ikura Y, Takeda M (1998) White matter changes in the gerbil brain under chronic cerebral hypoperfusion. Stroke; a journal of cerebral circulation 29:1058-1062.
Kvickstrom P, Eriksson B, van Westen D, Latt J, Elfgren C, Nilsson C (2011) Selective frontal neurodegeneration of the inferior fronto-occipital fasciculus in progressive supranuclear palsy (PSP) demonstrated by diffusion tensor tractography. BMC neurology 11:13.
Larson EB, Wang L, Bowen JD, McCormick WC, Teri L, Crane P, Kukull W (2006) Exercise is associated with reduced risk for incident dementia among persons 65 years of age and older. Annals of internal medicine 144:73-81.
Le Bihan D (2003) Looking into the functional architecture of the brain with diffusion MRI. Nature reviews Neuroscience 4:469-480.
Le Bihan D, Breton E, Lallemand D, Grenier P, Cabanis E, Laval-Jeantet M (1986) MR imaging of intravoxel incoherent motions: application to diffusion and perfusion in neurologic disorders. Radiology 161:401-407.
Le Bihan D, Mangin JF, Poupon C, Clark CA, Pappata S, Molko N, Chabriat H (2001) Diffusion tensor imaging: concepts and applications. Journal of magnetic resonance imaging : JMRI 13:534-546.
Lee CY, Tabesh A, Nesland T, Jensen JH, Helpern JA, Spampinato MV, Bonilha L (2014) Human brain asymmetry in microstructural connectivity demonstrated by diffusional kurtosis imaging. Brain research 1588:73-80.
Lee W, Park B, Han K (2013) Classification of diffusion tensor images for the early detection of Alzheimer's disease. Computers in biology and medicine 43:1313-1320.
Leipsic PFO (1901) Developmental (myelogenetic) localisation of the cerebral cortex in the human subject. The Lancet 158:1027-1030.
Leuze CW, Anwander A, Bazin PL, Dhital B, Stuber C, Reimann K, Geyer S, Turner R (2014) Layer-specific intracortical connectivity revealed with diffusion MRI. Cerebral cortex 24:328-339.
Liu Y, Spulber G, Lehtimaki KK, Kononen M, Hallikainen I, Grohn H, Kivipelto M, Hallikainen M, Vanninen R, Soininen H (2011) Diffusion tensor imaging and tract-based spatial statistics in Alzheimer's disease and mild cognitive impairment. Neurobiology of aging 32:1558-1571.

Liu-Ambrose T, Nagamatsu LS, Graf P, Beattie BL, Ashe MC, Handy TC (2010) Resistance training and executive functions: a 12-month randomized controlled trial. Archives of internal medicine 170:170-178.
Logothetis NK, Pauls J, Augath M, Trinath T, Oeltermann A (2001) Neurophysiological investigation of the basis of the fMRI signal. Nature 412:150-157.
Lorenzo Cd (2012) Historia de los trastornos de la mente. vol. 2015.
MacWilliams B (2003) Russian claims first in magnetic imaging. Nature 426:375-375.
Madden DJ, Spaniol J, Costello MC, Bucur B, White LE, Cabeza R, Davis SW, Dennis NA, Provenzale JM, Huettel SA (2009) Cerebral white matter integrity mediates adult age differences in cognitive performance. Journal of cognitive neuroscience 21:289-302.
Makris N, Kennedy DN, McInerney S, Sorensen AG, Wang R, Caviness VS, Jr., Pandya DN (2005) Segmentation of subcomponents within the superior longitudinal fascicle in humans: a quantitative, in vivo, DT-MRI study. Cerebral cortex 15:854-869.
Marks BL, Katz LM, Styner M, Smith JK (2011) Aerobic fitness and obesity: relationship to cerebral white matter integrity in the brain of active and sedentary older adults. British journal of sports medicine 45:1208-1215.
Marks BL, Madden DJ, Bucur B, Provenzale JM, White LE, Cabeza R, Huettel SA (2007) Role of aerobic fitness and aging on cerebral white matter integrity. Annals of the New York Academy of Sciences 1097:171-174.
Marlatt MW, Potter MC, Lucassen PJ, van Praag H (2012) Running throughout middle-age improves memory function, hippocampal neurogenesis, and BDNF levels in female C57BL/6J mice. Developmental neurobiology 72:943-952.
Martino J, Brogna C, Robles SG, Vergani F, Duffau H (2010) Anatomic dissection of the inferior fronto-occipital fasciculus revisited in the lights of brain stimulation data. Cortex 46:691-699.
MathWorks I (2005) MATLAB: the language of technical computing. Desktop tools and development environment, version 7: MathWorks.
Matsui H, Nishinaka K, Oda M, Niikawa H, Komatsu K, Kubori T, Udaka F (2007a) Depression in Parkinson's disease. Diffusion tensor imaging study. Journal of neurology 254:1170-1173.
Matsui H, Nishinaka K, Oda M, Niikawa H, Kubori T, Udaka F (2007b) Dementia in Parkinson's disease: diffusion tensor imaging. Acta neurologica Scandinavica 116:177-181.
Mayer CJ, Steinman L, Williams B, Topolski TD, LoGerfo J (2008) Developing a Telephone Assessment of Physical Activity (TAPA) questionnaire for older adults. Preventing chronic disease 5:A24.
McArdle WD, Katch FI, Katch VL (2010) Exercise physiology: nutrition, energy, and human performance: Lippincott Williams & Wilkins.
McKhann G, Drachman D, Folstein M, Katzman R, Price D, Stadlan EM (1984a) Clinical diagnosis of Alzheimer's disease: report of the NINCDS-ADRDA Work Group under the auspices of Department of Health and Human Services Task Force on Alzheimer's Disease. Neurology 34:939-944.
McKhann G, Drachman D, Folstein M, Katzman R, Price D, Stadlan EM (1984b) Clinical diagnosis of Alzheimer's disease: Report of the NINCDS-ADRDA Work Group under

the auspices of Department of Health and Human Services Task Force on Alzheimer's disease. Neurology 34:939-944.
Medicine AACoS (2009) ACSM's Resource Manual For Guidelines For Exercise Testing And Prescription Author: American College Of Sports Medicine.
Merrill JE, Ignarro LJ, Sherman MP, Melinek J, Lane TE (1993) Microglial cell cytotoxicity of oligodendrocytes is mediated through nitric oxide. Journal of immunology 151:2132-2141.
Middleton LE, Barnes DE, Lui LY, Yaffe K (2010) Physical activity over the life course and its association with cognitive performance and impairment in old age. Journal of the American Geriatrics Society 58:1322-1326.
Mielke MM, Kozauer NA, Chan KC, George M, Toroney J, Zerrate M, Bandeen-Roche K, Wang MC, Vanzijl P, Pekar JJ, Mori S, Lyketsos CG, Albert M (2009) Regionally-specific diffusion tensor imaging in mild cognitive impairment and Alzheimer's disease. NeuroImage 46:47-55.
Miller DJ, Duka T, Stimpson CD, Schapiro SJ, Baze WB, McArthur MJ, Fobbs AJ, Sousa AM, Sestan N, Wildman DE, Lipovich L, Kuzawa CW, Hof PR, Sherwood CC (2012) Prolonged myelination in human neocortical evolution. Proceedings of the National Academy of Sciences of the United States of America 109:16480-16485.
Mori S, van Zijl PC (2002) Fiber tracking: principles and strategies - a technical review. NMR in biomedicine 15:468-480.
Mori S, Wakana S, Van Zijl PC, Nagae-Poetscher L (2005) MRI atlas of human white matter.
Morris JC (1993) The Clinical Dementia Rating (CDR): current version and scoring rules. Neurology 43:2412-2414.
Mufson EJ, Binder L, Counts SE, DeKosky ST, de Toledo-Morrell L, Ginsberg SD, Ikonomovic MD, Perez SE, Scheff SW (2012) Mild cognitive impairment: pathology and mechanisms. Acta neuropathologica 123:13-30.
Mufson EJ, Brady DR, Kordower JH (1990) Tracing neuronal connections in postmortem human hippocampal complex with the carbocyanine dye DiI. Neurobiology of aging 11:649-653.
Mustroph ML, Chen S, Desai SC, Cay EB, DeYoung EK, Rhodes JS (2012) Aerobic exercise is the critical variable in an enriched environment that increases hippocampal neurogenesis and water maze learning in male C57BL/6J mice. Neuroscience 219:62-71.
Nakajima K, Uchida S, Suzuki A, Hotta H, Aikawa Y (2003) The effect of walking on regional blood flow and acetylcholine in the hippocampus in conscious rats. Autonomic neuroscience : basic & clinical 103:83-92.
Nealey T, Daignault RM, Cai Y (2014) Trade Secrets in Life Science and Pharmaceutical Companies. Cold Spring Harbor perspectives in medicine.
Neeper SA, Gomez-Pinilla F, Choi J, Cotman C (1995) Exercise and brain neurotrophins. Nature 373:109.
Nelson ME, Rejeski WJ, Blair SN, Duncan PW, Judge JO, King AC, Macera CA, Castaneda-Sceppa C, American College of Sports M, American Heart A (2007) Physical activity and public health in older adults: recommendation from the American College of Sports Medicine and the American Heart Association. Circulation 116:1094-1105.

Nestor PG, Kubicki M, Gurrera RJ, Niznikiewicz M, Frumin M, McCarley RW, Shenton ME (2004) Neuropsychological correlates of diffusion tensor imaging in schizophrenia. Neuropsychology 18:629-637.
NIA NIoA (2014) Inside the Brain: Unraveling the Mystery of Alzheimer's Disease. vol. 2015.
Nichols TE, Holmes AP (2002) Nonparametric permutation tests for functional neuroimaging: a primer with examples. Human brain mapping 15:1-25.
Nir TM, Jahanshad N, Villalon-Reina JE, Toga AW, Jack CR, Weiner MW, Thompson PM, Alzheimer's Disease Neuroimaging I (2013) Effectiveness of regional DTI measures in distinguishing Alzheimer's disease, MCI, and normal aging. NeuroImage Clinical 3:180-195.
Nolte J (2009) The human brain : an introduction to its functional anatomy. Philadelphia, PA: Mosby/Elsevier.
O'Donnell LJ, Westin CF (2011) An introduction to diffusion tensor image analysis. Neurosurgery clinics of North America 22:185-196, viii.
Oishi K, Lyketsos CG (2014) Alzheimer's disease and the fornix. Frontiers in aging neuroscience 6:241.
Onodera S, Hicks TP (2010) Carbocyanine dye usage in demarcating boundaries of the aged human red nucleus. PloS one 5:e14430.
Pallin DJ, Espinola JA, Camargo CA, Jr. (2014) US population aging and demand for inpatient services. Journal of hospital medicine : an official publication of the Society of Hospital Medicine 9:193-196.
Papagno C, Miracapillo C, Casarotti A, Romero Lauro LJ, Castellano A, Falini A, Casaceli G, Fava E, Bello L (2011) What is the role of the uncinate fasciculus? Surgical removal and proper name retrieval. Brain : a journal of neurology 134:405-414.
Parente DB, Gasparetto EL, da Cruz LC, Jr., Domingues RC, Baptista AC, Carvalho AC, Domingues RC (2008) Potential role of diffusion tensor MRI in the differential diagnosis of mild cognitive impairment and Alzheimer's disease. AJR American journal of roentgenology 190:1369-1374.
Paskavitz JF, Lippa CF, Hamos JE, Pulaski-Salo D, Drachman DA (1995) Role of the dorsomedial nucleus of the thalamus in Alzheimer's disease. Journal of geriatric psychiatry and neurology 8:32-37.
Perneczky R, Alexopoulos P, Kurz A (2014) Soluble amyloid precursor proteins and secretases as Alzheimer's disease biomarkers. Trends in molecular medicine 20:8-15.
Petersen SE, Posner MI (2012) The attention system of the human brain: 20 years after. Annual review of neuroscience 35:73-89.
Pihlajamaki M, Jauhiainen AM, Soininen H (2009) Structural and functional MRI in mild cognitive impairment. Current Alzheimer research 6:179-185.
Poupon C, Rieul B, Kezele I, Perrin M, Poupon F, Mangin JF (2008) New diffusion phantoms dedicated to the study and validation of high‐angular‐resolution diffusion imaging (HARDI) models. Magnetic Resonance in Medicine 60:1276-1283.
Power J, Mayer-Proschel M, Smith J, Noble M (2002) Oligodendrocyte precursor cells from different brain regions express divergent properties consistent with the differing time courses of myelination in these regions. Developmental biology 245:362-375.

Raj A, Kuceyeski A, Weiner M (2012) A network diffusion model of disease progression in dementia. Neuron 73:1204-1215.
Reid AT, Evans AC (2013) Structural networks in Alzheimer's disease. European neuropsychopharmacology : the journal of the European College of Neuropsychopharmacology 23:63-77.
Reuter M, Fischl B (2011) Avoiding asymmetry-induced bias in longitudinal image processing. NeuroImage 57:19-21.
Reuter M, Rosas HD, Fischl B (2010) Highly accurate inverse consistent registration: a robust approach. NeuroImage 53:1181-1196.
Reuter M, Schmansky NJ, Rosas HD, Fischl B (2012) Within-subject template estimation for unbiased longitudinal image analysis. NeuroImage 61:1402-1418.
Rosen WG, Mohs RC, Davis KL (1984) A new rating scale for Alzheimer's disease. The American journal of psychiatry 141:1356-1364.
Rudow G, O'Brien R, Savonenko AV, Resnick SM, Zonderman AB, Pletnikova O, Marsh L, Dawson TM, Crain BJ, West MJ, Troncoso JC (2008) Morphometry of the human substantia nigra in ageing and Parkinson's disease. Acta neuropathologica 115:461-470.
Ruscheweyh R, Willemer C, Kruger K, Duning T, Warnecke T, Sommer J, Volker K, Ho HV, Mooren F, Knecht S, Floel A (2011) Physical activity and memory functions: an interventional study. Neurobiology of aging 32:1304-1319.
Sachdev PS, Zhuang L, Braidy N, Wen W (2013) Is Alzheimer's a disease of the white matter? Current opinion in psychiatry 26:244-251.
Sadigh-Eteghad S, Talebi M, Farhoudi M (2012) Association of apolipoprotein E epsilon 4 allele with sporadic late onset Alzheimer`s disease. A meta-analysis. Neurosciences 17:321-326.
Saher G, Brugger B, Lappe-Siefke C, Mobius W, Tozawa R, Wehr MC, Wieland F, Ishibashi S, Nave KA (2005) High cholesterol level is essential for myelin membrane growth. Nature neuroscience 8:468-475.
Salat DH (2011) The declining infrastructure of the aging brain. Brain connectivity 1:279-293.
Schaller RR (1997) Moore's law: past, present and future. Spectrum, IEEE 34:52-59.
Scharfman HE, Chao MV (2013) The entorhinal cortex and neurotrophin signaling in Alzheimer's disease and other disorders. Cognitive neuroscience 4:123-135.
Scherder E, Eggermont L, Visscher C, Scheltens P, Swaab D (2011) Understanding higher level gait disturbances in mild dementia in order to improve rehabilitation: 'last in-first out'. Neuroscience and biobehavioral reviews 35:699-714.
Schmahmann JD, Pandya DN, Wang R, Dai G, D'Arceuil HE, de Crespigny AJ, Wedeen VJ (2007) Association fibre pathways of the brain: parallel observations from diffusion spectrum imaging and autoradiography. Brain : a journal of neurology 130:630-653.
Schnabel J, Rueckert D, Quist M, Blackall J, Castellano-Smith A, Hartkens T, Penney G, Hall W, Liu H, Truwit C (2001) A generic framework for non-rigid registration based on non-uniform multi-level free-form deformations. pp 573-581: Springer.
Schocke MF, Seppi K, Esterhammer R, Kremser C, Jaschke W, Poewe W, Wenning GK (2002) Diffusion-weighted MRI differentiates the Parkinson variant of multiple system atrophy from PD. Neurology 58:575-580.

Schwarz CG, Reid RI, Gunter JL, Senjem ML, Przybelski SA, Zuk SM, Whitwell JL, Vemuri P, Josephs KA, Kantarci K, Thompson PM, Petersen RC, Jack CR, Jr., Alzheimer's Disease Neuroimaging I (2014) Improved DTI registration allows voxel-based analysis that outperforms tract-based spatial statistics. NeuroImage 94:65-78.
Schwarz TL (2013) Mitochondrial trafficking in neurons. Cold Spring Harbor perspectives in biology 5.
Scola E, Bozzali M, Agosta F, Magnani G, Franceschi M, Sormani MP, Cercignani M, Pagani E, Falautano M, Filippi M, Falini A (2010) A diffusion tensor MRI study of patients with MCI and AD with a 2-year clinical follow-up. Journal of neurology, neurosurgery, and psychiatry 81:798-805.
Sen PN, Basser PJ (2005) A model for diffusion in white matter in the brain. Biophysical journal 89:2927-2938.
Seung S (2012) Connectome: How the brain's wiring makes us who we are: Houghton Mifflin Harcourt.
Sexton CE, Kalu UG, Filippini N, Mackay CE, Ebmeier KP (2011) A meta-analysis of diffusion tensor imaging in mild cognitive impairment and Alzheimer's disease. Neurobiology of aging 32:2322 e2325-2318.
Shirk SD, Mitchell MB, Shaughnessy LW, Sherman JC, Locascio JJ, Weintraub S, Atri A (2011) A web-based normative calculator for the uniform data set (UDS) neuropsychological test battery. Alzheimer's research & therapy 3:32.
Shu N, Wang Z, Qi Z, Li K, He Y (2011) Multiple diffusion indices reveals white matter degeneration in Alzheimer's disease and mild cognitive impairment: a tract-based spatial statistics study. Journal of Alzheimer's disease : JAD 26 Suppl 3:275-285.
Sjobeck M, Haglund M, Englund E (2006) White matter mapping in Alzheimer's disease: A neuropathological study. Neurobiology of aging 27:673-680.
Smith PJ, Blumenthal JA, Hoffman BM, Cooper H, Strauman TA, Welsh-Bohmer K, Browndyke JN, Sherwood A (2010) Aerobic exercise and neurocognitive performance: a meta-analytic review of randomized controlled trials. Psychosomatic medicine 72:239-252.
Smith SM (2002) Fast robust automated brain extraction. Human brain mapping 17:143-155.
Smith SM, Jenkinson M, Johansen-Berg H, Rueckert D, Nichols TE, Mackay CE, Watkins KE, Ciccarelli O, Cader MZ, Matthews PM, Behrens TE (2006) Tract-based spatial statistics: voxelwise analysis of multi-subject diffusion data. NeuroImage 31:1487-1505.
Smith SM, Jenkinson M, Woolrich MW, Beckmann CF, Behrens TE, Johansen-Berg H, Bannister PR, De Luca M, Drobnjak I, Flitney DE, Niazy RK, Saunders J, Vickers J, Zhang Y, De Stefano N, Brady JM, Matthews PM (2004a) Advances in functional and structural MR image analysis and implementation as FSL. NeuroImage 23 Suppl 1:S208-219.
Smith SM, Jenkinson M, Woolrich MW, Beckmann CF, Behrens TEJ, Johansen-Berg H, Bannister PR, De Luca M, Drobnjak I, Flitney DE (2004b) Advances in functional and structural MR image analysis and implementation as FSL. Neuroimage 23:S208-S219.

Smith SM, Nichols TE (2009) Threshold-free cluster enhancement: addressing problems of smoothing, threshold dependence and localisation in cluster inference. NeuroImage 44:83-98.
Song SK, Sun SW, Ju WK, Lin SJ, Cross AH, Neufeld AH (2003) Diffusion tensor imaging detects and differentiates axon and myelin degeneration in mouse optic nerve after retinal ischemia. NeuroImage 20:1714-1722.
Song SK, Yoshino J, Le TQ, Lin SJ, Sun SW, Cross AH, Armstrong RC (2005) Demyelination increases radial diffusivity in corpus callosum of mouse brain. NeuroImage 26:132-140.
Sperling R, Mormino E, Johnson K (2014) The evolution of preclinical Alzheimer's disease: implications for prevention trials. Neuron 84:608-622.
Stahl R, Dietrich O, Teipel SJ, Hampel H, Reiser MF, Schoenberg SO (2007) White matter damage in Alzheimer disease and mild cognitive impairment: assessment with diffusion-tensor MR imaging and parallel imaging techniques. Radiology 243:483-492.
Stejskal E, Tanner J (1965) Spin diffusion measurements: spin echoes in the presence of a time‐dependent field gradient. The journal of chemical physics 42:288-292.
Storandt M, Grant EA, Miller JP, Morris JC (2006) Longitudinal course and neuropathologic outcomes in original vs revised MCI and in pre-MCI. Neurology 67:467-473.
Stranahan AM, Khalil D, Gould E (2007) Running induces widespread structural alterations in the hippocampus and entorhinal cortex. Hippocampus 17:1017-1022.
Sullivan EV, Pfefferbaum A (2006) Diffusion tensor imaging and aging. Neuroscience and biobehavioral reviews 30:749-761.
Tang K, Xia FC, Wagner PD, Breen EC (2010) Exercise-induced VEGF transcriptional activation in brain, lung and skeletal muscle. Respiratory physiology & neurobiology 170:16-22.
Teipel SJ, Meindl T, Wagner M, Stieltjes B, Reuter S, Hauenstein KH, Filippi M, Ernemann U, Reiser MF, Hampel H (2010) Longitudinal changes in fiber tract integrity in healthy aging and mild cognitive impairment: a DTI follow-up study. Journal of Alzheimer's disease : JAD 22:507-522.
Teipel SJ, Wegrzyn M, Meindl T, Frisoni G, Bokde AL, Fellgiebel A, Filippi M, Hampel H, Kloppel S, Hauenstein K, Ewers M, group Es (2012) Anatomical MRI and DTI in the diagnosis of Alzheimer's disease: a European multicenter study. Journal of Alzheimer's disease : JAD 31 Suppl 3:S33-47.
Thies W, Bleiler L, Alzheimer's A (2013) 2013 Alzheimer's disease facts and figures. Alzheimer's & dementia : the journal of the Alzheimer's Association 9:208-245.
Thompson PM, Hayashi KM, de Zubicaray G, Janke AL, Rose SE, Semple J, Herman D, Hong MS, Dittmer SS, Doddrell DM, Toga AW (2003) Dynamics of gray matter loss in Alzheimer's disease. The Journal of neuroscience : the official journal of the Society for Neuroscience 23:994-1005.
Thompson PM, Mega MS, Woods RP, Zoumalan CI, Lindshield CJ, Blanton RE, Moussai J, Holmes CJ, Cummings JL, Toga AW (2001) Cortical change in Alzheimer's disease detected with a disease-specific population-based brain atlas. Cerebral cortex 11:1-16.

Tian Q, Erickson KI, Simonsick EM, Aizenstein HJ, Glynn NW, Boudreau RM, Newman AB, Kritchevsky SB, Yaffe K, Harris TB, Rosano C (2014a) Physical activity predicts microstructural integrity in memory-related networks in very old adults. The journals of gerontology Series A, Biological sciences and medical sciences 69:1284-1290.

Tian Q, Simonsick EM, Erickson KI, Aizenstein HJ, Glynn NW, Boudreau RM, Newman AB, Kritchevsky SB, Yaffe K, Harris T, Rosano C, Health ABCs (2014b) Cardiorespiratory fitness and brain diffusion tensor imaging in adults over 80 years of age. Brain research 1588:63-72.

Todd S, Barr S, Passmore AP (2013) Cause of death in Alzheimer's disease: a cohort study. QJM : monthly journal of the Association of Physicians 106:747-753.

Trejo JL, Carro E, Torres-Aleman I (2001) Circulating insulin-like growth factor I mediates exercise-induced increases in the number of new neurons in the adult hippocampus. The Journal of neuroscience : the official journal of the Society for Neuroscience 21:1628-1634.

Tseng BY, Gundapuneedi T, Khan MA, Diaz-Arrastia R, Levine BD, Lu H, Huang H, Zhang R (2013) White Matter Integrity in Physically Fit Older Adults. NeuroImage.

Tuch DS (2004) Q-ball imaging. Magnetic resonance in medicine : official journal of the Society of Magnetic Resonance in Medicine / Society of Magnetic Resonance in Medicine 52:1358-1372.

Vaillancourt DE, Spraker MB, Prodoehl J, Abraham I, Corcos DM, Zhou XJ, Comella CL, Little DM (2009) High-resolution diffusion tensor imaging in the substantia nigra of de novo Parkinson disease. Neurology 72:1378-1384.

Van der Borght K, Kobor-Nyakas DE, Klauke K, Eggen BJ, Nyakas C, Van der Zee EA, Meerlo P (2009) Physical exercise leads to rapid adaptations in hippocampal vasculature: temporal dynamics and relationship to cell proliferation and neurogenesis. Hippocampus 19:928-936.

van Praag H, Kempermann G, Gage FH (1999) Running increases cell proliferation and neurogenesis in the adult mouse dentate gyrus. Nature neuroscience 2:266-270.

van Praag H, Shubert T, Zhao C, Gage FH (2005) Exercise enhances learning and hippocampal neurogenesis in aged mice. The Journal of neuroscience : the official journal of the Society for Neuroscience 25:8680-8685.

Vidoni ED, Honea RA, Billinger SA, Swerdlow RH, Burns JM (2012a) Cardiorespiratory fitness is associated with atrophy in Alzheimer's and aging over 2 years. Neurobiology of aging 33:1624-1632.

Vidoni ED, Van Sciver A, Johnson DK, He J, Honea R, Haines B, Goodwin J, Laubinger MP, Anderson HS, Kluding PM, Donnelly JE, Billinger SA, Burns JM (2012b) A community-based approach to trials of aerobic exercise in aging and Alzheimer's disease. Contemporary clinical trials 33:1105-1116.

Voss MW, Erickson KI, Prakash RS, Chaddock L, Kim JS, Alves H, Szabo A, Phillips SM, Wojcicki TR, Mailey EL, Olson EA, Gothe N, Vieira-Potter VJ, Martin SA, Pence BD, Cook MD, Woods JA, McAuley E, Kramer AF (2013a) Neurobiological markers of exercise-related brain plasticity in older adults. Brain, behavior, and immunity 28:90-99.

Voss MW, Heo S, Prakash RS, Erickson KI, Alves H, Chaddock L, Szabo AN, Mailey EL, Wojcicki TR, White SM, Gothe N, McAuley E, Sutton BP, Kramer AF (2012) The

influence of aerobic fitness on cerebral white matter integrity and cognitive function in older adults: Results of a one-year exercise intervention. Human brain mapping.
Voss MW, Prakash RS, Erickson KI, Basak C, Chaddock L, Kim JS, Alves H, Heo S, Szabo AN, White SM, Wojcicki TR, Mailey EL, Gothe N, Olson EA, McAuley E, Kramer AF (2010) Plasticity of brain networks in a randomized intervention trial of exercise training in older adults. Frontiers in aging neuroscience 2.
Voss MW, Vivar C, Kramer AF, van Praag H (2013b) Bridging animal and human models of exercise-induced brain plasticity. Trends in cognitive sciences 17:525-544.
Wakana S, Caprihan A, Panzenboeck MM, Fallon JH, Perry M, Gollub RL, Hua K, Zhang J, Jiang H, Dubey P, Blitz A, van Zijl P, Mori S (2007) Reproducibility of quantitative tractography methods applied to cerebral white matter. NeuroImage 36:630-644.
Walhovd KB, Johansen-Berg H, Karadottir RT (2014) Unraveling the secrets of white matter - Bridging the gap between cellular, animal and human imaging studies. Neuroscience 276C:2-13.
Wang Z, Jia X, Liang P, Qi Z, Yang Y, Zhou W, Li K (2012) Changes in thalamus connectivity in mild cognitive impairment: evidence from resting state fMRI. European journal of radiology 81:277-285.
Watson PE, Watson ID, Batt RD (1980) Total body water volumes for adult males and females estimated from simple anthropometric measurements. The American journal of clinical nutrition 33:27-39.
Watson R, Blamire AM, Colloby SJ, Wood JS, Barber R, He J, O'Brien JT (2012) Characterizing dementia with Lewy bodies by means of diffusion tensor imaging. Neurology 79:906-914.
Weinstein AM, Voss MW, Prakash RS, Chaddock L, Szabo A, White SM, Wojcicki TR, Mailey E, McAuley E, Kramer AF, Erickson KI (2012) The association between aerobic fitness and executive function is mediated by prefrontal cortex volume. Brain, behavior, and immunity 26:811-819.
Weintraub S, Salmon D, Mercaldo N, Ferris S, Graff-Radford NR, Chui H, Cummings J, DeCarli C, Foster NL, Galasko D, Peskind E, Dietrich W, Beekly DL, Kukull WA, Morris JC (2009) The Alzheimer's Disease Centers' Uniform Data Set (UDS): the neuropsychologic test battery. Alzheimer disease and associated disorders 23:91-101.
Weuve J, Hebert LE, Scherr PA, Evans DA (2014) Deaths in the United States among persons with Alzheimer's disease (2010-2050). Alzheimer's & dementia : the journal of the Alzheimer's Association 10:e40-46.
Weuve J, Kang JH, Manson JE, Breteler MM, Ware JH, Grodstein F (2004) Physical activity, including walking, and cognitive function in older women. JAMA : the journal of the American Medical Association 292:1454-1461.
Wheeler-Kingshott CA, Cercignani M (2009) About "axial" and "radial" diffusivities. Magnetic resonance in medicine : official journal of the Society of Magnetic Resonance in Medicine / Society of Magnetic Resonance in Medicine 61:1255-1260.
Wikipedia.org (2014) Robert Brown (botanist).
Wilkins B, Lee N, Gajawelli N, Law M, Lepore N (2014) Fiber estimation and tractography in diffusion MRI: Development of simulated brain images and comparison of multi-fiber analysis methods at clinical b-values. NeuroImage.

Wiltshire K, Concha L, Gee M, Bouchard T, Beaulieu C, Camicioli R (2010) Corpus callosum and cingulum tractography in Parkinson's disease. The Canadian journal of neurological sciences Le journal canadien des sciences neurologiques 37:595-600.
Winkler AM, Ridgway GR, Webster MA, Smith SM, Nichols TE (2014) Permutation inference for the general linear model. NeuroImage 92:381-397.
Woolrich MW, Jbabdi S, Patenaude B, Chappell M, Makni S, Behrens T, Beckmann C, Jenkinson M, Smith SM (2009) Bayesian analysis of neuroimaging data in FSL. Neuroimage 45:S173-S186.
Wu CW, Chang YT, Yu L, Chen HI, Jen CJ, Wu SY, Lo CP, Kuo YM (2008) Exercise enhances the proliferation of neural stem cells and neurite growth and survival of neuronal progenitor cells in dentate gyrus of middle-aged mice. Journal of applied physiology 105:1585-1594.
Wyss JM, Van Groen T (1992) Connections between the retrosplenial cortex and the hippocampal formation in the rat: a review. Hippocampus 2:1-11.
Xie S, Xiao JX, Wang YH, Wu HK, Gong GL, Jiang XX (2005) Evaluation of bilateral cingulum with tractography in patients with Alzheimer's disease. Neuroreport 16:1275-1278.
Yoshikawa K, Nakata Y, Yamada K, Nakagawa M (2004) Early pathological changes in the parkinsonian brain demonstrated by diffusion tensor MRI. Journal of neurology, neurosurgery, and psychiatry 75:481-484.
Yu JT, Tan L, Hardy J (2014) Apolipoprotein E in Alzheimer's disease: an update. Annual review of neuroscience 37:79-100.
Zalesky A (2011) Moderating registration misalignment in voxelwise comparisons of DTI data: a performance evaluation of skeleton projection. Magnetic resonance imaging 29:111-125.
Zarei M, Patenaude B, Damoiseaux J, Morgese C, Smith S, Matthews PM, Barkhof F, Rombouts SA, Sanz-Arigita E, Jenkinson M (2010) Combining shape and connectivity analysis: an MRI study of thalamic degeneration in Alzheimer's disease. NeuroImage 49:1-8.
Zeineh MM, Holdsworth S, Skare S, Atlas SW, Bammer R (2012) Ultra-high resolution diffusion tensor imaging of the microscopic pathways of the medial temporal lobe. NeuroImage 62:2065-2082.
Zhan W, Kang GA, Glass GA, Zhang Y, Shirley C, Millin R, Possin KL, Nezamzadeh M, Weiner MW, Marks WJ, Jr., Schuff N (2012) Regional alterations of brain microstructure in Parkinson's disease using diffusion tensor imaging. Movement disorders : official journal of the Movement Disorder Society 27:90-97.
Zhang B, Xu Y, Zhu B, Kantarci K (2014) The role of diffusion tensor imaging in detecting microstructural changes in prodromal Alzheimer's disease. CNS neuroscience & therapeutics 20:3-9.
Zhang Y, Schuff N, Jahng GH, Bayne W, Mori S, Schad L, Mueller S, Du AT, Kramer JH, Yaffe K, Chui H, Jagust WJ, Miller BL, Weiner MW (2007) Diffusion tensor imaging of cingulum fibers in mild cognitive impairment and Alzheimer disease. Neurology 68:13-19.
Zheng Z, Shemmassian S, Wijekoon C, Kim W, Bookheimer SY, Pouratian N (2013) DTI correlates of distinct cognitive impairments in Parkinson's disease. Human brain mapping.

Zhou B, Liu Y, Zhang Z, An N, Yao H, Wang P, Wang L, Zhang X, Jiang T (2013) Impaired functional connectivity of the thalamus in Alzheimer's disease and mild cognitive impairment: a resting-state fMRI study. Current Alzheimer research 10:754-766.
Zhuang L, Wen W, Zhu W, Trollor J, Kochan N, Crawford J, Reppermund S, Brodaty H, Sachdev P (2010) White matter integrity in mild cognitive impairment: a tract-based spatial statistics study. NeuroImage 53:16-25.